IDENTIFICATION OF NATURAL MODIFIER AGAINST EPIGENETICS OF NEPHROLITHIASIS USING IN-SILICO APPROACH AND ITS APPLICABILITY IN IN-VITRO AND IN-VIVO MODELS

Thesis Submitted for the Award of the Degree of

DOCTOR OF PHILOSOPHY

in

Biotechnology

By

Nancy Bhura

Registration Number: 11917137

Supervised By

Dr. Jeena Gupta

Associate Professor

Department of Biochemistry

School of Bioengineering and Biosciences

LOVELY PROFESSIONAL UNIVERSITY, PUNJAB
2026

DECLARATION

I, hereby declare that the presented work in the thesis entitled "Identification of natural modifier against epigenetics of nephrolithiasis using in-silico approach and its applicability in in-vitro and in-vivo models" in fulfilment of the degree of **Doctor of Philosophy (PhD)** is the outcome of research work carried out by me under the supervision of **Dr. Jeena Gupta**, working as Associate Professor, in the Department of Biochemistry, School of Bioengineering and Biosciences of Lovely Professional University, Punjab, India. In keeping with the general practice of reporting scientific observations, due acknowledgements have been made whenever the works described here are based on the findings of other investigators. This work has not been submitted in part or whole to any other University or Institute for the award of any degree.

Name of the scholar: Nancy Bhura

Registration No.: 11917137

Department/School: Biotechnology (School of Bioengineering and Biosciences)

Lovely Professional University

Punjab, India

CERTIFICATE

This is to certify that the work reported in the Ph. D. thesis entitled "Identification of Natural Modifiers Against Epigenetics of Nephrolithiasis Using In-Silico Approach and its Applicability in In-Vitro and In-Vivo Models" submitted in fulfillment of the requirement for the reward of degree of **Doctor of Philosophy (Ph.D.)** in the Biotechnology department of School of Bioengineering and Biosciences, is a research work carried out by **Nancy Bhura**, 11917137, is bonafide record of his/her original work carried out under my supervision and that no part of thesis has been submitted for any other degree, diploma or equivalent course.

(Signature of Supervisor)

Name of supervisor: Dr. Jeena Gupta

Designation: Associate Professor

Department/school: Biochemistry, School of Bioengineering and Biosciences

University: Lovely Professional University

Abstract

Nephrolithiasis, commonly known as kidney stone disease, is a prevalent health condition affecting approximately 13% of the global population. The disease poses significant clinical challenges due to its high recurrence rate, leading to severe health complications and imposing a substantial burden on healthcare systems worldwide. Conventional treatment strategies, including increased fluid intake, dietary modifications, citrate supplementation, and surgical interventions such as extracorporeal shock wave lithotripsy (ESWL) and ureteroscopy, have shown limited success in reducing recurrence rates. This necessitates the exploration of alternative therapeutic strategies that can effectively target the underlying mechanisms of nephrolithiasis pathogenesis. Recent research suggests that epigenetic modifications play a crucial role in disease progression by influencing gene expression associated with oxidative stress, inflammation, and crystal formation. In this study, an integrated in-silico, in-vitro, and in-vivo approach was employed to identify potential natural epigenetic modifiers that can mitigate nephrolithiasis.

To systematically identify natural compounds with anti-nephrolithiatic potential, a comprehensive literature-based screening was conducted. This initial screening identified six key phytochemicals known for their epigenetic regulatory properties and potential protective effects against nephrolithiasis. Structural similarity searching expanded this selection to 67 related compounds. These compounds underwent a rigorous screening process, including Lipinski's rule of five for drug-likeness assessment, ADME (absorption, distribution, metabolism, and excretion) analysis for pharmacokinetic evaluation, and toxicity profiling to ensure safety. The Swiss Target Prediction and GeneCards databases were utilized to identify nephrolithiasis-associated molecular targets. Network pharmacology analysis revealed 191 common targets between the shortlisted phytochemicals and nephrolithiasis-related genes. Key regulatory genes were determined using Cytoscape's Cytohubba plugin and subsequently analyzed for biological significance through Gene Ontology (GO) and Kyoto Encyclopedia of Genes and Genomes (KEGG) pathway analysis. Molecular docking studies were performed to evaluate the binding affinities of the phytochemicals to disease-associated proteins, with a specific focus on epigenetic regulators such as sirtuins (SIRTs), histone deacetylases (HDACs), and DNA methyltransferases (DNMTs).

Among the shortlisted phytochemicals, 4-Vinylguaiacol, anethole, isoeugenol, nadolol, and silibinin demonstrated the most promising potential in modulating nephrolithiasis-associated

pathways. GO analysis indicated enrichment in biological processes related to oxidative stress response, inflammation modulation, and cellular homeostasis. Cellular component analysis suggested that these phytochemicals primarily localized within the nuclear lumen and nucleoplasm, reinforcing their role in epigenetic modulation. Molecular function analysis revealed their interaction with key enzymatic regulators, suggesting their potential to influence crystal formation, oxidative damage, and renal injury. KEGG pathway analysis further confirmed associations with signalling pathways involved in oxidative stress, apoptosis, and metabolic regulation, highlighting their therapeutic potential.

Beyond their impact on crystal formation, the antioxidant potential of these phytochemicals was evaluated using DPPH, ABTS, and FRAP assays, all of which demonstrated significant free radical scavenging activity. Cellular assays conducted on renal epithelial cells revealed that these phytochemicals conferred notable protective effects against oxidative stress-induced injury. Treated cells exhibited enhanced enzymatic antioxidant responses, with a marked reduction in reactive oxygen species (ROS) levels and lipid peroxidation. Notably, silibinin exhibited superior anti-crystallization effects by effectively inhibiting nucleation and aggregation, while Anethole demonstrated the highest oxalate depletion efficiency, surpassing the efficacy of conventional potassium citrate treatment.

Molecular docking studies provided further mechanistic insights, particularly regarding the interaction between the phytochemicals and epigenetic regulators. Among the evaluated targets, SIRT1 exhibited strong binding interactions with multiple phytochemicals, including anethole, isoeugenol, and silibinin. Detailed interaction analysis revealed significant binding at key residues such as GLU230, ASN226, and PHE273. To validate these interactions, molecular dynamics simulations were performed using the GROMACS software suite. Trajectory analysis employing the molecular mechanics Poisson–Boltzmann surface area (MM/PBSA) approach confirmed the stability of these interactions over a 100-nanosecond simulation period. Binding free energy calculations ranged from -12 to -16 kcal/mol, indicating a high affinity and stability of the phytochemical-protein complexes. Root-mean-square deviation (RMSD) and radius of gyration (Rg) analyses suggested that these interactions remained stable within a range of 0.2 to 1.1 nm, reinforcing the hypothesis that these natural compounds exert regulatory effects on epigenetic pathways involved in nephrolithiasis.

To translate these findings into a physiological context, in-vivo studies were conducted using an ethylene glycol (EG)-induced nephrolithiasis rat model. Histopathological examination of

kidney tissues from treated rats revealed that Silibinin administration significantly mitigated oxidative damage and calcium oxalate deposition. Biochemical analyses demonstrated improved renal function in treated animals, as evidenced by increased glomerular filtration rate (GFR) and reduced serum creatinine and blood urea nitrogen (BUN) levels. Antioxidant enzyme assays showed a marked increase in superoxide dismutase (SOD), catalase (CAT), and glutathione peroxidase (GPx) activity, alongside a significant reduction in malondialdehyde (MDA) levels, a key marker of lipid peroxidation. Immunohistochemical staining confirmed a substantial reduction in the expression of inflammatory markers and apoptosis-related proteins in treated kidney tissues, further supporting the protective role of these phytochemicals in mitigating nephrolithiasis-associated renal injury.

The kinetic effects of various phytochemicals on calcium oxalate monohydrate (COM) crystallization were also investigated, focusing on nucleation kinetics, surface energy, and critical nucleus formation. Induction time analysis at different supersaturation ratios (SRs), with and without phytochemical additives, revealed that all phytochemicals, along with potassium citrate, increased induction time, indicating a delayed nucleation process and inhibition of detectable crystal nuclei formation. UV-vis absorbance analysis further validated this trend.

Induction time data were utilised to determine surface energy and critical nucleus size using classical nucleation theory. The presence of phytochemicals generally reduced surface energy compared to the control, except for silibinin, which exhibited increased surface energy. X-ray diffraction (XRD) analysis confirmed that all formed crystals were primarily COM, with structural variations affecting surface energy. Gibbs free energy calculations demonstrated that Silibinin and Anethole significantly increased the free energy barrier (ΔGcr) for nucleus formation, suggesting their inhibitory effects on nucleation.

Fourier-transform infrared spectroscopy (FTIR) analysis identified characteristic COM peaks, confirming that phytochemicals did not alter fundamental molecular structures. Zeta potential measurements indicated enhanced system stability with reduced particle aggregation at higher SRs, with Silibinin exhibiting the most significant impact on stabilizing particle dispersion. Field emission scanning electron microscopy (FESEM) revealed that COM crystals formed in the absence of additives were more aggregated than those formed in the presence of phytochemicals. The presence of citrate and phytochemicals modulated calcium oxalate crystallization by interacting with calcium ions, altering crystal morphology.

This study represents a comprehensive investigation into the potential of natural epigenetic modifiers for nephrolithiasis treatment. By integrating computational, biochemical, and physiological methodologies, we identified and validated phytochemicals with promising anti-nephrolithiatic properties that exert their effects through oxidative stress reduction, crystal growth inhibition, and epigenetic modulation. The findings highlight the therapeutic potential of silibinin, anethole, and isoeugenol while providing a framework for further research into plant-derived epigenetic modulators. Future studies should focus on translating these findings into clinical applications through rigorous human trials and exploring additional interactions with epigenetic regulators such as non-coding RNAs and histone modifications. This study paves the way for developing novel, plant-based therapeutics targeting the epigenetic landscape of nephrolithiasis, offering an effective alternative to conventional treatment options with minimal adverse effects.

Graphical abstract

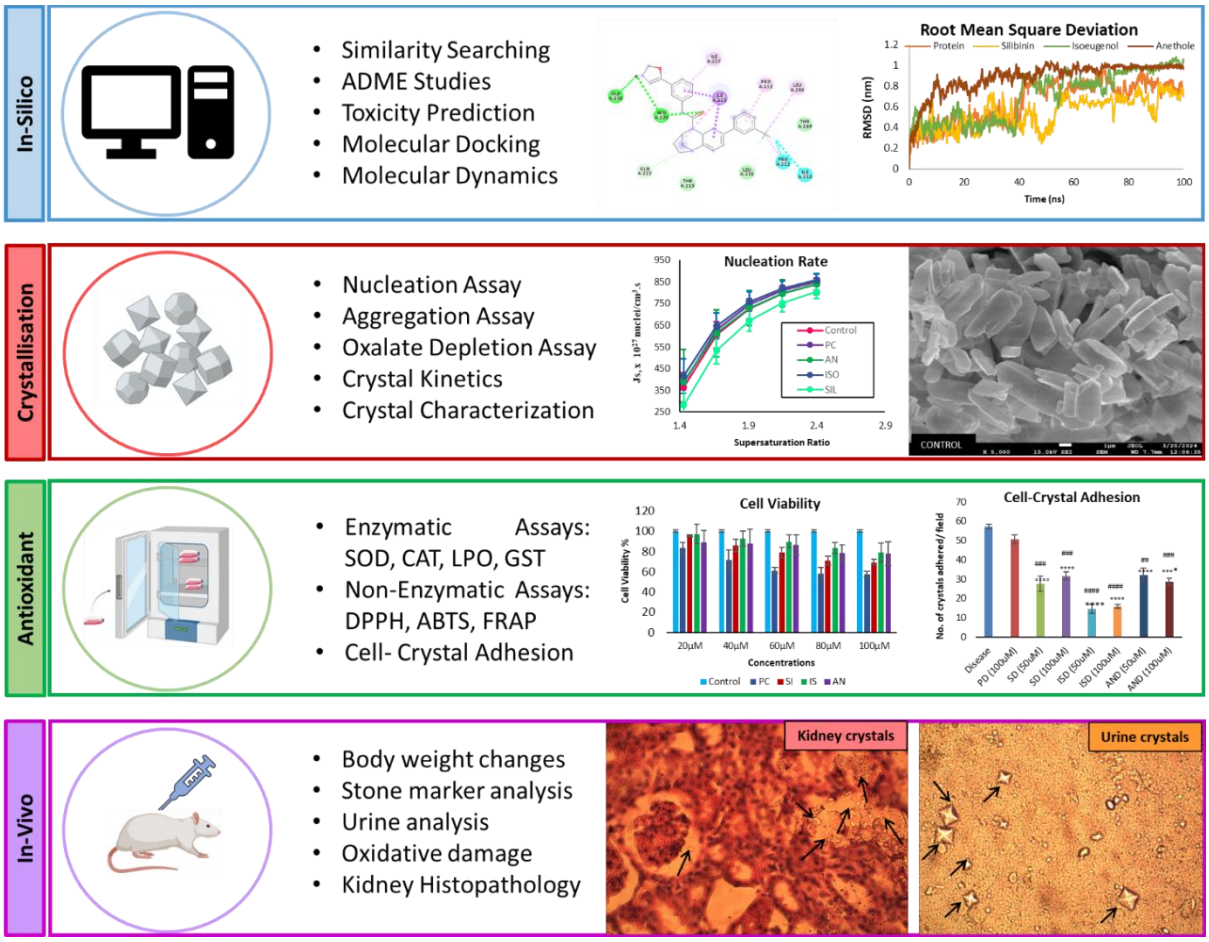

Multi-level screening of phytochemicals against nephrolithiasis

Summary of graphical abstract

Widespread kidney stones (nephrolithiasis) are on the rise across the globe due to dietary and lifestyle changes. Many surgical/ invasive procedures are available to treat them, but they come with other side effects like excessive blood loss, haematuria and pain, to name a few. To address this, we screened out natural modifiers that come from plant sources and can target the epigenetics of this disease. For this, we initially created a library containing a large number of molecules retrieved from similarity searching. This library was then screened for molecules having drug-likeness and good pharmacokinetic properties with the least toxicity. These filters gave us five molecules, namely 4-Vinylguaiacol, anethole, isoeugenol, nadolol, and silibinin, which were used for molecular docking. Among these five molecules, Anethole, Isoeugenol and Silibinin were chosen for molecular dynamics based on binding energy. These three molecules were subsequently used for in-vitro assays containing crystallization assays, crystal-

kinetics, and enzymatic and non-enzymatic assays. Lastly, based on the in-vitro results, silibinin was chosen for our in-vivo studies. It was found that indeed silibinin has calculi-dissolving properties, which paves the pathway for future clinical trials.

Acknowledgement

अल्पश्रुतं श्रुतवतां परिहासधाम्। त्वद्भक्तिरेव मुखरीकुरुते बलान्माम् ॥

यत्कोकिलः किल मधौ मधुरं विरौति। तच्चारुचूत कलिकानिकरैकहेतु ॥६॥

-Bhaktamar Stotra, Shloka 6

(Just as the cuckoo sings inspired by the blooming mango blossoms, this work is a humble expression of the guidance and higher inspiration I have received)

First and foremost, I would like to express my deepest and most heartfelt gratitude to my **parents**. Their love has been my foundation, encouragement my wings, and sacrifices the silent pillars holding up every success I've achieved. From the very beginning, they have believed in my dreams even when they were nothing more than distant flickers and stood by me without ever expecting anything in return. They bore the financial, emotional, and physical weight of this journey with grace and without a single complaint, creating a haven of peace and assurance so I could pursue my academic goals freely. This degree is as much theirs as it is mine, for it was completed not by my efforts alone but by the steady, selfless love that they poured into every stage of my life.

I sincerely thank my supervisor, **Dr. Jeena Gupta,** for her continuous guidance, insightful feedback, and immense patience throughout this journey. Beyond her role as a mentor, she was a pillar of emotional strength and unwavering support during the most challenging times. Her understanding nature, timely encouragement, and empathy helped me push through moments of self-doubt and mental fatigue. I consider myself fortunate to have worked under someone who not only nurtured my academic growth but also stood beside me with kindness and genuine care.

My heartfelt thanks to my seniors, **Rupal Dubey** and **Kriti Kushwaha**, for their timely help, advice, and support at crucial stages of my research. I am also deeply grateful to my labmates and dear friends, **Debojyoti Mandal** and **Sourbh Suren Garg**, for their camaraderie, healthy competition, and constant motivation, which kept me striving for excellence.

I would also like to express my appreciation to the lab technicians **Rahul sir, Onkar sir, Sandeep sir, Sunny sir, Kuldeep sir, and Madan bhaiya** whose behind-the-scenes efforts in managing chemicals and glassware ensured the smooth progress of my experimental work. Your dedication did not go unnoticed.

I thank **Dr. Navneet Khurrana** for his timely assistance in obtaining the necessary approvals and facilitating the animal studies with great care and professionalism. I am grateful to **Dr. Hamdy Ghafar**, my international collaborator, for his enthusiastic participation and valuable contribution to the kinetic studies. Our collaboration not only enriched my research but also expanded its scope in ways I hadn't imagined.

A special note of thanks to my friend **Rudra Mishra** from VIT Vellore. Despite being miles away, he extended generous help in conducting the in-silico studies, for which I remain indebted. I would also like to acknowledge an anonymous external evaluator at the BITS Goa conference, whose critical yet constructive feedback on my poster presentation prompted me to revisit my in-silico work. That interaction led me down a new path of exploration and collaboration in simulation studies, proving to be a turning point in my research.

With a heavy heart, I also acknowledge the sacrifice of the tiny creatures used during my research. I deeply regret the necessity of their use and recognize that no words can truly compensate for their lives. Their contribution was significant in validating my hypothesis, and I carry that responsibility with humility and respect.

To my husband, **Ronak**, my unwavering lighthouse in the darkest of nights. When I had lost sight of myself, when I believed I had failed in my own eyes, it was your strength that held me upright. You reminded me of who I am and what I'm capable of, with words so simple yet filled with the power to revive. You are the quiet hero behind these pages, the calm in my chaos, and the reason I kept going.

Lastly, I owe everything to my family for being the unwavering backbone of support throughout this long journey. Their love, understanding, and faith in me kept me grounded and consistent. To all my friends who have been constant sources of motivation and joy, and to the countless others who supported me in ways big and small you may not all be named here, but your contributions are deeply appreciated and never forgotten.

TABLE OF CONTENT

S.No	Chapter Titles	Page No.
1	**Chapter 1: Introduction**	**1**
2	**Chapter 2: Review of Literature**	**5-27**
2.1	Epidemiology of Nephrolithiasis	5
2.2	Pathophysiology and Risk Factors	6
2.3	Classification of Kidney Stones	6-8
	2.3.1: Classification Based on Composition	7
	2.3.2: Classification Based on Size and Treatment Approach	8
2.4	Treatment Modalities for Urolithiasis	8
2.5	Common Renal Anomalies Affecting Stone Management	9
2.6	Minimally Invasive Endourological Procedures	10
2.7	Key Differences Between URSL and RIRS	11
2.8	Limitations & Complications of Current Treatments	12
2.9	Role of Randall's Plaques in Stone Formation	14
2.10	Role of Reactive Oxygen Species (ROS) in Cellular Function	14
2.11	Oxidative Stress and Inflammation Formation	15
2.12	Types of Antioxidants and Their Protective Effects	18-19
	2.12.1: Endogenous Antioxidants	18
	2.12.2: Dietary and Exogenous Antioxidants	19
2.13	Other Contributing Factors of Nephrolithiasis	24
2.14	Significance of Epigenetics in the Aetiology of Stones	24
2.15	Stone Types and Pathogenesis	26
3	**Chapter 3: Hypothesis**	**28-29**
4	**Chapter 4: Aims and objectives**	**30**
5	**Chapter 5: Materials and methods**	**31-58**
5.1	Chemicals Procurement	31
5.2	Review of Literature, Similarity Searching and Ligand Compilation	31
5.3	Level 1 Screening: Based on Lipinski's Rule of Five (RO5)	32
5.4	Level 2 Screening: Based on ADME Studies	32

5.5	Level 3 Screening: Toxicity Prediction, A Crucial Step in Drug Development	33
5.6	Identification of Common Gene Targets for Nephrolithiasis	33
5.7	Protein-Protein Interaction Network Analysis	33
5.8	Gene Ontology and KEGG Pathway Enrichment Analysis	34
5.9	Molecular Docking	34-35
	5.9.1 Application of standardized protocol in the present study	34
	5.9.2 Docking validation	35
5.10	Molecular Dynamics Simulation (MDS)	35
5.11	MM/PBSA-Trajectory Analysis	36
5.12	Principal Component Analysis and Free Energy Landscape	36
5.13	Crystallization Assays	36-38
	5.13.1: Nucleation Assay	37
	5.13.2: Aggregation Assay	37
	5.13.3: Oxalate Depletion Assay	38
5.14	Crystallization Kinetics	38-41
	5.14.1: Experimental Design	39
	5.14.2: Surface Energy Calculation (γ)	40
	5.14.3: Particle Size and Zeta Potential	40
	5.14.4: Fourier Transform Infrared Spectroscopy (FTIR)	40
	5.14.5: X-Ray Diffraction	41
	5.14.6: Field Emission Scanning Electron Microscopy (FESEM)	41
5.15	Non-Enzymatic Anti-Oxidant Assays	42-43
	5.15.1: DPPH Assay	42
	5.15.2: ABTS Radical Scavenging Activity Assay	43
	5.15.3: Ferric Reducing Antioxidant Power (FRAP) Assay	43
5.16	Antioxidant Assays - Enzymatic	44-48
	5.16.1: MTT Assay	45
	5.16.2: Establishment of In-Vitro Nephrolithiasis Model	45
	5.16.3: Cell Lysate Preparation	46
	5.16.4: Tissue Homogenate Preparation	46
	5.16.5: Protein Estimation	47

	5.16.6: Estimation of In-Vitro Oxidative Biomarkers	48
5.17	Histone Isolation Protocol	51-55
	5.17.1 Western Blotting Protocol	52
	5.17.2: Transfer Assembly	54
	5.17.3: Transfer Method	54
	5.17.4: Processing of Western Blot	54
	5.17.5: Detection and Analysis	55
5.18	Animal Studies	55-58
	5.18.1: Nephrolithiasis Induction	55
	5.18.2: Experimental Design	56
	5.18.3: Body Weight, Organ Weight, and Kidney Morphology Measurement	57
	5.18.4: Serum and Urine Biochemical Analysis	57
	5.18.5: Preparation of Kidney Homogenate	57
	5.18.6: Stone Markers Estimation	58
	5.18.7: Renal Histopathology	58
5.19	Statistical Analysis	58
6	**Chapter 6: Results**	**59-158**
6.1	Data Mining and Similarity Searching	59
6.2	Level 1 Screening: Based on Lipinski's Rule of Five (RO5)	75
6.3	Level 2 Screening: Based on ADME Studies	77
6.4	Level 3 Screening: Based on Toxicity	80
6.5	Core Hub Genes in Nephrolithiasis Treatment Identified Through Phytochemical Targeting	82
6.6	Gene ontology and pathway analysis	84
6.7	Disease-phytochemical-target-pathway network construction	85
6.8	Level 4 Screening: Using Molecular Docking	86
6.9	Molecular Dynamics (MD) Assessment	96-102
	6.9.1: Root Mean Square Deviation (RMSD)	96
	6.9.2: Root Mean Square Fluctuation (RMSF)	97
	6.9.3: Radius of Gyration (Rg)	98
	6.9.4: Solvent Accessible Surface Area (SASA)	99

	6.9.5: Hydrogen Bonding	100
	6.9.6: Distance Between Protein and Ligand	102
6.10	MM/PBSA Binding Energy Analysis	103
6.11	Residue decomposition	104
6.12	PCA and FEL analysis	106
6.13	Crystallization Assays	108-123
	6.13.1: Nucleation Assay	111
	6.13.2: Aggregation Assay	116
	6.13.3: Oxalate Depletion Assay	121
6.14	Crystallization Kinetics	124-135
	6.14.1: Effect of Phytochemicals on Induction Time	124
	6.14.2: Surface Energy Calculation (γ)	124
	6.14.3: Nucleation Rate (Js)	126
	6.14.4: Calculation of Free Energy Change (ΔGcr) and Critical Nucleus Radius (r)	127
	6.14.5: Fourier Transform Infrared Spectroscopy (FTIR)	129
	6.14.6: Particle Size and Zeta Potential Measurements	132
	6.14.7: X-Ray Diffraction	132
	6.14.8: Field Emission Scanning Electron Microscopy (FESEM)	133
6.15	Non-Enzymatic Anti-Oxidant Assays	136-138
	6.15.1: DPPH Assay	136
	6.15.2: ABTS Assay	137
	6.15.3: FRAP Assay	137
6.16	Enzymatic Anti-Oxidant Assays	139-144
	6.16.1: MTT Assay	142
	6.16.2: Lipid Peroxidation	140
	6.16.3: Superoxide Dismutase (SOD)	140
	6.16.4: Glutathione-S-Transferase (GST)	141
	6.16.5: Catalase	141
	6.16.6: Cell-Crystal Adhesion Assay	143
6.17	Western Blotting	145
6.18	Animal Studies	146-158

	6.18.1: Effect of Silibinin on Body Weight, Organ Coefficient, and Kidney Morphology	146
	6.18.2: Effect of Silibinin on Serum, Urine Analysis and Stone Markers	148
	6.18.3: Effect of Silibinin on Renal Oxidative Damage	150
	6.18.4: Effect of Silibinin on Kidney Histopathology	156
7	**Chapter 7: Discussion**	**159-166**
8	**Chapter 8: Conclusion**	**167-169**
	Bibliography	170
	Conferences and workshops	201-209

LIST OF TABLES

Table 2.1	**Common terminology used by nephrologists**	**12**
Table 2.2	Cellular and animal evidence on phytochemicals used for inhibition and management of KS	22
Table 2.3	Phytochemicals possessing epigenetic modifying potential	25
Table 5.1	Sites and servers used for in-silico studies	31
Table 5.2	Experimental procedure of calcium oxalate at various supersaturations ratios	39
Table 5.3	Sample preparation in lowry's protein estimation	48
Table 5.4	Division of animals into various groups	56
Table 6.1	Phytochemicals involved in treatment of KS along with their epigenetic activity.	60
Table 6.2	Similarity searching of Catechin	61
Table 6.3	Similarity searching of Diosmin	64
Table 6.4	Similarity searching of Epigallocatechin-3-gallate	69
Table 6.5	Similarity searching of Quercetin	70
Table 6.6	Similarity searching of Rutin	72
Table 6.7	Similarity searching of Resveratrol	74
Table 6.8	List of similar compounds derived from parental compounds, validating Lipinski's rule.	75
Table 6.9	Solubility, CYP inhibition and Bioavailability score of shortlisted compounds	77
Table 6.10	Toxicity prediction and analysis of shortlisted compounds using different signaling pathways.	80
Table 6.11	Binding energy and interacting residues after performing molecular docking of shortlisted phytochemicals. Bold residues indicate hydrogen bonding	88
Table 6.12	MM/PBSA results of the protein-ligand complex from 0.1ns to 20ns simulation. Energy (E) is represented in Kcal/mol	103
Table 6.13	Size and potential of calcium oxalate with and without phytochemicals	132
Table 6.14	Groups used in sEnzymatic Anti-Oxidant Assays	140

Table 6.15	Morphological characteristics of kidney and organ coefficient	147
Table 6.16	Stone parameters in various animal groups	150
Table 6.17	Histopathological changes in the experimental groups.	157

LIST OF FIGURES

S. No	Title of Figures	Page no.
Figure 2.1	Extracorporeal shock wave lithotripsy (ESWL) [Supine position]	11
Figure 2.2	Proposed mechanism of regulation of SIRT1 in nephrolithiasis	17
Figure 6.1	Catechin	61
Figure 6.2	Diosmin	63
Figure 6.3	Epigallocatechin-3-gallate	68
Figure 6.4	Quercetin	70
Figure 6.5	Rutin	71
Figure 6.6	Resveratrol	73
Figure 6.7	2D structure of shortlisted phytochemicals	81
Figure 6.8	Boiled egg representation of shortlisted phytochemicals	82
Figure 6.9	Venn diagram showing targets of phytochemicals and nephrolithiasis disease where the intersection represents the number of common targets between the two sets	83
Figure 6.10	Protein-protein network of common targets between phytochemicals and nephrolithiasis	83
Figure 6.11	Dot plot diagram of three gene ontology processes and KEGG pathway analysis	85
Figure 6.12	Disease-phytochemical-target-pathway network	85
Figure 6.13	Overlay diagram of co-crystallized ligand (green) with docked ligand (pink)	89
Figure 6.14	Docking of the SIRT1 protein (PDB ID:4ZZJ) with Co-crystallized ligand: 3D visualization in PyMol (top), 2D visualization in Discovery Studio (bottom left) and Ligplot (bottom right).	90
Figure 6.15	Docking of the SIRT1 protein (PDB ID:4ZZJ) with 4-Vinylguaicol: 3D visualization in PyMol (top), 2D visualization in Discovery Studio (bottom left) and Ligplot (bottom right).	91

Figure 6.16	Docking of the SIRT1 protein (PDB ID:4ZZJ) with Anethole: 3D visualization in PyMol (top), 2D visualization in Discovery Studio (bottom left) and Ligplot (bottom right).	92
Figure 6.17	Docking of the SIRT1 protein (PDB ID:4ZZJ) with Isoeugenol: 3D visualization in PyMol (top), 2D visualization in Discovery Studio (bottom left) and Ligplot (bottom right).	93
Figure 6.18	Docking of the SIRT1 protein (PDB ID:4ZZJ) with Nadolol: 3D visualization in PyMol (top), 2D visualization in Discovery Studio (bottom left) and Ligplot (bottom right).	94
Figure 6.19	Docking of the SIRT1 protein (PDB ID:4ZZJ) with Co-crystallized Silibinin : 3D visualization in PyMol (top), 2D visualization in Discovery Studio (bottom left) and Ligplot (bottom right).	95
Figure 6.20	RMSD of Silibinin, Isoeugenol and Anethole along with protein for 100ns	96
Figure 6.21	RMSF of Silibinin, Isoeugenol and Anethole along with protein.	98
Figure 6.22	Radius of gyration of Silibinin, Isoeugenol and Anethole along with protein for 100ns	98
Figure 6.23	SASA of Silibinin, Isoeugenol and Anethole along with protein for 100ns.	99
Figure 6.24	Hydrogen bond of Silibinin, Isoeugenol and Anethole with protein for 100ns	100
Figure 6.25	Hydrogen Bond Pairs of Silibinin, Isoeugenol and Anethole with protein for 100ns	101
Figure 6.26	Distance between of Silibinin, Isoeugenol and Anethole with protein for 100ns	102
Figure 6.27	MM/PBSA binding energy over 100ns	104
Figure 6.28	Residue contribution plot A) Silibinin B) Isoeugenol, and C) Anethole	106
Figure 6.29	PCA plot of phytochemicals along with protein	106

Figure 6.30	FEL plots of phytochemicals A) Silibinin B) Isoeugenol C) Anethole D) Protein	108
Figure 6.31	Nucleation assay of all compounds at various time span A) 20µM B) 40µM C) 60µM D) 80µM E) 100µM	111
Figure 6.32	Nucleation assay of all compounds at various concentrations at 0 minutes.	112
Figure 6.33	Microscopic images of nucleation assay at various concentrations (20-100µM) observed under 100X magnification.	114
Figure 6.34	Number of crystals present at each concentration after observing under microscope.	115
Figure 6.35	Aggregation assay of all compounds at various time span A) 20µM B) 40µM C) 60µM D) 80µM E) 100µM.	118
Figure 6.36	Aggregation assay of all compounds at various concentrations	119
Figure 6.37	Microscopic images of aggregation assay at various concentrations (20-100µM) observed under 100X magnification.	120
Figure 6.38	Number of aggregates present at each concentration after observing under microscope.	121
Figure 6.39	Microscopic images of oxalate depletion assay at various concentrations (20-100µM) observed under 100X magnification.	122
Figure 6.40	Oxalate Depletion assay of all compounds at various concentrations at 0 minutes.	123
Figure 6.41	Effect of Supersaturation ratio on induction time (s) with and without inhibitors.	124
Figure 6.42	Surface energy of calcium oxalate with and without phytochemicals	125
Figure 6.43	Nucleation rate (Js) of calcium oxalate with and without phytochemicals	126
Figure 6.44	Free energy change of calcium oxalate with and without phytochemicals	128

Figure 6.45	Critical radius of nucleus changes of calcium oxalate with and without phytochemicals.	129
Figure 6.46	FTIR spectrum of all the groups.	130
Figure 6.47	XRD spectrum of calcium oxalate with and without phytochemicals.	133
Figure 6.48	SEM images at lower supersaturation (0.72) of A) Control B) potassium citrate C) Anethole D) Isoeugenol E) Silibinin	135
Figure 6.49	SEM images at higher supersaturation (2.4) of A) Control B) potassium citrate C) Anethole D) Isoeugenol E) Silibinin	136
Figure 6.50	Antioxidant activities of phytochemicals at various concentrations, where AA= Ascorbic acid, SI= Silibinin, IS= Isoeugenol and AN= Anethole.	139
Figure 6.51	Cell line toxicity assay using NRK-52E cell line.	139
Figure 6.52	Effect of phytochemicals on enzymatic anti-oxidant assays A) Lipid Peroxidation B) Superoxide dismutase (SOD) C) Glutathione-S-Transferase (GST) D) Catalase	143
Figure 6.53	Microscopic images of NRK-52E cell lines infected with crystals developed from sodium oxalate (2mM) at 100X magnification	144
Figure 6.54	Effect of phytochemicals on crystal adhered kidney cells	146
Figure 6.55	Histone 3 acetylation levels as determined by western blot in NRK-52E cell line upon no treatment (C), treatment with sodium oxalate (SO), Potassium Citrate (PC), silibinin (SIL), isoeugenol (ISO), anethole (AN).	146
Figure 6.56	Change in body weight of the experimental groups during four weeks	147
Figure 6.57	Urine microscopy of experimental groups at 100X	149
Figure 6.58	Effects of silibinin on renal lipid peroxidation (LPO).	151
Figure 6.59	Effects of silibinin on renal superoxide dismutase (SOD	152
Figure 6.60	Effect of silibinin on renal catalase (CAT).	153
Figure 6.61	Effects of silibinin on renal Glutathione S-transferase (GST) activity	154
Figure 6.62	Effects of silibinin on renal reduced glutathione (GSH)	155

Figure 6.63	Renal histopathology of experimental groups.	157
Figure 6.64	Histopathological findings of the kidneys in experimental groups	158

Abbreviations

ADME	Absorption, Distribution, Metabolism, And Excretion
AN	Trans-Anethole
ANOVA	Analysis Of Variance
BBB	Blood-Brain Barrier
BSA	Bovine Serum Albumin
CDNB	1-Chloro-2,4-Dinitrobenzene
CKD	Chronic Kidney Disease
COD	Calcium Oxalate Dihydrate
COM	Calcium Oxalate Monohydrate
DM	Diabetes Mellitus
DMEM	Dulbecco's Modified Eagle Medium
DMSO	Dimethyl Sulfoxide
DPPH	1,1 Diphenyl-2-Picrylhydrazyl
ECL	Enhanced Chemiluminescence0p
EDTA	Ethylenediamine Tetraacetic Acid
ESRD	End-Stage Renal Disorder
ESRD	End-Stage Renal Disease
GFR	Glomerular Filtration Rate
GST	Glutathione S Transferase
HDAC	Histone Deacetylase
HRP	Horseradish Peroxidase
HSP	Heat Shock Protein
IFN	Interferon
IL	Interleukins
IS	ISOEUGENOL
JNK	Jun N-Terminal Kinase
LPO	Lipid Peroxidation
LSB	Low Salt Buffer
MAP3K	Mitogen-Activated Protein Kinase Kinase Kinase
MAPK	Microtubule-Associated Protein Kinase
MAPKK	Mitogen-Activated Protein Kinase Kinase
MBD	Metabolic Bone Disease

MCP	Monocyte Chemoattractant Protein
MDA	Malondialdehyde
MIRNA	Micro RNA
MTOR	Mammalian Target of Rapamycin
MTT	3-(4,5-Dimethylthiazol-2-Yl)-2,5-Diphenyltetrazolium Bromide
NADPH	Nicotinamide Adenine Dinucleotide Phosphate Hydrogen
NBT	Nitroblue Tetrazolium
NF-KB	Nuclear Factor Kb
PBS	Phosphate Buffer Saline
PMSF	Phenylmethylsulfonyl Fluoride
PTMS	Post-Translational Modifications
ROS	Reactive Oxygen Species
SDS	Sodium Dodecyl Sulfate
SGL	Sodium-Glucose Transporter
SI	SILIBININ
SIRT1	Sirtuin-1
SOD	Superoxide Dismutase
STZ	Streptozotocin
TBA	Thiobarbituric Acid
TEF	Transcription Enhancer Factor
TGF-B	Transforming Growth Factor-B
TNF-A	Tumor Necrosis Factor-Alpha
WHO	World Health Organization

CHAPTER 1

INTRODUCTION

Nearly 13% of the world's population and 10% of North America's population and 12% of the Indian population are affected by nephrolithiasis, a figure expected to rise in the coming decades, further increasing the global healthcare burden (Sorokin et al., 2017; Haley et al., 2017; Hill et al., 2022; Singh et al., 2023). Most kidney stones (approximately 80%) are composed of calcium, primarily calcium oxalate (Yu et al., 2021). The rest include 10% struvite, 9% uric acid, and 1% cysteine (Evan, 2010; Petrović et al., 2021). The aetiology of kidney stones involves a complex interplay of dietary, genetic, and epigenetic factors (Shadman et al., 2017; Barghouthy et al., 2021). Kidney stones can impair renal function, cause hydronephrosis, and inflame renal tubular cells, ultimately leading to chronic kidney disease and significantly diminishing the quality of life (Sigurjonsdottir et al., 2015; Raja et al., 2020). Several factors contribute to the development of kidney stones, including geography, ethnicity, gender, and genetics. Conditions like hypertension, diabetes, and gout also raise the risk. In developed countries, high protein and salt intake contribute to stones, while in developing nations, malnutrition and limited water access are issues (Geraghty et al., 2023; Stamatelou and Goldfarb, 2023). Kidney stones are linked to other health problems, such as bone fractures and chronic kidney disease, and can contribute to cardiovascular diseases and metabolic syndrome (Taylor et al., 2016; Rule et al., 2010; Rule et al., 2009; Ferraro et al., 2013).

We always nucleate calcium oxalate crystals in the kidney because of the saturation of urine from calcium and oxalate, but it doesn't get noticed because the size of these crystals is <2µm. Since the kidney filters approximately 180 liters of blood/day, leading to the production of 1-2 liters of urine, calcium oxalate crystals need to grow more than 2µm in less than 10 minutes, which is tough to achieve normally. But when this happens, a single crystal grows to form stone via the Ostwald ripening mechanism. This stone is too large to pass through nephrons without affecting epithelial cells (Abdel-Aal EA et al., 2009; Daosukho, 2007).

Supersaturated solutions have molecular aggregations due to which crystallization takes place and when it achieves the size of the critical radius, the formation of nuclei takes place. This entire process is called nucleation. Nucleation is measured by induction time which is the time frame between the achievement of supersaturated solution and the appearance of first nuclei (Ilevbare et al., 2012), which later forms macroscopic crystals and is referred to as crystal growth. The crystallization of a molecule aids in better drug delivery formulation that could

either target nucleation or crystal growth or both (Chavan et al., 2016; Oucherif et al., 2013). Many techniques are available to study nucleation and crystal growth such as measuring turbidity, conductivity, focused beam reflectance measurement, bulk video imaging, etc. (Simon et al., 2009), but in this paper, we have used UV-visible spectroscopy as mentioned by Rathi et al., 2020, this technique minimises the lag time, quick and easy to measure induction time. Also, we used deionized water as the solution because simulated gastric fluid or buffer solution gives inconsistent results and also overestimates the supersaturation stability (Bevernage et al., 2010; Bevernage et al., 2013).

During normal cellular metabolism, hydrogen peroxide (H_2O_2)—like other reactive oxygen species (ROS)—is produced at low levels. However, excessive accumulation leads to cellular and extracellular matrix damage. Due to its small size and unequal charge distribution, H_2O_2 easily enters cells and interacts with metal ions (such as iron and copper), generating highly reactive radicals. These radicals damage cellular lipids, proteins, and nucleic acids, contributing to the pathogenesis of various diseases, including connective tissue disorders, cancer, and skin aging (Valko et al., 2007; Barja, 2004; Aruoma, 1998; Galicka et al., 2014). Thus, effective treatment strategies are needed to counteract ROS-related damage. When dissolved minerals start getting deposited in the kidney, it forms kidney stones which mainly get excreted through the urethra. Treatment of kidney stones was $2.1 billion in the year 2000 and is expected to double in the United States by the year 2030 (Antonelli et al., 2014). Risk factors of nephrolithiasis include diabetes, dyslipidemia, hypertension, obesity, and metabolic syndrome (Taylor et al., 2005; Johri et al., 2010; Kohjimoto et al., 2013). High levels of oxalate lead to increased oxidative damage, which is a key factor in kidney stone formation. The process involves several stages: crystal initiation, growth, aggregation, and eventual trapping in kidney tissues and tubules. This begins when there is an imbalance between substances (crystal inhibitors and crystal initiators already present in urine) that inhibit and promote crystal formation (Khan, 2013; Moe, 2006; Zhai et al., 2013).

While surgical treatments like percutaneous nephrolithotomy (PCNL) and lithotripsy can be effective, they often come with complications, such as kidney damage, high stone recurrence rates, reduced kidney function, and high costs (Butterweck and Khan, 2009). Despite advancements in minimally invasive technologies, stone recurrence remains a significant challenge, with rates as high as 50% after the first surgery (Spivacow et al., 2016; Chmiel et al., 2023). The global prevalence of kidney stones (KS) has risen significantly in recent years, creating substantial challenges for healthcare systems and impacting patient well-being (Scales

et al., 2012; Sorokin et al., 2017). This growing burden is further intensified by the recurrent nature of KS, increasing the demand for effective preventive strategies (Khan et al., 2016; Peerapen & Thongboonkerd, 2023). Additionally, the rising prevalence of metabolic disorders, such as obesity and diabetes, has further contributed to the increasing incidence of kidney stones, making it a significant global metabolic health concern (Kittanamongkolchai et al., 2018; Wong et al., 2016; Moftakhar et al., 2022).

Preventive and treatment strategies for kidney stones include increasing fluid intake, using thiazide diuretics, potassium citrate, and allopurinol, depending on the type and size of the stones (Mayans, 2019). Increasing health consciousness has led to higher consumption of fruits, vegetables, and supplements to address nutritional deficiencies (D'Angelo et al., 2019). There is also growing interest in dietary and herbal remedies (Kizivat et al., 2017). Polyphenols have demonstrated potential anti-stone effects in lab studies, suggesting they could be useful in treating kidney stones (Yasir et al., 2018; Dinnimath et al., 2017). Dietary factors play a crucial role in the development of kidney stones. Low water intake, reduced consumption of dairy products and tea, and high intake of salt, oxalate-rich foods, and processed foods have been associated with an increased risk of nephrolithiasis (Bhattacharya et al., 2022; Dahl et al., 2022). Other dietary contributors include excessive consumption of cakes, soft drinks, and biscuits, along with insufficient intake of nuts, seeds, vegetables, coffee, and alcoholic beverages, particularly wine (Ahmed et al., 2023; Siener, 2021). Moreover, there is rise in global surface temperature of earth due to climate change, which also increased the risk of kidney stone formation (Maline et al., 2024). In contrast to modern dietary patterns, traditional herbal medicine has long been recognized for its potential in preventing and treating nephrolithiasis. Diets rich in fruits, vegetables, and spices, as well as the use of herbal remedies, have shown promise in reducing kidney stone formation (Vanitha & Vyshnavi, 2020; Nirumand et al., 2018; Yadav et al., 2021). Recently, computational tools have gained prominence for their effective approach in designing and discovering new medicines for various diseases. Among these methods, molecular docking stands out as a cost-effective and time-saving approach with significant biological and pharmacological potential (Rampogu et al., 2018; Berg EL, 2014). Complementary techniques, such as pharmacophore modelling and network pharmacology, are often used in conjunction with molecular docking. However, conventional molecular docking typically targets only a single protein at a time. Plant-derived drugs leveraging in silico methods have shown promise against diseases such as COVID-19 (Souid et al., 2022; Devi et al., 2021), microbial infections (Nischitha et al., 2022), diabetes

(Noor et al., 2022), and cancer (Opo et al., 2021). Phytochemicals derived from these natural sources exhibit strong antioxidant and anti-inflammatory properties, drawing attention from pharmaceutical and biotechnological communities for their therapeutic potential. Notably, catechin, diosmin, epigallocatechin-3-gallate, quercetin, rutin, and resveratrol have demonstrated anti-calculi activity. These phytochemicals were chosen based on a literature survey we did to find the most potent phytochemicals at the time of performing this experiment.

Due to the limited treatment available to treat nephrolithiasis in most of the world, herbal medicine holds great interest as an alternative therapy (Khan et al., 2021; Kasote et al., 2017), since it limits stone recurrence with lesser side effects (Zeng et al., 2019) and less cost (Gilani, 2005). Recent research has highlighted the role of SIRT1 (Sirtuin 1), an NAD+-dependent histone deacetylase, in regulating oxidative stress and inflammation, both key factors in kidney stone formation. SIRT1 helps mitigate renal fibrosis and cellular injury by upregulating antioxidant pathways and deacetylating key proteins involved in apoptosis (Chang & Guarente, 2014; Ren et al., 2017; Zhang et al., 2017; Liu et al., 2018; Giannakou & Partridge, 2004). Its ability to regulate oxidative stress and inhibit cell injury (Ye et al., 2021) makes it a promising therapeutic target for nephrolithiasis.

CHAPTER 2

REVIEW OF LITERATURE

2.1 Epidemiology of Nephrolithiasis

Nephrolithiasis, or the formation of stones in the urinary system, is an escalating global health concern. It includes kidney stones (nephrolithiasis) and stones located elsewhere in the urinary tract (urolithiasis). The incidence has risen sharply across Asia, with reports indicating increases from 4.0% to 6.4% in China, 4.3% to 9.0% in Japan, 3.5% to 11.5% in South Korea, 1.4% to 16.9% in Thailand, and a prevalence of approximately 12% in India (Sorokin et al., 2017; Gamage et al., 2020; Liu et al., 2018; Singh et al., 2023).

In India alone, kidney stone disease affects nearly 2 million individuals annually, with the northwestern regions showing the highest prevalence. Based on reported incidence, the country has been divided into two major "stone belt" zones. The first belt spans North India, extending from Jammu & Kashmir through Punjab, Haryana, and Delhi to Uttar Pradesh. The second belt begins in Gujarat and ends in Jabalpur, Madhya Pradesh (Lohiya et al., 2017; Kakkar and Kakkar, 2021).

Several factors contribute to this region-specific growing burden, including environmental exposures, dietary habits, and genetic predisposition. High ambient temperatures, inadequate hydration, dependence on mineral-rich groundwater, and frequent consumption of oxalate- and calcium-rich foods, particularly those that are spicy or heavily processed, are key contributors to stone formation. These region-specific risk factors should be carefully considered when developing preventive and therapeutic strategies for managing urolithiasis in the Indian population (López and Hoppe, 2010; Sequira et al., 2023). While many cases remain asymptomatic, complications such as severe pain, recurrent infections, urinary obstruction, and renal impairment have become increasingly common. Alarmingly, more than 50% of patients experience a recurrence within five years, leading to a higher risk of chronic kidney disease (CKD), metabolic bone disease (MBD), and end-stage renal disease (ESRD) if left untreated (Khan et al., 2016). KS formation is a major cause of morbidity leading to chronic renal disease and, in some cases, loss of kidney function too (Alexander et al., 2012; El-Zoghby ZM et al., 2012). This metabolic disease is common in both developed and developing nations. The occurrence of KS varies with gender and race (Curhan, 2007). KS is more common in men than in women (Romero et al., 2010), and over 2-3% of stone formation also takes place in

children (Schwarz and Dwyer, 2006). In men, the peak age of KS formation is 30 years, while in women it is 35 and 55 years (Parmar, 2004).

2.2 Pathophysiology and Risk Factors

The management of kidney stones largely depends on their size, composition, and location. Stones smaller than 5 mm often pass spontaneously with minimal complications, while larger stones (≥10 mm) typically require intervention (Nephrolithiasis, 2016). Complex cases, such as staghorn calculi and anomalous kidney stones, present significant surgical challenges and frequently necessitate a combination of treatment modalities. According to the European Association of Urology (EAU) and American Urological Association (AUA) guidelines, surgical removal is recommended for symptomatic stones larger than 15 mm or in cases of urinary obstruction, recurrent infections, haematuria, or severe pain (Türk et al., 2011; Assimos et al., 2016). However, the optimal treatment strategy depends on multiple factors, including the stone's characteristics, the patient's health status, and available surgical expertise.

Given the high recurrence rates and potential complications associated with kidney stones, researchers continue to explore more effective and minimally invasive treatment options. Conventional methods such as extracorporeal shock wave lithotripsy (ESWL), ureteroscopy (URSL), and percutaneous nephrolithotomy (PCNL) have been refined with technological advancements, improving stone-free rates (SFR) and reducing postoperative complications. Additionally, emerging techniques like high-frequency laser lithotripsy (dusting, pop-dusting), miniaturized PCNL (mini-PCNL, microperc, super-mini PCNL), and combination approaches (ECIRS, hybrid laser techniques) have demonstrated promising outcomes in recent studies (Worcester et al., 2003; Sepe et al., 2006).

2.3 Classification of Kidney Stones

Among the various types of kidney stones, calcium oxalate (CaOx) stones account for 70–80% of cases, followed by uric acid, struvite, and cystine stones (Asplin, 2002). The formation of kidney stones is a complex and multifactorial process influenced by metabolic, dietary, genetic, and environmental factors. Increasing evidence suggests that nephrolithiasis is not just a localized urinary disorder but may be a systemic condition with underlying pathophysiological mechanisms resembling vascular calcification and bone mineralization (Worcester et al., 2003; Jungers et al., 2004). Hydroxyapatite deposits, commonly found in both atherosclerotic plaques and Randall's plaques, play a critical role in stone formation. Randall's plaques, composed

primarily of calcium phosphate (CaP), are located in the subepithelial regions of renal papillae and serve as a nucleation site for calcium oxalate crystallization (Gao et al., 2007; Icer & Gezmen-Karadag, 2018; Gao et al., 2010; Sepe et al., 2006). Several proteins, including matrix Gla protein (MGP) and osteopontin, have been identified as key regulators of these calcifications, making them potential therapeutic targets in stone prevention (Icer & Gezmen-Karadag, 2018; Gao et al., 2010).

Kidney stones can be classified based on their chemical composition and size, both of which are crucial in determining the most effective treatment approach.

2.3.1 Classification Based on Composition

KS is majorly composed of either calcium oxalate (CaOx) or calcium phosphate (CaP) in addition to magnesium ammonium phosphate (struvite) or uric acid stones (Sakhaee et al., 2012), and rare cases involve L-cystine, ammonium urate, or drug-induced xenostones (Poloni et al., 2016; Coe et al., 2005). These high variations of stone compositions among the affected population result in the need for personalized therapeutic management, which comprises a combination of dietary regulation, use of supplements/drugs, or surgical procedures to remove KS (Moe, 2005). The use of any therapeutic strategy is also based on the location, where the stone is actually located. This also helps in therapeutic preparation and extent upto which a surgery is required.

The chemical composition of kidney stones varies depending on metabolic factors, dietary habits, genetic predisposition, and underlying medical conditions. The four major types include:

- **Calcium Oxalate Stones** are the most prevalent type, accounting for the majority of kidney stone cases. These stones form due to high oxalate intake, low urine volume, and metabolic imbalances. Factors such as dehydration, high sodium consumption, and excessive intake of oxalate-rich foods (e.g., spinach, nuts, and chocolate) contribute to their formation (Sowers et al., 1998).
- **Uric Acid Stones:** These stones develop when urine becomes excessively acidic, leading to the crystallization of uric acid. Individuals with gout, metabolic syndrome, diabetes, or a high-protein diet are at greater risk. Unlike calcium-based stones, uric acid stones are often radiolucent and may be dissolved using alkalization therapy (Wiederkehr & Moe, 2011).

- **Struvite Stones:** Also known as infection stones, these are composed of magnesium ammonium phosphate and typically form in response to chronic urinary tract infections (UTIs) caused by urease-producing bacteria. These stones can grow rapidly and form staghorn calculi, which may require surgical removal due to their size and complexity (Stroup & Auge, 2010).
- **Cystine Stones:** Cystine stones are a rarer form of kidney stones resulting from a genetic disorder called cystinuria, which leads to excessive excretion of cystine in the urine. These stones tend to recur frequently and are often resistant to standard treatments, necessitating long-term medical management and hydration therapy to prevent formation (Edvardsson et al., 2013).

2.3.2 Classification Based on Size and Treatment Approach

The size of a kidney stone significantly impacts its likelihood of spontaneous passage and dictates the appropriate treatment method (Vijayakumar et al., 2018):

- **Small Stones (<5 mm):** These stones are typically small enough to pass through the urinary tract without intervention. Patients are often advised to increase fluid intake and may be prescribed pain relievers or alpha-blockers to facilitate passage.
- **Medium Stones (5–10 mm):** Stones of this size may not always pass naturally and may require medical intervention. Treatments such as extracorporeal shock wave lithotripsy (ESWL) or medication-assisted stone expulsion (using citrate or alkalization therapy) may be recommended.
- **Large Stones (>10 mm):** Larger stones usually require surgical removal, as they pose a higher risk of urinary obstruction, infections, and kidney damage. Common surgical interventions include ureteroscopy with laser lithotripsy (URSL), percutaneous nephrolithotomy (PCNL), and, in complex cases, a combination of procedures.

Classifying kidney stones based on composition and size is essential for determining the most effective treatment strategy. While small stones may pass naturally, larger or more complex stones often require intervention to prevent complications and improve patient outcomes.

2.4 Treatment Modalities for Urolithiasis

Multiple factors, including the stone's size, location, composition, and clinical symptoms, determine the management of urolithiasis. While small stones (<5 mm) often pass

spontaneously with adequate hydration and medical support, larger stones (>10 mm) or those causing complications such as pain, infection, or urinary obstruction typically require intervention. The treatment choice aims to maximize stone clearance, prevent recurrence, and minimize complications, hospitalization time, and invasiveness (Gottlieb et al., 2018).

Endourology and laser technology advancements have significantly improved the effectiveness of minimally invasive approaches, reducing the need for open surgeries. Treatment modalities are broadly categorized into non-invasive and minimally invasive techniques. Non-invasive treatments, such as extracorporeal shock wave lithotripsy (ESWL), are preferred for smaller stones likely to pass naturally (McClinton et al., 2020). Minimally invasive procedures, including ureteroscopy with laser lithotripsy (URSL/RIRS) and percutaneous nephrolithotomy (PCNL), are good options for larger, more complex stones or those resistant to ESWL. In some cases, hybrid and combination therapies improve stone-free rates (SFR) and reduce complications (Sani et al., 2025).

Each treatment method has its indications, benefits, and limitations, and the decision is often made based on patient-specific factors such as anatomical variations, kidney function, stone burden, and associated comorbidities.

2.5 Common Renal Anomalies Affecting Stone Management

Common renal anomalies affecting stone management include:

- **Horseshoe Kidney:** In this condition, the two kidneys are fused at the lower poles, altering their normal orientation and making percutaneous access more challenging. Modified PCNL access techniques and fluoroscopic guidance are often required (Abed et al., 2012).
- **Ectopic Kidney:** When the kidney is located outside its normal position, such as in the pelvis, standard PCNL or ureteroscopy may not be feasible. In such cases, laparoscopic or robotic-assisted stone removal may be necessary (Goel et al., 2006).
- **Malrotated Kidney:** Due to abnormal rotation, the pelvicalyceal system is misaligned, making retrograde ureteroscopy and standard PCNL difficult. These cases require customized percutaneous access planning based on preoperative imaging (Binbay et al., 2011).

For patients with renal anomalies, robotic-assisted PCNL and ureteroscopy are emerging as promising minimally invasive alternatives, offering better precision, improved instrument control, and reduced complication rates.

2.6 Minimally Invasive Endourological Procedures

Minimally invasive endourological procedures provide more effective and targeted treatment options for kidney stones that are too large (>10 mm), too dense, or resistant to ESWL. These approaches allow for direct visualisation, fragmentation, and removal of stones while minimising trauma to surrounding kidney and ureteral tissues. Over the past two decades, advancements in endoscopic technology, laser lithotripsy, and miniaturised surgical instruments have significantly improved stone-free rates (SFR), reduced complications, and accelerated patient recovery (He et al., 2024).

Unlike extracorporeal shock wave lithotripsy (ESWL), which relies on externally generated shock waves to fragment stones, endourological procedures involve directly inserting an endoscope into the urinary tract to access the stone. This ensures higher precision, real-time visualisation, and improved stone clearance, especially for stones that are dense, impacted, or located in difficult anatomical positions (Malinaric et al., 2023). This method is most effective for stones smaller than 20 mm. It is particularly recommended for those in the renal pelvis or upper ureter, where gravity and urine flow assist in stone clearance (Figure 2.1).

The two primary minimally invasive procedures for stone treatment are ureteroscopic lithotripsy (URSL) and retrograde intrarenal surgery (RIRS). Both utilise laser lithotripsy to break down stones into smaller fragments that can either be removed or naturally passed in the urine (Jain et al., 2021).

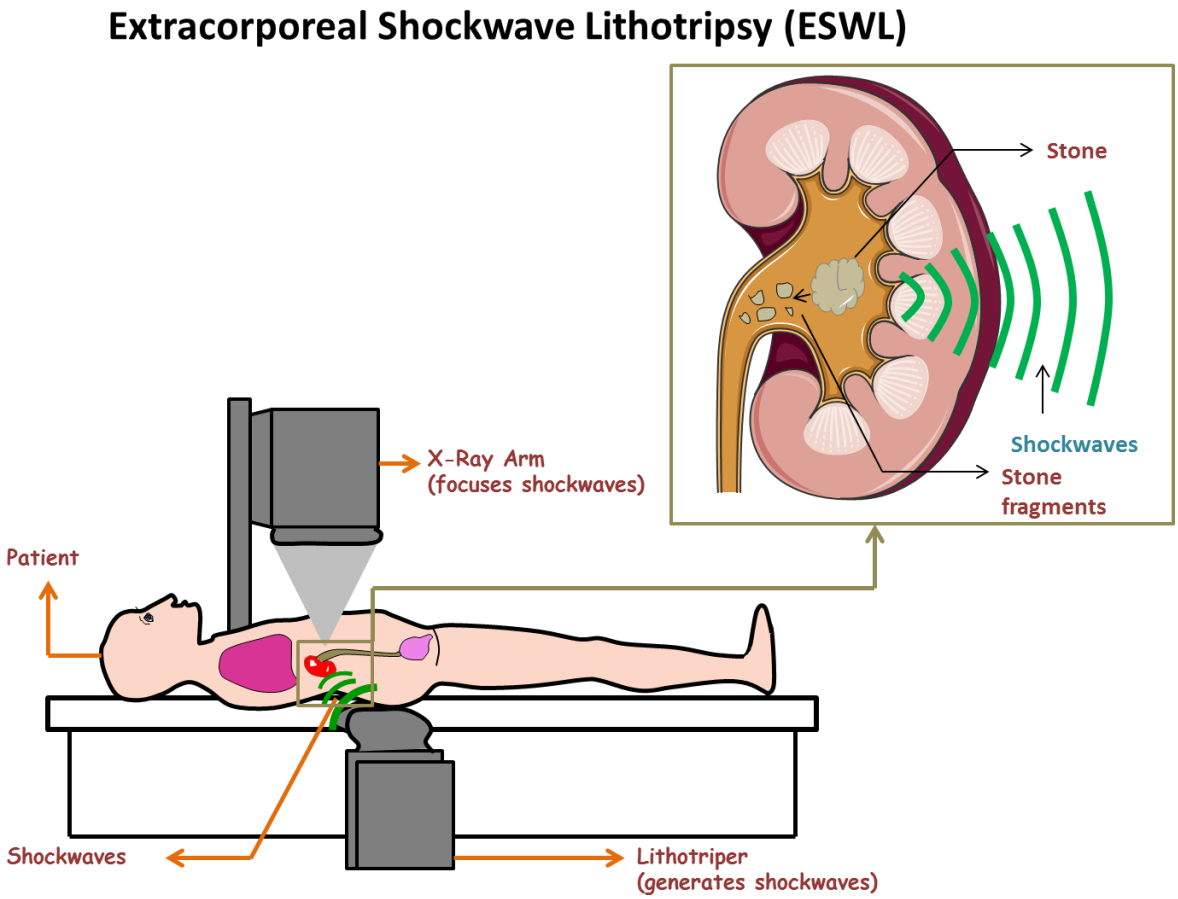

Figure 2.1: Extracorporeal shock wave lithotripsy (ESWL) [Supine position]

2.7 Key Differences Between URSL and RIRS

- **URSL (Ureteroscopic Lithotripsy)** is primarily used for ureteral stones and involves the use of a semi-rigid ureteroscope, which provides better stability and control during the procedure. This approach is especially effective for stones lodged in the distal, mid, or proximal ureter (El-Abd et al., 2022).
- **RIRS (Retrograde Intrarenal Surgery)** is used to treat kidney stones and requires a flexible ureteroscope designed to navigate the intricate structure of the renal collecting system. This flexibility allows access to challenging locations, such as the lower calyx, where stones may be difficult to reach with conventional rigid instruments (Gauhar et al., 2023).

Once the stone is located, a fiber-optic laser probe is passed through the working channel of the ureteroscope to perform laser lithotripsy (Alexander et al., 2015). The most commonly used laser technology is the Holmium:YAG laser, which emits pulsed energy selectively absorbed

by water molecules and biological tissues, ensuring precise stone fragmentation with minimal damage to surrounding structures (Lambert et al., 2011).

2.8 Limitations & Complications of Current Treatments

Despite significant advancements in kidney stone treatment, each modality comes with inherent limitations and potential complications that can impact treatment success and patient recovery. The choice of intervention depends on various factors, including stone size, location, composition, and the patient's overall health. However, even the most effective treatments are not without risks. The three most widely used techniques—extracorporeal shock wave lithotripsy (ESWL), percutaneous nephrolithotomy (PCNL), and laser lithotripsy (used in ureteroscopic lithotripsy (URSL) and retrograde intrarenal surgery (RIRS))—each have specific drawbacks that must be carefully considered. The selection of the appropriate treatment requires a balanced approach, considering both efficacy and potential adverse effects (Kim et al., 2020; Sani et al., 2025).

Extracorporeal shock wave lithotripsy (ESWL) remains a preferred non-invasive option for small-to-moderate kidney stones. However, its success largely depends on stone composition, size, and location. Hard stones, such as cystine and calcium oxalate monohydrate, tend to resist fragmentation, often necessitating multiple sessions or alternative treatments (Skolarikos et al., 2006). Additionally, ESWL is less effective for lower calyx stones due to gravitational challenges that hinder fragment clearance. Another major limitation of ESWL is its unpredictability in fragmenting stones into passable sizes, often resulting in the accumulation of stone debris in the urine.

Nephrolithiasis results in severe pain on the sides of the abdomen, resulting in the presence of blood in the urine. Often the terminologies for kidney stones like cystinuria, hypercalciuria, hyperuricosuria, hypocitraturia or oxaluria are unanimously used but they all possess different meanings. Hence to clarify these common terminologies related to KS they are summarized in Table 2.1.

Table 2.1 Common terminology used by nephrologists

Medical terms	**Meaning**	**Causes**	**Occurrence**
Cystinuria	Cysteine rich urine	Mutation in SLC3A1 and SLC7A9	1-2 % adults & 6-8% children

Hypercalciuria	Calcium rich urine	Excess vitamin D intake, sarcoidosis, Cushing's syndrome, glucocorticoid use, cancer, hyperthyroidism, Paget's disease, or renal tubular acidosis	5-10 %
Hyperuricosuria	Excessive amounts of uric acid in the urine (800mg/day in men and 750mg/day in women)	Excessive dietary intake of purine-rich foods	
Hypocitraturia	Less than 320 mg/day urinary citrate excretion	Distal renal tubular acidosis (type 1), bowel dysfunction, hypokalemia, and a high-protein, low-alkali diet.	20% - 60% of stone former
Primary hyper-oxaluria type 1, 2 and 3	Accumulation of oxalate along with calcium in kidney and bladder	Mutation in AGXT, GRHPR and HOGA1 respectively	Rare
Renal tubular acidosis (Type 1-distal)	Unable to excrete acid into urine leading to highly acidic blood or impaired renal hydrogen ion excretion	Autoimmune disease Sjögren syndrome or Rheumatoid arthritis, Nephrocalcinosis, Kidney transplantation, Chronic obstructive uropathy drugs (mainly amphotericin B, ifosfamide, and lithium), Cirrhosis, Sickle cell anemia, medullary sponge kidney	Rare
Renal tubular acidosis (Type 2-proximal)	Impaired bicarbonate resorption	Fanconi syndrome, Light chain nephropathy due to multiple myeloma, drugs (mainly acetazolamide, sulfonamides, ifosfamide, outdated tetracycline, or streptozocin)	Very rare

Renal tubular acidosis (Type 3)	Combination of type 1 and type 2	--	Very rare
Renal tubular acidosis (Type 4-generalized)	Abnormal aldosterone production or response	diabetic nephropathy, HIV/AIDS, amyloidosis, Addison's disease, urinary tract obstruction, sickle cell disease, lupus, removal or destruction of both adrenal glands, and kidney transplant rejection.	Most common among renal tubular acidosis

2.9 Role of Randall's Plaques in Stone Formation

The formation of kidney stones is driven by intricate processes, including the accumulation of immune cells, collagen fibers, and interstitial cells, all of which are influenced by calcification triggered by inflammation and oxidative stress (Peerapen and Thongboonkerd, 2023). Crystal-cell adhesion can lead to mitochondrial dysfunction, oxidative stress activation, and apoptosis. Altered adhesion in renal tubular epithelial cells contributes to phenotypic changes in nephrocalcinosis. Osteopontin (OPN), matrix GLA protein (MGP), and the CLDN14 gene play key roles in kidney stone formation by influencing calcification and epithelial permeability (Lai et al., 2022). In the interstitial pathway, calcium phosphate (CaP) crystals initially deposit along the basement membrane of Henle's loop, eventually forming inflammatory plaques. These plaques can subsequently erode into the urinary collecting system, facilitating CaOx crystallisation (Tamborino et al., 2024; Ushimoto et al., 2023). This progression underscores the impact of inflammation and oxidative stress on kidney stone formation and related renal dysfunction (Sun et al., 2020; Liu et al., 2019; Knauf et al., 2013).

Oxidative stress plays a key role in kidney stone formation, and antioxidants may help in prevention and treatment. Studies suggest that vitamin E, N-acetylcysteine, and green tea can reduce crystal buildup, support kidney function, and enhance antioxidant enzyme activity, making them potential therapeutic options for urolithiasis (Huang et al.,2006; Thamilselvan and Menon, 2005). Jeong et al. reported that green tea supplementation enhanced the activity of antioxidant enzymes (SOD, CAT, GSH), which helped reduce crystal deposition (Jeong et al., 2006).

2.10 Role of Reactive Oxygen Species (ROS) in Cellular Function

The term ROS refers to free radicals (atoms and molecules with unpaired electrons) as well as their metabolites. It includes free radicals and their byproducts, such as superoxide anion, nitric oxide, hydroxyl radical, and hydrogen peroxide (Khan, 2013). Under normal conditions, enzymes regulate ROS levels, allowing them to participate in cellular signaling and regulatory functions. Antioxidants like superoxide dismutase (SOD), catalase (CAT), and glutathione (GSH) help neutralize excess ROS (Sies et al., 2022; Roy et al., 2023). However, excessive ROS production and reduced antioxidant capacity can lead to oxidative stress (OS), contributing to inflammation and cellular damage (Manea, 2010; Ray et al., 2012).

Oxalate-driven reactive oxygen species (ROS) contribute to calcium oxalate (CaOx) kidney stone formation by impairing monocyte and macrophage function. Exposure to oxalate triggers oxidative stress, disrupts mitochondrial activity, and lowers IL-10 levels, weakening immune defenses and facilitating crystal formation. Treatment with MitoQ and IL-10 helps counteract these effects, highlighting ROS as a potential target for preventing CaOx stones (Kumar et al., 2023).

Inhibitors of crystallization such as citrate, magnesium, uromoduline, pyrophosphate and promoters of crystallization such as oxalate, calcium, phosphate, urate, cysteine in the urine urine, exceeding supersaturation with consecutive aggregation, nucleation, and stone growth at Randall's plaque leads to the formation of kidney stone (Halbritter, 2021). Other than abnormal metabolism of minerals inflammation, oxidative stress and irregular crystallization inhibition also allows deposition of CaP in the interstitial tissue of the renal papilla or renal tubules or vessels (Taylor and Stoller, 2015). With the aggregation and calcification of plaques, oxidative and inflammatory reactions subsequently promote the further formation of stones (Khan, 2014).

2.11 Oxidative Stress and Inflammation Formation

Crystal-cell adhesion generates reactive oxygen species, which in turn secretes massive inflammatory cytokines and inflammatory cascade in renal tubular epithelial cells, which gets activated, resulting in intrarenal inflammation and injury to renal tubular epithelial cells (RTECs) (Narula et al., 2016). It is also reported that Nod-like receptor protein 3 (NLRP3) inflammasome facilitates this renal inflammation (Mulay et al., 2012). This cytoplasmic protein complex (NLRP3 inflammasome) activates caspase-1, causing the maturation of interleukin (IL)-1β and IL-18 and then induces pyroptosis which is a proinflammatory form of cell death (He et al., 2016), which also leads to kidney disease progression.

Class of small (18–25 nt in length) endogenous noncoding RNAs also called as microRNAs (miRNAs) controls gene expression at the posttranscriptional level (Lan et al., 2017). Some of them has been identified to have differential expression profiles in CaOx crystal-induced renal tubular epithelial cells by renal tubular epithelial cells (Wang et al., 2014). Epithelioid morphology of RTECs is supported by miR-141-3p, which also represses renal interstitial fibrosis (Zhang et al., 2020). One study reported that overexpression of miR-141-3p alleviated CaOx crystal-induced renal tubular epithelial cells injury by affecting NLRP3-mediated pyroptosis, (Gan et al., 2022). When RTECs were exposed to CaOx in invitro (HK-2) cell lines, this induces apoptosis by increasing the altered gene expression via the p38 mitogen-activated protein kinase pathway (Alelign and Petros, 2018) . CaOx also induces oxidative stress by increasing the contents of LDH and MDA but reducing the content of SOD, thus leading to RTEC injury in HK-2 cells (Khan, 2013; Gan et al., 2022) .To Another study reported that elevated oxalate levels in HK-2 cells leads to increased transcriptional activation of IL-2R beta mRNA, which drives to IL-2R beta protein levels at high levels, resulting into the cellular changes like induction of inflammation (Koul et al., 2014).

Sirt3 plays a crucial role in reducing reactive oxygen species (ROS) and maintaining mitochondrial function, which is essential in preventing oxidative damage and inflammation in kidney stone formation (Xi et al., 2019). Oxalate disrupts mitochondrial function in monocytes, leading to oxidative stress and inflammatory responses (Patel et al., 2018). Overexpression of Sirt3 activates the NRF2/HO-1 signaling pathway, reducing apoptosis and calcium oxalate (CaOx) crystal adhesion to renal tubular cells (Xi et al., 2019; Xu et al., 2023). These findings highlight the significance of targeting mitochondrial dysfunction to mitigate inflammation and kidney stone development. SIRT1 represses the NOTCH signaling pathway and promotes macrophage polarization towards the M2 phenotype, thereby reducing CaOx crystal deposition, apoptosis, and kidney damage (Song et al., 2023). It also protects the kidney against crystal formation and associated inflammation by inhibiting TLR4 signaling and limiting M1 macrophage polarization. This suppression reduces oxidative injury (ROS) and mitochondrial damage in tubular epithelial cells under both in-vitro and in-vivo conditions (Duan et al., 2023). Similarly, FKBP5 deficiency has been shown to attenuate calcium oxalate stone formation by inhibiting NF-κB signaling, thereby reducing cell–crystal adhesion, apoptosis, and pro-inflammatory M1 macrophage polarization (Song et al., 2023).. Furthermore, SIRT1 expression was found to be downregulated in nephrolithiasis patients,

animal models, and cell cultures (Ye et al., 2021), highlighting its potential as a promising therapeutic target for nephrolithiasis. A possible mechanism is shown in Figure 2.2.

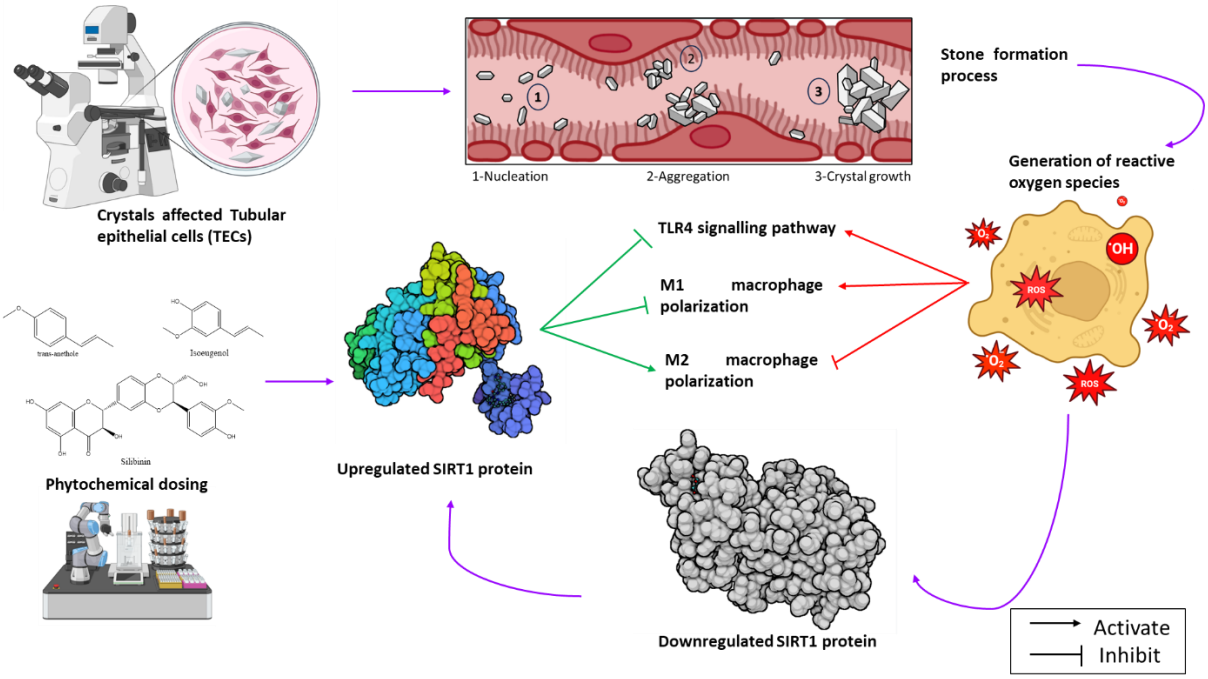

Figure 2.2: Proposed mechanism of regulation of SIRT1 in nephrolithiasis

Kidney stone formation occurs primarily via two distinct mechanisms: the intratubular pathway and the interstitial (Randall's plaque) pathway. The intratubular pathway involves supersaturation of urine, followed by nucleation, growth, and aggregation of crystals within renal tubules. These crystals adhere to the renal tubular epithelial cells, causing cellular injury and triggering downstream pathological responses such as oxidative stress and apoptosis. This epithelial damage leads to altered expression of key adhesion molecules, including cadherin 4 (CDH4), which facilitates stronger binding of crystals to the tubular surface and contributes to local inflammation and tissue remodeling (Taguchi et al., 2015; Thongboonkerd, 2019).

Additionally, crystal-cell adhesion has been linked to mitochondrial dysfunction, enhanced reactive oxygen species (ROS) production, and the progression of nephrocalcinosis, during which epithelial cells may undergo phenotypic changes. Important regulators such as osteopontin (OPN) and matrix Gla protein (MGP) have been implicated in modulating crystal adhesion and inflammation. Moreover, the CLDN14 gene, which controls paracellular ion permeability through epithelial tight junctions, has been significantly associated with increased susceptibility to nephrolithiasis (Lai et al., 2022).

In the interstitial pathway, stone formation is initiated by the deposition of calcium phosphate (CaP) crystals, particularly hydroxyapatite, at the basement membrane of Henle's loop. Over time, this leads to the development of inflammatory plaques, which can penetrate the urinary collecting system and act as niduses for calcium oxalate (CaOx) crystal deposition when exposed to urine (Tamborino et al., 2024; Ushimoto et al., 2023). The formation and progression of these plaques are closely linked to chronic inflammation and oxidative stress, both of which contribute to renal damage and functional decline (Sun et al., 2020).

A thorough understanding of these molecular and cellular mechanisms is essential for the identification of novel therapeutic targets aimed at interrupting early events in crystal adhesion, oxidative injury, and inflammatory responses, thereby improving treatment strategies for kidney stone disease.

2.12 Types of Antioxidants and Their Protective Effects

2.12.1 Endogenous Antioxidants

Reactive oxygen species (ROS) formed by calcium oxalate deposition can be prevented or reduced by endogenous antioxidants such as superoxide dismutase (SOD), CAT, and glutathione peroxidase (GSH-Px) (Khan, 2005; Ozturk et al., 2019).

Superoxide Dismutase (SOD): Superoxide dismutase (SOD) plays a vital role in preventing kidney stone formation by counteracting reactive oxygen species (ROS) and minimizing oxidative stress. A decline in SOD function can elevate ROS levels, triggering calcium oxalate monohydrate (COM)-related oxidative damage and inflammation, which facilitate stone development. Tsujihata et al. reported that atorvastatin (ATO) boosts SOD function, presenting a potential strategy for kidney stone prevention (Kang et al., 2020; Tsujihata et al., 2008; Tsujihata et al., 2011). Furthermore, ursolic acid (UA), a pentacyclic triterpene known for its anti-inflammatory effects has been found to restore Nrf2/HO-1 protein and SOD activity, helping to alleviate oxidative injury and inflammation linked to stone formation (Liu, 1995; Jia et al., 2021).

Glutathione (GSH): Song and group studied ferroptosis induced by oxalate in HK-2 cells and found that significant reduction in glutathione (GSH) levels and increased malondialdehyde (MDA) in oxalate-treated cells indicate that oxalate disrupts GSH metabolism, leading to oxidative stress and lipid peroxidation (Song et al., 2021). Since GSH, catalyzed by GPX4, plays a key role in detoxifying lipid peroxides, its depletion may contribute to oxidative damage

and ferroptosis (Lu et al., 2018). This disruption in redox balance can promote renal tubular injury and inflammation, creating a favorable environment for calcium oxalate crystal formation and kidney stone development. Therefore, maintaining GSH homeostasis may be crucial in preventing oxalate-induced oxidative stress and kidney stone formation (Lu et al., 2018; Song et al., 2021).

2.12.2 Dietary and Exogenous Antioxidants

Vitamin C: Vitamin C acts as a powerful antioxidant, but excessive intake can raise oxalate levels, increasing the risk of calcium oxalate kidney stones (Ferraro et al., 2016; Knight et al., 2016). Formation of kidney stone is inversely related to vitamin c intake (Liu et al., 2023). While the FDA recommends 90 mg daily for adults, higher doses, such as 162.8 mg, may help lower serum uric acid (Bae et al., 2014). Balanced intake is essential to gain benefits while minimizing kidney stone risk.

Vitamin E: Vitamin E helps prevent kidney stones by reducing crystal-induced renal damage through its antioxidant and anti-inflammatory effects. It improves urinary biochemistry and regulates crystal-inhibiting proteins. When combined with polyacrylic acid, it enhances stone prevention by inhibiting both crystal aggregation and renal injury, making it a potential therapy for nephrolithiasis and reducing stone recurrence (Sridharan et al., 2022).

Catechins: Catechin plays a crucial role in kidney stone prevention by enhancing mitochondrial function, lowering oxidative stress, and suppressing apoptosis-related gene activity. Research also indicates its effectiveness in restoring antioxidant defenses and inhibiting crystal formation in vivo. Furthermore, catechin reduces melamine-induced crystal accumulation by modulating oxidative stress, apoptosis, and key signaling pathways, highlighting its potential as a therapeutic agent against kidney stones (Zhai et al., 2013).

Apigenin: Azimi et al. reported that apigenin strongly reduces crystal deposition in urolithiatic rats by inhibiting the TGF-β pathway while exhibiting significant antioxidant properties (Azimi et al., 2021). Similarly, researchers found that vitexin, an apigenin 8-C-glucoside, prevents pyroptosis, blocks the epithelial–mesenchymal transition in renal tubular epithelial cells, and limits macrophage infiltration, effectively reducing crystal accumulation and oxidative stress-induced kidney injury (Ding et al., 2021).

Quercetin: Quercetin plays a significant role in nephrolithiasis prevention through its antioxidant and protective effects on renal cells. Park et al. identified quercetin's ability to

inhibit lipid peroxidation while enhancing superoxide dismutase (SOD) and catalase (CAT) activity, helping to mitigate oxidative stress in urolithiasis (Park et al., 2008). Additionally, Guzel et al. demonstrated that quercetin may suppress oxidative damage by inhibiting the p38-MAPK pathway (Guzel et al., 2021). Another protective mechanism involves quercetin's ability to reinforce the epithelial barrier, reducing the reabsorption of sodium, calcium, and water, which in turn decreases the likelihood of kidney stone formation (Gamero-Estevez et al., 2019).

A derivative of quercetin, hyperoside (quercetin 3-O-galactoside), has also shown protective effects against oxalate-induced oxidative stress in HK-2 cells by activating the Nrf2/HO-1/NQO1 pathway (86). Zhu et al. further explored the combined effects of quercetin and hyperoside in urolithiatic rats and found a significant reduction in crystal deposition (87). Furthermore, Yuan et al. investigated the androgen receptor (AR)/NOX2 pathway, revealing that kaempferol, a compound structurally related to quercetin, alleviated calcium oxalate (CaOx) crystal-induced oxidative stress and crystal accumulation by suppressing AR/NOX2 signaling. This study also showed a dose-dependent decrease in renal CaOx crystal deposition with increasing kaempferol concentration (Chen et al., 2018).

These findings highlight quercetin and its derivatives as potential therapeutic agents for preventing kidney stone formation by reducing oxidative stress, maintaining epithelial integrity, and modulating key signaling pathways involved in nephrolithiasis.

Epigallocatechin gallate (EGCG): a key compound in green tea, has shown potential in protecting against nephrolithiasis by reducing oxidative stress and preventing crystal attachment to kidney cells. Jeong et al. observed that EGCG lowers reactive oxygen species (ROS) production in NRK-52E cells exposed to oxalate, thereby minimizing oxidative damage (Jeong et al., 2006). Kanlaya et al. further demonstrated that EGCG decreases the expression of alpha-enolase, a protein that facilitates calcium oxalate (CaOx) crystal adhesion to renal tubular cells. This reduction leads to a decline in crystal binding and subsequent deposition (Kanlaya et al., 2016). Additionally, EGCG helps preserve the structural integrity of renal tubular cells by preventing microvillar damage induced by calcium oxalate monohydrate (COM) crystals. This protective effect is achieved by suppressing oxidized protein expression, which is associated with cellular damage in kidney stone formation (Fong-ngern et al., 2017).

These studies highlight EGCG's role in nephrolithiasis prevention by alleviating oxidative stress, limiting crystal adherence, and safeguarding kidney cells, suggesting its potential as a therapeutic agent for kidney stone management.

Resveratrol: a polyphenolic stilbene with strong antioxidant properties, plays a protective role in nephrolithiasis by reducing oxidative stress, inflammation, and crystal deposition. Hong et al. found that resveratrol downregulates NADPH oxidase subunits, MCP-1, OPN, TGF-β1, TGFR-I/II, and hyaluronan in oxalate-treated renal epithelial cells, preventing stone formation (Hong et al., 2013). Oksay et al. suggested its involvement in the p38-MAPK and NF-κB pathways in rat models (Oksay et al., 2017). Additionally, Wu et al. demonstrated that resveratrol enhances TFEB expression in NRK-52E cells, promoting autophagy and further reducing oxidative stress and crystal accumulation (Wu et al., 2021). These findings suggest resveratrol as a promising therapeutic agent for kidney stone prevention.

Vitamin D: It regulates calcium absorption and excretion, impacting kidney stone formation. Both excessive and insufficient intake can increase the risk, with its active form, 1,25-dihydroxyvitamin D, strongly linked to stone development. Personalized medical guidance is essential to balance supplementation and prevent kidney stones (Zhang et al., 2024).

Diosmin: Diosmin, a natural bioflavonoid commonly found in citrus fruits, plays a protective role against nephrolithiasis by regulating calcium oxalate (CaOx) crystal formation and deposition. Research indicates that diosmin helps prevent CaOx accumulation in the kidneys of ethylene glycol-induced nephrolithiatic rats while also reducing degenerative alterations in the renal cortex and medulla (Noorafshan et al., 2013). Furthermore, in vitro studies suggest that diosmin exhibits a dual modulatory effect during crystallization, increasing the number and mass of CaOx crystals while simultaneously decreasing their size and growth. Additionally, diosmin enhances CaOx self-aggregation and extracellular matrix invasion but suppresses CaOx–cell interactions, emphasizing its potential in kidney stone prevention (Khamchun et al., 2021).

Rutin: Rutin and curcumin help prevent calcium oxalate urolithiasis, likely by reducing urinary levels of stone-forming components while also exhibiting anti-inflammatory and antioxidant properties (Ghodasara et al., 2010). The surface area is increased by rutin-based nanorods through the transformation of calcium oxalate from its monohydrated to dihydrate form. Osteopontin expression in MDCK cells is regulated, proinflammatory signaling in human

leukemia monocytic macrophages is suppressed, and cell viability is restored (Saha and Mishra, 2022). All the properties of these phytochemicals are summarized in Table 2.2

Table 2.2. Cellular and animal evidence on phytochemicals used for inhibition and management of KS

Photochemical	In Vitro/In Vivo	Model	Result	Reference
Catechin	In vivo	Ethylene glycol (EG) induced nephrolithiasis in rat	(i) OPN, (d) MDA, 8-OhdG (d)Renal calcium crystallization	Wang et al., 2023
	In vivo	co-exposure to melamine (MEL) and cyanuric acid (CYA) in rats	(d) crystal deposition and pathological damage	Wang et al., 2023
Diosmin	In vivo	EG-induced nephrolithiasis in rat	(d) Capillary hyper-permeability (d) Degeneration of glomeruli and tubules, Restoring the diameter of the capillaries and vessels in the cortex	Noorafshan et al., 2013
	In vitro	Calcium oxalate monohydrate (COM)-induced in MDCK	(d) crystal cell adhesion induces crystal internalization	Khamchun et al., 2021
	In vitro	COM-induced Madin–Darby canine kidney (MDCK) cells	(d) α-enolase protein expression (d) crystal-binding capability	Kanlaya et al., 2024
Epigallocatechin-3-gallate	In vitro	COM-induced Madin–Darby	(d) HSP90 surface expression (d) crystal aggregation and crystal-cell adhesion	Kanlaya et al., 2024
	In vivo	Oxalate-induced renal stone in rats	(d) Excretion of urinary oxalate (d) Activities of urinary gammaglutamyl transpeptidase and N-acetylglucosaminidase	Cupisti et al., 2023
	In vivo	Sodium oxalate + gentamicin	(d) urinary stone formation (i) antioxidative action	Li et al., 2024

Quercetin	In vivo	EG-induced nephrolithiasis in rat	(d) Urinary crystal deposit formation (i) urine volume	Nagula et al., 2023
	In vivo	EG-induced nephrolithiasis in rat	(d) Oxidative damage (i) Serum paraoxonase 1 (PON1)	Amengual-Cladera et al., 2011
	In vivo	EG-induced nephrolithiasis in rat	Prevention of stone formation Inhibition of calcium oxalate urolithiasis	Ghodasara et al., 2010
	In vivo	EG-induced nephrolithiasis in rat	(d) Malondialdehyde levels (d) p38 MAPK expression	Guzel et al., 2021
Rutin	In silico	Docking against glycolate oxidase and lactate dehydrogenase	High binding affinity towards the target proteins	Mohamed et al., 2024
	In-vitro	COM-induced Madin–Darby canine kidney (MDCK) cells	restored cell viability (d) oxidative stress	Saha and Mishra, 2022
	In vivo	EG-induced nephrolithiasis in rat	(d) calcifications and (i) tissue viability	Saha and Mishra, 2022
Resveratrol	In vitro	COM-induced Madin–Darby canine kidney (MDCK) cells	(d) crystal cell adhesion induces crystal internalization (d) crystal growth	Peerapen et al., 2024
	In vivo	glyoxylic acid monohydrate-induced rats	(d) CaOx crystal deposition (d) oxidative stress	Wu et al., 2021
	In vitro	Oxalate induced in NRK-52E	(d) cell damage (d) oxidant species overexpression	Wu et al., 2021

Here (i) demonstrates increasing trend; (d) demonstrates decreasing trend.

Kidney stone formation is a complex process influenced by oxidative stress, inflammation, and metabolic imbalances. Various antioxidants, including endogenous enzymes (SOD, CAT, GSH) and dietary compounds (vitamins C, E, quercetin, resveratrol, EGCG), play crucial roles in reducing oxidative damage and preventing crystal accumulation. Targeting mitochondrial dysfunction and inflammatory pathways may offer promising therapeutic strategies. A

balanced intake of antioxidants, along with personalized medical approaches, can help mitigate the risk and recurrence of kidney stones.

2.13 Other contributing factors of nephrolithiasis

Despite advancements in KS treatment, its high prevalence and recurrence remain major health and socioeconomic concerns (Shoag et al., 2015). Contributing factors include obesity, with studies indicating a correlation between KS incidence and BMI (Body Mass Index) and waist circumference, particularly in women (Taylor et al., 2005). Hypertension is another associated factor, especially in women (Gillen et al., 2005). Both environmental and genetic factors play crucial roles in KS development. Although monogenic diseases such as cystinuria, Dent's disease, and primary hyperoxaluria contribute to stone formation, the role of inheritance in idiopathic stone formation remains unclear (Coe et al., 2005). KS also exhibits a familial tendency, with environmental factors influencing disease expression (Goldfarb et al., 2005). Dehydration due to inadequate fluid intake is the most common environmental risk factor, along with dietary factors such as excessive sodium and animal protein consumption (Sayer, 2017). In some cases, KS can result from insoluble drugs or their metabolites, leading to iatrogenic stones (Tattevin et al., 2013). The prevalence of KS is rising in many Asian countries (Liu et al., 2018), further emphasizing the need for novel therapeutic strategies (Morgan and Pearle, 2016). Current KS management includes increased fluid intake and pharmaceutical interventions to dissolve stones, though these treatments have limitations (Assadi and Moghtaderi, 2017).

2.14 Significance of Epigenetics in the Aetiology of Stones

Recent research highlights the significance of gene expression modifications in disease mechanisms. Epigenetics, which refers to heritable changes in gene expression without altering DNA sequences, plays a vital role in gene regulation and disease development. Factors influencing epigenetic modifications include environmental influences such as lifestyle, diet, and social status (Moore, 2017). Epigenetic mechanisms significantly impact phenotypic outcomes, cellular maintenance, and disease progression, including cancer (Bonini and Berger, 2017). Epigenetics also serves as a link between various biological domains across different time scales (Nicoglou and Merlin, 2017). Bioinformatics approaches, such as identifying high-density CpG islands, enable the measurement of epigenetic changes (Bakulski & Fallin, 2014). Over the past decade, phytochemicals have garnered attention as effective, safe, and low-cost bioactive compounds for various treatments targeting their epigenetic modification potential as

shown in Table 2.3. Dietary polyphenols, derived from plants, are the most abundant antioxidants in human diets, with over 8,000 structural variants found in fruits and vegetables (Han et al., 2007).

Table 2.3: Phytochemicals possessing epigenetic modifying potential

Phytochemical	Model organism	Effectiveness	Epigenetic targets	Reference
Resveratrol	*Toxoplasma gondii*	(d) H3 and H4K16 acetylation (i) H2A.X phosphorylation	alteres transcription levels, induces DNA damage,	Contreras et al., 2021
	MDA-MB-231 and BT-549-Luc TNBC cells	(i) histone acetylation of CDH1 and CDKN1A	represses the metastatic capacity via up-regulation of *CDH1* and *CDKN1A*	Sakamoto et al., 2023
Catechin	Nalm6 cell line	(d) DNA methyltransferases (DNMT1 and DNMT3B)	Induces apoptosis via epigenetic mechanisms	Afgar et al., 2024
	HT29 cell line	DNA methylation of *SRXN1* promoter region	Protecting cells against reductive stress	Jakubek et al., 2023
Epigallocatechin -3-gallate (EGCG)	*Staphylococcus aureus*	Alters orfx-mediated ribosomal methylation	Antimicrobial treatment and drug resistance	Zeferino et al., 2022
	FaDu and SCC-1 cells	(d) DNA methylation (d) DNMT activity	reactivate epigenetically silenced tumor suppressors	Agarwal et al., 2023
	Chondrocyte cell C28/I2.	RAGE (receptor of advanced glycation end products) promoter hypermethylation	Protective effects on chondrocytes against Osteoarthritis	Wu et al., 2023
Rutin	Db/db mice	(d) HDAC1 (d) PI3K / AKT/ mTOR phosphorylation	Restores autophagy by HDAC1 inhibition	Dong et al., 2023
	Sprague–Dawley rats	(i) PI3K, p-AKT, and p-GSK-3β phosphorylation	Neuroprotective effect against brain damage	Thabet et al., 2018

Here (i) demonstrates increasing trend; (d) demonstrates decreasing trend.

Given the importance of epigenetics in gene regulation, this study aims to identify natural molecules targeting epigenetic pathways against nephrolithiasis. In-silico studies offer a cost-effective and efficient method to screen large numbers of molecules against specific targets, reducing the time and resources required for laboratory and clinical trials. Structural similarity searching helps detect remote homology and predict compound functionality based on known molecules. Molecular dynamics simulations aid in identifying significant amino acid stability changes (Lu et al., 2016), while molecular docking studies have become a crucial tool in drug discovery due to their rapid results, low costs, and the availability of free tools (Morris et al., 1998). Our objective is to perform in-silico structural similarity searches to identify potential epigenetic modifiers for KS, followed by in-vitro and in-vivo validation of their efficacy.

2.15 Stone Types and Pathogenesis

KS formation occurs in four major steps:

1. **Crystal Nucleation** – The initial stage of the crystallization process is characterized by the formation of distinct crystal nuclei. This phenomenon of aggregation is considered homogeneous when occurring within the bulk of the solution and heterogeneous when taking place on extremely small solid particles, such as amorphous clusters or crystalline particles.
2. **Aggregation** – Clusters of crystals, when they stick together in the form of aggregates.
3. **Growth** – When these aggregates start growing in size and volume.
4. **Retention** – when the crystal grows large enough to obstruct the pathway of urine passage. Stones remain within the kidney or urinary tract, leading to symptoms Epigenetic or molecular modifiers could play a key role in disrupting these processes, potentially reducing KS formation.

In summary, KS remains a significant global health concern, necessitating innovative approaches for prevention and treatment. Epigenetic studies and computational drug discovery hold promise in identifying novel therapeutic targets, offering hope for more effective management of nephrolithiasis.

Based on the data given in Tables 2.2 and 2.3, we have targeted a few phytochemicals and screened them for KS and its epigenetic modifications. Furthermore, structural similarity

searching helped us in identifying new phytochemicals with unexplored activity against KS, which may lead towards progressive research. Also, the relationship between phytochemicals and their epigenetic modification ability will open the door towards epigenome modifying drugs, a field which has started growing recently.

CHAPTER 3

HYPOTHESIS

Nephrolithiasis, commonly known as kidney stone disease, is a significant global health issue affecting nearly 12% of the population. Among kidney stones, calcium oxalate (CaOx) is the most prevalent, accounting for approximately 75% of cases. Despite advancements in medical and surgical treatments, recurrence remains a persistent challenge, emphasizing the need for alternative therapeutic approaches. Current treatment options, such as surgical removal, pharmacological interventions, and dietary modifications, often fail to prevent stone recurrence, highlighting the urgency for safer and more effective solutions. Emerging research suggests that oxidative stress, inflammation, and metabolic imbalances play a crucial role in kidney stone pathogenesis. The process of stone formation involves several stages, including urinary supersaturation with stone-forming ions, nucleation, crystal growth, aggregation, and retention within renal tubules. Hyperoxaluria, a key risk factor for kidney stone formation, triggers excessive reactive oxygen species (ROS) production, leading to oxidative damage, mitochondrial dysfunction, and inflammation in renal epithelial cells. These factors create a favorable environment for CaOx crystallization, further exacerbating renal injury. Given the complexity of nephrolithiasis, an effective treatment strategy should target multiple pathways simultaneously.

Natural phytochemicals have gained considerable attention as potential therapeutic agents due to their antioxidant, anti-inflammatory, and epigenetic-modulating properties. These bioactive compounds, derived from plants, have demonstrated promising results in preventing stone formation by inhibiting oxidative stress, modulating inflammation, and interfering with calcium oxalate crystallization. Furthermore, plant-derived molecules have been recognized for their role in epigenetic regulation, which may help reverse pathological changes associated with nephrolithiasis and metabolic disorders. Numerous plant extracts have demonstrated promising anti-lithiatic properties in traditional and experimental medicine; however, the majority of such studies focus on crude extracts rather than isolating and characterizing specific phytochemicals. This lack of molecular resolution makes it difficult to pinpoint the exact compound responsible for the observed therapeutic effects.While polyphenol-rich extracts have been tested for their antioxidant potential in nephrolithiasis, very few studies have systematically evaluated purified, well-characterized molecules for their anti-crystallization properties.

This study aims to explore the therapeutic potential of phytochemicals in preventing nephrolithiasis using a multidisciplinary approach encompassing in-silico, in-vitro, and in-vivo analyses. Computational screening techniques will be employed to identify phytochemicals with structural similarities to known anti-nephrolithiatic compounds, based on the hypothesis that similar molecular structures exhibit comparable biological activities. The identified candidates will be further assessed for their efficacy in inhibiting calcium oxalate crystallization, reducing oxidative stress, and modulating inflammatory pathways through laboratory and animal model studies. By integrating computational modeling, biochemical validation, and physiological assessments, this research seeks to provide a strong foundation for the development of plant-based nephrolithiasis therapies. The findings may lead to the identification of safer, more effective alternatives to existing treatments, minimizing the risk of recurrence and associated complications. Additionally, the insights gained from this study could open new avenues for clinical trials, evaluating the potential of phytochemicals in nephrolithiasis management. The broader implications of this research extend beyond kidney stone disease, offering a framework for investigating plant-derived bioactive compounds in various metabolic and inflammatory disorders.

CHAPTER 4

AIMS AND OBJECTIVES

Aims

Synthetic drugs are used to treat nephrolithiasis or kidney stones (KS), but they are loaded with side effects. So, we need to look for alternatives with no side effects. We seek to identify such naturally occurring epigenetic modifiers that are structurally related to the already present medicines, then test their binding affinity and molecular interaction with SIRT-1 in silico, investigate them in reducing oxidative stress and the associated epigenetic changes, and further validate our findings with the help of in vitro (cell culture) as well as in vivo (SD rats) models. The following objectives were created to accomplish the study's goals listed below.

Objectives

1. In-silico studies, including structural similarity searching and molecular docking of known epigenetic modifiers to screen promising novel natural molecules that can prove protective against KS

2. To establish a successful in vitro and in vivo model of nephrolithiasis associated with various types of stones and evaluate the beneficial effects of potential natural molecules.

3. To evaluate the histone acetylation modifying potential of selected bioactive components and study epigenetics mechanism.

CHAPTER 5
MATERIALS AND METHODS

5.1 Chemicals procurement

Silibinin, Isoeugenol, and trans-Anethole were procured from Sigma, while potassium citrate and sodium oxalate were obtained from SRL, ethylene glycol and ammonium chloride from Loba Chemie, Calcium and magnesium testing kits were sourced from TRUEchemie, India. All other reagents for enzymatic assays were of analytical grade unless stated otherwise. Calcium chloride dihydrate ($CaCl_2 \cdot 2H_2O$) and sodium oxalate ($Na_2C_2O_4$) used as reactants were analytically pure and obtained from Loba Chemie. Anethole (trans), Isoeugenol, and Silibinin were purchased from Sigma-Aldrich (Gillingham, UK) and Potassium citrate was purchased from SRL, India, which also contained 0.01% oxalate. All other chemicals used were of analytical grade unless otherwise specified. The NRK-52E cell line was procured from NCCS, Pune, India.

5.2 Review of Literature, Similarity searching and ligand compilation

Table 5.1: Sites and servers used for in-silico studies

Software name	**Purpose**	**Website**
DrugBank	Similarity searching and 2D/3D structure	https://go.drugbank.com/
mCule	Druglikeliness	https://mcule.com/apps/property-calculator/
SwissADME	ADME studies	http://www.swissadme.ch/index.php
ProTox-II	Toxicity	https://tox-new.charite.de/protox_II/index.php?site=compound_search_similarity
AutoDock Vina	Molecular Docking	https://vina.scripps.edu/
UCSF Chimera	3D Visualization	https://www.cgl.ucsf.edu/chimera/
Discovery Studio	2D Visualization	https://discover.3ds.com/discovery-studio-visualizer-download
LigPlot+	2D Visualization	https://www.ebi.ac.uk/thornton-srv/software/LigPlus/install.html
CHARMM-GUI	Input file generation	https://www.charmm-gui.org/

GROMACS	Molecular dynamics (MDS)	https://www.gromacs.org/
MM-PBSA	Post MDS	https://valdes-tresanco-ms.github.io/gmx_MMPBSA/dev/

In chemical databases, similarity searching identifies molecules structurally similar to a user-defined reference structure, evaluated through quantitative measures of intermolecular similarity. In this study, "similarity searching" was performed using the said tab in DrugBank database (https://go.drugbank.com/), a comprehensive, freely accessible online resource providing detailed information on drugs and their targets (Wishart et al., 2018). The similarity threshold was set at 0.6, ensuring a significant resemblance to the reference structures. The threshold value was selected based on previous reports (Muñoz et al., 2017). Ligands structurally similar to six shortlisted phytochemicals (identified through literature review) were retrieved in SMILES format for subsequent analyses. The database was accessed in September 2024 to ensure the inclusion of the most up-to-date information. Similarity searching was also employed in our previous papers (Shafi et al., 2024; Kushwaha et al., 2024)

5.3 Level 1 screening: Based on Lipinski's rule of five (RO5)

To evaluate drug-likeness, all ligands were initially screened for violations of Lipinski's rule of five (RO5). According to RO5, an orally active drug should meet the following criteria: a) Fewer than 5 hydrogen bond donors, b) Fewer than 10 hydrogen bond acceptors, c) molecular weight of less than 500 Da, d) logP (octanol-water partition coefficient) value of less than 5, and e) No more than one violation of the above parameters. Ligands were analyzed for RO5 compliance using the mCule property calculator tool (https://mcule.com/apps/property-calculator/), ensuring only those adhering to these criteria were shortlisted for further studies.

5.4 Level 2 Screening: Based on ADME studies

ADME, which stands for absorption, distribution, metabolism, excretion, and toxicity, is critical for understanding the pharmacokinetics of a drug molecule. Poor ADME profiles are a significant cause of attrition in drug discovery projects (Daina and Zoete, 2016). Consequently, assessing these properties before synthesis and in vivo studies is crucial for the success of drug candidates.

Traditionally, ADME profiling involves extensive experimental procedures, which are both time-consuming and costly (Yadav and Mohite, 2020). To address these challenges, in silico ADME studies have emerged as an efficient alternative. In this study, we utilized SwissADME (http://www.swissadme.ch/index.php) to evaluate various pharmacokinetic and safety parameters of the shortlisted compounds. The parameters analysed included water solubility, CYP2C19 inhibition, CYP2C9 inhibition, CYP2D6 inhibition, bioavailability score, and alerts from PAINS (Pan Assay Interference Structures) and BRENK.

5.5 Level 3 Screening: Toxicity Prediction, A Crucial Step in Drug Development

Complications in the drug discovery process often necessitate comprehensive toxicity studies to ensure the safety and viability of potential drug candidates. These studies assess whether compounds exhibit harmful effects such as hepatotoxicity, mutagenicity, cytotoxicity, or interference with critical signalling pathways, including nuclear receptor and stress response pathways. In this study, we employed the ProTox-II server (https://tox-new.charite.de/protox_II/index.php?site=compound_search_similarity) for in silico toxicity prediction. This tool offers a reliable and efficient method to evaluate potential toxicological risks associated with the ligands under investigation (Banerjee et al., 2018).

5.6 Identification of Common Gene Targets for Nephrolithiasis

To determine gene targets associated with nephrolithiasis, we used the GeneCards database (https://www.genecards.org/) with the keywords “nephrolithiasis” and “kidney stones” (Stelzer et al., 2016). This comprehensive database provided a list of genes implicated in the disease. Phytochemicals shortlisted after rigorous screenings were uploaded to the Swiss Target Prediction server (http://swisstargetprediction.ch/) to predict their potential biological targets (Daina et al., 2019). The targets identified for each phytochemical were merged, and duplicates were removed to compile a list of unique targets. To identify overlapping targets between the phytochemicals and nephrolithiasis-associated genes, we used Venny 2.1, a powerful tool for comparing datasets (Oliveros JC and Venny, 2007). This analysis enabled the identification of common targets, offering insights into the molecular interactions and pathways that these phytochemicals may modulate in the context of nephrolithiasis.

5.7 Protein-Protein Interaction Network Analysis

The common targets between nephrolithiasis-associated genes and phytochemicals were uploaded to the STRING database (https://string-db.org) with *Homo sapiens* selected as the

reference organism and 0.7 threshold (high confidence) was used. The STRING platform provides insights into protein-protein interactions, enabling the identification of functional connections among the targets.

5.8 Gene Ontology and KEGG Pathway Enrichment Analysis

Gene ontology (GO) and Kyoto Encyclopedia of Genes and Genomes (KEGG) pathway enrichment analyses were conducted using ShinyGO v0.81 (http://bioinformatics.sdstate.edu/go/). These analyses aimed to elucidate the biological functions and pathways associated with the identified hub genes crucial to nephrolithiasis. GO analysis categorized the hub genes into three major domains: Biological Processes (BP), Cellular Components (CC), Molecular Functions (MF).

KEGG pathway analysis identified the signaling pathways and metabolic networks enriched among the hub genes. These pathways included those linked to nephrolithiasis and related comorbidities. A significance threshold of $p < 0.05$ was applied to ensure robust results, and the top 30 pathways in each category were retained for detailed interpretation (Ge et al., 2020; Luo et al., 2013).

5.9 Molecular docking

Most of the time, it accurately predicts binding between ligand and protein by assessing the binding affinity and hydrogen bonding and hence is a crucial step in the drug discovery process (López-Vallejo et al., 2011; Meng et al., 2011).

5.9.1 Application of standardized protocol in the present study

In the present study, proteins were selected based on human species, availability of co-crystallized ligands and higher degree value based on the number of genes. Before performing molecular docking using AutoDock Vina (Trott & Olson, 2010; Eberhardt et al., 2021), preparation of the protein and ligands in 3D format is required. The 3D structure of human SIRT1 was obtained from the Protein Data Bank (PDB ID: 4ZZJ) (Dai et al., 2015), which contains the SIRT1/activator/substrate complex. This open heterodimeric protein consists of chain A (SIRT1) and chain B (a p53-derived peptide substrate). The protein also includes an allosteric region, where residues 183–243 bind a non-hydrolyzable NAD+ analogue (Carba-Nicotinamide Adenine-Dinucleotide), and a small molecule (4TQ) binds at the activator region (residues 244–512).

Docking parameters were as follows: the grid size dimensions were 60 × 60 × 60 Å in the X, Y, and Z axes, with a grid spacing of 0.375 Å. The grid center was set to (-0.827, 45.618, -1.076) to cover the active site of SIRT1. All ligands were downloaded from ChemSpider (http://www.chemspider.com/Default.aspx) in 3D format. Protein and ligand preparations were performed using AutoDock Vina, including the removal of water molecules, addition of hydrogen atoms, merging of non-polar hydrogens, and addition of Gasteiger charges. The final structures were saved in pdbqt format. Protein-ligand complex interactions were visualized in 3D using UCSF Chimera (Pettersen et al., 2004), while 2D interactions were analyzed and compared using BIOVIA Discovery Studio 2020 and LigPlot+ version 2.2.7 (Wallace et al., 1995). These software tools are open source and freely available for academic users.

5.9.2 Docking validation

To ensure the reliability of our molecular docking approach, we first validated the protocol through a redocking experiment using the crystal structure of the target protein–ligand complex (PDB ID: 4ZZJ). The co-crystallized ligand was extracted and re-introduced into the original binding site, employing AutoDock Vina with parameters consistent with those used in subsequent virtual screening analyses. The optimal binding pose, identified by the lowest binding affinity (−7.9 kcal/mol), was converted to .pdb format for comparison. Structural alignment between the docked and experimental ligand was performed in PyMOL, where atom correspondence was manually curated and the pair_fit command was applied to facilitate calculation of the root mean square deviation (RMSD).

5.10 Molecular dynamics simulation (MDS)

The dynamic behaviour of any protein-ligand complex with time can be explored using MDS, which is the most commonly used approach in drug discovery. It analyses the movements of atoms and molecules in a simulated environment and gives crucial insights into their interaction stability, along with orientational fluctuation and conformational changes. The top three hits with the lowest binding energy were selected for MDS. CHARMM-GUI solution builder was used to generate input files of proteins and protein-ligand complex for MDS calculations (Lee et al., 2016; Jo et al., 2008). Solvation of complexes was done in TIP3P water in a rectangular box, Na+ and Cl- ions were added (0.15M) at 303.15K temperature & atmospheric pressure (1 bar) to neutralize the system and mimic physiological conditions in Monte-Carlo fashion followed by imposition of periodic boundary conditions (PBC) in XYZ directions (Mark & Nilsson, 2001). System energy minimization was done at the steepest descent algorithm of

5000 steps. All the MDS runs and calculations were performed in GROMACS (2021.4 version) (Abraham et al., 2015). Using an NPT (constant number, volume, temperature) ensemble, the system was equilibrated at 310K temperature and 1 bar pressure and was run for 100 ns. The pressure was maintained by a modified Berendsen thermostat (Huang et al., 2017) and Parrinello-Rahmanbarostat (Bussi et al., 2007), (Parrinello & Rahman, 1980). To evaluate the changes in the docked complex in the hydrated simulated environment, two physical properties namely RMSD (root mean square deviation) and RMSF (root mean square fluctuations) were evaluated alongside the radius of gyration, solvent accessible surface area (SASA) (Bondi, 1694) and number of hydrogen bond using GROMACS.

5.11 MM/PBSA-Trajectory analysis

MM-PBSA (molecular mechanics/Poisson–Boltzmann surface area) which is open-source software was used for estimating the binding free energy of protein-ligand complex. The binding free energy of any complex can be described from the following equation (Genheden & Ryde, 2015):

$$\Delta G \text{ (Binding)} = \Delta G\ (Complex) - (\Delta G\ Protein + \Delta G\ Ligand)$$

Where $\Delta G\ (Complex)$ represents the total energy of protein and ligand, $\Delta G\ Protein$ and $\Delta G\ Ligand$ represent individual free energies, respectively.

5.12 Principal Component Analysis and Free Energy Landscape

Principal component analysis (PCA) of protein and complex for 100ns trajectory was performed using gmx_covar and gmx_anaeig module of GROMACS software. After removing rotation and translation coordinates, PCA captures the intrinsic motion of the system (Kume et al., 2017). Fluctuation intensity of the protein was measured using the first two components (PC1 and PC2) (Amadei et al., 1993). Gmx_sham module was used for plotting free energy landscape (FEL) which analyze energy and conformation of the complex (Bashyal et al., 2024).

5.13. Crystallization assays

Reagents required in these assays are:

- Calcium chloride: 4mM
- Calcium chloride: 50mM

- Sodium oxalate: 7mM
- Sodium oxalate: 50mM
- Tris: 0.05 mol/L
- NaCl: 0.15 mol/L
- Sodium acetate buffer (pH 5.7)
- Tris-HCl buffer

5.13.1 Nucleation Assay

The nucleation assay is an essential technique used to study how crystals form and how certain substances can prevent or slow down this process. This is particularly important in understanding kidney stone formation, where calcium oxalate (CaOx) crystals play a major role. By using this assay, researchers can test different compounds to see if they can effectively stop or reduce the early stages of stone formation.

Crystal formation begins when tiny solute particles in a supersaturated solution come together to form stable crystal nuclei. The nucleation assay measures how well an inhibitor can slow or prevent this process by monitoring changes in the solution's turbidity (cloudiness) over time.

- **Without an inhibitor**: Calcium oxalate crystals form rapidly, making the solution more turbid.
- **With an inhibitor**: If a compound has nucleation-inhibiting properties, it slows down crystal formation, resulting in a clearer solution for a longer period.

The nucleation assay of compounds was performed as described in the literature (Abu et al., 2020). Briefly, 4 mM calcium chloride and 7 mM sodium oxalate were prepared in Tris buffer (0.05 mol/L Tris and 0.15 mol/L NaCl, pH 6.5) and added to various concentrations of the compounds. The assay was measured at 620 nm to calculate the inhibition rate and evaluate the effect on calcium oxalate crystal formation.

% Nucleation inhibition = [(OD of control- OD of sample)/ (OD of control] *100

5.13.2 Aggregation Assay

An aggregation assay is a test used to study how small calcium oxalate crystals clump together to form larger kidney stones. This test helps researchers understand the process of stone formation and identify substances that can slow down or prevent crystal aggregation,

potentially reducing the risk of kidney stones. The goal of the aggregation assay is to measure how well a substance can prevent tiny kidney stone crystals from sticking together.

The aggregation assay of compounds was performed following the methodology described by (Abu et al., 2020). Calcium oxalate crystals were synthesized by mixing equal volumes of 50 mM calcium chloride and 50 mM sodium oxalate solutions, maintaining the mixture at 60°C for 1 hour. The resulting crystals were then dried and evaporated at 37°C. These crystals were subsequently dissolved in Tris buffer (0.05 mol/L Tris and 0.15 mol/L NaCl, pH 6.5) and treated with various concentrations of the test compounds. The extent of calcium oxalate aggregation was assessed by measuring the absorbance at 620 nm, which corresponds to the percentage inhibition rate.

% Aggregation inhibition = [(OD of control- OD of sample)/ (OD of control] *100

5.13.3 Oxalate depletion assay

The Oxalate Depletion Assay is a test that helps researchers understand how well a substance can lower oxalate levels in a solution. This is important because too much oxalate in the urine is a key factor in the formation of kidney stones, especially calcium oxalate stones. By using this assay, scientists can identify potential treatments or natural compounds that may help prevent kidney stones by reducing oxalate levels in the body.

The oxalate depletion assay was conducted following the methodology outlined by Zaki et al., 2019). In this assay, a 1.5 mg/mL calcium oxalate slurry was prepared in sodium acetate buffer (pH 5.7). The reaction mixture consisted of calcium chloride and sodium oxalate at a concentration of 0.004 M each, combined with Tris-HCl buffer (0.01 M Tris-HCl and 0.09 M sodium chloride, pH 7.4). Various concentrations of the test compounds were added to this mixture. The growth of calcium oxalate crystals was monitored by measuring absorbance at 214 nm over 10 minutes, and the percentage inhibition was calculated.

% Growth inhibition = [(OD of control- OD of sample)/ (OD of control] *100

5.14 Crystallization Kinetics

To study the rate of nucleation, it is important to study the kinetics of crystallization. Here we have taken equimolar solutions of calcium chloride and sodium oxalate and prepared different supersaturation ratios as mentioned in Equation 1. In the beaker containing calcium chloride and inhibitors, sodium oxalate was added and mixed using a magnetic stirrer on a medium

speed and samples were withdrawn at regular intervals and were measured using a spectrophotometer at 560nm wavelength to measure induction time. Induction time is the time between the supersaturation of the solution and the first appearance of crystal nuclei in the solution (Amjad, 1985; Abdel-Aal EA et al., 2017). We have taken the supersaturation ratio from 0.72 to 2.4 as a possible range to measure induction time.

5.14.1 Experimental Design

The effect of phytochemicals along with potassium citrate as positive control was done by studying their effect on various supersaturation levels mentioned in Table 5.2 which was calculated as mentioned in equation 1; potassium citrate also oxalates ions which was less than 0.1%, hence not taken into account while calculating supersaturation ratio.

$$S = \frac{C}{(C*)} \qquad (1)$$

Where S = supersaturation ratio

C = solute concentration

C* = solute solubility

Table 5.2: Experimental procedure of calcium oxalate at various supersaturations ratios

Supersaturation ratio	**CaCl2 (0.01M) V, mL**	**Na2C2O4 (0.01M) V, mL**	**DI-water V, mL**	**Inhibitor (0.001M) V, mL**
0.72	3	3	84	10
0.96	4	4	82	10
1.2	5	5	80	10
1.43	6	6	78	10
1.67	7	7	76	10
1.91	8	8	74	10
2.15	9	9	72	10
2.4	10	10	70	10

5.14.2 Surface energy calculation (γ)

The relation between inverse log square of supersaturation ratio (1/ $\log^2 S$) and log induction time over a range of supersaturation ratio (1.43 to 2.4) was used for calculation of surface energy of nuclei and free energy barrier derived from classical homogenous nucleation theory (Oxtoby, 1992). To understand the nucleation rate and crystal growth, it is critical to determine surface energy or interfacial tension, which can be calculated from the equation 2**.** Here B is the slope of log induction time and 1/ $\log^2 S$, R is the gas constant, T is the absolute temperature, β is the geometric shape factor, V is molar volume, NA is Avogadro number and f(θ) is the Correction factor.

$$\gamma 3 = B * \frac{(2.3RT)3}{RT\beta V2NAf(\theta)} \qquad (2)$$

5.10.4 Nucleation rate

The rate of nuclei formed per unit time is referred to as the nucleation rate and is calculated from equation 3 (Lancia et al., 1999; Myerson, 2002).

$$\boldsymbol{Js = F\frac{exp[-\beta\gamma 3V2NAf(\theta)]}{(RT)3ln2S}} \qquad (3)$$

Js = nucleation rate

F = Frequency constant (10^{30} nuclei/cm^3) (Izmailov et al., 1999)

5.14.3 Particle Size and Zeta Potential

To assess the particle size of the prepared crystals, a particle size analyzer (Malvern S90) was used, which works based on dynamic light scattering (DLS). For this analysis, Millipore water served as the medium, and the particle emulsions were prepared at a concentration of 1 mg/ml. Each sample was measured three times at a 90-degree angle to ensure accuracy, with all experiments conducted at a stable temperature of 25°C.

In addition to particle size, the zeta potential was also measured using the Malvern zeta potential analyzer. This instrument determines the surface charge of particles by analyzing their movement under an electric field. Like the particle size analysis, the zeta potential measurements were conducted at 25°C to maintain consistency. These analyses help understand the stability and dispersion of the nanoformulation, which is crucial for its effectiveness in biological applications.

5.14.4 Fourier transform infrared spectroscopy (FTIR)

To track any changes in crystals, Fourier Transform Infrared (FTIR) spectroscopy was used, a technique that helps identify molecular structures based on how they absorb infrared light. The FTIR spectra were recorded using a Perkin Elmer Spectrum 2 spectrometer to analyze the chemical composition and potential structural modifications in the formulation.

For more precise measurements, a Nicolet iS50 FT-IR spectrometer from Thermo Scientific was used, equipped with a thermally controlled diode laser to ensure stable and accurate readings. The FTIR spectrum was recorded over a broad range of 4000 to 500 cm^{-1}, covering key vibrational frequencies of functional groups within the nanoformulation. This analysis helps in detecting any chemical interactions, bonding changes, or structural modifications that might have occurred during the formulation process, providing valuable insights into the stability and integrity of the nanoformulation.

5.14.5 X-Ray Diffraction

X-ray diffraction was measured using Monochromatic Kα1 radiation in the 10–60°, 2θ range at a scan rate of 1° min^{-1}. Obtained peaks were compared with calcium oxalate monohydrated JCPDS card no. 00-020-0231 and 00-001-0008 for calcium citrate hydrate.

5.14.6 Field Emission Scanning Electron Microscopy (FESEM)

To closely examine the surface structure and morphology of the crystals, Field Emission Scanning Electron Microscopy (FESEM) was utilized. FESEM is a highly advanced imaging technique that provides exceptional depth resolution and highly detailed surface images at the nanometer scale.

For this analysis, a JEOL JSM 6610LV FESEM (Peabody, MA, USA) was used, known for its ability to produce high-resolution images that reveal the ultrafine details of a material's surface. The sample preparation process involved applying a thin layer of the nanoformulation onto an aluminum stub using double-sided adhesive carbon tape to ensure proper adherence.

To enhance the image quality and conductivity, the sample was subjected to a gold sputter coating in an argon atmosphere using a high-vacuum evaporator. This coating prevents electron charging during the scanning process and improves the visibility of surface features. Once prepared, the sample was examined under the FESEM at various magnifications, allowing for a detailed visualization of the crystal's structure and morphology and the best ones were

reported in the results and discussions. These high-resolution photomicrographs provided valuable insights into the shape, texture, and surface characteristics of the prepared formulation, helping researchers understand its structural integrity and potential applications.

5.15 Non-Enzymatic Anti-Oxidant Assays

Reagents required in these assays are:

- DPPH (2,2-diphenyl-1-picrylhydrazyl): 0.16 mM
- Methanol: 100%
- Ascorbic Acid: 20-100 µM
- ABTS: 7mM
- Potassium persulfate: 2.45 mM
- Phosphate buffer: 0.2M
- Potassium ferricyanide: 1%
- Trichloroacetic acid: 10%
- Ferric chloride: 0.1%
- Distilled water

5.15.1 DPPH Assay

Principle

The assay measures the ability of antioxidants to neutralize DPPH radicals. The nitrogen atom in DPPH, which contains an unpaired electron, is reduced when it accepts a hydrogen atom from an antioxidant, forming the corresponding hydrazine.

Procedure

In this assay, a 0.16 mM DPPH solution was prepared in methanol, and 2 mL of this solution was mixed with 1 mL of varying concentrations of phytochemicals prepared in methanol. The mixture was incubated in the dark for 30 minutes, followed by absorbance measurement at 517 nm, as described in previous studies (Yen et al., 1995). Ascorbic acid was used as the standard. And DPPH in methanol was served as blank. The DPPH solution was optimized such that the reading of blank comes around 0.7. DPPH scavenging activity was then calculated from the following equation:

$$\text{DPPH scavenging activity}(\%) = [(A0 - A1)/ A0] * 100$$

Where A0 = absorbance of blank

A1 = absorbance of the test sample

5.15.2 ABTS Radical Scavenging Activity Assay

Principle

ABTS radicals are produced by reacting ABTS salt with a strong oxidizing agent, such as potassium permanganate or potassium persulfate. The reduction of the blue-green ABTS radical by antioxidants that donate hydrogen is assessed by the decrease in its characteristic long-wavelength absorbance spectrum.

Procedure

The ABTS assay was performed following published protocols with slight modifications (Seke et al., 2021). A 7 mM ABTS solution was prepared in water and mixed with an equal volume of 2.45 mM potassium persulfate. The mixture was stored in the dark overnight to generate ABTS radicals. The solution's absorbance was measured at 734 nm and diluted with water to approximately 0.70 to prepare the ABTS working solution. For the assay, 1 mL of each test compound at different concentrations was mixed with 2 mL of ABTS working solution, and absorbance was recorded at 734 nm. Ascorbic acid was used as the standard. And ABTS in water was served as blank. ABTS solution was optimized such that the reading of blank comes around 0.7. ABTS scavenging activity was then calculated from the following equation:

$$\text{ABTS scavenging activity}(\%) = [(A0 - A1)/\ A0] * 100$$

Where A0 = absorbance of blank

A1 = absorbance of the test sample

5.15.3 Ferric reducing antioxidant power (FRAP) Assay

Principle

The FRAP assay is based on the reduction of Fe^{3+} to Fe^{2+} by pH. The reaction is conducted at an acidic pH of 3.6 to maintain iron solubility. At low pH, the ionization potential is decreased, facilitating hydrogen atom transfer, while the redox potential is increased, making it the dominant reaction mechanism.

Procedure

The iron reduction capacity was measured following previously published methods (Karagözler et al., 2008; Ouahhoud et al., 2022). Different concentrations of test compounds (1 mL) were mixed with 2.5 mL of 0.2 M phosphate buffer and 2.5 mL of 1% potassium ferricyanide. The mixture was then incubated at 50°C for 20 minutes. After incubation, the samples were cooled to room temperature, and 2.5 mL of 10% trichloroacetic acid was added to stop the reaction. The mixtures were then centrifuged at 3,000 rpm for 30 minutes to collect the supernatant. To the supernatant, 500 µL of freshly prepared 0.1% $FeCl_3$ (ferric chloride) and 2.5 mL of distilled water were added. Finally, absorbance was measured at 700 nm. Ascorbic acid was used as the standard. FRAP solution was optimized such that the reading of blank comes around 0.7. FRAP scavenging activity was then calculated from the following equation:

$$\text{FRAP scavenging activity}(\%) = [(A0 - A1)/ A0] * 100$$

Where A0 = absorbance of blank

A1 = absorbance of the test sample

5.16 Antioxidants assays -enzymatic

Reagents required in these assays are:

- NRK-52E cell line: 1flask
- Dulbecco's Modified Eagle Medium (DMEM): 1 pack
- Fetal Bovine Serum (FBS): 500ml
- MTT: 5 mg
- DMSO: 50ml
- Phosphate Buffered Saline (PBS): 500ml
- Trypsin: 200ml
- Antibiotic: 50ml
- Sodium oxalate: 2mM
- Tris-HCl buffer (pH 7.1): 150 mM
- Ferrous sulfate: 1 mM
- Ascorbic acid: 1.5 mM
- Trichloroacetic acid: 10%

- Thio barbituric acid (pH 7): 0.375%
- Sodium carbonate buffer: 50 mM in 0.1 mM EDTA, pH 10.8
- Nitro-blue tetrazolium: 96 µM in 95% ethanol
- Hydroxylamine hydrochloride: 20 mM, pH 6.0,
- Triton X-100: 0.6%
- Potassium phosphate buffer: 100 mM, pH 6.5
- Reduced glutathione: 1 mM, pH 6.5
- 1-Chloro-2,4-dinitrobenzene (CDNB): 1 mM
- Hydrogen peroxide: 100%
- Phosphate buffer: 200ml
- Sodium carbonate: 2%
- NaOH: 0.1N
- CuSO4: 1%
- Sodium potassium tartrate: 2%
- Folin's Ciocalteau's Reagent: 50%
- BSA: 20mg

5.16.1 MTT ASSAY

Principle

The MTT (3-(4,5-dimethylthiazol-2-yl)-2,5-diphenyltetrazolium bromide) assay is a colorimetric technique used for evaluating cell viability, proliferation, and cytotoxicity. It is based on the conversion of the yellow MTT reagent into purple formazan crystals by viable cells through the enzymatic activity of mitochondrial dehydrogenase

Procedure

NRK-52E cells were obtained from the National Centre for Cell Science (NCCS) in Pune, India, and cultured in a medium containing 25 mM glucose. Upon reaching 70% confluency, the cells were trypsinized and seeded into 96-well plates, allowing them to adhere and achieve 70% confluency in a serum-free medium. Subsequently, the cells were treated with varying concentrations (20-100µM) of Silibinin, Isoeugenol, and Trans-Anethole for 24 hours. After treatment, the growth medium was removed, and the cells were incubated with a 0.5 mg/mL MTT solution dissolved in phosphate-buffered saline (PBS) for 4 hours to facilitate the

formation of formazan crystals. The crystals were then dissolved using dimethyl sulfoxide (DMSO) for 30 minutes, and absorbance was measured at 570 nm using a microplate reader.

5.16.2 Establishment of in-vitro nephrolithiasis model

This assay was performed with slight modifications to the method outlined by Chaiyarit et al. (2024). NRK-52E cells were cultured in 6-well plates, and once they reached 70% confluency, the standard medium was replaced with a serum-free medium. The cells were then allocated into different groups. Disease induction was carried out by exposing the cells to 2000 µM sodium oxalate, along with the respective treatment groups, followed by a 24-hour incubation. After incubation, the media was removed from the plates, washed with PBS and stored at -80°C for further analysis.

5.16.3 Cell lysate preparation

To prevent protein degradation and modification, we supplemented the lysis solution with protease and phosphate inhibitors, ensuring optimal protein yield during cell lysis. After treating the cells in a 6-well plate as per the experimental protocol, we washed them with ice-cold phosphate-buffered saline (PBS). To maintain acetylation levels, they added 5 mM sodium butyrate to the lysis solution. The lysis buffer was then applied to the plate, and the cells were scraped off using a cell scraper. The collected lysate was transferred to microcentrifuge tubes and centrifuged at 1700 rpm for 7 minutes in a chilled microcentrifuge. The supernatant was preserved for further analysis, while the pellet was discarded.

5.16.4 Tissue homogenate preparation

The homogenate was prepared using a Dounce homogenizer with a buffer solution containing 0.1M Ethylenediamine tetraacetic acid (EDTA) and 0.1M Tris chloride, which was mixed and adjusted to a pH of 7.4. Beta-mercaptoethanol was added to the buffer before the homogenization of cells and tissues. The homogenizing tube was kept in an ice-filled beaker throughout the process. The cells were homogenized using a motor-driven Teflon pestle rotating at 3000 revolutions per minute. The resulting homogenate was filtered through cotton gauze and stored in labeled plastic vials at -18°C until further use. This 10% homogenate (1g of cells in 9 ml of buffer) was used as the starting material for subsequent dilutions with appropriate buffers to obtain the required working homogenate fraction.

Cell/tissue were then divided into three groups: 1) tissue homogenate/cell-lysate, 2) post-nuclear supernatant (PNS), and 3) Post mitochondrial supernatant (PMS)

5.16.4.1 Post nuclear supernatant (PNS) preparation

Centrifugation was performed on the cell homogenate at 10,000 rpm for five minutes at 4°C in a C-24 REMI cold centrifuge to separate the nuclear pellet and supernatant. The PNS was then isolated and stored at -18°C for subsequent use.

5.16.4.2 Post mitochondrial supernatant (PMS) preparation

To generate the PMS, the removal of the nuclear pellet was performed, and centrifugation of the supernatant was conducted for 10 minutes at 10,000 g at 4°C to achieve the separation of the mitochondrial pellet. The PMS was subsequently stored at -18°C for various assays.

5.16.5 Protein estimation

Tissue homogenate/cell-lysate, PNS, and PMS were then used for protein estimation. The protein content was quantified following the standardized method established by Lowry et al., 1951, employing a standard curve derived from bovine serum albumin (BSA).

Principle

This method is based on the presence of the amino acids' tyrosine and tryptophan. A colored complex was formed through the reaction of Folin's reagent with proteins. The interaction of aromatic amino acids in the protein with copper in an alkaline environment led to the reduction of phosphomolybdate, resulting in color production. The intensity of the color was proportional to the amount of aromatic amino acids present.

Reagents preparation:

- Reagent A: 2% sodium carbonate in 0. 1N NaOH
- Reagent B: 1% $CuSO_4$ in double-distilled water
- Reagent C: 2% sodium potassium tartrate in double-distilled water
- Lowry's Reagent: Mix Reagent A, Reagent B, and Reagent C in a ratio of 49: 0. 5: 0.5 (v/v)
- Folin's Ciocalteu's Reagent: Dilute with double-distilled water in a ratio of 1: 1 (v/v)
- Stock Protein Standard: 20mg/ml bovine serum albumin (BSA)

Procedure

Table 5.3 Sample preparation in lowry's protein estimation

Reagents	**Blank(ml)**	**Standard(ml)**	**Test(ml)**
DDW	1	0.9	0.9
Standard	-	0.1	-
Test Sample	-	-	0.1
Lowry's Reagent	5 ml to each	5 ml to each	5 ml to each
Incubate tubes at 37degrees C for 15 min and then			
Add 0.5 ml of Folin's Ciocalteau's Reagent. Then again			
Incubated tubes for 30 min at 37degrees C			
Recorded absorbance at 670nm			

5.16.6 Estimation of In-vitro oxidative biomarkers

In vitro antioxidant activity was evaluated using NRK-52E cells. Different groups were assigned for all in-vitro estimations of antioxidant activities: the control group (without treatment), the disease group (treated with 2mM sodium oxalate), the LD group (treated with 50 µM as the low dose of experimental samples under diseased conditions), and the HD group (treated with 100 µM as the high dose of experimental samples under diseased conditions).

5.16.6.1 Lipid peroxidation (LPO)

It is measured by the method of Beuge and Aust (1978)

Principle

Free radicals can cause damage to Poly unsaturated fatty acids by Peroxidation mainly by OH^- and O_2^-. The product of Peroxidation is Malondialdehyde (MDA) which is identified to react with Thiobarbituric acid (TBA) to give pale red color absorbance at 535nm.

Reagents:

- 150mM Tris-HCl buffer(pH=7.1)
- 1.5mM Ascorbic acid
- 1mM $FeSO_4$
- 10% Trichloroacetic acid
- 0.375% Thiobarbituric acid pH=7)

Procedure

Table 5.4**:** Procedure of LPO estimation

Reagent	**Blank(ml)**	**Test(ml)**
Tris-HCl buffer	0.1	0.1
$FeSO_4$	0.1	0.1
Ascorbic acid	0.1	0.1
DDW	0.7	0.6
Sample	-	0.1
Incubated @ 37ºC for 15 min, and the reaction was stopped by adding		
TCA	1	1
TBA	2	2

- Incubated for 15 min in boiling water bath followed by cooling and centrifuging at 3000 rpm for 10 min.
- The supernatant and absorbance were taken at 532nm.
- LPO concentration was calculated, and the result was expressed as nmoles of MDA formed /ml.

5.16.6.2 Superoxide dismutase (SOD)

The SOD is estimated by the method of Kono (1978) in cell homogenate.

Principle

The reduction of Nitroblue Tetrazolium dye to blue-colored formazan occurs due to superoxide radicals, which are generated by the auto-oxidation of hydroxylamine hydrochloride. Superoxide dismutase (SOD) prevents the reduction of NBT by interfering with hydroxylamine hydrochloride. The enzyme activity is determined by measuring the extent of inhibition.

Reagents

- 50mM Sodium Carbonate buffer in 0.1mM EDTA (pH=10.8)
- 96µM Nitro Blue Tetrazolium in 95% ethanol.
- 0.6% Triton X-100 in DDW
- 20mM Hydroxylamine HCl (pH=6.0)

Procedure

Table 5.5**:** Procedure of SOD estimation

Reagents	Blank(ml)	Test(ml)
Buffer	1.35	1.3
Hydroxylamine HCl	0.1	0.1
Triton X-100	0.1	0.1
NBT	0.5	0.5
Keep tubes for 2 min		
Sample	-	0.05

The blue color that was developed was measured at 560nm at intervals of 30sec for 2min.

Calculations

The concentration of enzyme that gives a half-maximal inhibition of NBT reduction is known as one unit of the enzyme activity.

5.16.6.3 Estimation of Catalase

It is measured in PNS according to the method of Luck (1971).

Principle

Catalase is an enzyme that decomposes H_2O_2 to H_2O

Reagents

- Phosphate Buffer (0.2M, pH=7.0)
- Solution A: 1.79gm of KH_2PO_4 in 200ml of DDW
- Solution B: 3.52gm of $NaHPO_4.2H_2O$ in 300 ml of DDW
- Solution C = Mix Solutions A and B in a ratio of 3:7 (pH=7.0)
- Working phosphate buffer = 160µl of H_2O_2 in 100 ml of Phosphate buffer

Procedure

Reagents	Blank	Test
Sample	25 µl	25 µl
Phosphate buffer+ H_2O_2	-	3.0 ml
Phosphate buffer- H_2O_2	3.0 ml	-

O.D. was measured at 240nm for 2 minutes at the interval of 30 seconds.

Enzyme activity for catalase was calculated using the Molar extinction coefficient of $43.6M^{-1}cm^{-1}$.

The results are expressed in µmoles of H_2O_2 decomposed/min/mg protein.

5.16.6.4 Estimation of GST

It is performed by the method by Habig et al, 1974 in PMS.

Principle

It is an enzyme that catalyzes the reaction of 1-chloro-2,4-dinitrobenzene (CDNB) with the sulphydryl group of Glutathione.

The conjugate of CDNB-Glutathione absorbs at 340nm.

Reagents

- 100mM of Potassium phosphate buffer(pH=6.5)
- 1mM GSH (reduced glutathione) (pH=6.5)
- Dissolve 61 mg of CDNB in 5.0 ml of distilled alcohol (1mM CDNB)

Procedure

Reagents	**Blank(ml)**	**Test(ml)**
Buffer	1	1
DDW	1.65	1.55
GSH	0.3	0.3
Sample	-	0.1
CDNB	0.05	0.05

The absorbance is checked at 340nnm at intervals of 1 min for 5 min.

5.16.7 Crystal-adhesion assay

This assay was conducted with slight modifications to the method described by (Chaiyarit et al. 2024). NRK-52E cells were cultured in 6-well plates and upon reaching 70% confluency, the regular medium was replaced with a serum-free medium. The cells were then divided into multiple groups. Disease induction was achieved by treating the cells with 2000 µM sodium oxalate, along with the treatment groups, and incubating for 24 hours. After washing with PBS, the cells were visualized under an inverted phase-contrast microscope, and cell counts were performed from 15 random fields per sample. The concentration of sodium oxalate and the choice of positive control were based on the study by Sun et al. 2021.

5.17 Histone isolation protocol

The nuclear pellet was resuspended in a low salt buffer (LSB), followed by the addition of 22.7µl of 0.2 M HCl. The mixture was then subjected to sonication at 40-50 kHz for 10 seconds, with 1-minute intervals, and the process was repeated three times. Subsequently, the mixture was centrifuged at 13,000 rpm for 30 minutes, and the supernatant was retained. To the collected supernatant, 20% TCA was added, vortexed thoroughly for proper mixing, and incubated in an ice bath for 30 minutes. The mixture underwent another round of centrifugation at 13,000 rpm for 30 minutes. The resulting pellet was resuspended in 1 ml of 0.25% acetone-HCl, vortexed, and centrifuged again at 13,000 rpm for 30 minutes, with the process repeated once more. The tubes were then sealed with parafilm and stored at 0°C overnight. Finally, the pellet was resuspended in chilled distilled water

5.17.1 Western blotting protocol

Principle

It utilizes the simple principle in which first the protein is separated according to molecular weight through electrophoresis and then followed by binding of this protein to the support called blot which allows its detection with the help of antibodies specific to the protein.

Reagents

- Separating gel buffer, pH 8.8(100ml)
  - Tris-18.2 gm Set pH 8.8
  - Sodium dodecyl sulfate (SDS) -400mg
- Stacking gel buffer, pH 6.8(100ml)
  - Tris-6.05gm Set pH 6.8
  - SDS -400mg
- Acrylamide 30x(100ml)
  - Acrylamide -29.2gm
  - Bis-acrylamide -0.8gm
- Staining buffer (500ml)
  - Methanol-250ml
  - Acetic acid-50ml
  - Brilliant blue-1.5g
- Destaining buffer(500ml)
  - Methanol-250ml
  - Acetic acid-50ml
  - Water -250ml

- 4x Sample buffer(10ml)
  - 1M Tris -0.2g
  - SDS -0.8g
  - Glycerol -4ml
  - B-mercaptoethanol -4ml
  - 10% Bromophenol blue -10µl
  - APS -1ml (100mg in 1ml water)
- 1x Running buffer (1 litre)
  - Tris 3 gm
  - Glycine 14.4 gm
  - SDS 1 gm

Reagents	**Stacking Gel**	**Separating gel**
Water	2.83 ml	6.10 ml
Separating buffer	2.5 ml	2.5 ml
30% acrylamide	4.7 ml	1.3 ml
APS	33.3 µl	50 µl
TEMED	6.7 µl	10 µl
Polymerise for half an hour		

- ***First step: SDS-PAGE***

- Extracted 0.5 µg histone sample was taken and suspended in a sample buffer. Samples were heated at 95ºC for 5 minutes.
- Samples were centrifuged to restore the sample volume.
- Stalking buffer and separating buffer were prepared.
- Histone samples were loaded in the wells per lane, also pre-stained protein standard was loaded.
- The gel was run at a voltage of 70 V till stalking and after that gel was run at 140 V for 1-2 hours.

Setup for transfer

- A transfer buffer was prepared to fill the tank during the transfer process.
- After successful SDS-PAGE, the gel was removed from the cassette. The stalk and
- well area of gel was cut off.

- The gel was put in a transfer buffer and shaken for 10 minutes.
- The nitrocellulose membrane was soaked in the transfer buffer for 30 minutes.

➢ **Second step: Western blotting**

Transfer buffer 500ml

- Tris -1.5gm
- Glycine -7.2 gm
- Distilled water (make up volume 500ml)

Tris-Buffered saline (TBS) (pH 7.2)

- 5M Nacl-30ml
- 2M tris-10ml
- Milli que water -955 ml

TBST (pH 7.2)

- TBS-500ml
- 0.5% Tween 20

2X Blocking buffer

- BSA (Bovine serum albumin)- 400mg in 20ml TBS (for 1 blot)
- TBS-500ml

Primary antibody

Secondary antibody

5.17.2 Transfer assembly

- The cassette was taken and opened to make an assembly
- The sandwich was made by placing a foam pad on one side of the cassette followed by a sheet of filter paper followed by gel on top of the filter paper.
- On top of the gel, the nitrocellulose membrane was applied, followed by the second sheet of filter paper, then the second pad of foam pad.
- The cassette was closed after making this sandwich.

5.17.3 Transfer method

- The cassette that has a sandwich assembly was placed in the transfer tank.
- The cathode (-) should face the gel side of the cassette, while the membrane side should face the anode.
- A transfer buffer was added to the transfer tank up to the mark.
- The apparatus was run at 10-15 V for 1 to 2 hours till the transfer was complete.
- After transfer, the sandwich was removed from the cassette and carefully disassembled using forceps.

- After that ponceau staining was used to verify the successful transfer of histone proteins

5.17.4 Processing of western blot

- ***Blocking*** – In this step, we used BSA as a blocking buffer. The membrane was blocked by placing it in a blocking buffer for 2 hrs at room temperature (RT) using 2X BSA/0.1% tris buffer saline (TBS) while continuing shaking.
- ***Incubation with primary antibody***- The membrane was incubated at 4ºC overnight with the antibody.
- ***Washing-*** The blot was washed with 0.1% of tris buffer saline tween TBST 4 times. Washing was done 2 times for 5 minutes followed by 2 times 10 min washes.
- ***Incubation with secondary antibody-*** The membrane was incubated with a secondary antibody for 1hr with continuous shaking @ 37ºC.
- ***Washing-*** The blot was washed with 0.1% of tris buffer saline tween TBST 4 times. Washing was done 2 times for 5 minutes followed by 2 times 10 min washes.
- The blot was developed.

5.17.5 Detection and analysis

The ECL (enhanced chemiluminescence) technology and ECL Hyperfilm were used to detect proteins (Amersham Biosciences). Quantification of western blots was done by densitometric analysis and the exposures have a linear dynamic range. The Image J software was used for densitometric analysis.

Analysis of western blot was carried out employing the following antibody:

- Rabbit anti- [aceylated histone H3 (Lys9/14)] antibody (1:5000 dilution; Santa Cruz Biotechnology).
- Rabbit anti-histone H3 antibody (1:5000 dilution; Santa Cruz Biotechnology).
- HRP-conjugated anti-rabbit secondary antibodies (diluted 1:20000; Santa Cruz Biotechnology).

5.18 Animals Studies

Sprague Dawley male rats weighing 160-200g were obtained from the institute's animal facility. They were kept in standard conditions and had free access to food and water. The study followed the guidelines of the CPCSEA, Ministry of Social Justice and Environment, and Government of India, and received approval from the Institutional Animal Ethical Committee (Approval no. LPU/IAEC/2022/08).

5.18.1 Nephrolithiasis induction

We created a calcium oxalate (CaOx) crystal nephrolithiasis rat model as described by Yousefi et al., 2018, using ethylene glycol in their drinking water for 28 days and administering ammonium chloride by oral gavage for the first three days of the first and third weeks to promote stone formation Table 5.8 and Figure 5.1.

5.18.2 Experimental design

Thirty-six male Sprague-Dawley rats were divided into six groups of six (Table 5.4). Group 1: Control group, given 0.5% Carboxymethyl cellulose (CMC), food, and water for 28 days. Group 2: Received 100 mg/kg silibinin dissolved in 0.5% CMC for 28 days, with food and water. Groups 3-6: Received 1% ethylene glycol in drinking water for 28 days and 1% ammonium chloride orally for the first three days of the first and third weeks. Groups 4-6: Also received potassium citrate (2.5 g/kg) and silibinin (50 mg/kg and 100 mg/kg), respectively for 28 days. The potassium citrate concentration was based on a published study (Yousefi et al., 2018), and the silibinin dosage was referenced from literature related to diabetes (Liu et al., 2019).

Table 5.4: Division of animals into various groups

Groups	**Treatment**	**Dose of test compounds**	**No. of animals**
Group 1	Control group	-	6
Group 2	Silibinin *per se* treated group	100 mg/kg, p.o. daily for 4 consecutive weeks	6
5ml/kg of 1% (v/v) EG for 4 weeks + 2 ml of 1% ammonium chloride for 1st three days of the 1st and 3rd week will be given			
Group 3	Disease *per se* group (negative control group)	-	6
Group 4	Disease + Potassium citrate treated positive control group	2.5 gm/kg	6
Group 5	Disease + Silibinin low dose treated group	50 mg/kg	6
Group 6	Disease + Silibinin high dose treated group	100 mg/kg	6

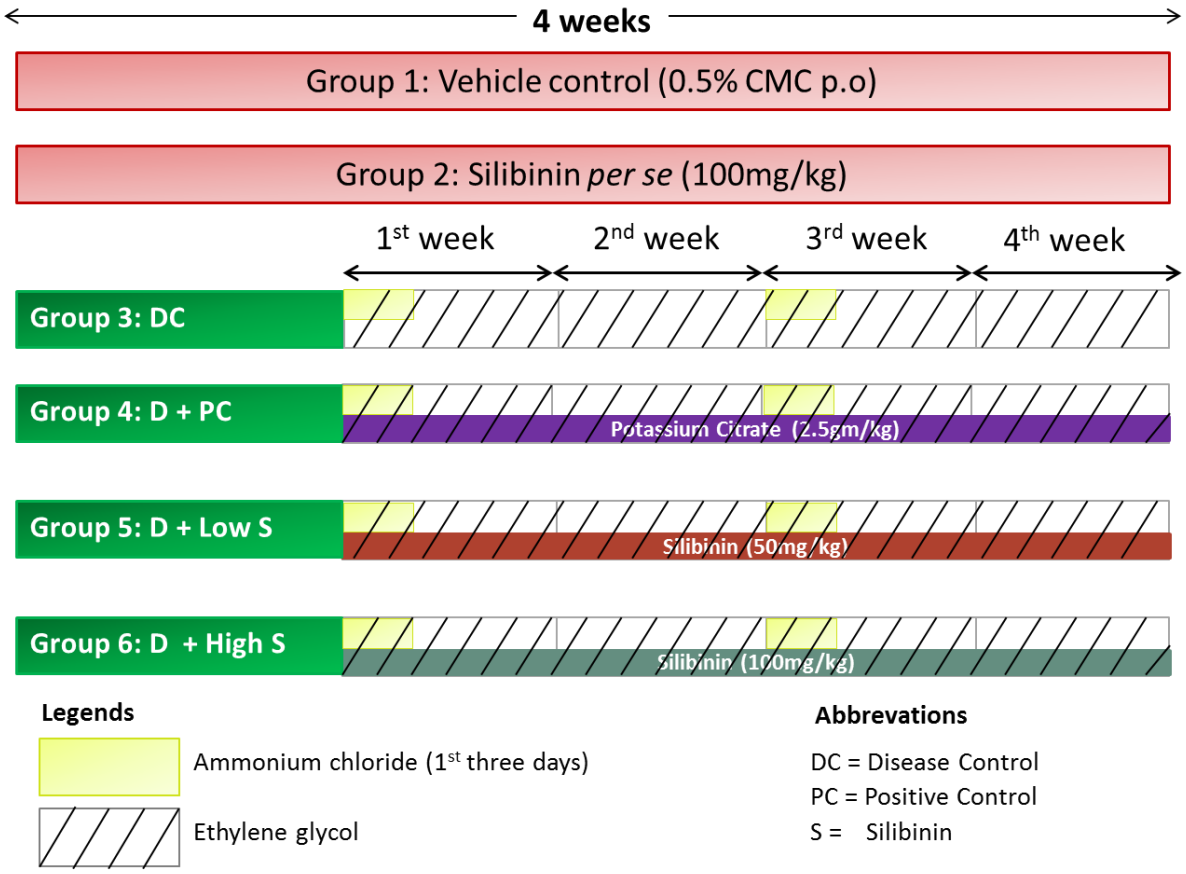

Figure 5.1: Timeline used for animal dosing

5.18.3 Body weight, organ weight, and Kidney morphology measurement

The body weight of each rat was measured weekly until the study ended. At the conclusion, kidney and liver weights were recorded to calculate their coefficients using the organ-to-body weight ratio. After dissection, the kidneys were carefully removed, and their length, width, and thickness were measured with a vernier caliper.

5.18.4 Serum and Urine Biochemical Analysis

The rats were placed in metabolic cages for 24 hours to collect urine before they were sacrificed. Urine was analyzed microscopically to detect crystals, followed by biochemical tests. Blood was collected through cardiac puncture, and serum was separated by centrifugation for the analysis of urea, uric acid, and creatinine levels. Water consumption and urinary output were measured at the end of the study.

5.18.5 Preparation of Kidney Homogenate

On the last day of study, the rats chosen for biochemical analysis were sacrificed by cervical dislocation at the end of the study. A 10% (w/v) homogenate in 0.1 M phosphate buffer (pH 7.4) was made after the tissues were removed. The homogenate was then centrifuged for 15 minutes at 3000 rpm, and the clear supernatant was collected for use in several biochemical tests to determine the levels of SOD, CAT, GST, and LPO.

5.18.6 Stone Markers Estimation

Calcium, magnesium, and potassium levels in tissue homogenate were analysed according to the manufacturer's protocol using an autoanalyzer.

5.18.7 Renal Histopathology

Following sacrifice and decapitation, the rats were dissected, and the kidneys were promptly removed and fixed in 10% neutral buffered formalin for 48 hours. The fixed kidneys were then processed for paraffin embedding and sectioning. Using a microtome, 5 μm thick sections were prepared, passed through a xylene-alcohol series, and stained with alum hematoxylin and eosin (H&E). The stained sections were then examined under a microscope to assess histopathological alterations.

5.19 Statistical analysis

All the results were persuasive as mean ± SEM. The one-way analysis of variance (ANOVA) followed by the Tukey test using GraphPad Prism software, was used to analyze the statistics of behavioural and biochemical data.The difference was considered to be significant when the level of significance was 5% ($p<0.05$).

CHAPTER 6

RESULTS

6.1 Data mining and similarity searching

Drug discovery has traditionally relied on the principle of molecular similarity, which suggests that structurally similar compounds often exhibit comparable biological activity. Earlier approaches primarily focused on two-dimensional molecular analysis to optimize lead compounds, but recent advancements have shifted towards three-dimensional conformational comparisons for improved drug target prediction, repurposing, and scaffold-hopping. However, the pharmaceutical industry faces significant challenges due to the rising costs of drug development and declining approval rates, necessitating innovative strategies for discovering effective therapeutics. One promising approach involves integrating Ayurvedic knowledge with modern drug discovery, utilizing historical medicinal practices to identify potential therapeutic agents from plant sources. In this study, structural similarity searches and molecular docking using AutoDock Vina were employed to screen compounds for their binding potential against target proteins. The most promising candidates, selected based on their favorable binding energy, subsequently underwent ADME analysis to evaluate their pharmacokinetic properties and drug-likeness, followed by toxicity assessments, molecular docking, and molecular dynamics simulations. This comprehensive and systematic methodology aims to identify naturally derived compounds that can be repurposed or developed into novel therapeutics with enhanced efficacy and minimal side effects, thereby addressing the growing need for safer and more effective treatment options (Kumar and Zhang, 2018; Atanasov et al., 2021).

Through this process, six phytochemicals—Quercetin, Resveratrol, Diosmin, Epigallocatechin-3-gallate, Rutin, and Catechin—were identified as potential candidates for further investigation (Table 6.1). Table 6.1 Briefs about phytochemicals reported in KS simultaneously with their epigenetic activity. But these epigenetic activities were reported with respect to other diseases like cancer. so here we are exploring this with respect to KS. These compounds will be subjected to in silico, in vitro, and in vivo studies to assess their therapeutic effects, particularly in managing nephrolithiasis and related conditions. This integrated approach highlights the potential of plant-based therapeutics in modern medicine, paving the way for the development of safer, more effective treatment options for complex diseases.

Table 6.1: Phytochemicals involved in treatment of KS along with their epigenetic activity.

S.No	Phytochemical	Nephrolithiasis activity	Epigenetic activity
1	Catechin	Reduces renal papillary calcification along with renal calcium crystallization reduction	Downregulating HDACs and DNMT1 expression in prostate cancer (Izzo et al., 2020)
2	Diosmin	Decreases degeneration of glomeruli and tubules, restoring the diameter of the capillaries and vessels in the cortex	Diosmin acted as a DNA hypomethylating agent in MCF-7 cells and DNA hypermethylating gent in SK-BR-3 cells (Lewinska et al., 2017).
3	Epigallocatechin -3-gallate	Decreases excretion of urinary oxalate and crystal-binding capability	Decreases histone acetylation, p300 and HDACs 1 & 2 binding at NF-kBp65 promoter regions
4	Quercetin	Decreases urinary crystal deposit formation	Restoring HAT/HDAC balance through ERK activation in cortex and hippocampus of OVX mice (Aggarwal et al., 2020)
5	Rutin	Inhibit calcium oxalate urolithiasis	DHT - 3,4-dihydroxytoluene (Rutin metabolite) reduces histone hyperacetylation in nonalcoholic fatty liver disease (Lee et al., 2020)
6	Resveratrol	Prevent hyperoxaluria by preventing oxidative stress factors and Randall plaque formation caused by free oxygen radicals (Oksay et al., 2017)	Increases Sirtuin activity and decreases activity of MMP9

Below-mentioned table shows the similar structures of the above-mentioned compounds:

Catechin: An antioxidant flavonoid, occurring especially in woody plants as both (+)-catechin and (-)-epicatechin (cis) forms. Also known as Cianidanol (2R,3S)-catechin, Catechuic acid, Cianidanolum, D-Catechol (source: drugbank) (Figure 6.1).

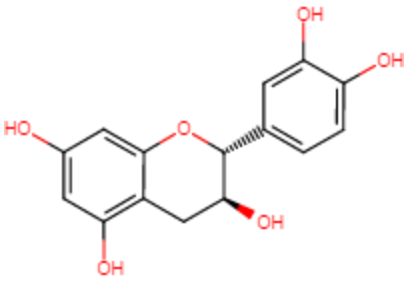

Figure 6.1: Catechin

Table 6.2: Similarity searching of Catechin

S.No	Similarity	Structure	SMILES	Drug bank	Compound Name
1	0.867	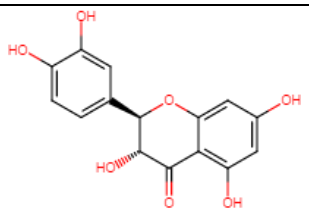	O[C@@H]1[C@H](OC2=CC(O)=CC(O)=C2C1=O)C1=CC=C(O)C(O)=C1	DB02224	Taxifolin C15H12O7 Mono mass: 304.058302738
2	0.867	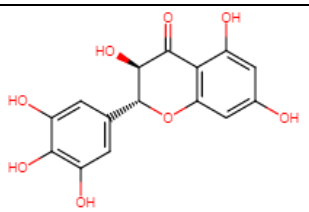	O[C@@H]1[C@H](OC2=C(C(O)=CC(O)=C2)C1=O)C1=CC(O)=C(O)C(O)=C1	DB15645	Dihydromyricetin $C_{15}H_{12}O_8$ Mono mass: 320.05321736
3	0.795	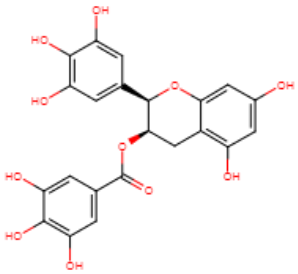	OC1=CC(O)=C2C[C@@H](OC(=O)C3=CC(O)=C(O)C(O)=C3)[C@H](OC2=C1)C1=CC(O)=C(O)C(O)=C1	DB12116	Epigallocatechin gallate $C_{22}H_{18}O_{11}$ Mono mass: 458.084911418

4	0.787	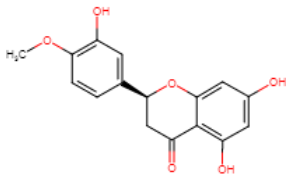	COC1=C(O)C=C(C=C1)[C@@H]1CC(=O)C2=C(O)C=C(O)C=C2O1	DB01094	Hesperetin C16H14O6 Mono mass: 302.07903818
5	0.749	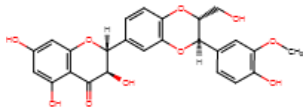	[H][C@@]1(OC2=C(O[C@@H]1CO)C=CC(=C2)[C@@]1([H])OC2=C(C(O)=CC(O)=C2)C(=O)[C@@H]1O)C1=CC(OC)=C(O)C=C1	DB09298	Silibinin $C_{25}H_{22}O_{10}$ Mono mass: 482.121296908
6	0.722	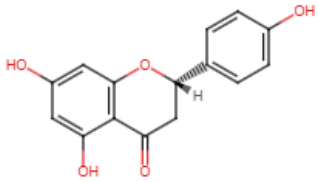	[H][C@]1(CC(=O)C2=C(O1)C=C(O)C=C2O)C1=CC=C(O)C=C1	DB03467	Naringenin
7	0.718	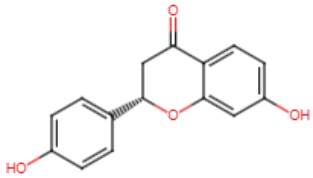	OC1=CC=C(C=C1)[C@@H]1CC(=O)C2=CC=C(O)C=C2O1	DB03601	5-deoxyflavanone $C_{15}H_{12}O_4$ Mono mass: 256.073558872
8	0.703	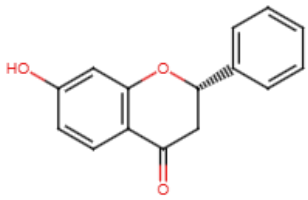	OC1=CC2=C(C=C1)C(=O)C[C@H](O2)C1=CC=CC=C1	DB04274	(2S)-7-hydroxyflavanone $C_{15}H_{12}O_3$ Mono mass: 240.07864425
9	0.691	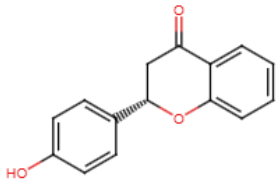	OC1=CC=C(C=C1)[C@@H]1CC(=O)C2=CC=CC=C2O1	DB04429	4-Hydroxyflavanone $C_{15}H_{12}O_3$ Mono mass: 240.07864425

10	0.641	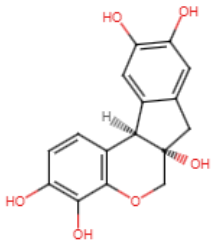	[H][C@]12C3=CC(O)=C(O)C=C3C[C@@]1(O)COC1=C2C=CC(O)=C1O	DB16871	Hematoxylin $C_{16}H_{14}O_6$ Mono mass: 302.079038171
11	0.629	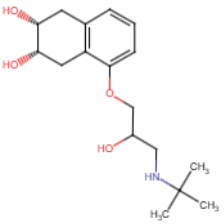	CC(C)(C)NCC(O)COC1=CC=CC2=C1C[C@H](O)[C@H](O)C2	DB01203	Nadolol $C_{17}H_{27}NO_4$ Mono mass: 309.194008357

Diosmin: It is a semisynthetic drug indicated for the treatment of venous disease. Diosmin is a flavone that can be found in the plant Teucrium gnaphalodes. Diosmin is available as a prescription medicine in several European countries, and is available as a nutritional supplement in the United States and the rest of Europe. It should be noted that clinical studies have been inconclusive and no articles have been published pertaining to its use in the treatment of vascular disease. When used in rats, diosmin has been effective at mitigating hyperglycaemia, and may also have anti-neurodegenerative properties (Figure 6.2).

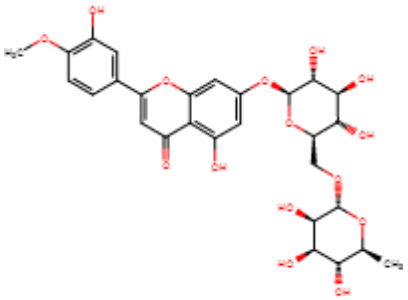

Figure 6.2: Diosmin

Table 6.3: Similarity searching of Diosmin

S.No	Similarity	Structure	SMILE	Drug bank Id	Compound Name
1	0.993	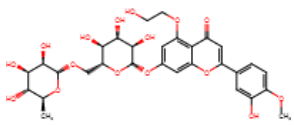	COC1=CC=C(C=C1O)C1=CC(=O)C2=C(OCCO)C=C(O[C@@H]3O[C@H](CO[C@@H]4O[C@@H](C)[C@H](O)[C@@H](O)[C@H]4O)[C@@H](O)[C@H](O)[C@H]3O)C=C2O1	DB13490	Hidrosmin C30H36O16 Mono mass: 652.200335079
2	0.852	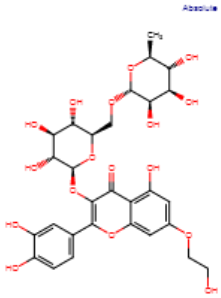	C[C@@H]1O[C@@H](OC[C@H]2O[C@@H](OC3=C(OC4=CC(OCCO)=CC(O)=C4C3=O)C3=CC=C(O)C(O)=C3)[C@H](O)[C@@H](O)[C@@H]2O)[C@H](O)[C@H](O)[C@H]1O	DB13764	Monoxerutin $C_{29}H_{34}O_{17}$ Mono mass: 654.179599635
3	0.834	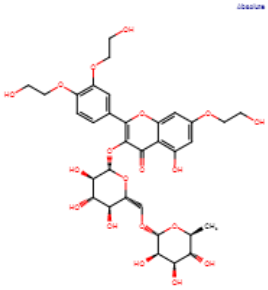	C[C@@H]1O[C@@H](OC[C@H]2O[C@@H](OC3=C(OC4=CC(OCCO)=CC(O)=C4C3=O)C3=CC(OCCO)=C(OCCO)C=C3)[C@H](O)[C@@H](O)[C@@H]2O)[C@H](O)[C@H](O)[C@H]1O	DB13124	Troxerutin $C_{33}H_{42}O_{19}$ Mono mass: 742.232029162

4	0.827	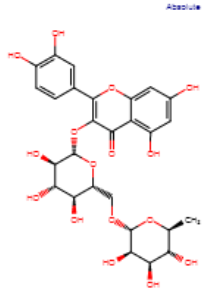	C[C@@H]1O[C@@H](OC[C@H]2O[C@@H](OC3=C(OC4=CC(O)=CC(O)=C4C3=O)C3=CC(O)=C(O)C=C3)[C@H](O)[C@@H](O)[C@@H]2O)[C@H](O)[C@H](O)[C@H]1O	DB01698	Rutin $C_{27}H_{30}O_{16}$ Mono mass: 610.153384912
5	0.812	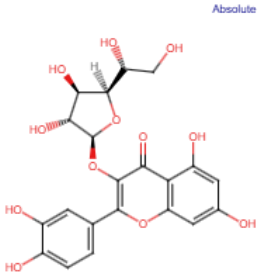	[H][C@@]1(O[C@@H](OC2=C(OC3=C(C(O)=CC(O)=C3)C2=O)C2=CC=C(O)C(O)=C2)[C@H](O)[C@H]1O)[C@H](O)CO	DB16403	Isoquercitrin $C_{21}H_{20}O_{12}$ Mono mass: 464.095476084
6	0.809	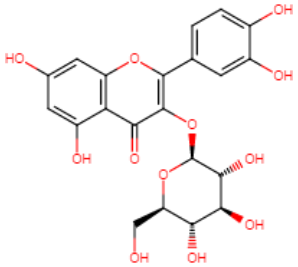	OC[C@H]1O[C@@H](OC2=C(OC3=C(C(O)=CC(O)=C3)C2=O)C2=CC=C(O)C(O)=C2)[C@H](O)[C@@H](O)[C@@H]1O	DB12665	Isoquercetin $C_{21}H_{20}O_{12}$ Mono mass: 464.095476104
	0.773	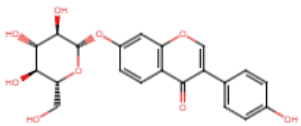	OC[C@H]1O[C@@H](OC2=CC3=C(C=C2)C(=O)C(=CO3)C2=CC=C(O)C=C2)[C@H](O)[C@@H](O)[C@@H]1O	DB02115	Daidzin $C_{21}H_{20}O_9$ Mono mass: 416.110732238
	0.753	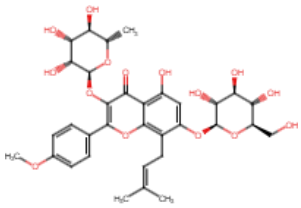	COC1=CC=C(C=C1)C1=C(O[C@@H]2O[C@@H](C)[C@H](O)[C@@H](O)[C@H]2O)C(=O)C2=C(O)C=C(O[C@@H]3O[C@H](CO)[C@@H](O)[C@H](O)[C@H]3O)C(CC=C(C)C)=C2O1	DB12052	Icariin $C_{33}H_{40}O_{15}$ Mono mass: 676.236720588

	0.719	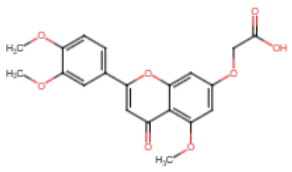	COC1=CC=C(C=C1OC)C1=CC(=O)C2=C(OC)C=C(OCC(O)=O)C=C2O1	DB12058	Recoflavone $C_{20}H_{18}O_8$ Mono mass: 386.10016754
	0.695	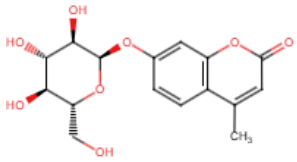	CC1=CC(=O)OC2=C1C=CC(O[C@H]1O[C@H](CO)[C@@H](O)[C@H](O)[C@H]1O)=C2	DB02639	7-(alpha-D-Glucopyranosyloxy)-4-methyl-2H-1-benzopyran-2-one $C_{16}H_{18}O_8$ Mono mass: 338.100167552
	0.695	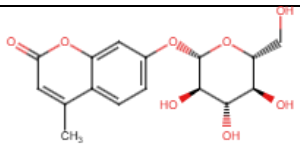	CC1=CC(=O)OC2=CC(O[C@@H]3O[C@H](CO)[C@@H](O)[C@H](O)[C@H]3O)=CC=C12	DB13177	4-methylumbelliferyl beta-D-glucoside $C_{16}H_{18}O_8$ Mono mass: 338.100167552
	0.688	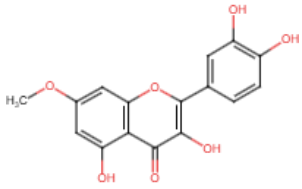	COC1=CC2=C(C(O)=C1)C(=O)C(O)=C(O2)C1=CC(O)=C(O)C=C1	DB16772	Rhamnetin $C_{16}H_{12}O_7$ Mono mass: 316.058302726
	0.668	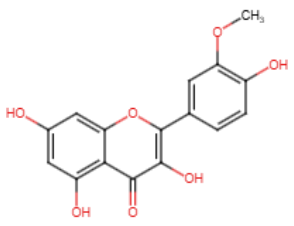	COC1=C(O)C=CC(=C1)C1=C(O)C(=O)C2=C(O)C=C(O)C=C2O1	DB16767	Isorhamnetin $C_{16}H_{12}O_7$ Mono mass: 316.058302726

	0.668	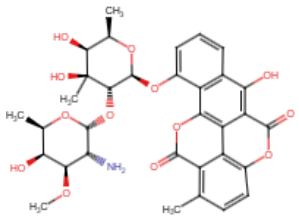	CO[C@@H]1[C@@H](N)[C@@H](O[C@H]2[C@H](OC3=CC=CC4=C3C3=C5C(C(=O)OC6=C5C(=C(C)C=C6)C(=O)O3)=C4O)O[C@H](C)[C@H](O)[C@]2(C)O)O[C@H](C)[C@@H]1O	DB05129	Elsamitrucin $C_{33}H_{35}NO_{13}$ Mono mass: 653.210840211
	0.664	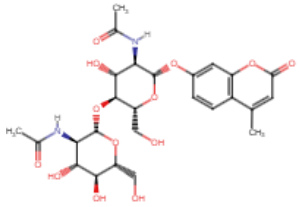	[H]N([C@H]1[C@H](O[C@@H]2[C@@H](CO)O[C@@H](OC3=CC4=C(C=C3)C(C)=CC(=O)O4)[C@H](N([H])C(C)=O)[C@H]2O)O[C@H](CO)[C@@H](O)[C@@H]1O)C(C)=O	DB02759	4-methyl-umbelliferyl-N-acetyl-chitobiose $C_{26}H_{34}N_2O_{13}$ Mono mass: 582.206089184
	0.664	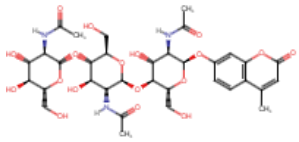	[H]N([C@H]1[C@H](O[C@@H]2[C@@H](CO)O[C@@H](O[C@@H]3[C@@H](CO)O[C@H](OC4=CC5=C(C=C4)C(C)=CC(=O)O5)[C@H](N([H])C(C)=O)[C@H]3O)[C@H](N([H])C(C)=O)[C@H]2O)O[C@H](CO)[C@@H](O)[C@@H]1O)C(C)=O	DB04268	Methylumbelliferyl chitotriose $C_{34}H_{47}N_3O_{18}$ Mono mass: 785.285461715
	0.66	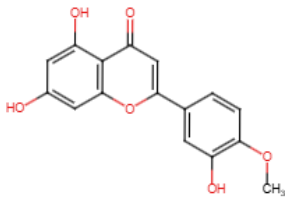	COC1=C(O)C=C(C=C1)C1=CC(=O)C2=C(O1)C=C(O)C=C2O	DB11259	Diosmetin $C_{16}H_{12}O_6$ Mono mass: 300.063388116

	0.656	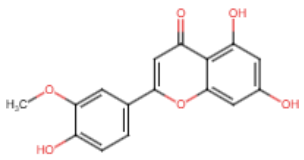	COC1=CC(=CC=C1O)C1=CC(=O)C2=C(O)C=C(O)C=C2O1	DB17283	Chrysoeriol $C_{16}H_{12}O_6$ Mono mass: 300.063388106
	0.653	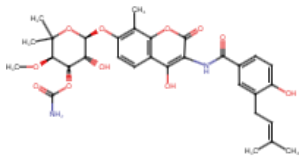	CO[C@@H]1[C@@H](OC(N)=O)[C@@H](O)[C@H](OC2=C(C)C3=C(C=C2)C(O)=C(NC(=O)C2=CC=C(O)C(CC=C(C)C)=C2)C(=O)O3)OC1(C)C	DB01051	Novobiocin $C_{31}H_{36}N_2O_{11}$ Mono mass: 612.231910004

Epigallocatechin-3-gallate: Epigallocatechin gallate has been investigated for the treatment of Hypertension and Diabetic Nephropathy (Figure 6.3).

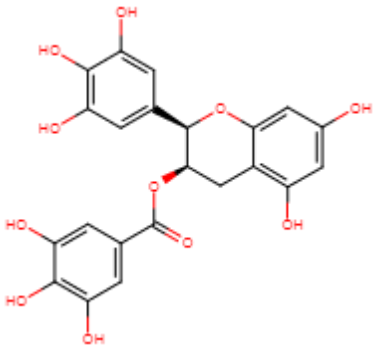

Figure 6.3: Epigallocatechin-3-gallate

Table 6.4: Similarity searching of Epigallocatechin-3-gallate

S. No	Similarity	Structure	SMILES:	Drug bank Id	Compound Name

1	0.8	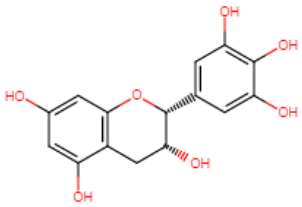	O[C@@H]1CC2=C(O[C@@H]1C1=CC(O)=C(O)C(O)=C1)C=C(O)C=C2O	DB3823	Epigallocatechin $C_{15}H_{14}O_7$ Mono mass: 306.073952802
2	0.8	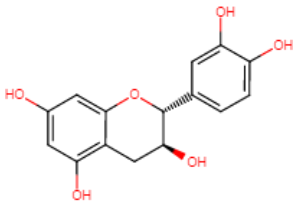	O[C@H]1CC2=C(O)C=C(O)C=C2O[C@@H]1C1=CC=C(O)C(O)=C1	DB14086	Cianidanol $C_{15}H_{14}O_6$ Mono mass: 290.07903818
3	0.77	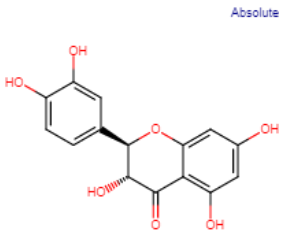	O[C@@H]1[C@H](OC2=CC(O)=CC(O)=C2C1=O)C1=CC=C(O)C(O)=C1	DB2224	Taxifolin $C_{15}H_{12}O_7$ Mono mass: 304.058302738
4	0.747	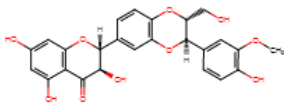	[H][C@@]1(OC2=C(O[C@@H]1CO)C=CC(=C2)[C@@]1([H])OC2=C(C(O)=CC(O)=C2)C(=O)[C@@H]1O)C1=CC(OC)=C(O)C=C1	DB09298	Silibinin $C_{25}H_{22}O_{10}$ Mono mass: 482.121296908
5	0.708	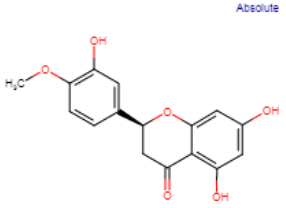	COC1=C(O)C=C(C=C1)[C@@H]1CC(=O)C2=C(O)C=C(O)C=C2O1	DB01094	Hesperetin $C_{16}H_{14}O_6$ Mono mass: 302.07903818

Quercetin: It is a flavonol widely distributed in plants. It is an antioxidant, like many other phenolic heterocyclic compounds. Glycosylated forms include rutin and quercetin (Figure 6.4).

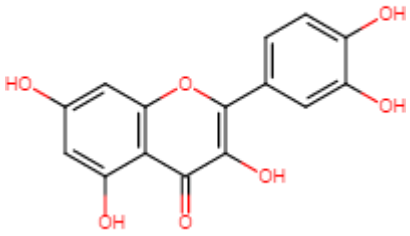

Figure 6.4: Quercetin

Table 6.5: Similarity searching of Quercetin

S.No	Similarity	Structure	SMILES	Drug bank Id	Compound Name
1	0.959	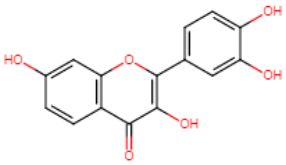	OC1=CC2=C(C=C1)C(=O)C(O)=C(O2)C1=CC=C(O)C(O)=C1	DB07795	Fisetin $C_{15}H_{10}O_6$ Mono mass: 286.047738052
2	0.946	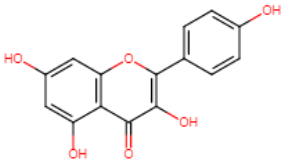	OC1=CC=C(C=C1)C1=C(O)C(=O)C2=C(O1)C=C(O)C=C2O	DB01852	Kaempherol $C_{15}H_{10}O_6$ Mono mass: 286.047738052
3	0.884	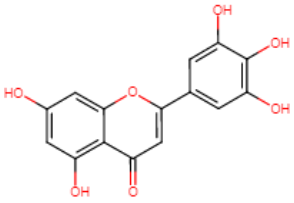	OC1=CC(O)=C2C(=O)C=C(OC2=C1)C1=CC(O)=C(O)C(O)=C1	DB08230	Tricetin $C_{15}H_{10}O_7$ Mono mass: 302.042652674
4	0.85	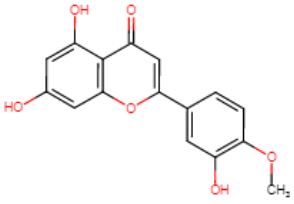	COC1=C(O)C=C(C=C1)C1=CC(=O)C2=C(O1)C=C(O)C=C2O	DB11259	Diosmetin $C_{16}H_{12}O_6$ Mono mass: 300.063388116

5	0.833	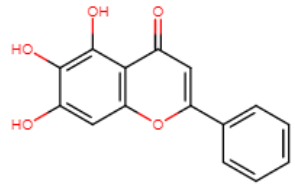	OC1=CC2=C(C(O)=C1O)C(=O)C=C(O2)C1=CC=CC=C1	DB16101	Baicalein $C_{15}H_{10}O_5$ Mono mass: 270.052823422

Rutin: A flavonol glycoside found in many plants, including buckwheat; tobacco; forsythia; hydrangea; viola, etc. It has been used therapeutically to decrease capillary fragility (Figure 6.5).

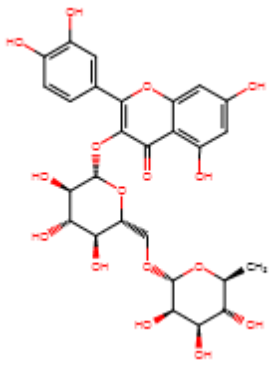

Figure 6.5: Rutin

Table 6.6: Similarity searching of Rutin

S. No	**Similarity**	**Structure**	**SMILES**	**Drug bank Id**	**Compound Name**

1	0.991	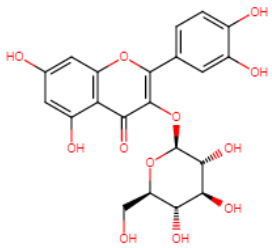	OC[C@H]1O[C@@H](OC2=C(OC3=C(C(O)=CC(O)=C3)C2=O)C2=CC=C(O)C(O)=C2)[C@H](O)[C@@H](O)[C@@H]1O	DB12665	**Isoquercetin** $C_{21}H_{20}O_{12}$ Mono mass: 464.095476104
2	0.983	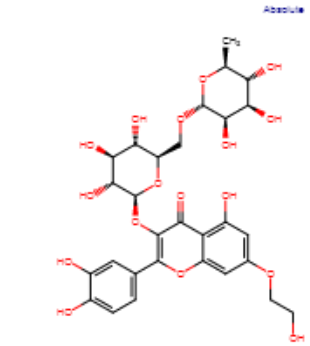	C[C@@H]1O[C@@H](OC[C@H]2O[C@@H](OC3=C(OC4=CC(OCCO)=CC(O)=C4C3=O)C3=CC=C(O)C(O)=C3)[C@H](O)[C@@H](O)[C@@H]2O)[C@H](O)[C@H](O)[C@H]1O	DB13764	**Monoxerutin** $C_{29}H_{34}O_{17}$ Mono mass: 654.179599635
3	0.959	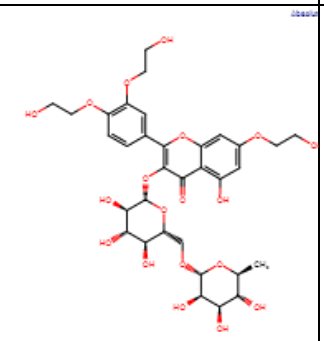	C[C@@H]1O[C@@H](OC[C@H]2O[C@@H](OC3=C(OC4=CC(OCCO)=CC(O)=C4C3=O)C3=CC(OCCO)=C(OCCO)C=C3)[C@H](O)[C@@H](O)[C@@H]2O)[C@H](O)[C@H](O)[C@H]1O	DB13124	**Troxerutin** $C_{33}H_{42}O_{19}$ Mono mass: 742.232029162
4	0.842	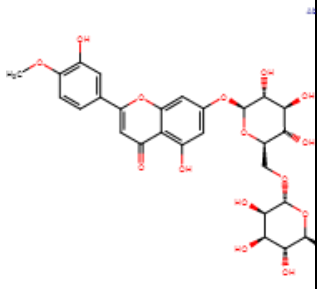	COC1=C(O)C=C(C=C1)C1=CC(=O)C2=C(O)C=C(O[C@@H]3O[C@H](CO[C@@H]4O[C@@H](C)[C@H](O)[C@@H](O)[C@H]4O)[C@@H](O)[C@H](O)[C@H]3O)C=C2O1	DB08995	**Diosmin** $C_{28}H_{32}O_{15}$ Mono mass: 608.174120354

5	0.835	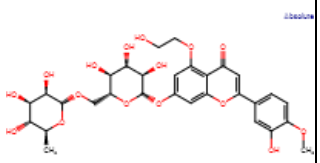	COC1=CC=C(C=C1O)C1=CC(=O)C2=C(OCCO)C=C(O[C@@H]3O[C@H](CO[C@@H]4O[C@@H](C)[C@H](O)[C@@H](O)[C@H]4O)[C@@H](O)[C@H](O)[C@H]3O)C=C2O1	DB1349	**Hidrosmin** $C_{30}H_{36}O_{16}$ Mono mass: 652.200335079

Resveratrol (3,5,4'-trihydroxystilbene): It is a polyphenolic phytoalexin. It is a stilbenoid, a derivate of stilbene, and is produced in plants with the help of the enzyme stilbene synthase. It exists as cis-(Z) and trans-(E) isomers. The trans- form can undergo isomerisation to the cis-form when heated or exposed to ultraviolet irradiation. In a 2004 issue of Science, Dr. Sinclair of Harvard University said resveratrol is not an easy molecule to protect from oxidation. It has been claimed that it is readily degraded by exposure to light, heat, and oxygen. However, studies find that Trans-resveratrol undergoes negligible oxidation in normal atmosphere at room temperature (Figure 6.6).

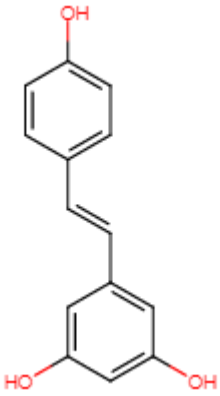

Figure 6.6: Resveratrol

Table 6.7: Similarity searching of Resveratrol

S. No	Similarity	Structure	SMILES	Drug bank Id	Compound Name
1	0.966	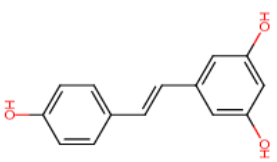	OC1=CC(\C=C\C2=CC=C(O)C(O)=C2)=CC(O)=C1	DB08399	Piceatannol $C_{14}H_{12}O_4$ Mono mass: 244.073558866

2	0.8	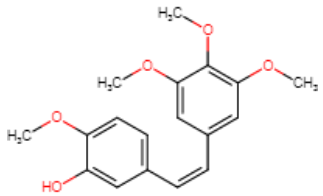	COC1=CC=C(\C=C/C2=CC(OC)=C(OC)C(OC)=C2)C=C1O	DB14680	Combretastatin A4 $C_{18}H_{20}O_5$ Mono mass: 316.131073744
3	0.761	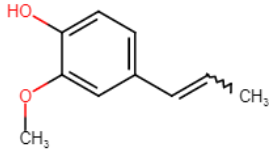	COC1=CC(C=CC)=CC=C1O	DB14188	Isoeugenol $C_{10}H_{12}O_2$ Mono mass: 164.083729626
4	0.757	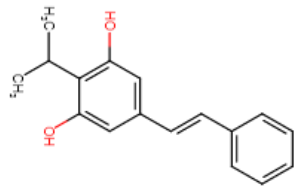	CC(C)C1=C(O)C=C(\C=C\C2=CC=CC=C2)C=C1O	DB06083	Tapinarof $C_{17}H_{18}O_2$ Mono mass: 254.13067982
5	0.719	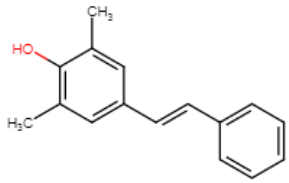	CC1=CC(\C=C\C2=CC=CC=C2)=CC(C)=C1O	DB08100	2,6-dimethyl-4-[(E)-2-phenylethenyl] phenol $C_{16}H_{16}O$ Mono mass: 224.120115134

Table 6.2 to Table 6.7 reports similarity searching of various phytochemicals. Their other properties like mol wt. and SMILE structures have also been drawn so as to use in ADME and toxicity studies. These structures were then compiled; duplicates were removed and used for multiple screening.

6.2 Level 1 screening: Based on Lipinski's rule of five (RO5)

Initially, six parent compounds were selected for similarity searching, which yielded 67 similar compounds. These compounds were subjected to Lipinski's rule of five (RO5) for screening, resulting in the selection of 51 molecules that satisfied the RO5 criteria. Detailed results are provided in Table 6.8.

The analysis showed that most compounds exhibited consistent patterns within their respective groups. For example, similar compounds derived from Catechin, Quercetin, and Resveratrol adhered to Lipinski's rule, supporting the hypothesis that "similar structures possess similar activity." However, this hypothesis holds true only to a certain extent, as not all classes demonstrated a uniform pattern in adhering to the criteria. This indicates variability in the activity and properties of compounds within and across structural groups.

Table 6.8: List of similar compounds derived from parental compounds, validating Lipinski's rule.

Parent Compound	**Similar compound**	**Similarity score**	**Lipinski rule**
Catechin	Cianidanol	1	Yes
	Hesperetin	0.787	Yes
	Silibinin	0.749	Yes
	Naringenin	0.722	Yes
	Sakuranetin	0.72	Yes
	5-deoxyflavanone	0.718	Yes
	(2S)-7-hydroxyflavanone	0.703	Yes
	4-Hydroxyflavanone	0.691	Yes
	Hematoxylin	0.641	Yes
	Nadolol	0.629	Yes
Diosmin	Hidrosmin	0.993	No
	Daidzin	0.773	Yes
	Icariin	0.753	No
	Elsamitrucin	0.668	No
	4-methyl-umbelliferyl-N-acetyl-chitobiose	0.664	No
	Methylumbelliferyl chitotriose	0.664	No
	Diosmetin	0.66	Yes
	Chrysoeriol	0.656	Yes
	Eupatilin	0.64	Yes

	Caflanone	0.638	Yes
	Methylumbelliferyl sialic acid	0.636	No
	Tricetin	0.631	Yes
	Luteolin	0.631	Yes
Epigallocatechin -3-gallate	Epigallocatechin	0.795	Yes
	Epicatechin	0.795	Yes
	Taxifolin	0.799	Yes
	Dihydromyricetin	0.799	Yes
	Hesperidin	0.679	No
	Erteberel	0.624	Yes
	rotenone	0.623	Yes
Quercetin	Myricetin	1	Yes
	Fisetin	0.965	Yes
	Isorhamnetin	0.952	Yes
	Rhamnetin	0.948	Yes
	Kaempherol	0.92	Yes
	Morin	0.88	Yes
	Apigenin	0.81	Yes
	Baicalein	0.784	Yes
	Hispidulin	0.782	Yes
	Chrysin	0.78	Yes
	Icaritin	0.747	Yes
	recoflavone	0.742	Yes
	flavone	0.675	Yes
	beta-Naphthoflavone	0.673	Yes
	alpha-Naphthoflavone	0.67	Yes
Rutin	Isoquercitrin	0.984	No
	Isoquercetin	0.981	No
	Monoxerutin	0.975	No
	Troxerutin	0.948	No
	Coumermycin A1	0.63	No
	Quercetin-3'-O-phosphate	0.656	No
	Vitexin	0.637	Yes
	esculin	0.622	Yes
	Clorobiocin	0.619	No
	Thiocolchicoside	0.612	No
	Rifalazil	0.606	No

Resveratrol	Piceatannol	0.958	Yes
	Pterostilbene	0.841	Yes
	Combretastatin A4	0.775	Yes
	Isoeugenol	0.723	Yes
	Tapinarof	0.711	Yes
	2,6-dimethyl-4-[(E)-2-phenylethenyl]phenol	0.667	Yes
	5-(3,3-Dihydroxypropeny)-3-Methoxy-Benzene-1,2-Diol	0.663	Yes
	3,4-Dihydroxycinnamic Acid	0.663	Yes
	Anethole	0.641	Yes
	4-Vinylguaiacol	0.639	Yes
	Sinapic acid	0.625	Yes

6.3 Level 2 Screening: Based on ADME studies

51 molecules selected in the initial screening were further subjected to ADME analysis, evaluating parameters such as water solubility, CYP2C19, CYP2C9, and CYP2D6 inhibition, bioavailability score, PAINS (Pan-Assay Interference Compounds), and BRENK alerts. Molecules with high or moderate solubility, non-CYP inhibition properties, a good bioavailability score, and no PAINS or BRENK alerts were retained for further study (Table 6.9).

Table 6.9: Solubility, CYP inhibition and bioavailability score of shortlisted compounds.

Compounds	**Water Solubility**	**CYP2C19 Inhibitor**	**CYP 2C9 Inhibitor**	**CYP2D6 Inhibitor**	**Bioavailibility Score**	**Pains**	**Brenk**
Hesperetin	Soluble	No	No	No	0.55	0	0
Silibinin	Moderately Soluble	No	No	No	0.55	0	0
Naringenin	Soluble	No	No	No	0.55	0	0
Sakuranetin	Moderately Soluble	Yes	No	No	0.55	0	0
5-Deoxyflavanone	Soluble	No	No	No	0.55	0	0
Cianidanol	Soluble	No	No	No	0.55	1	1
(2S)-7-Hydroxyflavanone	Moderately Soluble	No	No	No	0.55	0	0
4-Hydroxyflavanone	Moderately Soluble	No	No	No	0.55	0	0

Hematoxylin	Soluble	No	No	No	0.55	1	1
Nadolol	Soluble	No	No	No	0.55	0	0
Daidzin	Soluble	No	No	No	0.55	0	0
Diosmetin	Moderately Soluble	No	Yes	Yes	0.55	0	0
Chrysoeriol	Moderately Soluble	No	Yes	Yes	0.55	0	0
Eupatilin	Moderately Soluble	No	Yes	Yes	0.55	0	0
Caflanone	Moderately Soluble	No	Yes	No	0.55	0	1
Tricetin	Soluble	No	No	Yes	0.55	1	1
Luteolin	Soluble	No	No	Yes	0.55	1	1
Epigallocatechin	Soluble	No	No	No	0.55	1	1
Epicatechin	Soluble	No	No	No	0.55	1	1
Taxifolin	Soluble	No	No	No	0.55	1	1
Dihydromyricetin	Soluble	No	No	No	0.55	1	1
Erteberel	Moderately Soluble	Yes	No	Yes	0.55	0	1
Rotenone	Poorly Soluble	Yes	Yes	Yes	0.55	0	1
Fisetin	Soluble	No	No	Yes	0.55	1	1
Myricetin	Soluble	No	No	No	0.55	1	1
Isorhamnetin	Soluble	No	No	Yes	0.55	0	0
Rhamnetin	Soluble	No	No	Yes	0.55	1	1
Kaempherol	Soluble	No	No	Yes	0.55	0	0
Morin	Soluble	No	No	Yes	0.55	0	0
Apigenin	Moderately Soluble	No	No	Yes	0.55	0	0
Baicalein	Moderately Soluble	No	No	Yes	0.55	1	1
Hispidulin	Moderately Soluble	No	No	Yes	0.55	0	0
Chrysin	Moderately Soluble	No	No	Yes	0.55	0	0
Icaritin	Moderately Soluble	No	Yes	No	0.55	0	1
Recoflavone	Moderately Soluble	No	Yes	No	0.56	0	0
Flavone	Poorly Soluble	Yes	No	No	0.55	0	0

Beta-Naphthoflavone	Poorly Soluble	Yes	No	No	0.55	0	1
Alpha-Naphthoflavone	Poorly Soluble	Yes	No	No	0.55	0	1
Vitexin	Soluble	No	No	No	0.55	0	0
Esculin	Soluble	No	No	No	0.55	0	1
Piceatannol	Soluble	No	Yes	No	0.55	1	2
Combretastatin A4	Moderately Soluble	Yes	Yes	Yes	0.55	0	1
Isoeugenol	Soluble	No	No	No	0.55	0	0
Tapinarof	Moderately Soluble	Yes	Yes	Yes	0.55	0	1
Anethole	Soluble	No	No	No	0.55	0	0
Pterostilbene	Moderately Soluble	Yes	Yes	Yes	0.55	0	0
3,4-Dihydroxycinnamic Acid	Soluble	No	No	No	0.56	1	2
4-Vinylguaiacol	Soluble	No	No	No	0.55	0	0
2,6-Dimethyl-4-[(E)-2-Phenylethenyl]Phenol	Moderately Soluble	Yes	No	Yes	0.55	0	1
5-(3,3-Dihydroxypropeny)-3-Methoxy-Benzene-1,2-Diol	Soluble	No	No	No	0.55	1	2
Sinapic Acid	Soluble	No	No	No	0.56	0	1

Compounds failing to meet these criteria were eliminated, leaving 12 molecules that satisfied all the ADME requirements (Table 6.10). The final shortlisted molecules were Hesperetin, Silibinin, Naringenin, 5-Deoxyflavanone, (2S)-7-Hydroxyflavanone, 4-Hydroxyflavanone, Nadolol, Daidzin, Vitexin, Isoeugenol, Anethole, and 4-Vinylguaiacol. These molecules were selected for subsequent analysis due to their favourable pharmacokinetic profiles.

6.4 Level 3 Screening: Based on toxicity

From the above ADME criteria, 12 molecules were initially shortlisted (Table 6.10). The specific parameters used for this step, as detailed in the methodology section, were applied to

further refine the selection. This filtering process eliminated 7 molecules, leaving 5 final candidates: 4-Vinylguaiacol, Anethole, Isoeugenol, Nadolol, and Silibinin (Figure 6.7). These molecules were carried forward for subsequent experiments.

Table 6.10: Toxicity prediction and analysis of shortlisted compounds using different signaling pathways (IN- inactive, AC-active).

Compounds	**HPT**	**MTG**	**CYT**	**AR**	**AR-LBD**	**Aromatase**	**ER**	**ER-LBD**	**PPAR-γ**	**NRF2/ ARE**	**HSE**	**MMP**	**p53**
Hesperetin	IN	IN	IN	IN	IN	IN	AC	AC	IN	IN	IN	AC	IN
Silibinin	**IN**	**IN**	**IN**	**IN**	**IN**	**IN**	**IN**	**IN**	**IN**	**IN**	**IN**	**IN**	**IN**
Naringenin	IN	IN	AC	IN	IN	IN	AC	AC	AC	IN	IN	AC	AC
5-deoxyflavanone	IN	IN	IN	IN	IN	IN	AC	AC	IN	IN	IN	AC	IN
(2S)-7-hydroxyflavanone	IN	IN	AC	IN	IN	IN	AC	IN	IN	IN	IN	AC	IN
4-Hydroxyflavanone	IN	IN	AC	IN	IN	IN	AC	IN	IN	IN	IN	AC	IN
Nadolol	**IN**	**IN**	**IN**	**IN**	**IN**	**IN**	**IN**	**IN**	**IN**	**IN**	**IN**	**IN**	**IN**
Daidzin	IN	IN	IN	IN	IN	IN	IN	IN	IN	IN	IN	IN	AC
Vitexin	IN	AC	AC	IN	IN	IN	IN	IN	IN	IN	IN	IN	IN
Isoeugenol	**IN**	**IN**	**IN**	**IN**	**IN**	**IN**	**IN**	**IN**	**IN**	**IN**	**IN**	**IN**	**IN**
Anethole	**IN**	**IN**	**IN**	**IN**	**IN**	**IN**	**IN**	**IN**	**IN**	**IN**	**IN**	**IN**	**IN**
4-Vinylguaiacol	**IN**	**IN**	**IN**	**IN**	**IN**	**IN**	**IN**	**IN**	**IN**	**IN**	**IN**	**IN**	**IN**

*Bold compounds were taken for further studies

Table abbrevations: Hepatotoxicity (HPT), Mutagenicity (MTG), Cytotoxicity (CYT), androgen receptor (AR), androgen receptor ligand binding domain (AR-LBD), aromatase, estrogen receptor alpha (ER), estrogen receptor ligand binding domain (ERLBD), and peroxisome proliferator-activated receptor gamma (PPAR-γ), Nuclear factor (erythroid-derived 2)-like 2/antioxidant responsive element (nrf2/ARE), Heat shock factor response element (HSE), Mitochondrial Membrane Potential (MMP) and Phosphoprotein (Tumor Suppressor) p53.

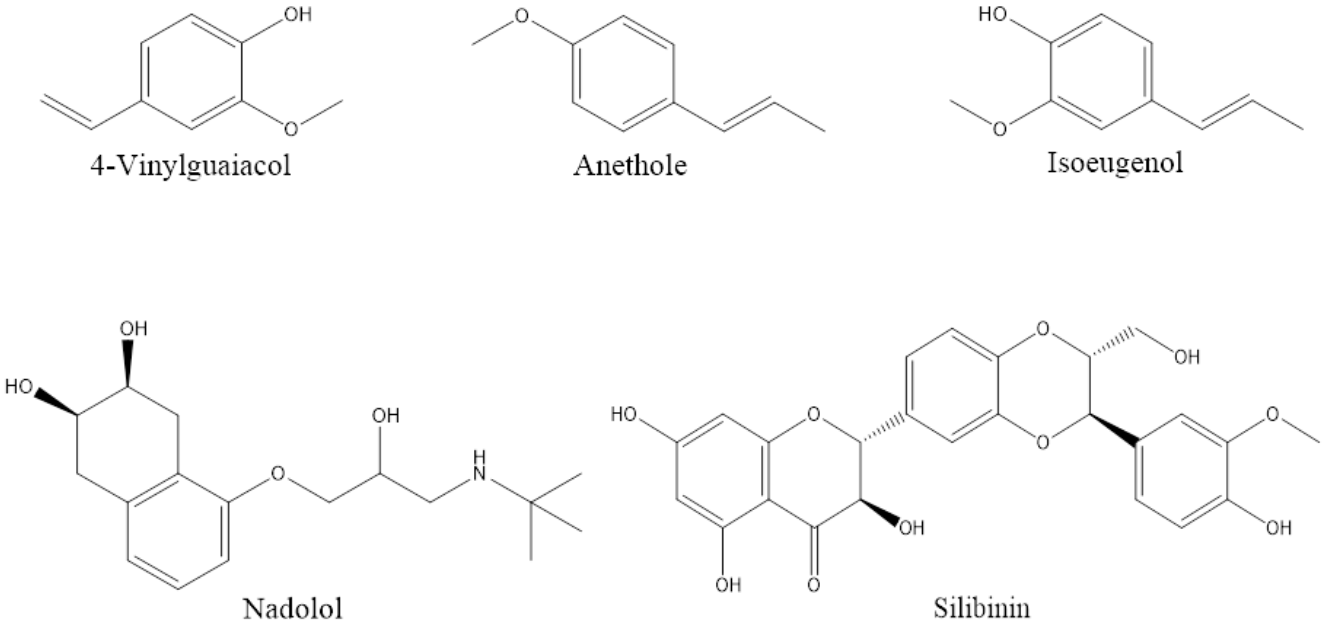

Figure 6.7: 2D structure of shortlisted phytochemicals.

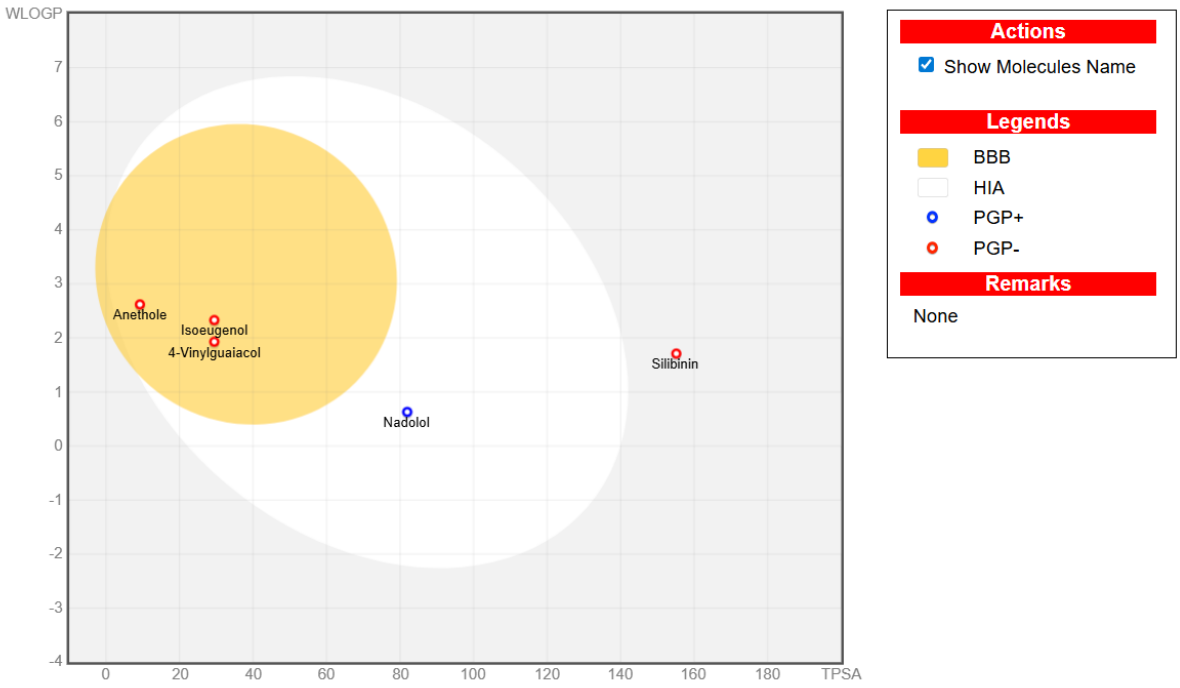

Fig 6.8: Boiled egg representation of shortlisted phytochemicals

The Boiled-Egg diagram is used for a straightforward assessment of passive gastrointestinal absorption indicated by the white section and BBB indicated by the yellow section. Additionally, blue and red points represent P-glycoprotein (P-gp) positivity and negativity concerning the position of small molecules in the WLOGP-versus-TPSA graph. The Boiled egg plots in Figure 6.8 depict 4-Vinylguaiacol, Anethole, Isoeugenol, Nadolol, and Silibinin

6.5 Core Hub Genes in Nephrolithiasis Treatment Identified Through Phytochemical Targeting

After applying multiple screenings using Lipinski's rule of five, ADME, and toxicity filters, five compounds 4-Vinylguaiacol, anethole, isoeugenol, nadolol, and silibinin—were shortlisted, with their 2D structures shown in Figure 6.7. Each phytochemical was then analyzed using Swiss Target Prediction, yielding 100 unique genes per compound, which were further filtered against duplicates. After merging, 329 compound genes remained, which were mapped against 3,713 disease-related targets, resulting in 191 common targets as shown in the Venn diagram in Figure 6.9.

These common targets were uploaded to the STITCH database to visualize the protein-protein interaction (PPI) network, depicted in Figure 6.10. Using Homo sapiens as the target organism and setting the minimum interaction score to 0.7, the network comprised 191 nodes and 628

edges, with an average node degree of 6.58. The PPI enrichment p-value was < 1.0e-16. Here, the nodes represent relevant targets, while the edges indicate protein-protein interactions.

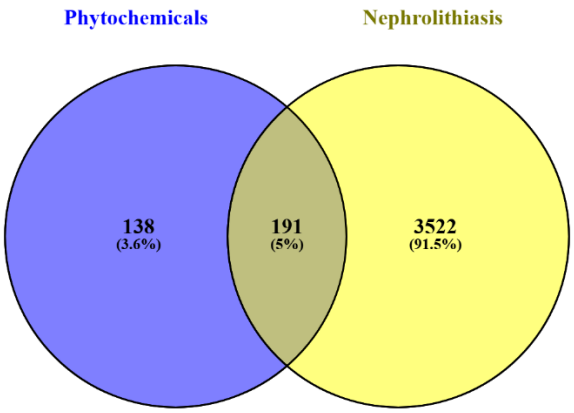

Figure 6.9: Venn diagram showing targets of phytochemicals and nephrolithiasis disease where the intersection represents the number of common targets between the two sets.

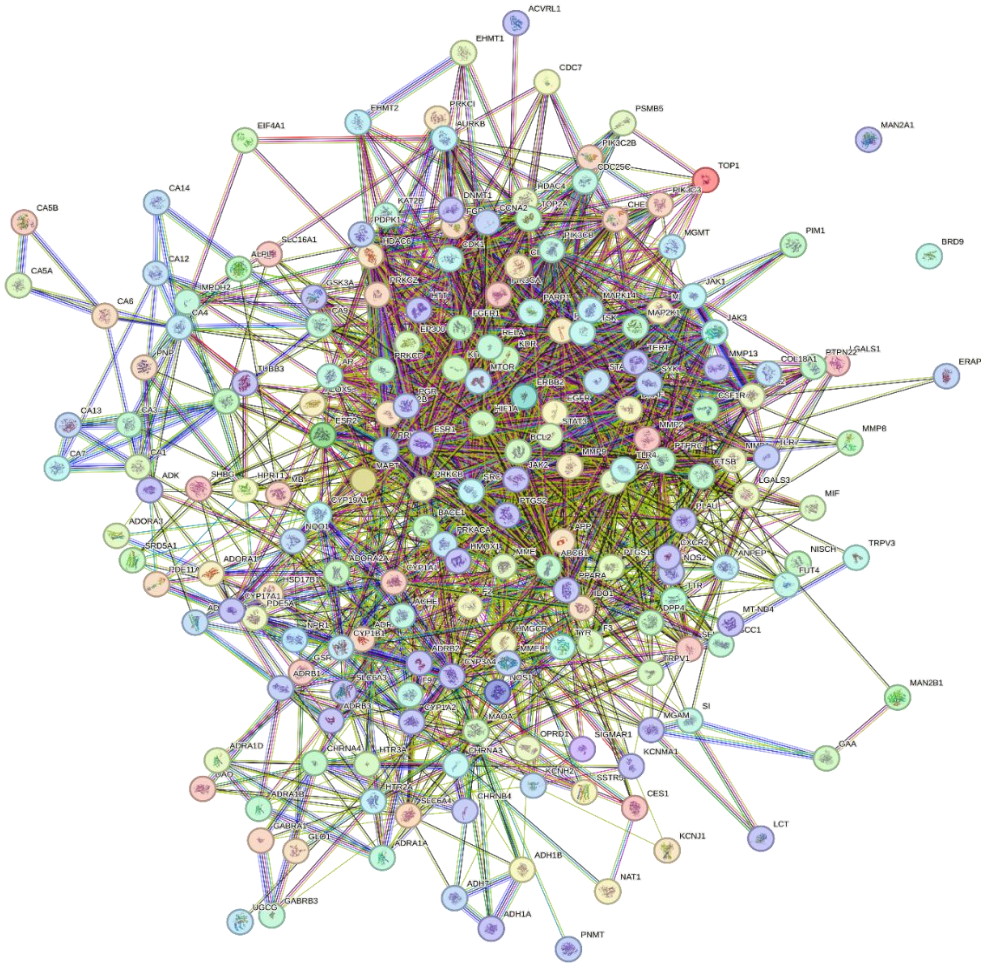

Figure 6.10: Protein-protein network of common targets between phytochemicals and nephrolithiasis

6.6 Gene ontology and pathway analysis

Gene ontology (GO) and KEGG pathway analysis were performed to assess the function and enriched pathways associated with nephrolithiasis-related genes using the ShinyGO 0.81 server. The analysis identified the top 30 biological pathways affecting biological properties such as biological process (BP), cellular component (CC), and molecular function (MF), as depicted in Figure 6.11 based on the number of genes involved.

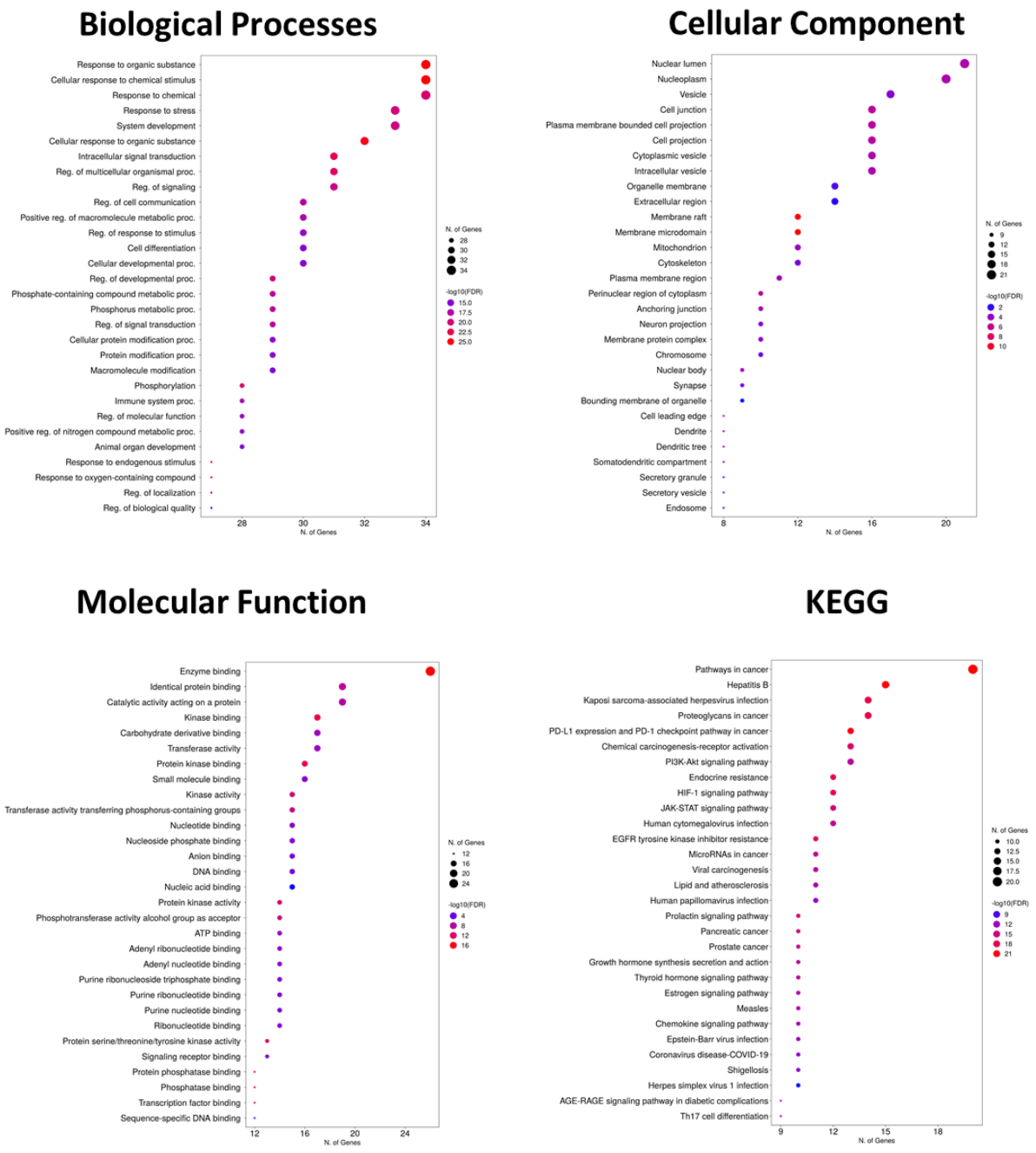

Figure 6.11: Dot plot diagram of three gene ontology processes and KEGG pathway analysis**.** Here, the size of the dot indicates the number of genes large dot confers a large gene number on a scale of blue to red, where red refers to high fold enrichment.

A total of 1517 statistically significant GO terms were found, including 100 BP, 217 CC, and 300 MF terms. The top BP terms included response to organic substance, cellular response to chemical stimulus, and response to chemical. The top CC terms were nuclear lumen, nucleoplasm, and vesicle, while the top MF terms included enzyme binding, identical protein binding, and catalytic activity acting on a protein. Furthermore, 190 significant KEGG pathways were identified, with key pathways involved in cancer, Hepatitis B, and Kaposi sarcoma-associated herpesvirus infection, highlighting the diverse biological activities of the shortlisted phytochemicals and disease-associated key genes.

6.7 Disease-phytochemical-target-pathway network construction

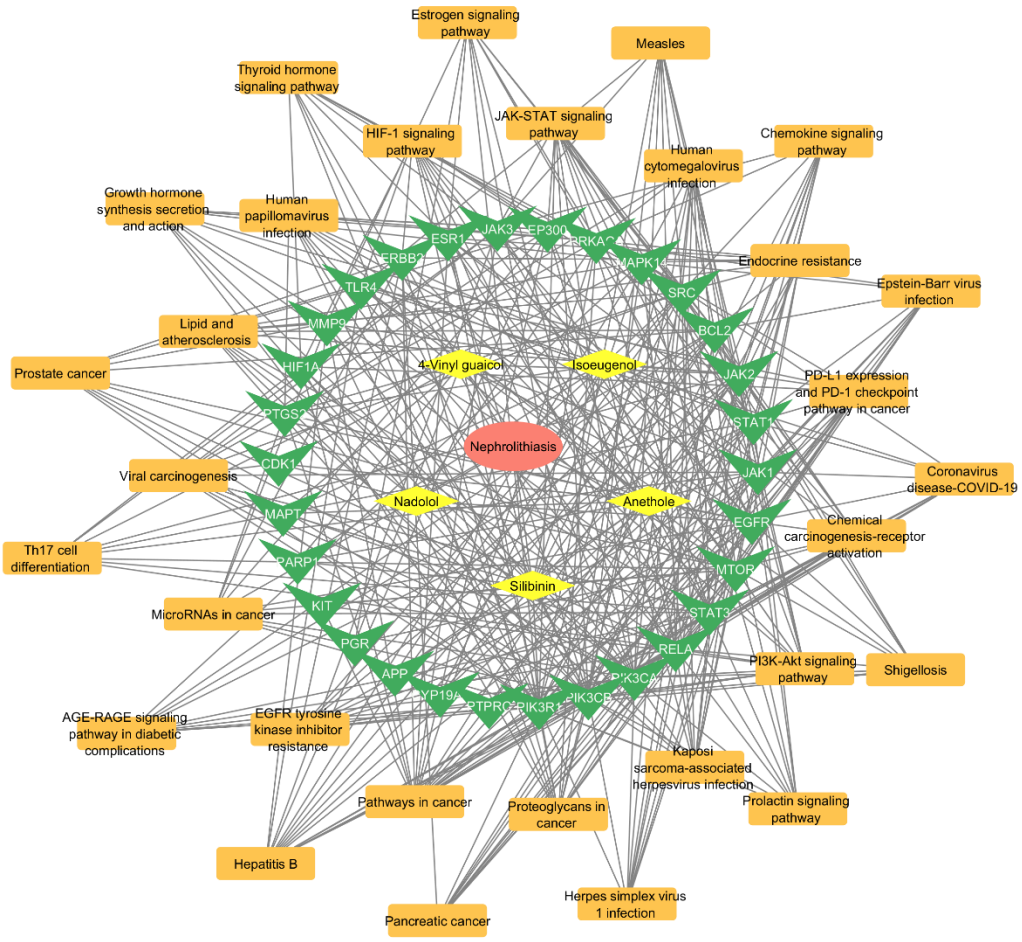

Figure 6.12: Disease-phytochemical-target-pathway network**.** Here innermost circle (brick red) represent disease, the outer circle (yellow) represents phytochemicals, the inverted triangle (green) represents targets and the rectangle (light orange) represents pathways.

A disease-phytochemical-target-pathway network was constructed and analyzed using the Network Analyzer tool in Cytoscapeas shown in Figure 6.12. The targets of the selected phytochemicals were as follows:

- **4-Vinylguaiacol** targets include RELA, SRC, PARP1, MAPT, PTGS2, ERBB2, EGFR, CDK1, JAK1, JAK2, and PGR.
- **Anethole** targets include RELA, ESR1, PTGS2, TLR4, MAPT, CYP19A1, APP, JAK1, JAK2, STAT3, JAK3, EGFR, PTPRC, PARP1, and CDK1.
- **Isoeugenol** targets include RELA, PTGS2, ESR1, EGFR, MAPT, CYP19A1, PARP1, SRC, APP, STAT3, EP300, MMP9, JAK1, and JAK2.
- **Nadolol** targets include PRKACA, EGFR, CDK1, and MTOR.
- **Silibinin** targets include MAPT, STAT1, SRC, BCL2, MAPK14, KIT, HIF1A, CYP19A1, APP, MMP9, MTOR, PIK3CB, PIK3CA, PARP1, ESR1, PRKACA, and PIK3R1.

Among all the phytochemicals, silibinin exhibited the highest number of gene targets, highlighting its broad potential in addressing nephrolithiasis-related pathways and interactions.

6.8 Level 4 Screening: Using molecular docking

Comparison of the docked pose with the crystallographic ligand (4TQ) revealed a close overlap within the binding pocket, as illustrated in Figure 6.13. Quantitative assessment yielded an RMSD of 1.970 Å, indicating that the docking parameters were able to effectively reproduce the experimentally observed binding conformation. These findings demonstrate that the implemented docking strategy is reliable and appropriate for application in virtual screening workflows. The molecular docking analysis of shortlisted phytochemicals with SIRT1 (PDB ID: 4ZZJ) provided valuable insights into their binding affinities, interacting residues, and potential inhibitory effects. The docking studies were performed using Discovery Studio and LigPlot, with the results highlighting key interactions, including hydrogen bonding and hydrophobic interactions. The binding energies of the compounds ranged from -5.0 kcal/mol to -7.9 kcal/mol, with stronger binding affinities indicating better stability of the ligand-protein complex (Table 6.11).The co-crystallized ligand exhibited the strongest binding energy of -7.9 kcal/mol, interacting with ILE227, GLU230, PRO212, LEU206, THR209, ILE223, ASN226, GLN222, THR219, LEU215, PRO211, and ILE210 in Discovery Studio and PRO293,

PHE273, ASP277, GLY278, ALA281, TYR280, ALA284, and PRO288 in LigPlot. This serves as a reference for comparing the efficacy of other phytochemicals (Figure 6.14).

4-Vinylguaiacol demonstrated the weakest binding energy of -5.0 kcal/mol, interacting with GLY261, ILE316, PHE312, GLN345, ASN346, ILE347, PHE273, ALA262, VAL445, PHE297, and PHE414 in Discovery Studio and ALA262, ASN346, GLY261, GLN345, PHE297, and PHE273 in LigPlot. The absence of strong hydrogen bonding and fewer stabilising interactions suggests relatively weaker binding compared to other phytochemicals (Figure 6.15).

Anethole exhibited a binding energy of -5.9 kcal/mol, interacting with ILE347, PHE297, VAL412, PHE413, HIS363, PHE414, VAL445, ILE411, GLN345, and PHE312 in Discovery Studio and VAL445, PHE414, PHE297, ILE316, PHE312, PRO271, ALA262, and PHE273 in LigPlot. The moderate binding affinity indicates potential inhibitory activity, although additional validation is required (Figure 6.16).

Isoeugenol had a binding energy of -6.4 kcal/mol, showing interactions with PHE312, ALA262, GLY263, ARG274, ASP272, GLY440, SER441, SER442, LEU443, LYS444, GLN345, VAL445, and PHE273 in Discovery Studio and GLY440, SER442, LEU443, SER441, GLN345, PHE273, and ALA262 in LigPlot. The presence of multiple hydrogen bonds suggests a relatively stable binding pose (Figure 6.17).

Nadolol exhibited a binding energy of -5.8 kcal/mol, with Discovery Studio revealing interactions with GLN294, PRO293, ARG274, PHE273, TYR658, SER275, ARG276, ASP277, ILE279, TYR280, ALA281, LYS444, and GLY278 and LigPlot showing similar residues, including PHE273, GLN294, PRO293, SER275, ARG276, GLY278, ALA281, TYR280, ASP277, TYR658, and ARG274. Despite moderate binding energy, the presence of hydrogen bonds enhances its potential inhibitory effect (Figure 6.18).

Silibinin exhibited a high binding affinity among the tested compounds with a binding energy of -7.4 kcal/mol. The interacting residues identified in Discovery Studio included ASP272, PHE273, SER441, SER442, LYS444, PRO293, ARG274, GLN294, ASP292, TYR658, SER659, ALA262, VAL445, HIS363, and PHE297, whereas LigPlot analysis confirmed interactions with GLN294, ASP292, PRO293, TYR658, ARG274, SER442, ALA262, PHE273, PHE297, and LYS444. The presence of hydrogen bonding interactions with key residues suggests strong stabilization within the active site (Figure 6.19).

Overall, the molecular docking studies indicate that Silibinin, with its strong binding affinity and extensive hydrogen bonding interactions, holds the most promise as a SIRT1 modulator in nephrolithiasis treatment. Isoeugenol and Anethole also exhibit moderate potential, whereas 4-Vinylguaiacol and Nadolol show weaker binding interactions.

Table 6.11: Binding energy and interacting residues after performing molecular docking of shortlisted phytochemicals. Bold residues indicate hydrogen bonding.

Compounds	**Binding energy**	**Discovery Studio Interacting Residues**	**Ligplot Interacting Residues**
Co-crystallized	-7.9	ILE227, **GLU230,** PRO212, LEU206, THR209, ILE223, **ASN226,** GLN222, THR219, LEU215, PRO211, ILE210	PRO293, PHE273, ASP277, GLY278, ALA281, TYR280, ALA284, PRO288
4-Vinylguaiacol	-5	GLY261, ILE316, PHE312, **GLN345, ASN346,** ILE347, PHE273, ALA262, VAL445, PHE297, PHE414	ALA262, **ASN346,** GLY261, GLN345, PHE297, PHE273
Anethole	-5.9	ILE347, PHE297, VAL412, PHE413, HIS363, PHE414, VAL445, ILE411, GLN345, PHE312	VAL445, PHE414, PHE297, ILE316, PHE312, PRO271, ALA262, PHE273
Isoeugenol	-6.4	PHE312, ALA262, GLY263, ARG274, ASP272, GLY440, **SER441,** SER442, LEU443, LYS444, GLN345, VAL445, PHE273	GLY440, **SER442, LEU443, SER441,** GLN345, PHE273, ALA262,
Nadolol	-5.8	GLN294, PRO293, ARG274, PHE273, TYR658, **SER275,** ARG276, ASP277, ILE279, TYR280, **ALA281,** LYS444, GLY278	**PHE273,** GLN294, PRO293, **SER275,** ARG276, **GLY278, ALA281,** TYR280, ASP277, TYR658, ARG274
Silibinin	-7.4	ASP272, **PHE273,** SER441, SER442, LYS444, PRO293, ARG274, **GLN294, ASP292,** TYR658, **SER659,** ALA262, VAL445, HIS363, PHE297	**GLN294,** ASP292, PRO293, TYR658, **ARG274, SER442,** ALA262, **PHE273,** PHE297, LYS444

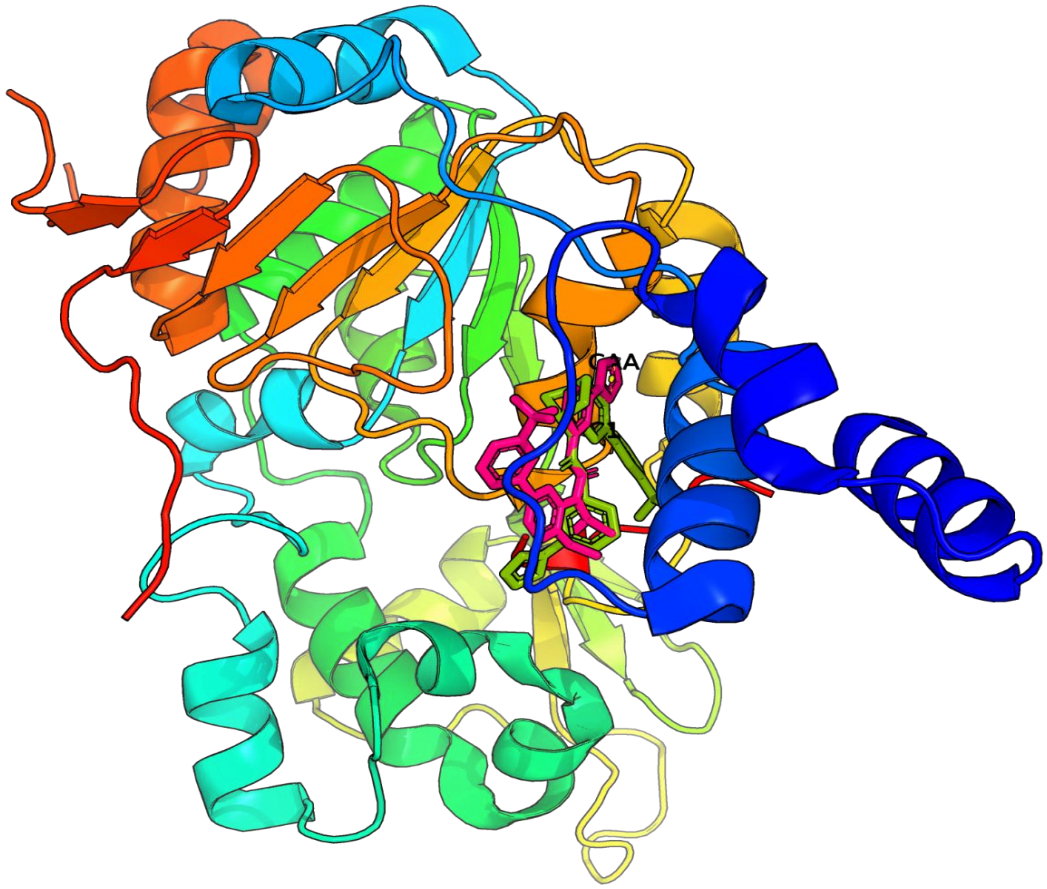

Figure 6.13: Overlay diagram of co-crystallized ligand (green) with docked ligand (pink)

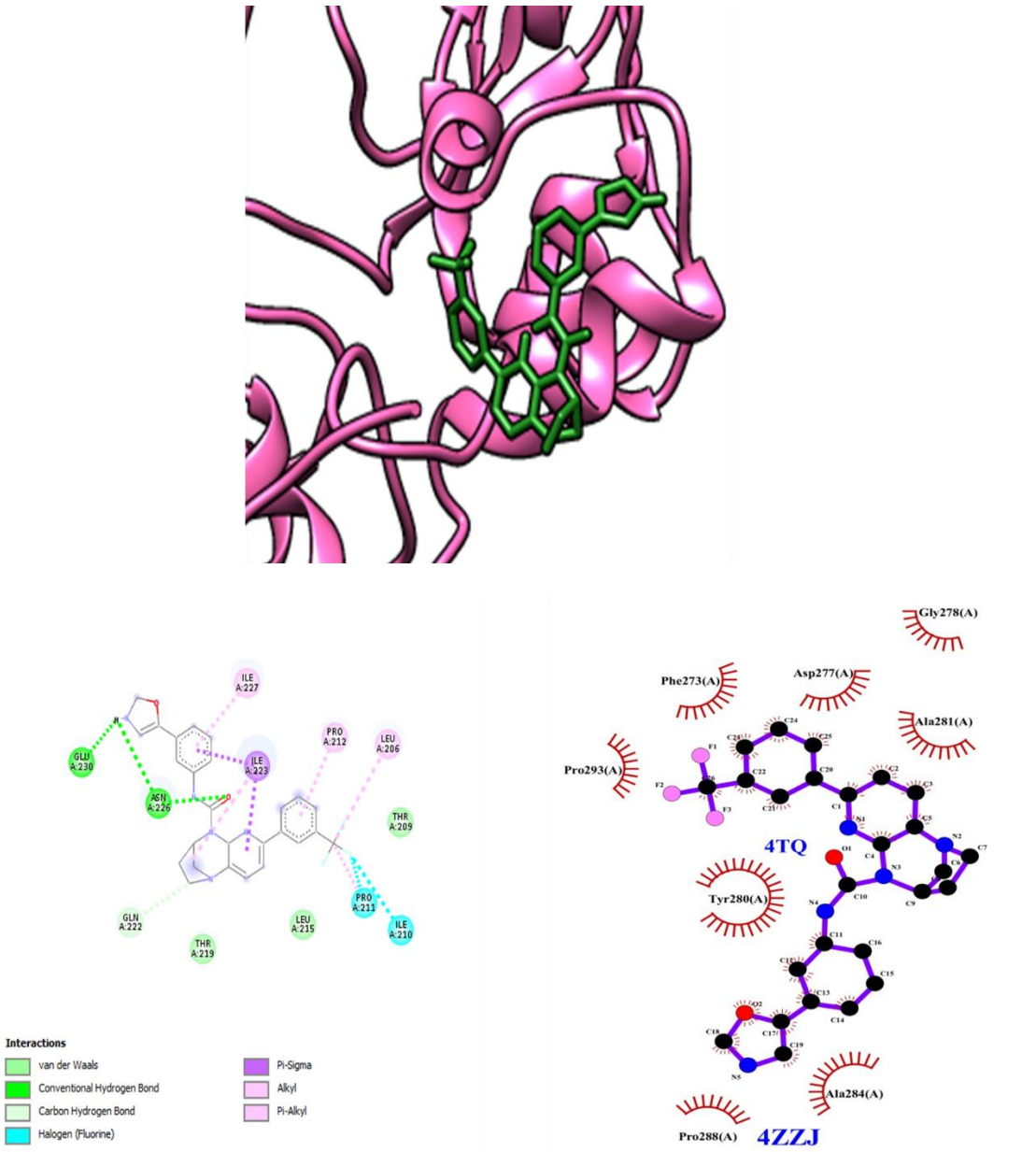

Figure 6.14: Docking of the SIRT1 protein (PDB ID:4ZZJ) with Co-crystallized ligand : 3D visualization in PyMol (top), 2D visualization in Discovery Studio (bottom left) and Ligplot (bottom right).

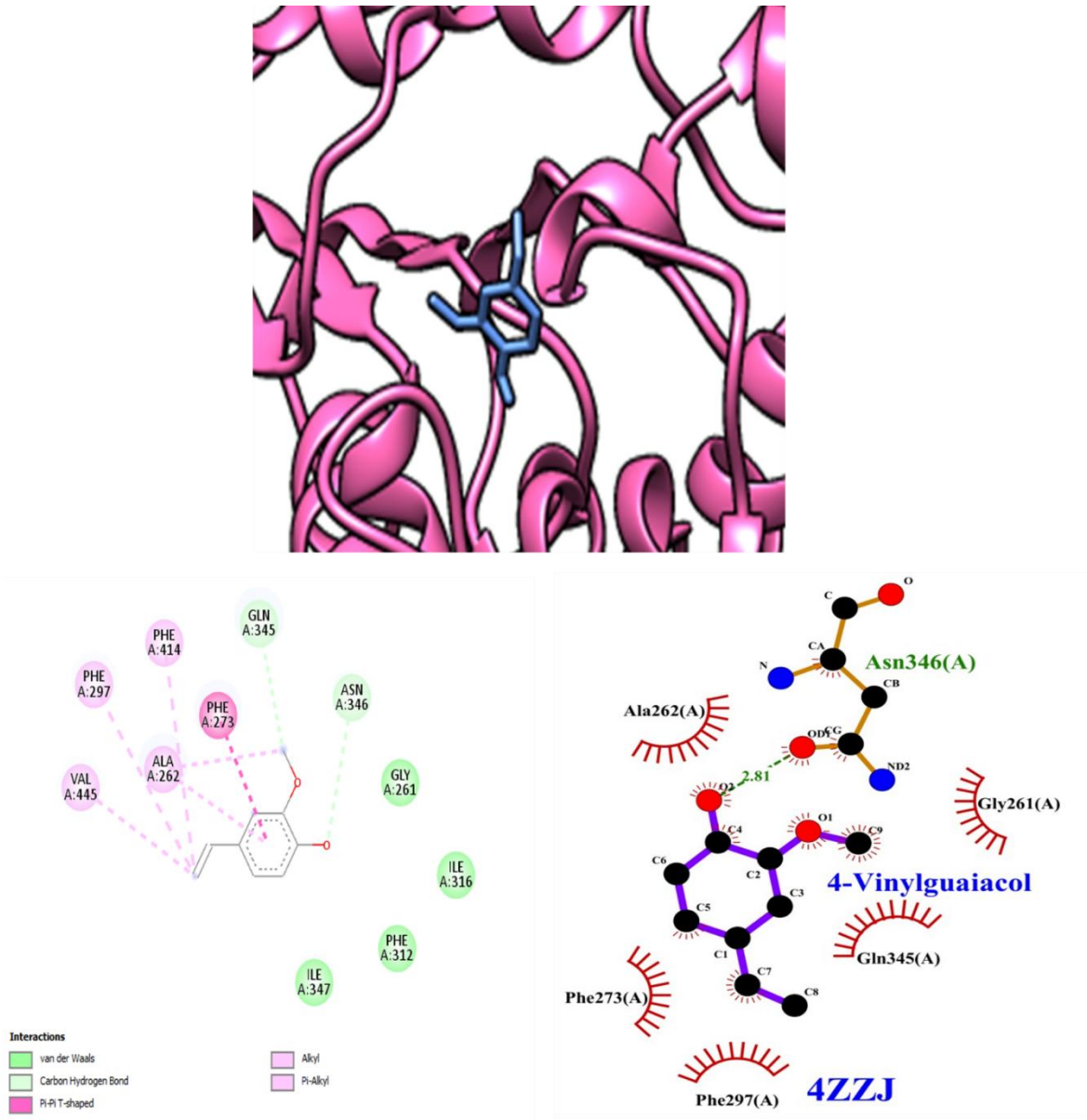

Figure 6.15: Docking of the SIRT1 protein (PDB ID:4ZZJ) with 4-Vinylguaicol: 3D visualization in PyMol (top), 2D visualization in Discovery Studio (bottom left) and Ligplot (bottom right).

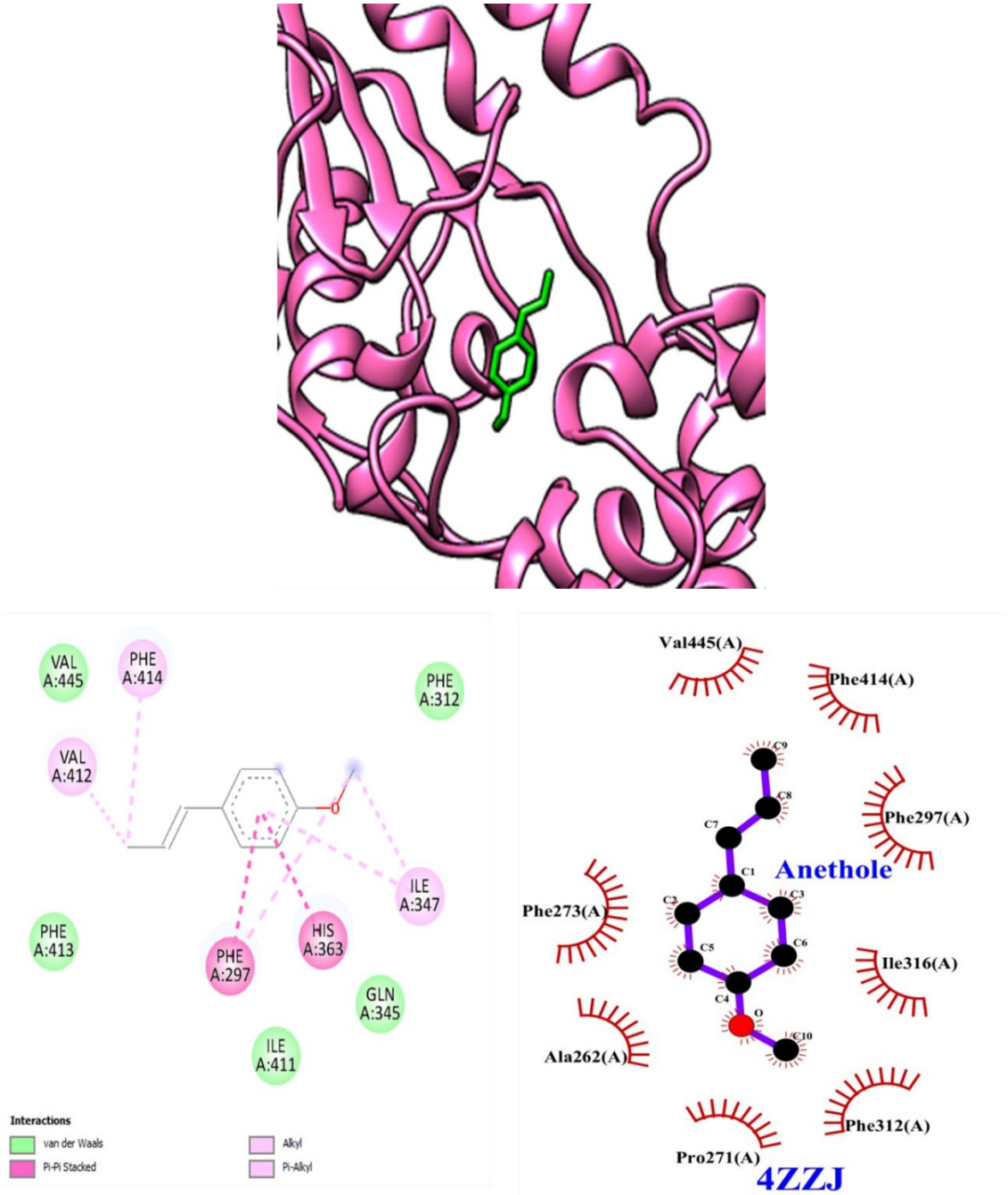

Figure 6.16: Docking of the SIRT1 protein (PDB ID:4ZZJ) with anethole: 3D visualization in PyMol (top), 2D visualization in Discovery Studio (bottom left) and Ligplot (bottom right).

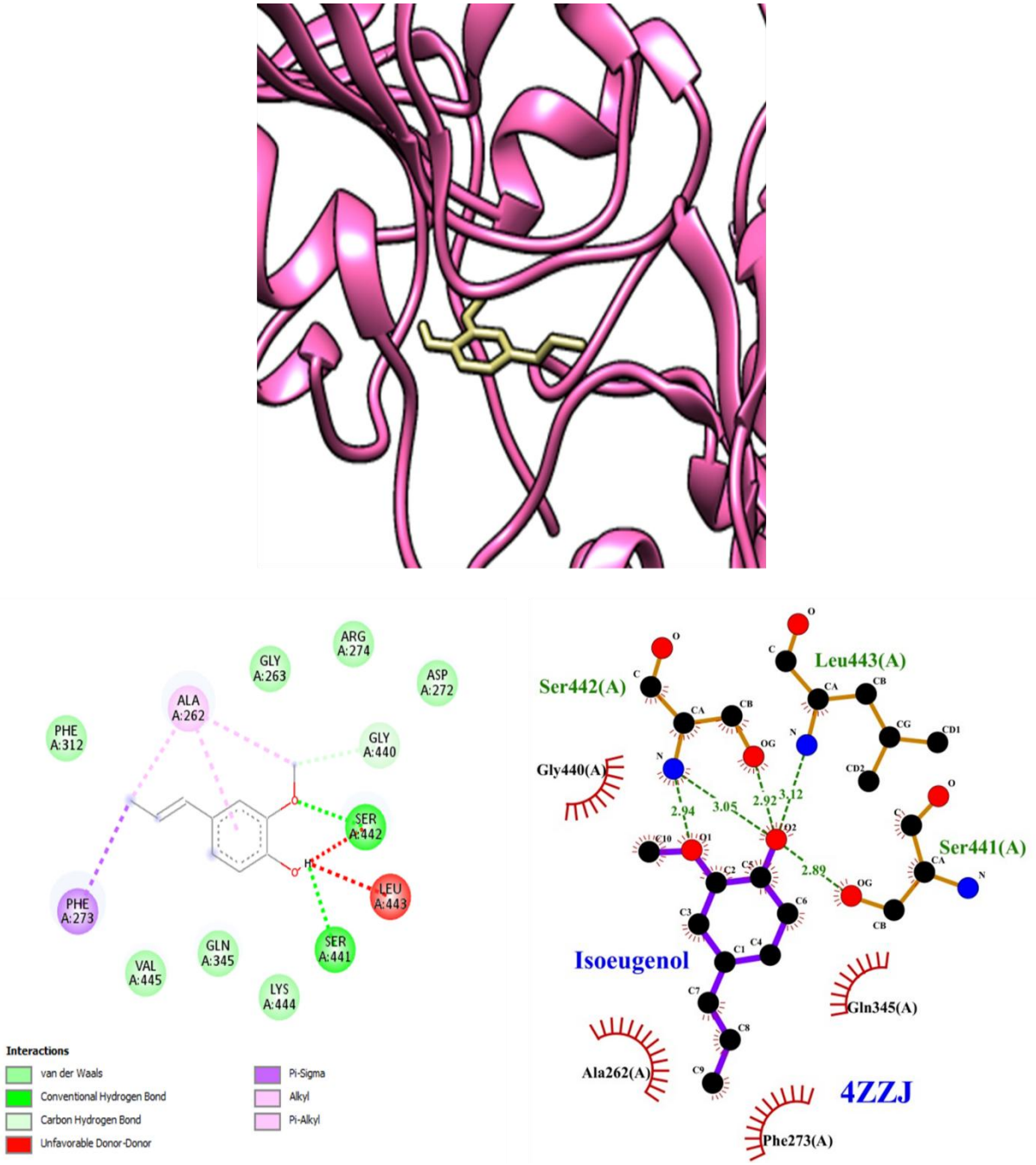

Figure 6.17: Docking of the SIRT1 protein (PDB ID:4ZZJ) with isoeugenol: 3D visualization in PyMol (top), 2D visualization in Discovery Studio (bottom left) and Ligplot (bottom right).

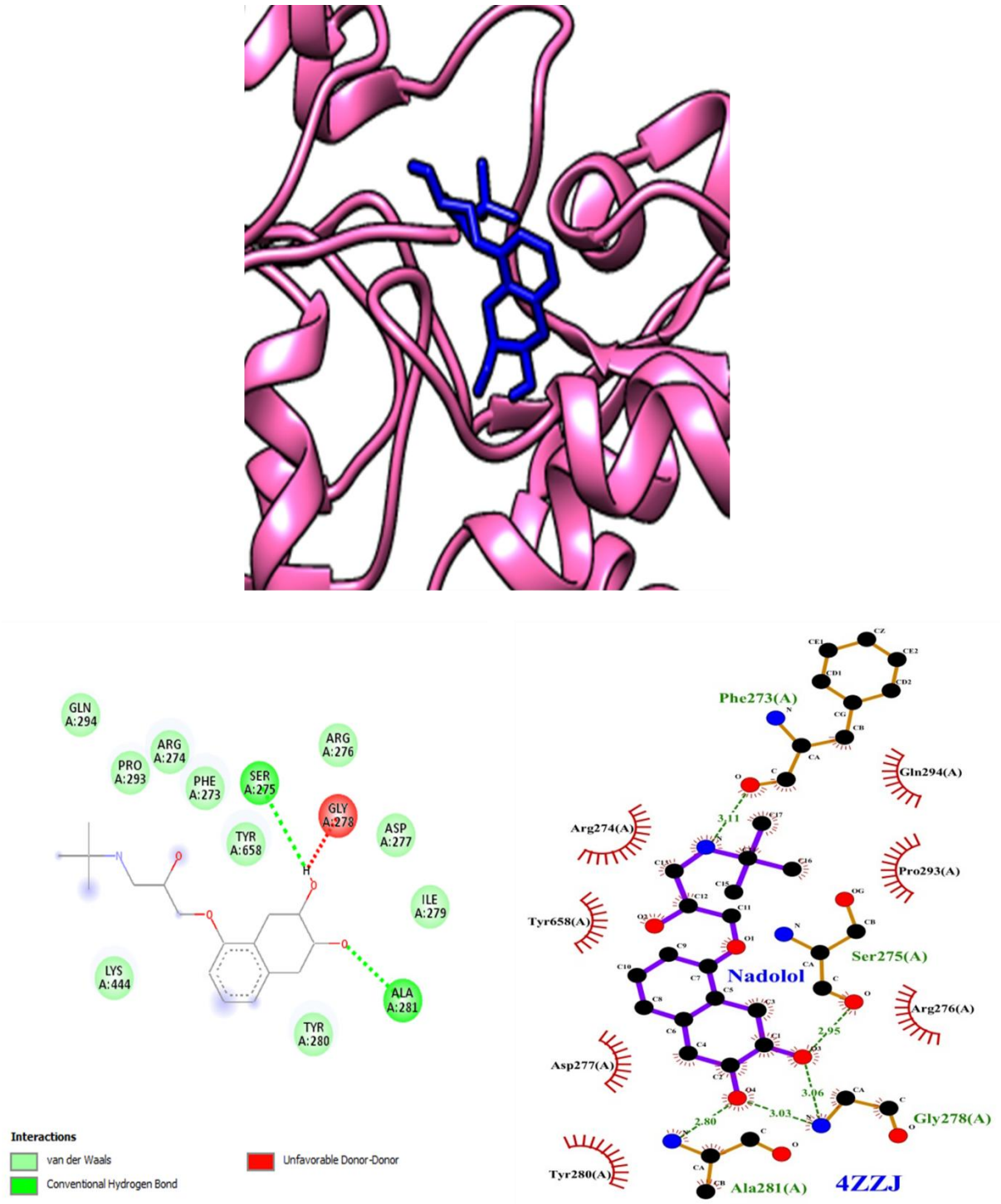

Figure 6.18: Docking of the SIRT1 protein (PDB ID:4ZZJ) with nadolol: 3D visualization in PyMol (top), 2D visualization in Discovery Studio (bottom left) and Ligplot (bottom right).

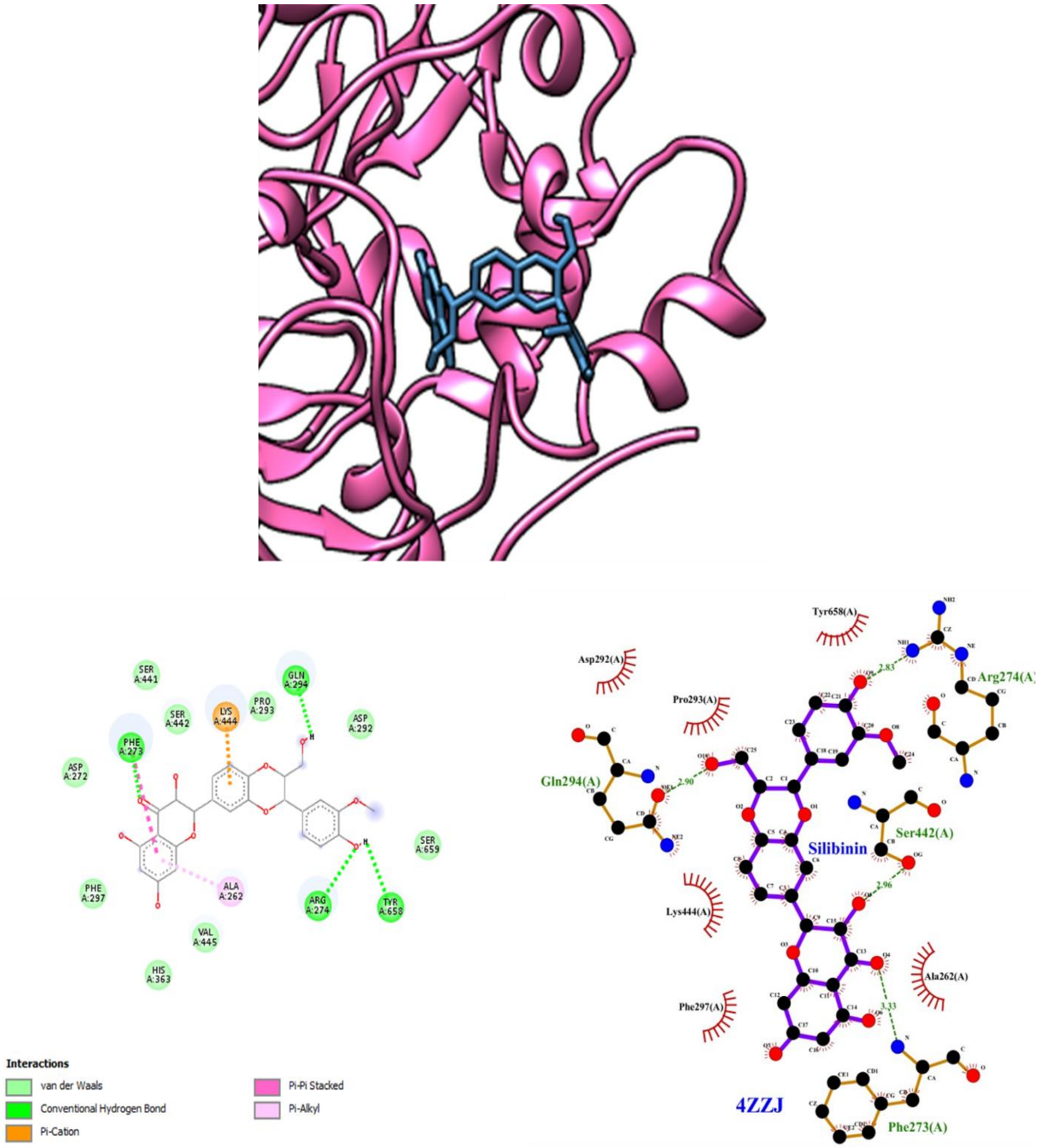

Figure 6.19: Docking of the SIRT1 protein (PDB ID:4ZZJ) with silibinin: 3D visualization in PyMol (top), 2D visualization in Discovery Studio (bottom left) and Ligplot (bottom right).

6.9 Molecular dynamics (MD) assessment

Anethole, isoeugenol, and silibinin were evaluated for molecular dynamics studies. In MD various parameters were analyzed to study the stability and conformation of protein-ligand complexes such as RMSD, RMSF, number of hydrogen bonds, SASA, and radius of gyration.

6.9.1 Root Mean Square Deviation (RMSD)

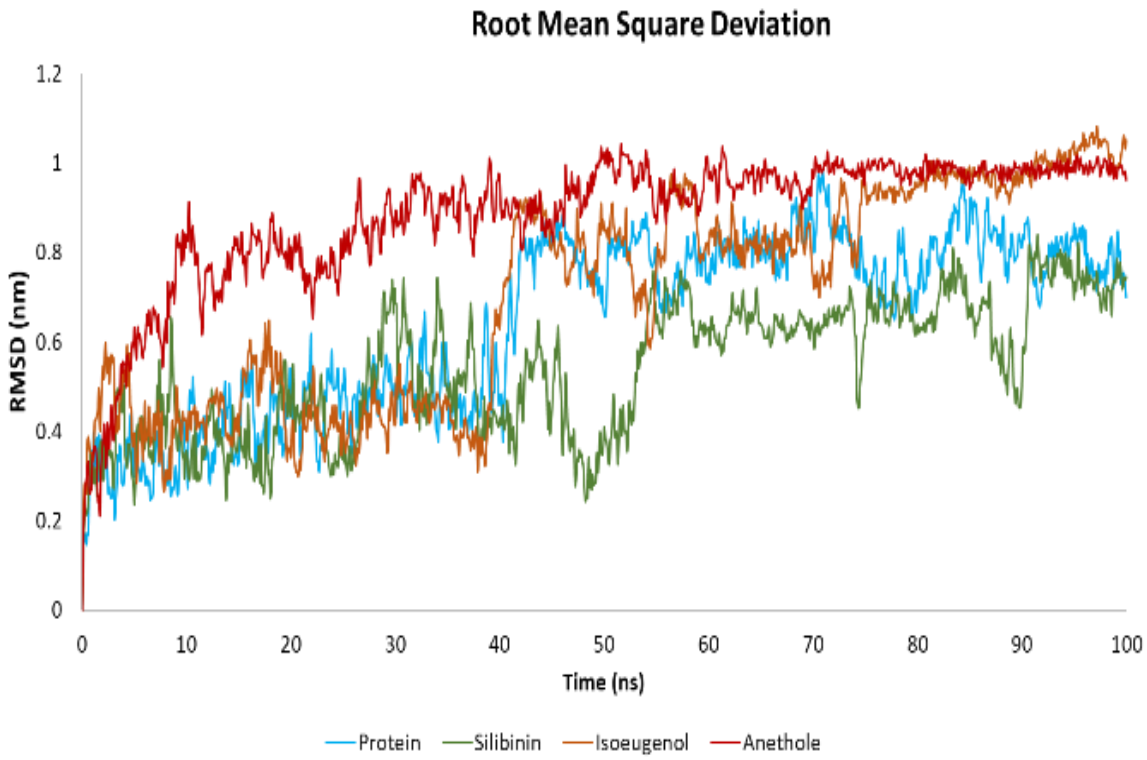

Figure 6.20: RMSD of silibinin, isoeugenol and anethole along with protein for 100ns

The stability of the protein-ligand complex over a 100 ns simulation is assessed using Root Mean Square Deviation (RMSD), which measures atomic positional changes over time. RMSD provides insights into both stability and flexibility within the simulated environment by evaluating structural deviations in the protein and protein-ligand complex. A lower RMSD value signifies structural stability and a strong interaction between the ligand and the binding pocket, indicating minimal conformational changes and a well-maintained binding throughout the simulation. In contrast, a higher RMSD value suggests structural fluctuations, which may impact ligand retention and overall complex stability. Consistently low RMSD values indicate

that the ligand remains securely bound within the active site, while higher fluctuations reflect alterations in protein dynamics, potentially leading to weaker binding or ligand displacement. In this study, RMSD was analysed for both the apo (unbound) and ligand-bound protein states, as depicted in Figure 6.20. Initially, fluctuations are observed in the RMSD plot for all three compounds, which is expected as the system undergoes equilibration. However, anethole and isoeugenol exhibit greater stability over time, with their RMSD values stabilising after an initial adjustment period. In contrast, silibinin shows slightly higher deviations, suggesting a relatively less stable binding. The results indicate that the protein, along with its complexes with silibinin, isoeugenol, and anethole, remains relatively stable throughout the simulation, reinforcing the potential of these phytochemicals in maintaining strong molecular interactions within the binding site.

6.9.2 Root Mean Square Fluctuation (RMSF)

RMSF analysis evaluates the flexibility of individual residues within a protein structure during a molecular dynamics simulation. It measures the extent of atomic displacement over time, providing insights into the stability and mobility of different protein regions. Higher RMSF values indicate regions with greater movement, suggesting structural flexibility and potential instability. In contrast, lower RMSF values signify stable interactions, where residues maintain their positions with minimal fluctuations. This analysis is crucial in understanding ligand-induced conformational changes and identifying binding site stability, as excessive fluctuations in key residues may compromise ligand retention and overall protein function. In this study, RMSF was calculated for three ligand-protein complexes and the apo-protein over a 100 ns simulation to evaluate deviations from the original positions. The results revealed that key binding site residues exhibited relatively low RMSF values for silibinin, anethole, and the protein, indicating strong ligand retention. In contrast, isoeugenol showed slightly higher fluctuations, suggesting a more flexible binding interaction. The RMSF graph (Figure 6.21) demonstrates that fluctuations remained below 2 nm for most of the simulation, except at the beginning and end of the curve, likely due to the presence of loop or turn regions in the protein structure. The majority of the residues exhibited deviations under 0.6 nm, reinforcing the stability of the protein-ligand complexes throughout the simulation.

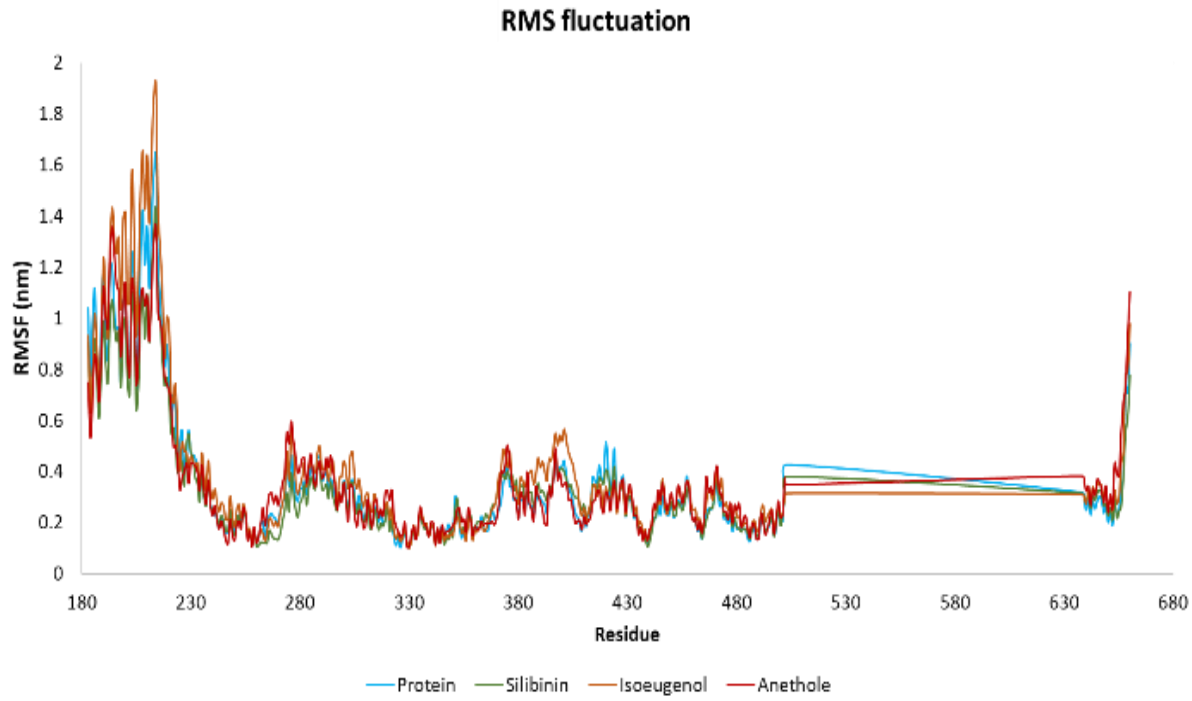

Figure 6.21: RMSF of silibinin, isoeugenol and anethole along with protein.

6.9.3 Radius of Gyration (Rg)

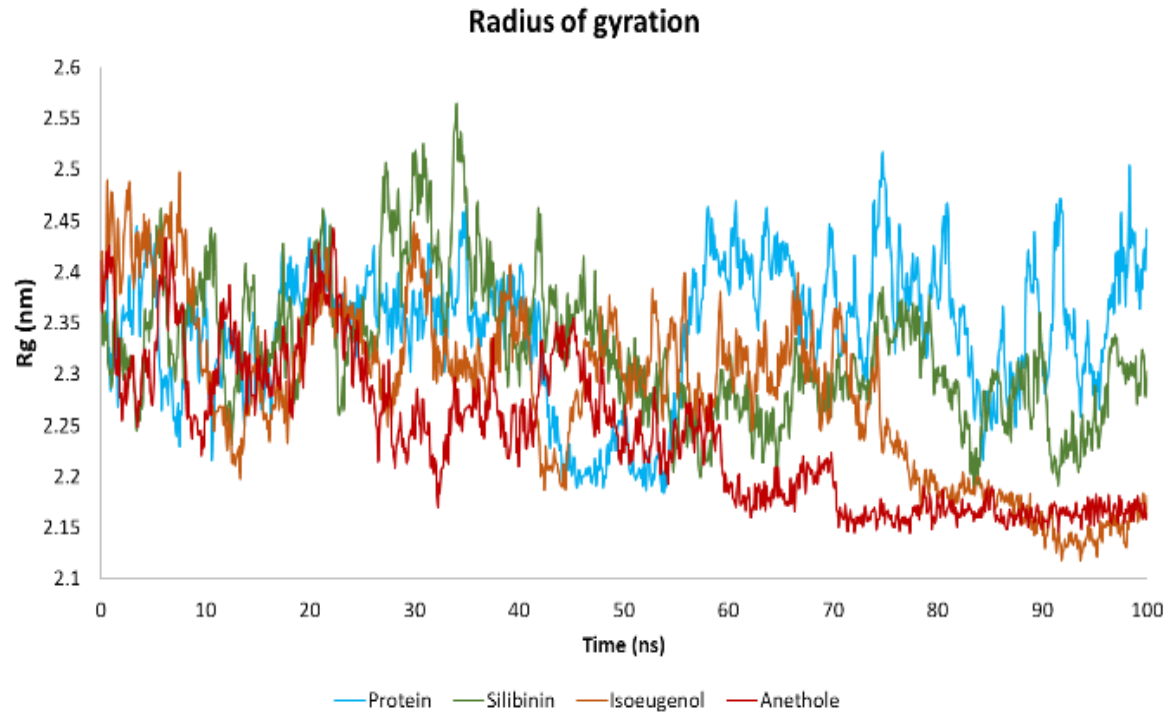

Figure 6.22: Radius of gyration of silibinin, isoeugenol and anethole along with protein for 100ns

The radius of gyration (Rg) is a key parameter used to assess the compactness and structural stability of a protein throughout a molecular dynamics simulation. It measures the distribution of atomic mass around the center of mass, providing insights into protein folding and rigidity. A lower and stable Rg value indicates that the protein maintains a well-folded and compact conformation, suggesting structural integrity and stability. Conversely, fluctuations in Rg may indicate conformational changes, unfolding events, or flexibility within the protein structure.

In this study, the Rg analysis was performed to compare the compactness of the protein in both apo (unbound) and ligand-bound states. The results revealed that all ligand-bound complexes exhibited relatively stable Rg values, indicating that ligand binding did not induce significant structural perturbations. Minor fluctuations observed in certain complexes suggest slight conformational rearrangements, but these variations remained within an acceptable range, confirming that the protein retained its structural stability throughout the simulation. The consistent Rg values observed across different conditions further support the notion that the protein-ligand complexes maintained their compact and well-folded states during the 100 ns simulation period, as depicted in Figure 6.22.

6.9.4 Solvent Accessible Surface Area (SASA)

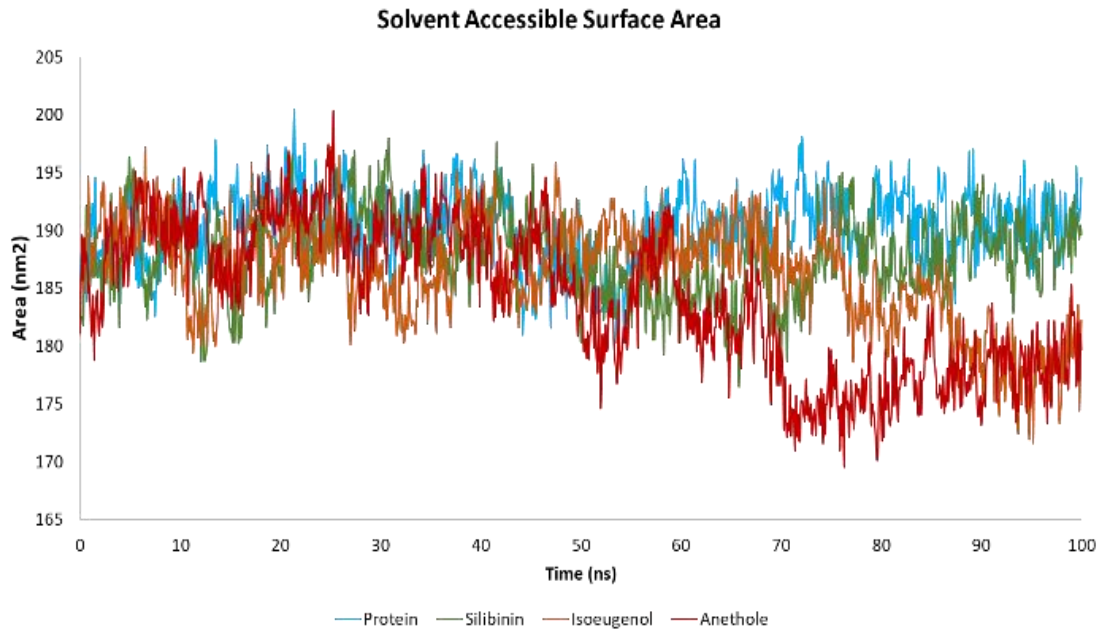

Figure 6.23: SASA of silibinin, isoeugenol and anethole along with protein for 100ns

Solvent Accessible Surface Area (SASA) is an essential parameter used to evaluate the extent to which a protein or protein-ligand complex is exposed to the surrounding solvent during a

molecular dynamics simulation. It provides insights into the stability of ligand binding, as a decrease in SASA typically indicates that the ligand is more deeply embedded within the protein's binding pocket, forming stable interactions. Conversely, an increase in SASA suggests greater solvent exposure, which may imply weaker binding or conformational changes in the protein structure.

In this study, SASA was analyzed to assess the degree of solvent exposure for both the apo-protein and ligand-bound complexes over the 100 ns simulation period (Figure 6.23). The results demonstrated that Isoeugenol and Anethole exhibited lower SASA values compared to the apo-protein and Silibinin, suggesting that these ligands were more tightly enclosed within the binding pocket, contributing to greater binding stability. The SASA values fluctuated between 170-200 nm^2 throughout the simulation, indicating that the overall structure of the protein and protein- ligand complexes remained stable. Minimal variations in SASA further support the notion that the protein retained its compactness and did not undergo significant conformational changes upon ligand binding. These findings reinforce the stability of the ligand-protein interactions and the structural integrity of the complexes over the course of the simulation.

6.9.5 Hydrogen Bonding

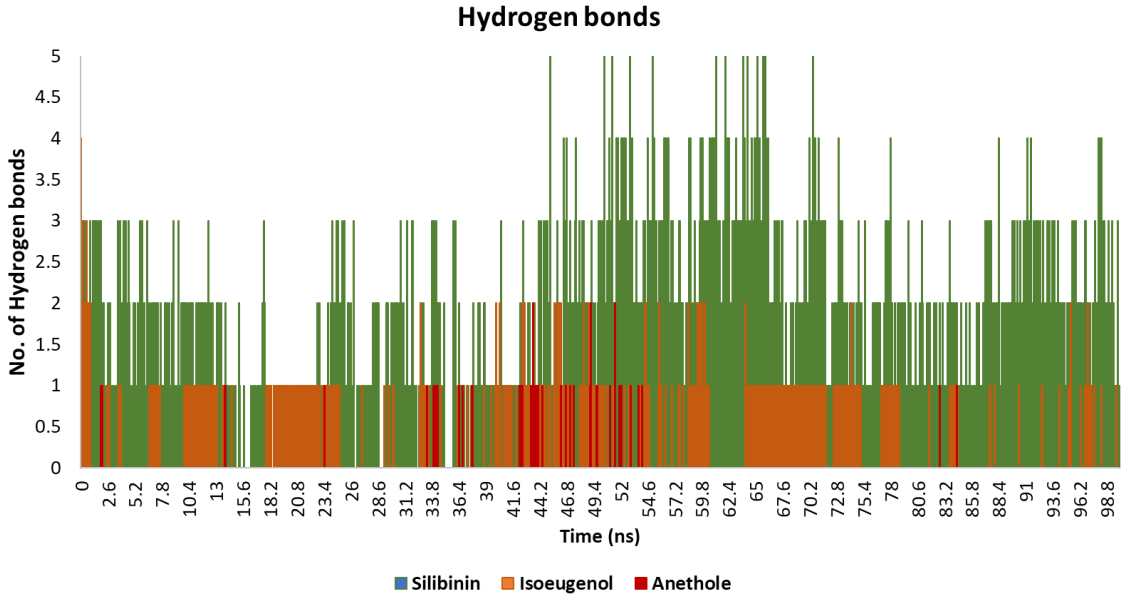

Figure 6.24: Hydrogen bond of Silibinin, Isoeugenol and Anethole with protein for 100ns

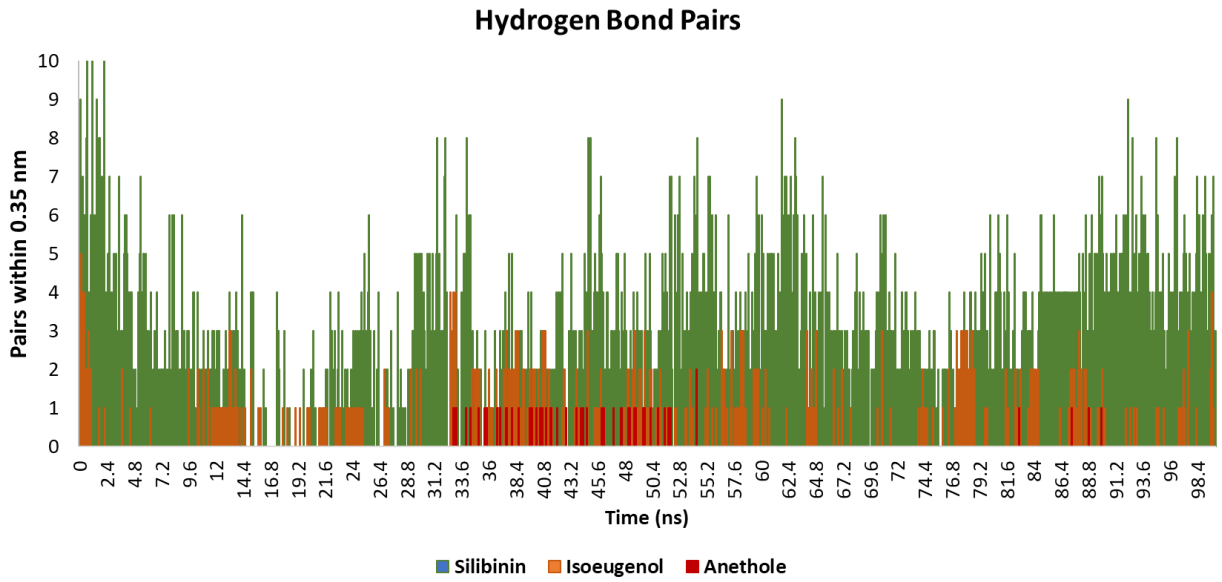

Figure 6.25: Hydrogen Bond Pairs of silibinin, isoeugenol and anethole with protein for 100ns.

Hydrogen bonds are critical for the stability and integrity of protein-ligand interactions, as they contribute significantly to binding affinity and complex stabilisation. A higher number of hydrogen bonds generally correlates with stronger and more stable interactions, whereas fewer hydrogen bonds may indicate weaker binding and increased flexibility of the ligand within the protein's active site.

In this study, molecular dynamics (MD) simulations were used to evaluate hydrogen bond formation between the selected ligands and the target protein throughout the simulation trajectory. The results indicated that silibinin formed the highest number of hydrogen bonds, maintaining consistent interactions with the protein, which contributed to its enhanced stability. Isoeugenol exhibited a moderate number of hydrogen bonds, while anethole formed the least, suggesting a comparatively weaker binding affinity.

Post-MDS, trajectory files were analysed to quantify the number of hydrogen bonds, providing insights into ligand-protein interaction stability over time. The hydrogen bond fluctuations observed during the simulation indicated that silibinin maintained stable interactions, reinforcing its strong binding affinity. Conversely, the lower number of hydrogen bonds in anethole suggests that it may have a more transient interaction with the protein, leading to reduced stability. The results, as depicted in Figure 6.24 and Figure 6.25, highlight the role of hydrogen bonding in ligand retention and overall protein-ligand complex stabilisation.

6.9.6 Distance between protein and ligand

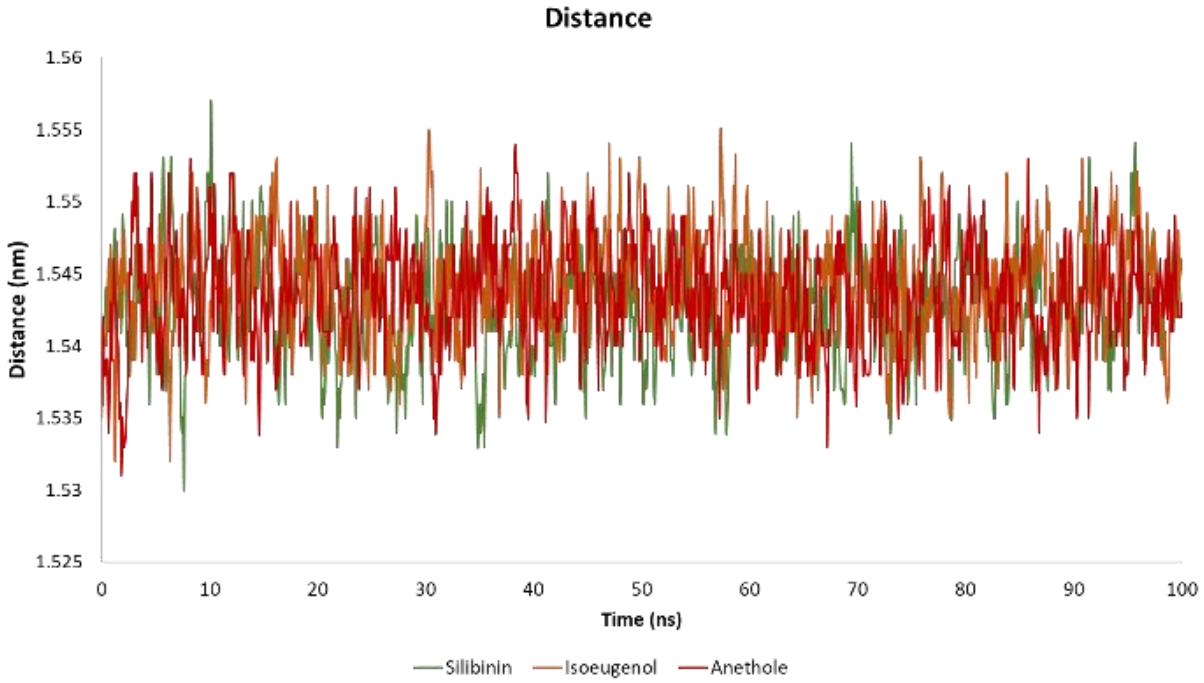

Figure 6.26: Distance between silibinin, isoeugenol and anethole with protein for 100ns.

The proximity between a ligand and its target protein plays a crucial role in determining the strength and stability of their interaction. A shorter distance between the ligand and key protein residues generally indicates stronger binding as it facilitates stable molecular interactions, including hydrogen bonding, van der Waals forces, and hydrophobic interactions. Conversely, larger fluctuations in distance may suggest a weaker or less stable binding affinity.

In this study, molecular dynamics (MD) simulations were used to assess the distance between the ligand and the protein throughout the simulation trajectory. The results demonstrated that the selected compounds maintained relatively stable interactions with key binding site residues. Furthermore, distance analysis confirmed that the protein-ligand separation remained under 1.56 nm for all the studied compounds, signifying stable binding throughout the simulation period (Figure 6.26). The minimal fluctuations in distance reaffirm the structural stability of the protein-ligand complex, providing insights into the binding efficiency of the tested phytochemicals. These findings further validate the reliability of molecular docking results and highlight the potential of the identified compounds in maintaining strong and stable interactions with the protein target.

6.10 MM/PBSA Binding Energy Analysis

Table 6.12: MM/PBSA results of the protein-ligand complex from 100ns simulation. Energy (E) is represented in KJ/mole

Energy (KJ/mole)	Silibinin	Isoeugenol	Anethole
Van der Waal Energy	-156.690 ± 0.20	-85.939 ± 0.10	-91.378 ± 0.10
Electrostatic Energy	-99.579 ± 0.30	-23.179 ± 0.16	-15.857 ± 0.08
Polar solvation Energy	187.485 ± 0.31	66.400 ± 0.14	58.408 ± 0.10
SASA Energy	-18.367 ± 0.01	-10.711 ± 0.01	-10.292 ± 0.00
Binding Energy	**-87.151 ± 0.20**	**-53.429 ± 0.11**	**-59.119 ± 0.08**

We have used gmx mmpbsa module to perform MM/PBSA, which gave summarised binding energy of phytochemicals in Table 6.12. Silibinin had the strongest binding energy (-87.151 KJ/mole), whereas not much difference in binding energy between isoeugenol and anethole was observed. All three phytochemicals interacted well with the protein, which can be seen from their negative binding energy. With MM/PBSA analysis, we also found that this negative binding energy is imparted mainly due to Van der Waals energy, followed by electrostatic Energy. The binding energy trajectory over 100ns is depicted in Figure 6.27. Silibinin also had the strongest binding in Autodock Vina.

In recent times, MM/PBSA has been used as an advanced technology for estimating binding energies of complexes (Genheden & Ryde, 2015). Although it is computationally expensive, it gives more reliable binding energy as compared to the traditional docking method. Data shows that all the ligands have very good binding energy with very little standard deviation, as depicted in Table 6.12. Vander wall interactions played a major role in stabilising the protein-ligand complex here, as they contributed more negative values than their other energy counterparts.

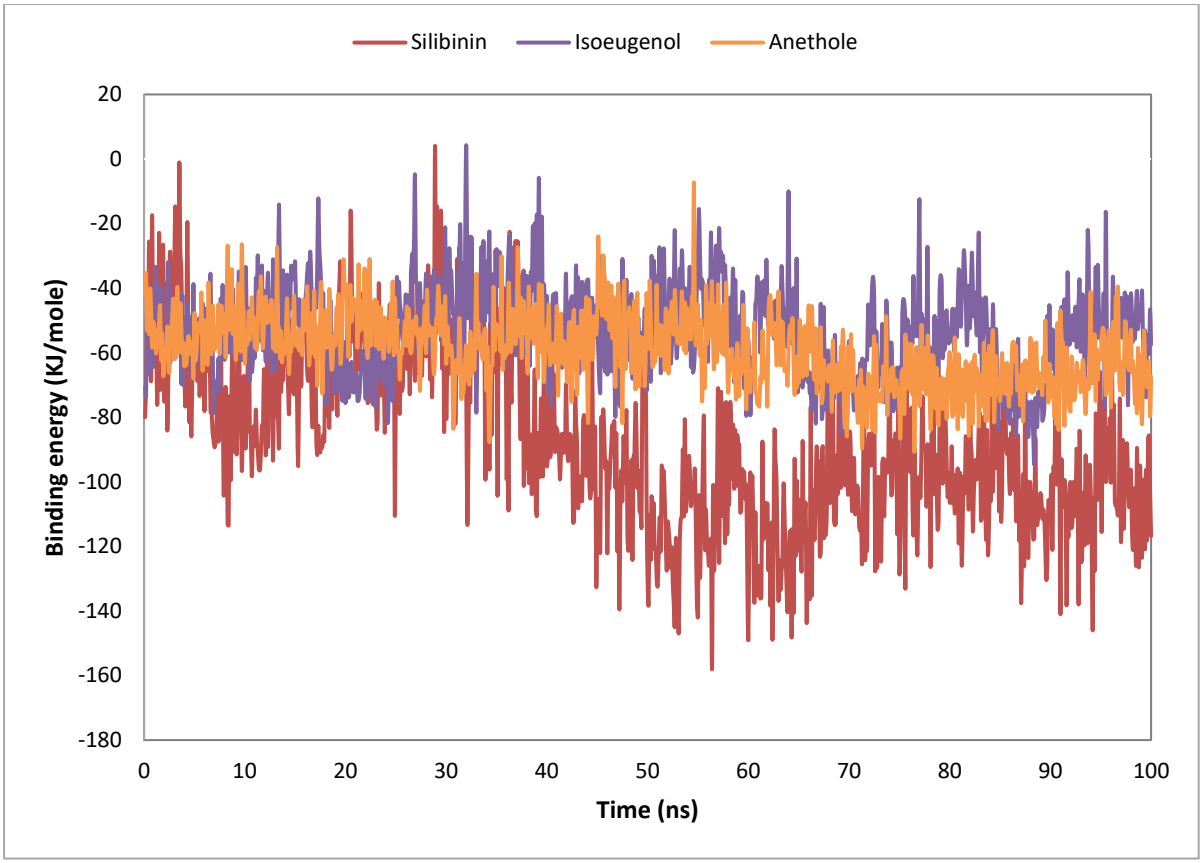

Figure 6.27: MM/PBSA binding energy over 100ns.

6.11 Residue decomposition

Residue decomposition analysis revealed that silibinin binding involves a wider array of stabilising residues, particularly ASP274 and ARG272, contributing substantially to binding affinity. In contrast, isoeugenol is predominantly stabilised by ARG272, while Anethole shows weaker and fewer favourable interactions, mostly hydrophobic (Figure 6.28). These findings correlate well with MM/PBSA binding energies and FEL analysis, confirming silibinin as the most tightly bound ligand.

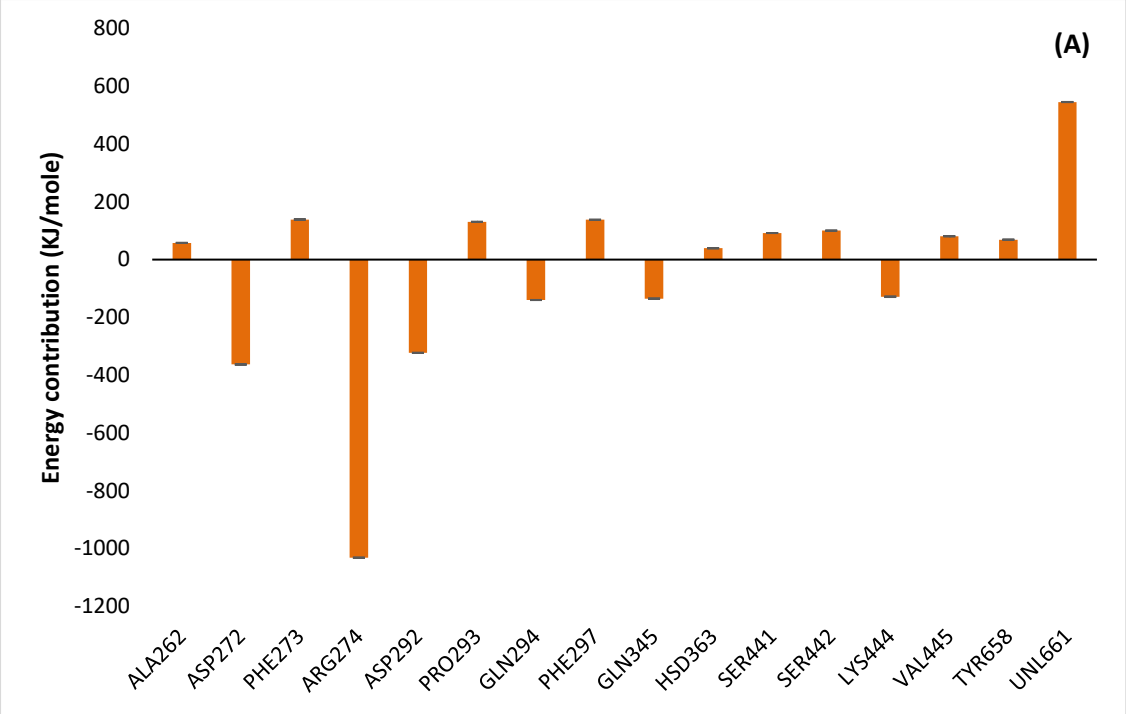
(A)
Energy contribution (KJ/mole)
800
600
400
200
0
-200
-400
-600
-800
-1000
-1200
ALA262
ASP272
PHE273
ARG274
ASP292
PRO293
GLN294
PHE297
GLN345
HSD363
SER441
SER442
LYS444
VAL445
TYR658
UNL661

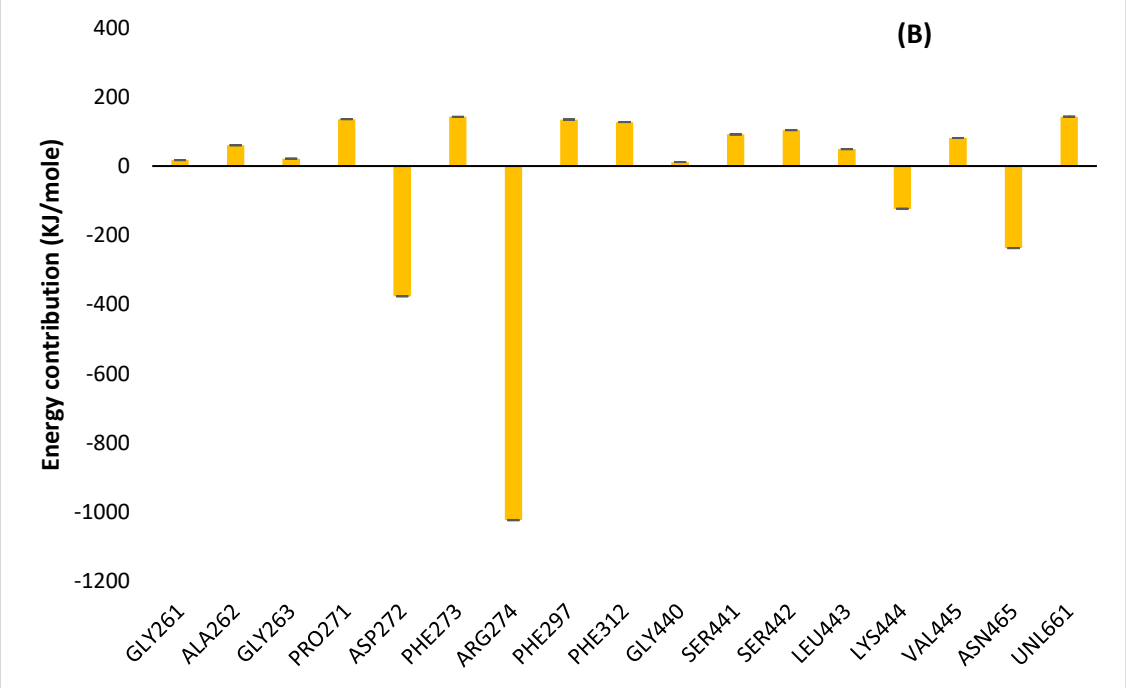
(B)
Energy contribution (KJ/mole)
400
200
0
-200
-400
-600
-800
-1000
-1200
GLY261
ALA262
GLY263
PRO271
ASP272
PHE273
ARG274
PHE297
PHE312
GLY440
SER441
SER442
LEU443
LYS444
VAL445
ASN465
UNL661

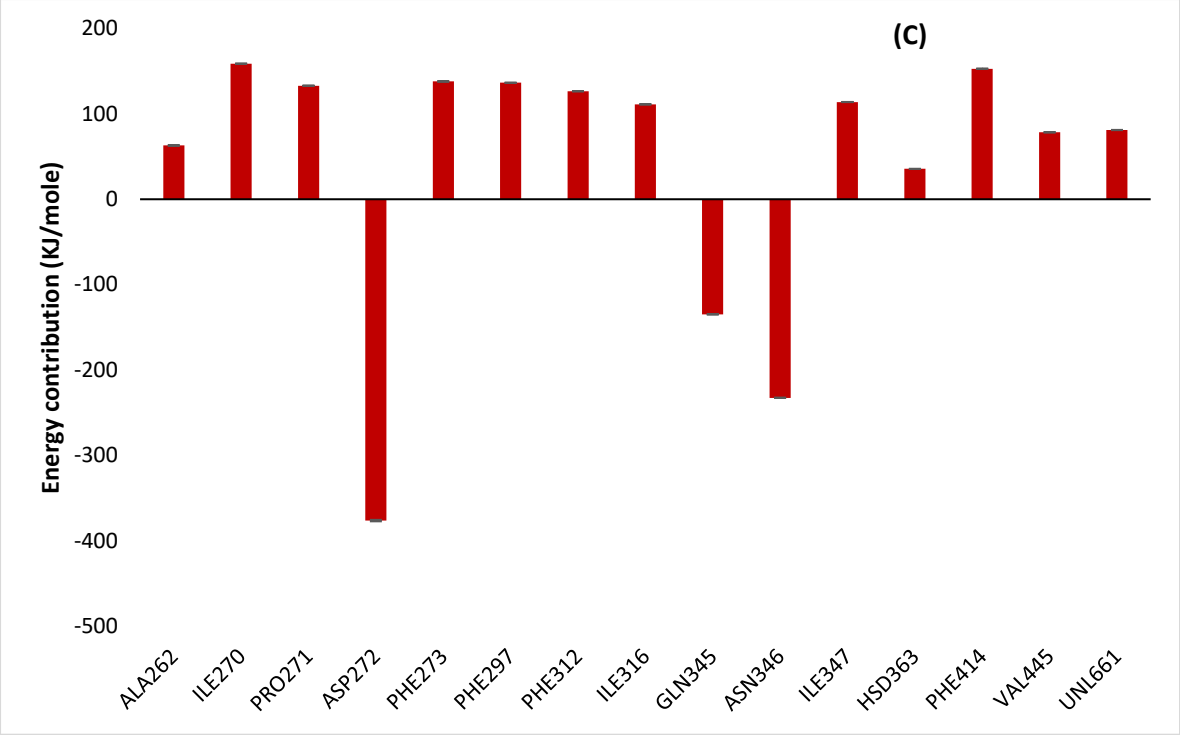

Figure 6.28: Residue contribution plot A) Silibinin, B) Isoeugenol, and C) Anethole

6.12 PCA and FEL analysis

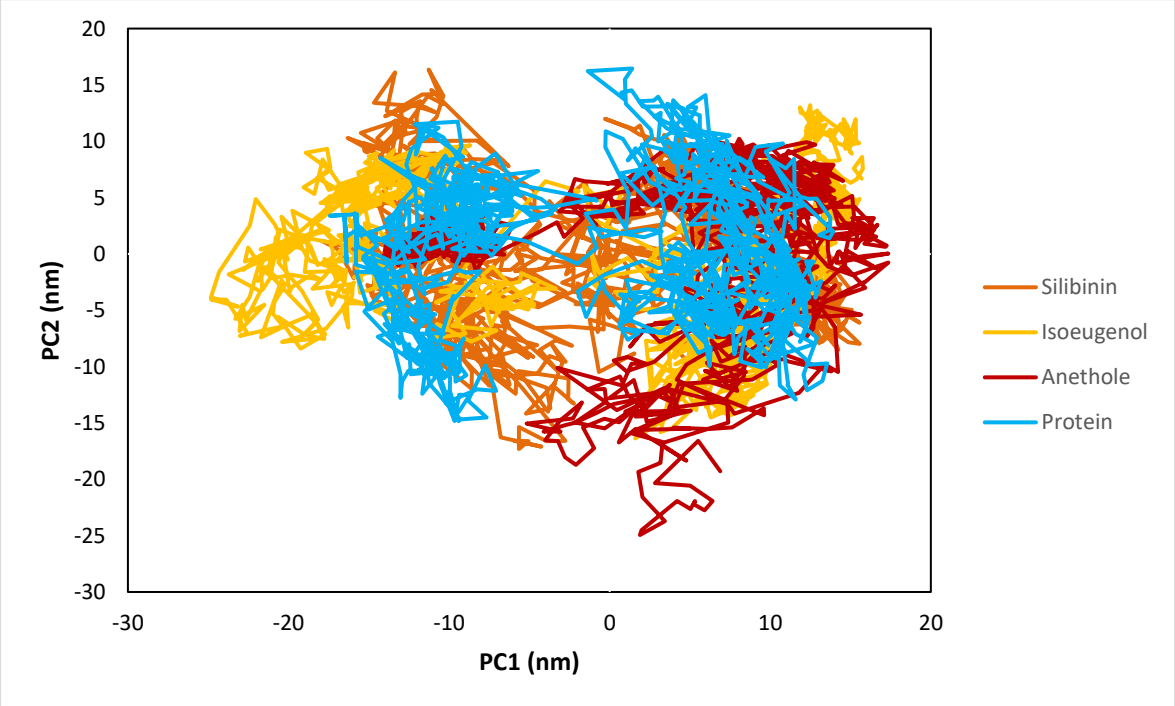

Figure 6.29: PCA plot of phytochemicals along with protein

The first two principal components (PC1 and PC2) were used for 2D projection in Figure 6.29, which shows the motion of the protein in the complex. Projection of the first two eigen vectors of the phytochemicals along with the protein (cyan) is highlighted here. PCA analysis revealed that silibinin-bound protein complex explored a narrower conformational space, indicating greater structural stability upon ligand binding. In contrast, anethole and isoeugenol displayed broader distributions, suggesting increased flexibility. The unbound protein (apo form) exhibited the highest conformational diversity, affirming the stabilising effect of ligand interaction. These results are in strong agreement with the MM/PBSA binding energy estimates. The diagonalised covariance matrices for silibinin, isoeugenol, anethole, and protein were 152.401 nm^2, 254.054 nm^2, 180.408 nm^2, and 184.231 $nm^{2,}$ respectively. Isoeugenol had the maximum eigen values whereas anethole had the least eigen values.

Folding and conformation of the protein decide the fate of its function (Prada-Gracia et al., 2009; Maisuradze et al., 2010). FEL aids in characterising the protein conformation and its free energy. The conformational variability parameter measures how different the sampled conformations are from each other. The free energy parameter shows how stable and easy to access they are compared to each other, which further helps in elucidating the biological function of proteins and aids in the drug design process (Baidya et al., 2022). The free energy landscape (Gibbs energy) plot that analyses the folding and unfolding nature of macromolecules in native and complex states for PC1 and PC2 of all the phytochemicals, along with protein, is shown in Figure 6.30. Here, red, yellow, blue and green spots denote folded structure with low free energy, intermediate energy, an unfolded structure with high Gibbs free energy and a metastable time frame of biomolecules, respectively (Uk and Tk, 2020). Free energy landscape (FEL) analysis revealed that the silibinin-bound system exhibited the most stable conformation, with a well-defined deep energy basin. In contrast, Anethole and Isoeugenol showed broader and more dispersed low-energy regions, reflecting greater conformational variability. The apo-protein explored the widest area of conformational space, reinforcing the stabilising effect of ligand binding observed in MM/PBSA and PCA analyses.

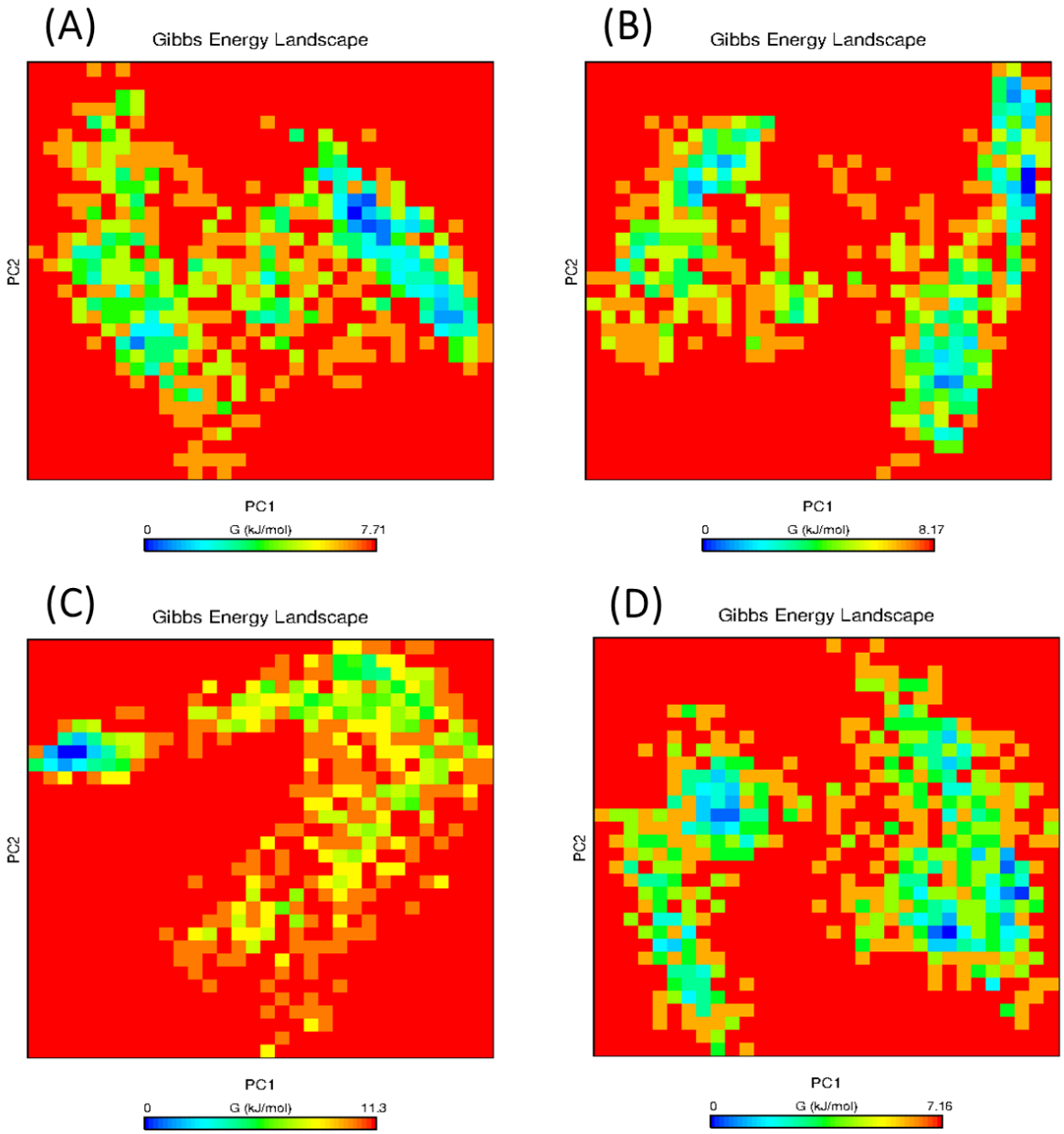

Figure 6.30: FEL plots of phytochemicals A) Silibinin, B) Isoeugenol, C) Anethole and D) Protein.

6.13 Crystallization assays

6.13.1 Nucleation assay

Crystallization assays are critical in understanding the production and prevention of nucleation, particularly for calcium oxalate crystals, which are the major ingredients of kidney stones. The nucleation assay used in this study assesses the inhibitory potential of several phytochemicals at different doses and time intervals. This study sheds light on the effectiveness of these chemicals in avoiding crystal formation, which is critical for designing therapeutic options

against nephrolithiasis. The results, depicted in microscopic pictures and statistical graphs, show substantial patterns in nucleation inhibition that change with concentration, time, and compound specificity.

6.13.1.1 Time-Dependent Nucleation Assay

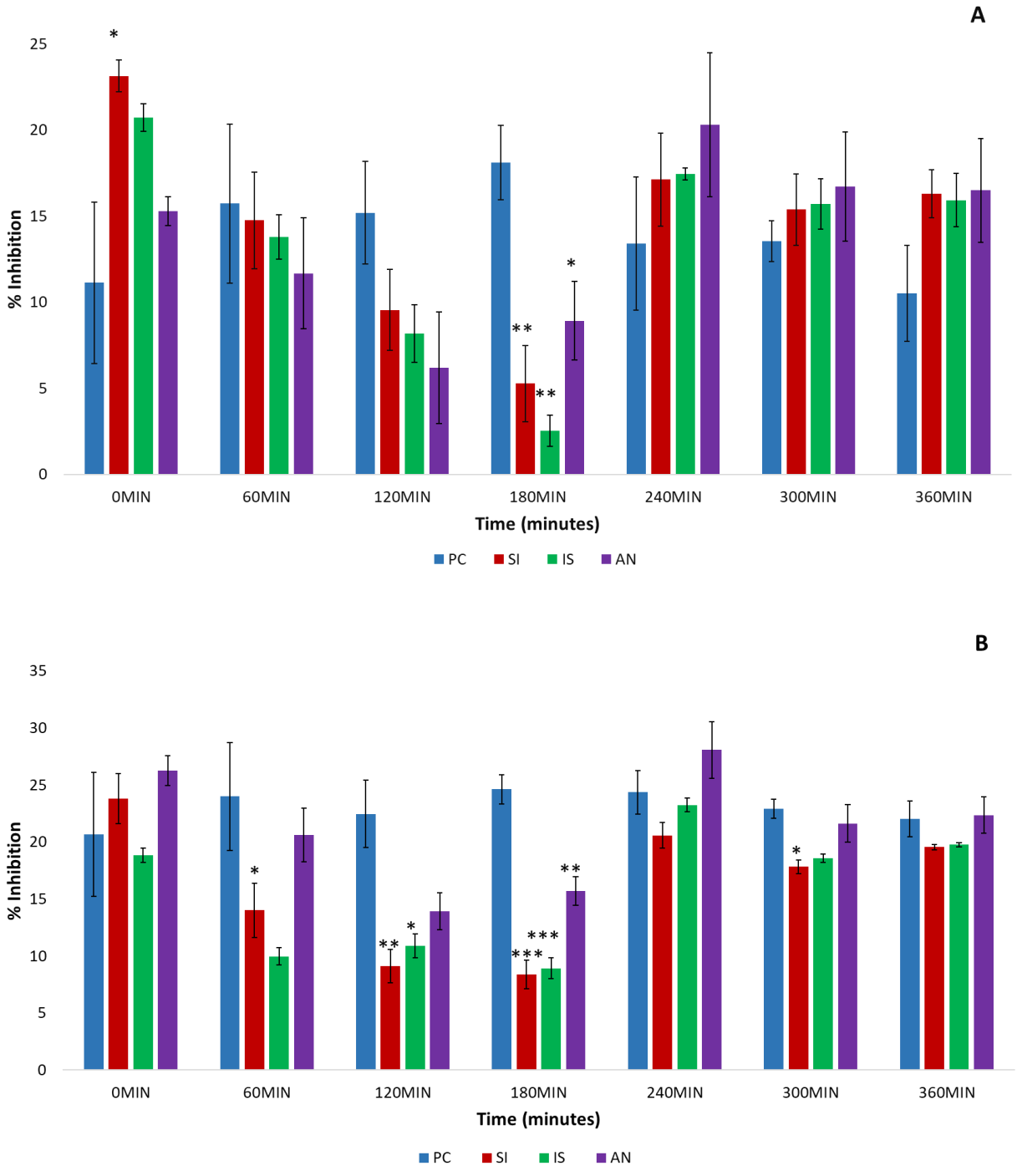

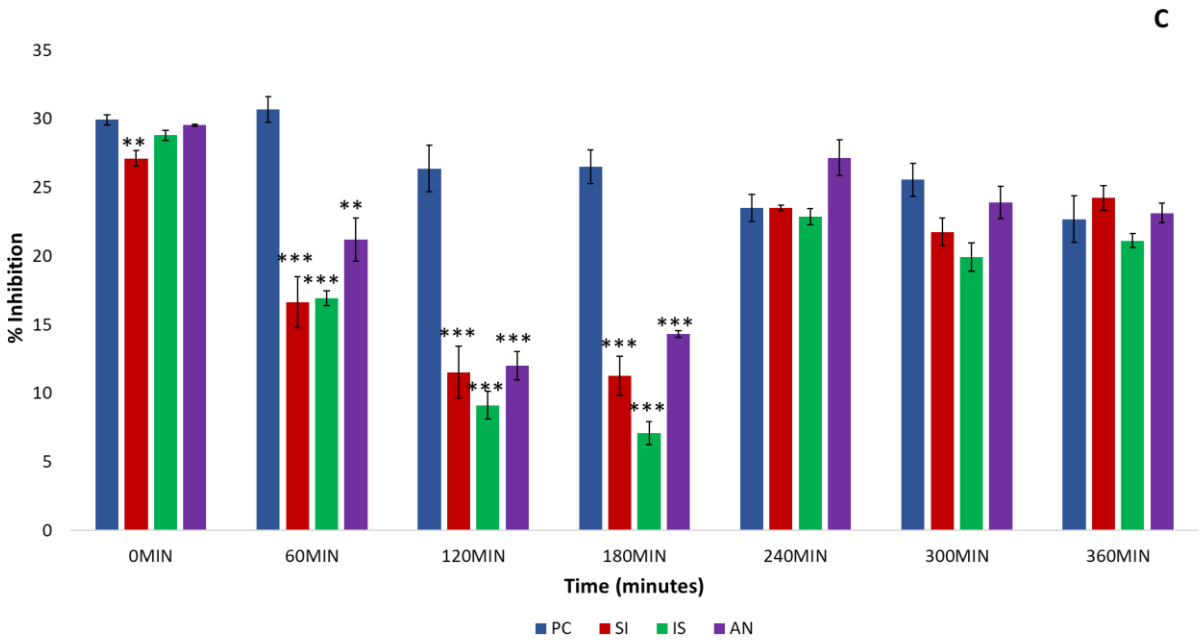
C
% Inhibition
35
30
25
20
15
10
5
0
0MIN
60MIN
120MIN
180MIN
240MIN
300MIN
360MIN
Time (minutes)
PC
SI
IS
AN

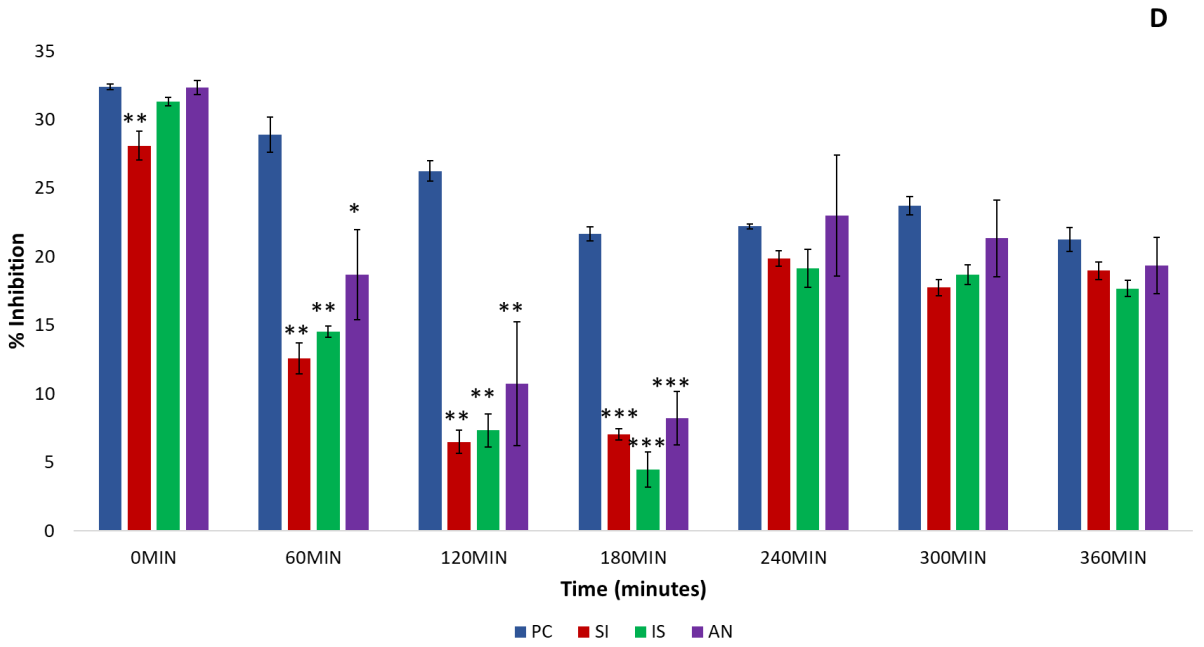
D
% Inhibition
35
30
25
20
15
10
5
0
0MIN
60MIN
120MIN
180MIN
240MIN
300MIN
360MIN
Time (minutes)
PC
SI
IS
AN

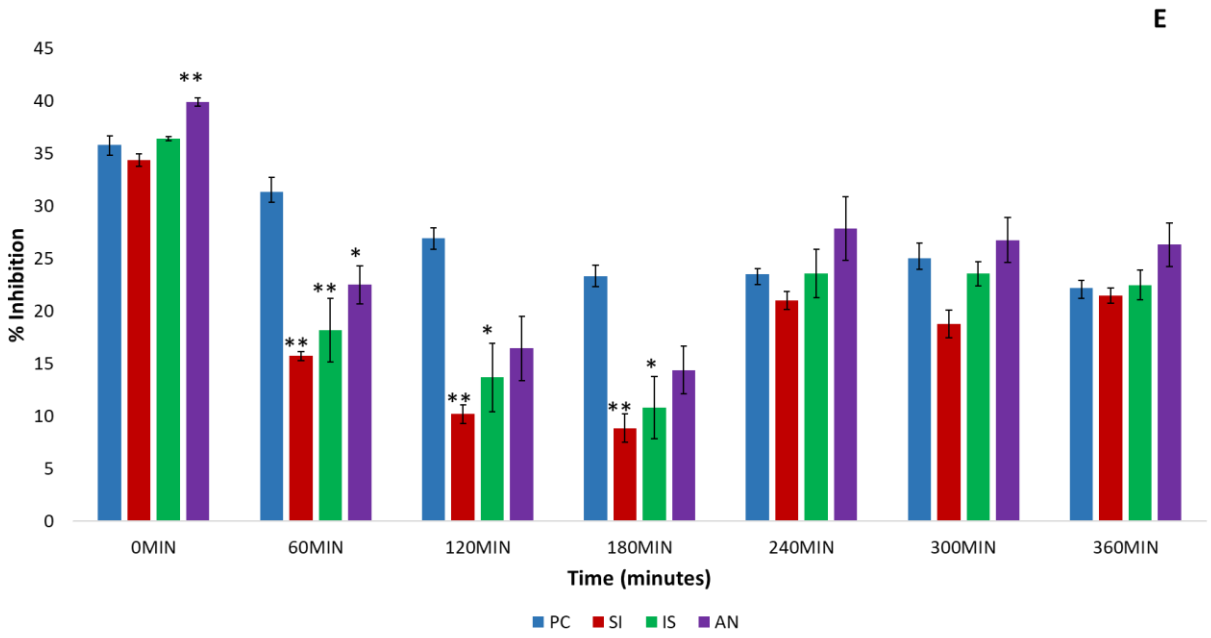

Figure 6.31: Nucleation assay of all compounds at various periods: A) 20µM, B) 40µM, C) 60µM, D) 80µM, E) 100µM. Values are expressed as mean ±SEM (n = 3) *P < 0.05, **P < 0.01, ***P < 0.001 vs PC

At 20 µM, silibinin is significant at 0 minutes (P < 0.05) and at 180 minutes (P < 0.01), indicating a delayed but sustained inhibitory effect. Isoeugenol and anethole also exhibit significant inhibition at 180 minutes (P < 0.01 and P < 0.05, respectively) (Figure 6.31A).

At 40 µM, silibinin demonstrates progressive inhibition, with significant reductions observed at 60 minutes (P < 0.05), 120 minutes (P < 0.01), 180 minutes (P < 0.001), and 300 minutes (P < 0.05). This suggests that silibinin's inhibitory activity increases over time, reinforcing its potential as a long-term inhibitor of nucleation (Figure 6.31B).

For isoeugenol at 40 µM, significant changes occur at 120 minutes (P < 0.05) and 180 minutes (P < 0.001), while anethole shows significance at 180 minutes (P < 0.01). These findings indicate that while anethole and isoeugenol exhibit inhibitory effects, they may not be as potent or consistent as silibinin at this concentration. Silibinin and Isoeugenol show highly significant inhibition (P < 0.001) at 60, 120, and 180 minutes (Figure 6.31C).

Anethole also exhibits strong inhibition at 60 minutes (P < 0.01), 120 minutes (P < 0.001), and 180 minutes (P < 0.001) (Figure 6.31C).

At 80µM, silibinin and Isoeugenol remain significantly inhibitory at 60 minutes ($P < 0.01$), 120 minutes ($P < 0.01$), and 180 minutes ($P < 0.001$). Anethole is also effective, showing significant inhibition at 60 minutes ($P < 0.05$), 120 minutes ($P < 0.01$), and 180 minutes ($P < 0.001$) (Figure 6.31D).

At 100µM, silibinin maintains significant inhibition at 60 minutes ($P < 0.01$), 120 minutes ($P < 0.01$), and 180 minutes ($P < 0.01$). Isoeugenol follows a similar trend, with significance at 60 minutes ($P < 0.01$), 120 minutes ($P < 0.05$), and 180 minutes ($P < 0.05$). Anethole shows significant inhibition at 0 minutes ($P < 0.05$) and 60 minutes ($P < 0.05$), reinforcing its effectiveness (Figure 6.31E).

The time-dependent nucleation assay assesses inhibition over 360 minutes, providing further insights into the long-term effects of the compounds. All tested phytochemicals show a dose-dependent increase in inhibition, except isoeugenol, which exhibits an unexpected reduction in inhibition at 40 µM. The time-course study helps determine whether the inhibitory effects are transient or sustained over an extended period.

6.13.1.2 Nucleation Assay of all concentrations in a single time point

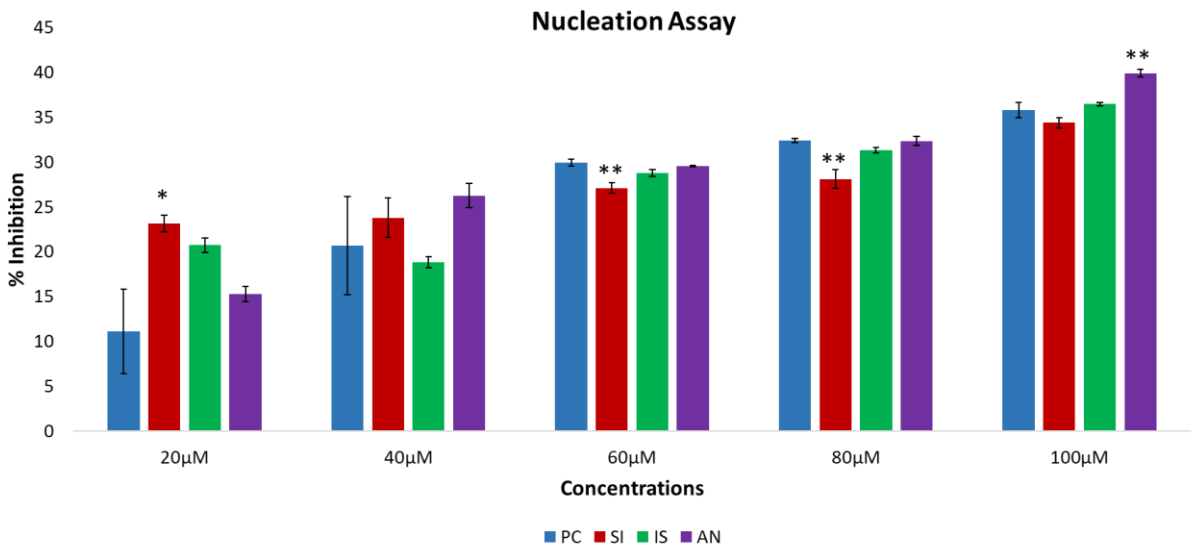

Figure 6.32: Nucleation assay of all compounds at various concentrations at 0 minutes. Values are expressed as mean ±SEM (n = 3) *$P < 0.05$, **$P < 0.01$, vs PC.

The quantitative data from the nucleation assay corroborate the microscopic observations. silibinin shows significantly better inhibition than potassium citrate at 20 µM ($P < 0.05$),

suggesting its superior efficacy in reducing crystal formation at lower concentrations. The inhibition remains significant at 60 μM and 80 μM ($P < 0.01$), though these values remain slightly lower than those observed in the PC group. Interestingly, anethole exhibits superior inhibition at 100 μM ($P < 0.01$), demonstrating its effectiveness at higher doses. However, isoeugenol does not show a significant difference from PC, indicating that its inhibitory potential may be lower than that of silibinin and anethole (Figure 6.32).

6.13.1.3 Microscopic Observations and Crystals Count of Nucleation Assay

Microscopic imaging at 100X magnification provides a qualitative view of crystal formation in different experimental groups. The control group shows a significant presence of crystals, highlighting the natural propensity for nucleation under experimental conditions. In contrast, the treatment and positive control (PC) groups exhibit a progressive reduction in crystal formation as the concentration of the compounds increases from 20 μM to 100 μM. This visual evidence suggests a dose-dependent inhibition of nucleation, which is a desirable characteristic in potential therapeutic agents for kidney stone prevention. The decrease in crystal number with increasing concentrations indicates that higher doses of these phytochemicals might effectively suppress nucleation (Figure 6.33). Very much aligned with the microscopic observation, crystals decreased significantly and inversely proportionately with concentrations of the phytochemicals, especially at higher concentrations, which indicates these phytochemicals can reduce the number of crystals in a given area (Figure 6.34).

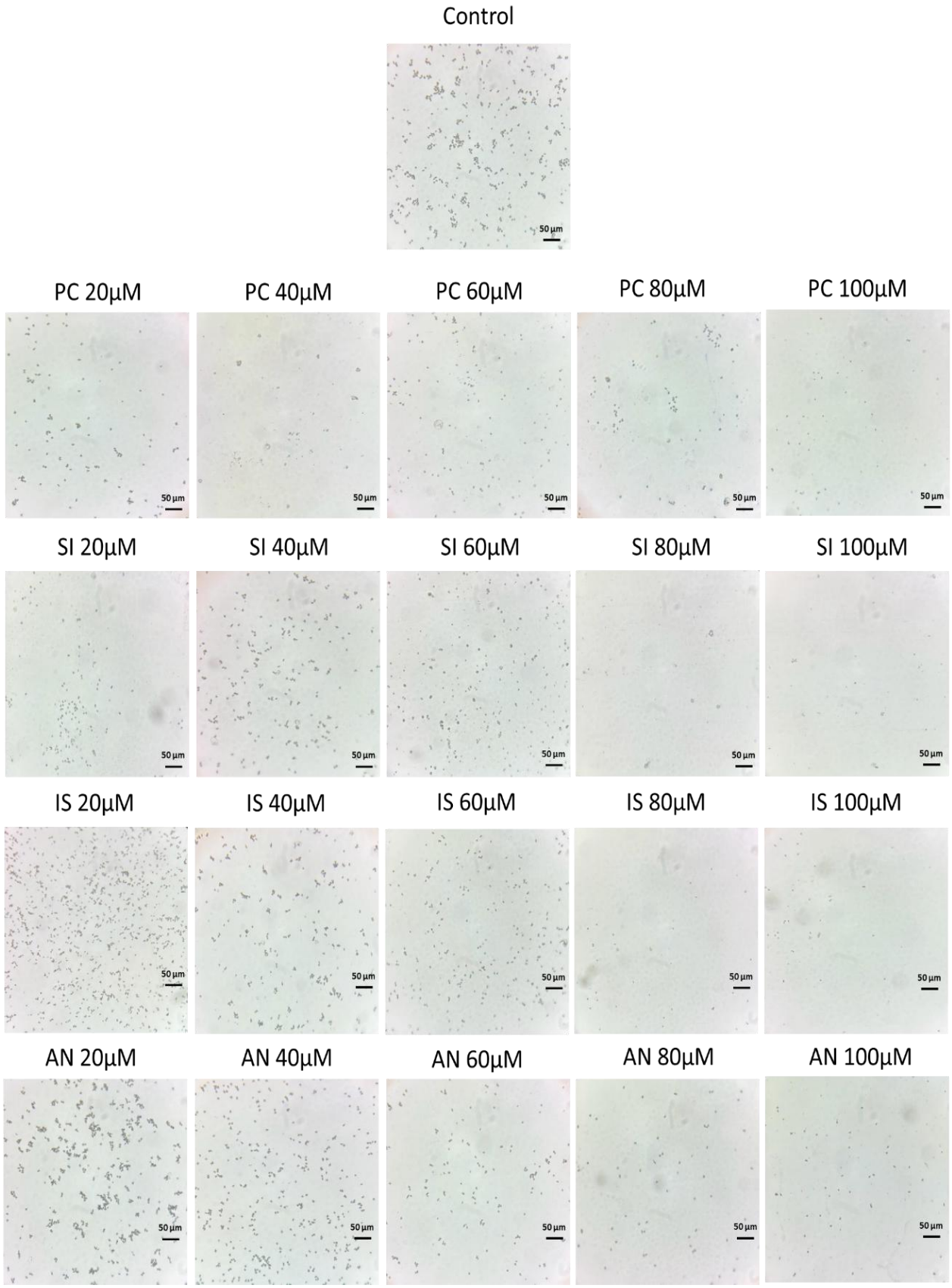

Figure 6.33: Microscopic images of nucleation assay at various concentrations (20-100µM) observed under 100X magnification.

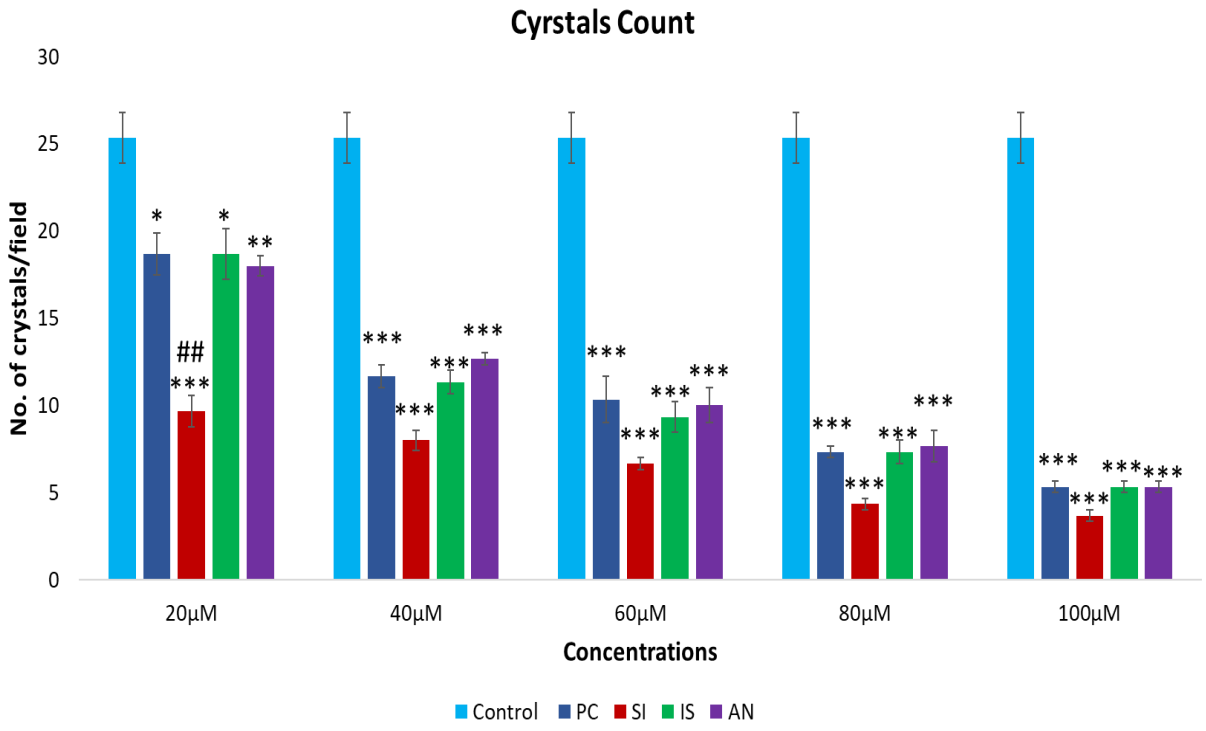

Figure 6.34: Number of crystals present at each concentration after observing under a microscope. Mean ±SEM (n = 3) *P < 0.05, **P < 0.01, ***P< 0.001, vs control, ## P<0.01 vs PC.

The findings from this study highlight several key trends:

1. **Dose-Dependent Inhibition:** Higher concentrations lead to greater reductions in nucleation, confirming the effectiveness of increasing phytochemical concentration for better inhibition.

2. **Time-Dependent Effects:** Some compounds, particularly silibinin, exhibit increasing inhibition over time, whereas others, such as Isoeugenol, show inconsistent effects at certain concentrations.

3. **Comparative Potency:**
    - **Silibinin** is the most effective inhibitor, showing consistent inhibition at multiple concentrations and time points.

- **Anethole** exhibits the strongest inhibition at 100 µM, suggesting its potential as a high-dose therapeutic agent.
- **Isoeugenol** shows mixed results, with effectiveness varying across concentrations and time points.

Interestingly, the expected time-dependent increase in inhibition was not observed in this study, unlike previously reported results by Abbas and Saadi (2023). This discrepancy may be attributed to differences in experimental setups, highlighting the need for standardised testing conditions in future studies.

6.13.2 Aggregation Assay

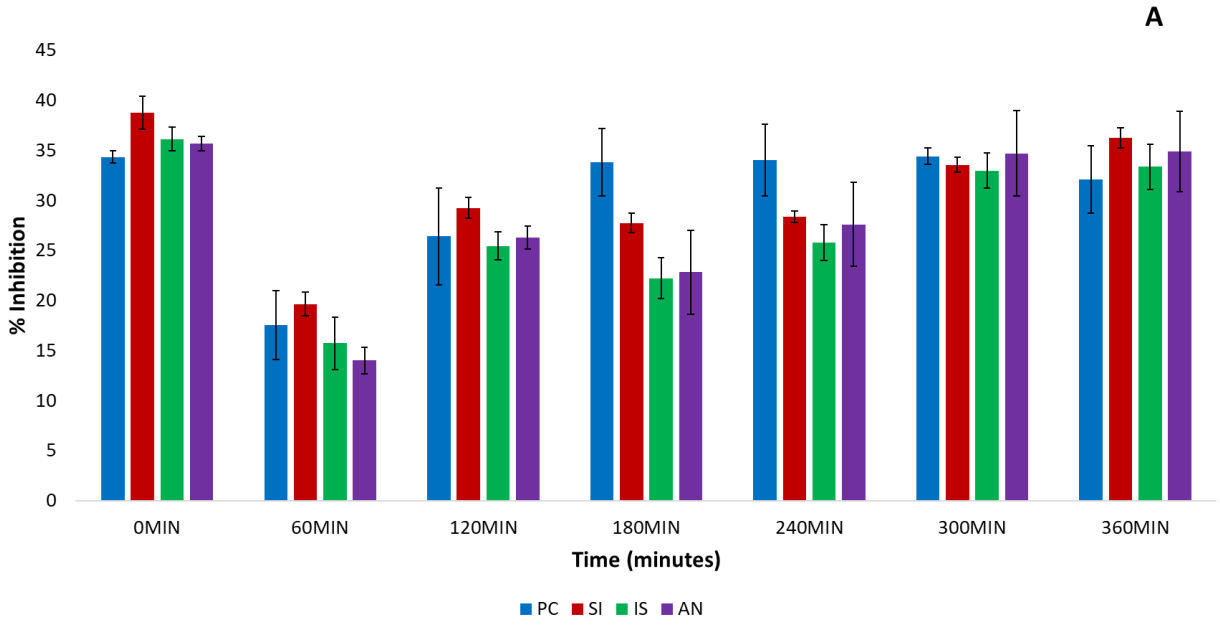

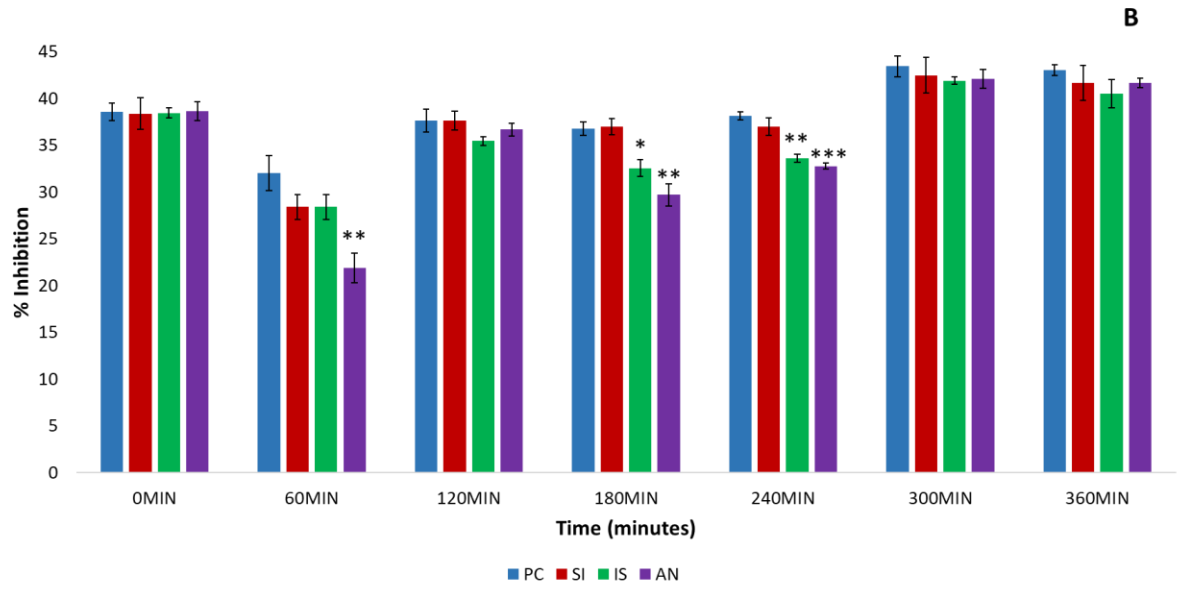
B
% Inhibition
0
5
10
15
20
25
30
35
40
45
**
*
**
**
***
0MIN
60MIN
120MIN
180MIN
240MIN
300MIN
360MIN
Time (minutes)
PC
SI
IS
AN

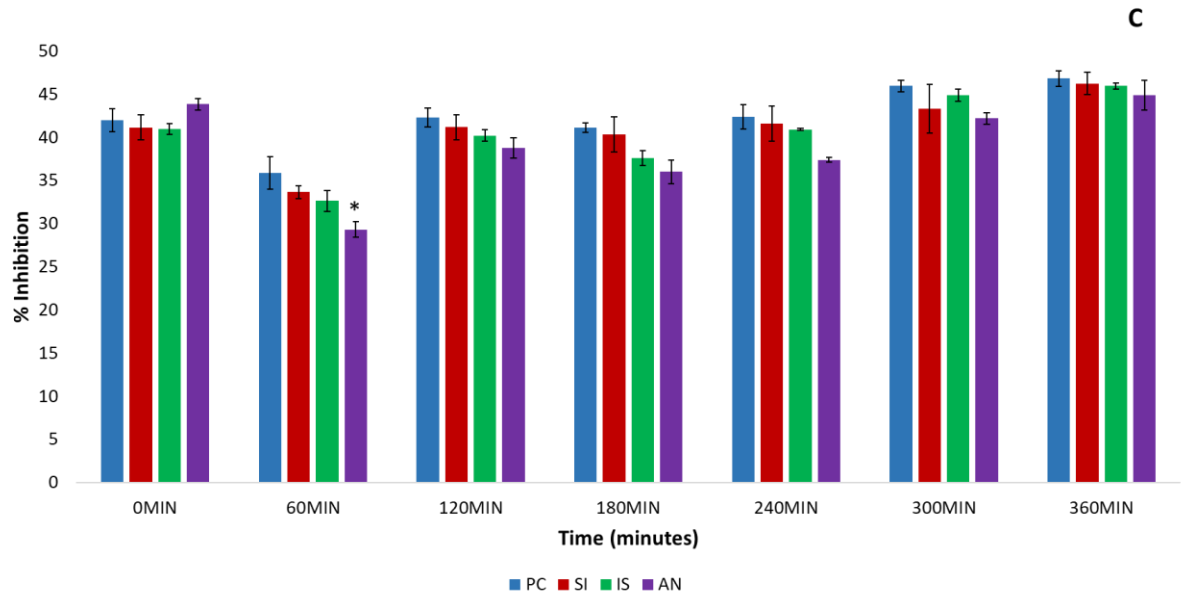
C
% Inhibition
0
5
10
15
20
25
30
35
40
45
50
*
0MIN
60MIN
120MIN
180MIN
240MIN
300MIN
360MIN
Time (minutes)
PC
SI
IS
AN

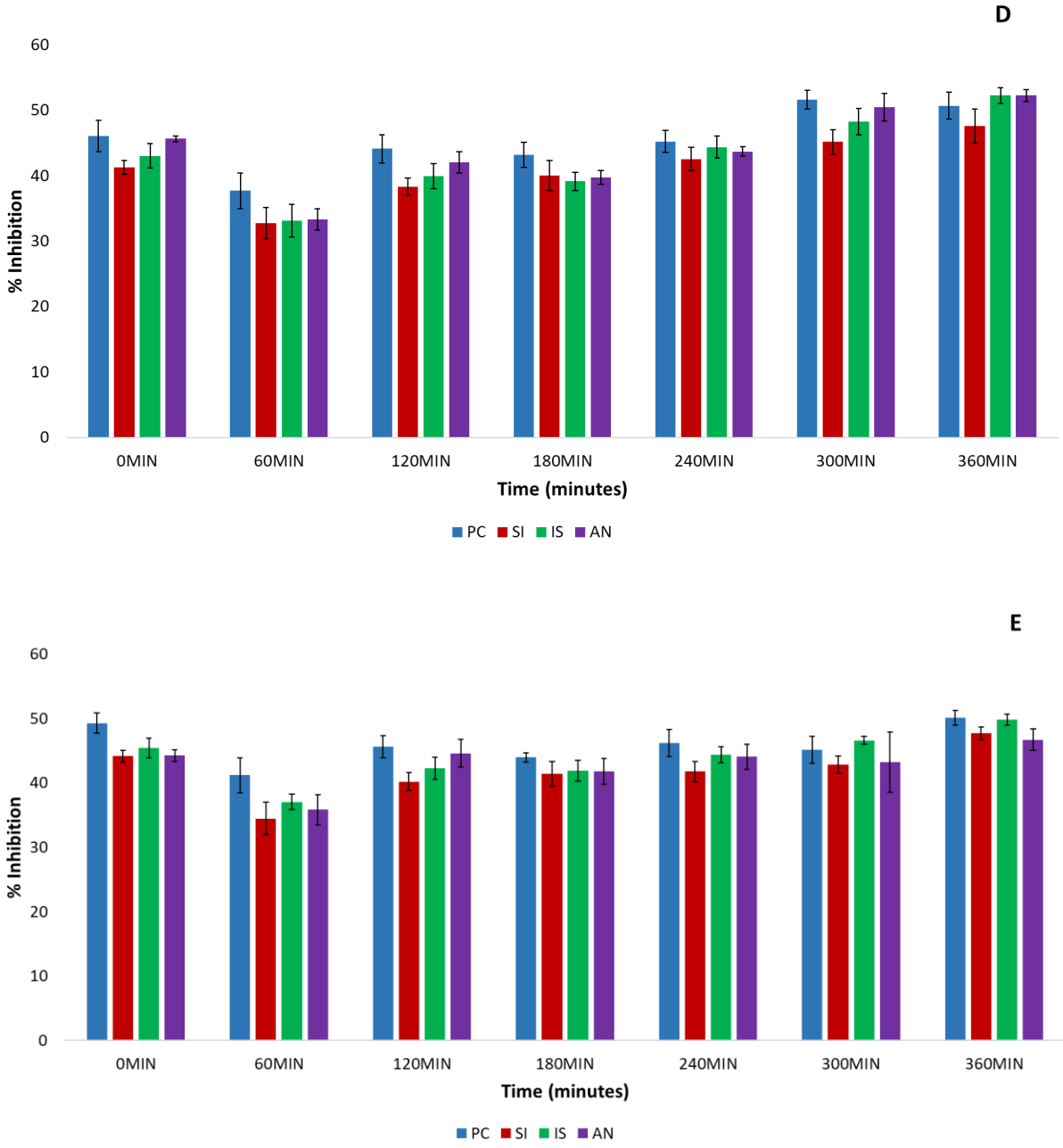

Figure 6.35: Aggregation assay of all compounds at various time span A) 20µM B) 40µM C) 60µM D) 80µM E) 100µM. Values are expressed as mean ±SEM (n = 3) *P < 0.05, **P < 0.01, ***P < 0.001 vs PC

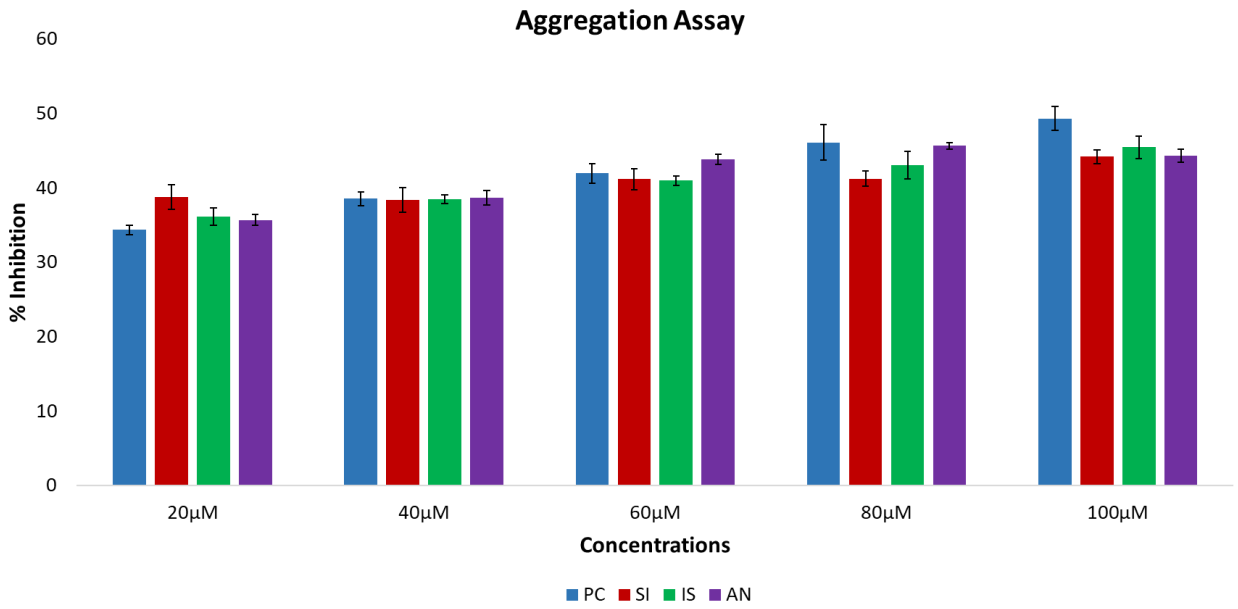

Figure 6.36: Aggregation assay of all compounds at various concentrations. Values are expressed as mean ±SEM (n = 3).

An aggregation assay over 360 minutes duration offers little significance, as can be seen in Figure 6.35. Silibinin didn't show any significant changes compared to PC across all the concentrations from Figure 6.35A to 6.35B. Isoeugenol did show some significant change, as can be seen in Figure 6.35B at 180 minutes ($p<0.05$) and 240 minutes ($p<0.01$). Anethole, on the other hand, showed significant changes at 60 minutes ($p<0.01$), 180 minutes ($p<0.01$) and 240 minutes ($p<0.001$) in Figure S2B and at 60 minutes ($p<0.05$) in Figure 6.25C. Dose dependent increase was observed for aggregation inhibition which was in the range of 35-50%. There weren't any significant changes observed when compared to PC in aggregation assay as can be seen in Figure 6.36.

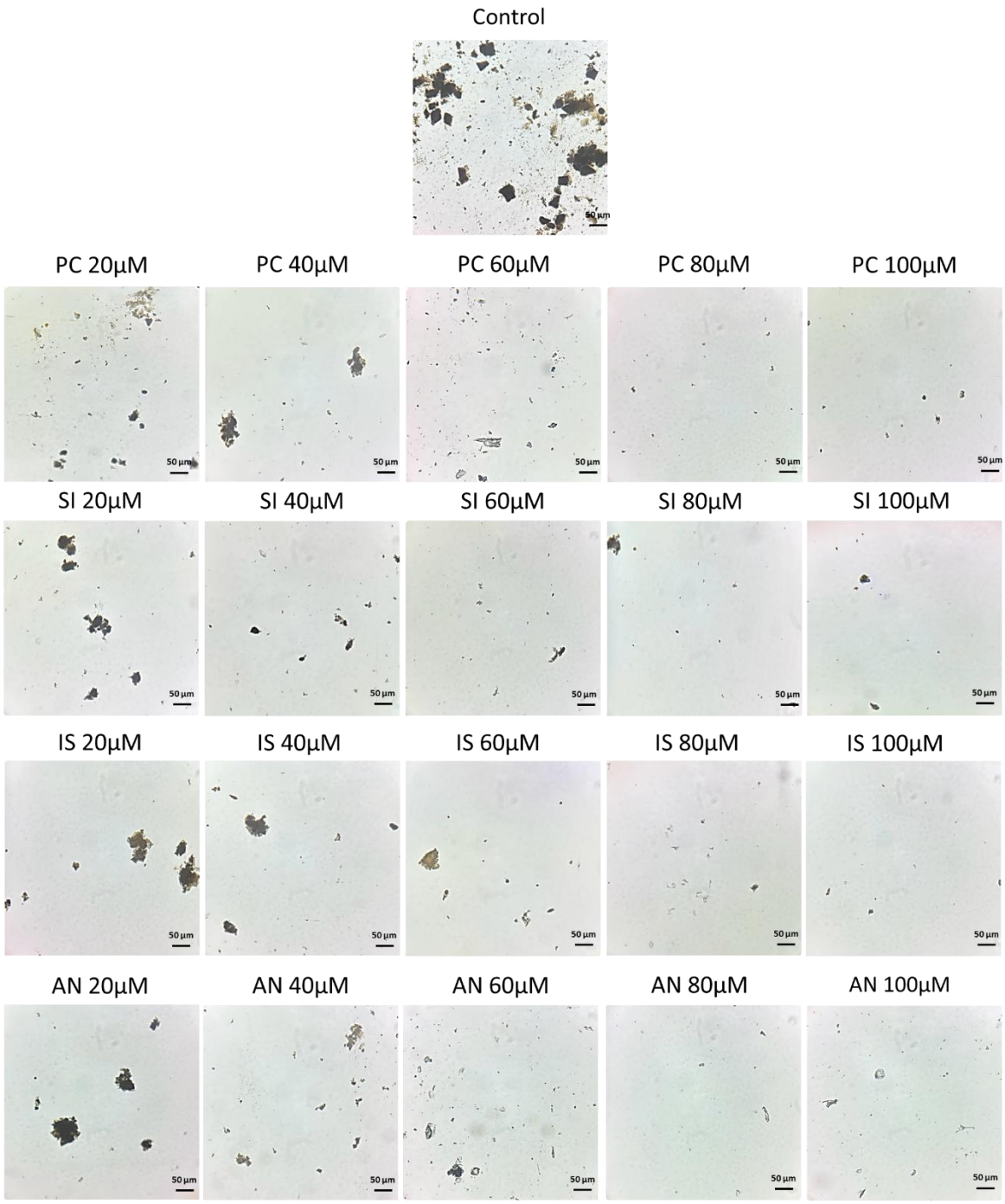

Figure 6.37: Microscopic images of aggregation assay at various concentrations (20-100µM) observed under 100X magnification.

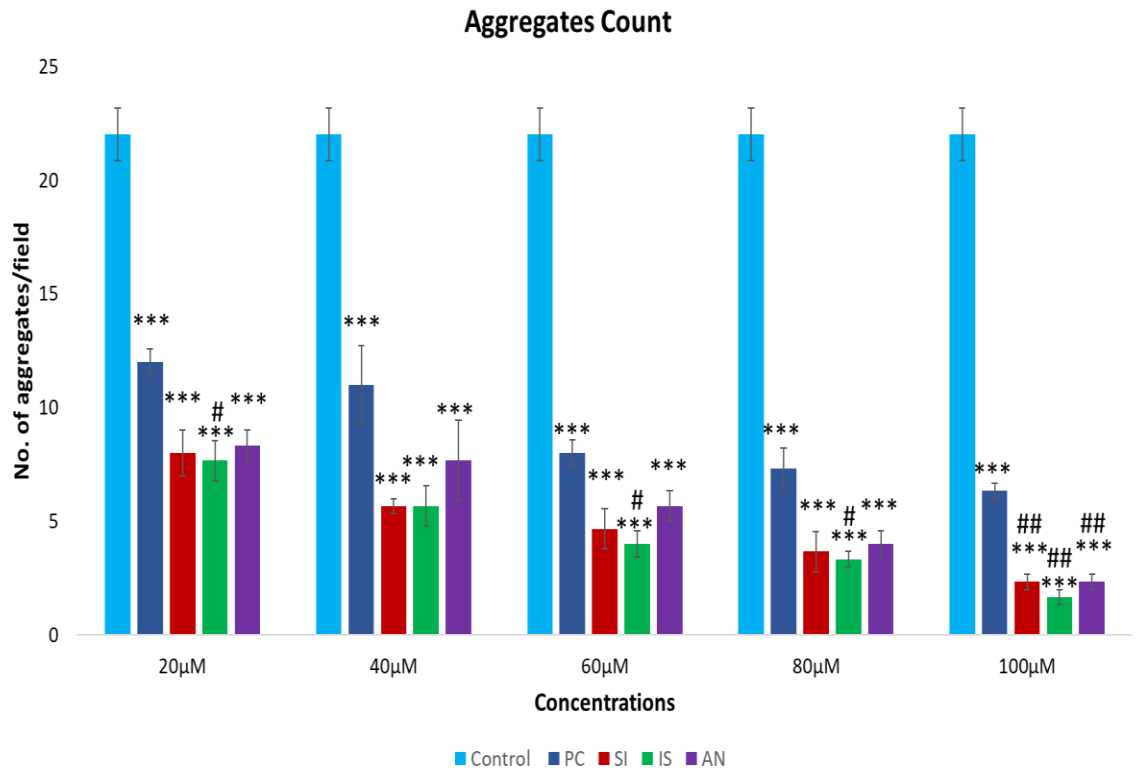

Figure 6.38: Number of aggregates present at each concentration after observing under a microscope. Mean ±SEM (n = 3) *P < 0.05, **P < 0.01, ***P< 0.001, vs control, #P < 0.05, ## P<0.01 vs PC.

Microscopic observation in Figure 6.37 revealed that the control group had large aggregates. On the contrary, the treatment group had low aggregates and even lower as we went towards the higher concentration, hence dose dose-dependent decrease was observed. Very much aligned with the microscopic observation, aggregate count decreased significantly and inversely proportionately with concentrations of the phytochemicals, especially at higher concentrations, which indicates these phytochemicals can reduce the number of aggregates in a given area (Figure 6.38).

6.13.3 Oxalate depletion assay

After the oxalate depletion assay, when the crystals were visualised under the microscope, as can be seen in Figure 6.39, the control had few irregular-shaped crystals, while the treatment and positive control groups had significantly reduced the number as well as the size of the crystals.

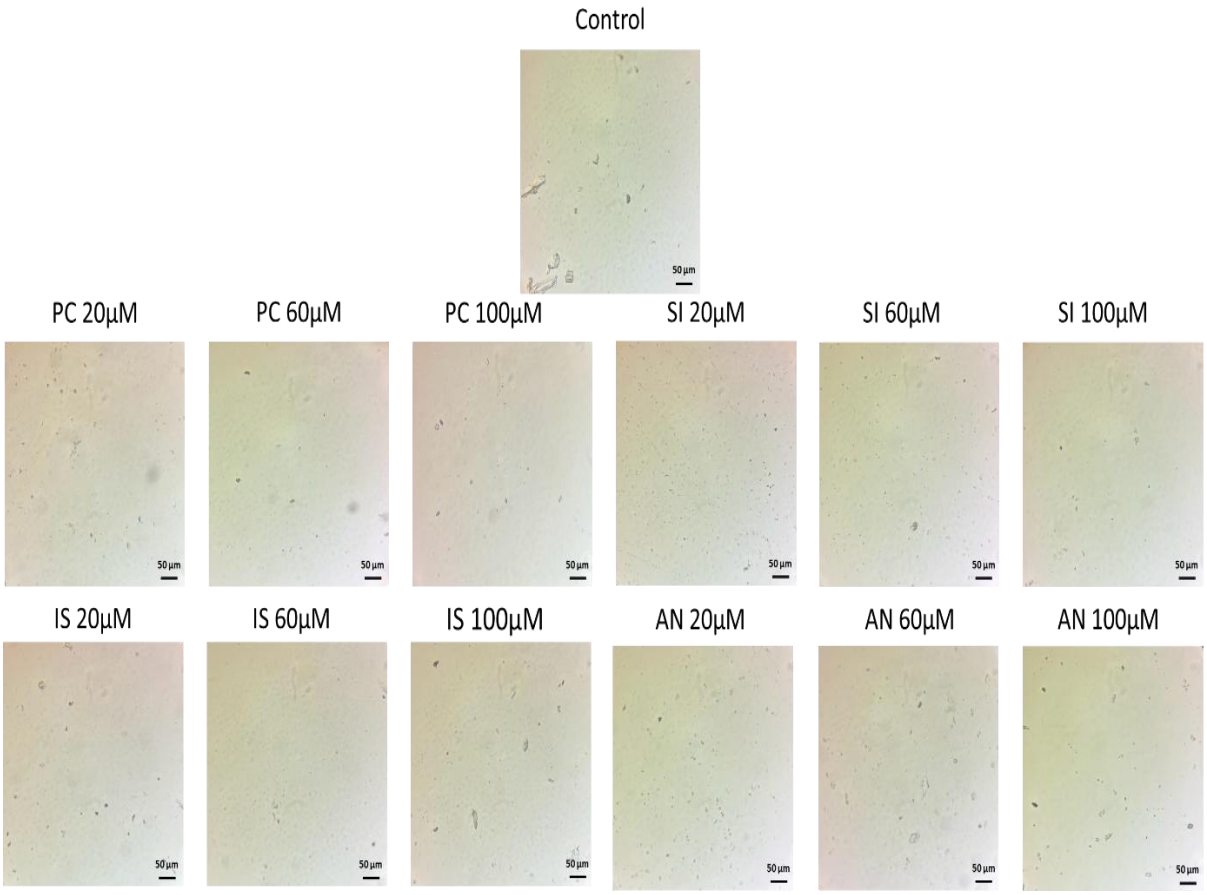

Figure 6.39: Microscopic images of oxalate depletion assay at various concentrations (20-100µM) observed under 100X magnification.

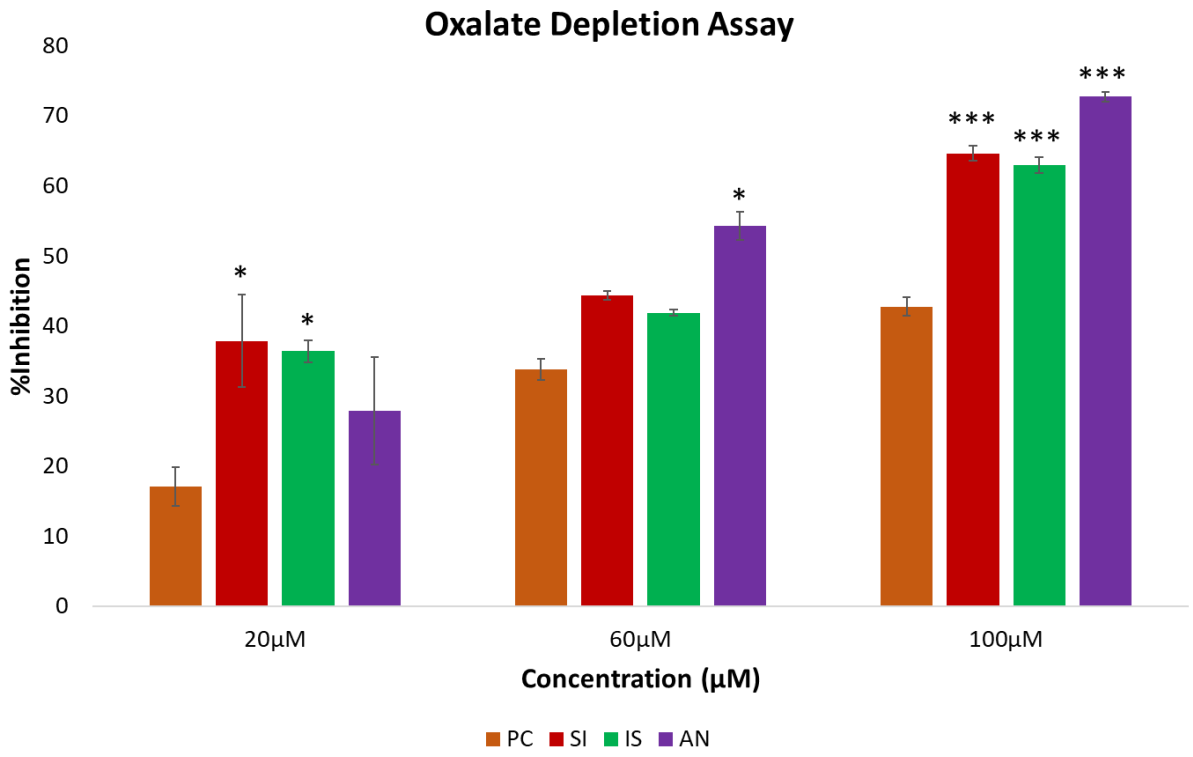

Figure 6.40: Oxalate Depletion assay of all compounds at various concentrations at 0 minutes. Values are expressed as mean ±SEM (n = 3). *P < 0.05, **P < 0.01, ***P<0.001, vs PC

In the case of the oxalate depletion assay, as can be seen in Figure 6.40, all the compounds showed a dose-dependent increase inhibition. Silibinin (37.86 ± 1.48 %, p<0.05) and Isoeugenol (36.36 ± 1.29%) showed significantly better inhibition than PC (17.05 ± 2.76%) at 20µM concentration. Anethole showed better inhibition (54.24 ± 1.98%, p<0.05) than PC (33.78 ± 6.60%) at 60µM concentration. At 100µM, all three compounds, Silibinin (64.60 ± 0.41%, p<0.001), Isoeugenol (62.98 ±1.12%, p<0.001) and Anethole (72.72 ± 0.69%, p<0.001) showed better inhibition than PC (42.77 ± 1.57%).

6.14 Crystallization Kinetics

6.14.1 Effect of phytochemicals on induction time

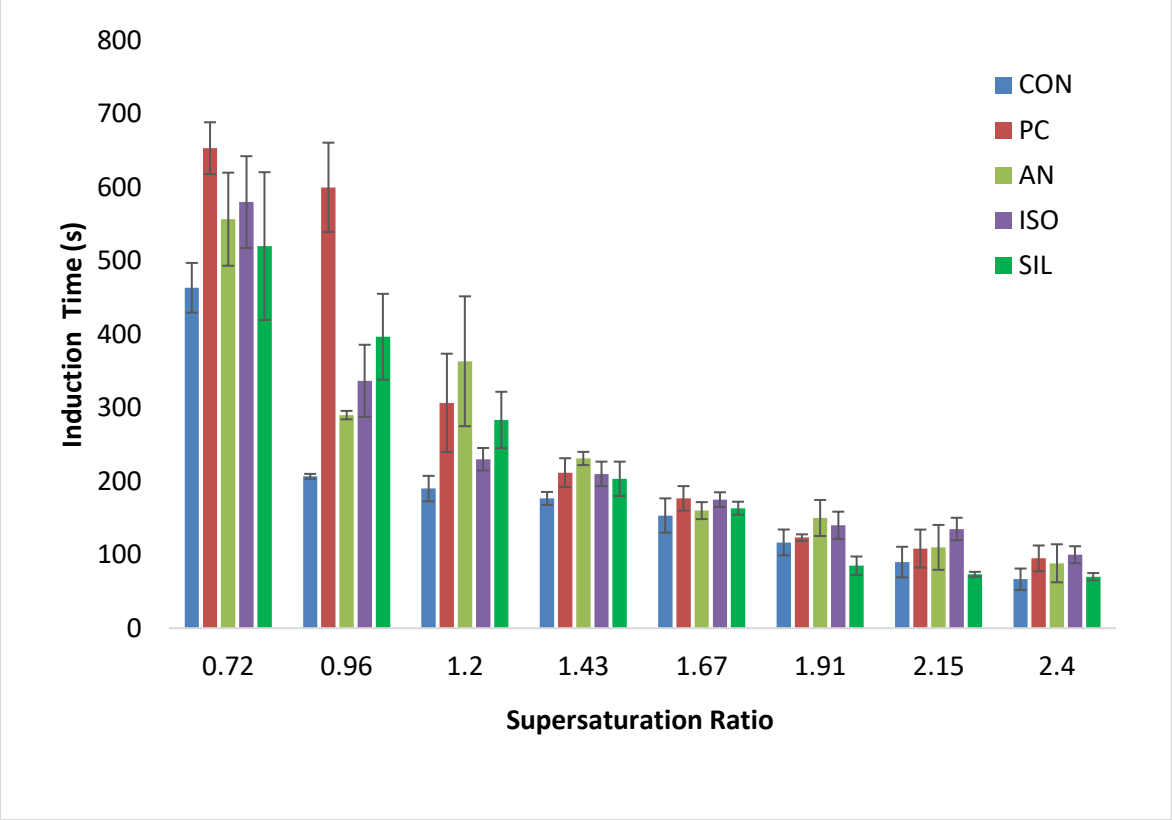

Figure 6.41: Effect of Supersaturation ratio on induction time (s) with and without inhibitors. The data are presented as mean ± SEM (n=3) of measurements from three independent experiments.

Figure 6.41 displays the induction time results at different supersaturation ratios (SRs) with and without phytochemicals (control). The findings indicate that all phytochemicals, along with potassium citrate, increased the induction time across all tested SRs. This implies that the system took a longer time to nucleate detectable crystals. Additionally, UV–vis absorbance was analysed under varying SRs in the presence and absence of phytochemicals.

The induction time data were further utilised to determine the surface energy and critical nucleus size of calcium oxalate monohydrate (COM) using classical nucleation theory.

6.14.2 Surface energy calculation (γ)

The relation between inverse log square of supersaturation ratio ($1/ \log^2 S$) and log induction time over a range of supersaturation ratio (1.43 to 2.4) was used for calculation of surface

energy of nuclei and free energy barrier derived from classical homogenous nucleation theory (Oxtoby, 1992). To understand the nucleation rate and crystal growth, it is critical to determine surface energy or interfacial tension, which can be calculated from the equation 2. Here B is slope of log induction time and 1/ $\log^2 S$, R is gas constant, T is absolute temperature, β is geometric shape factor, V is molar volume, NA is Avogadro number and f(θ) is the Correction factor.

$$\gamma 3 = B * \frac{(2.3RT)3}{RT\beta V2NAf(\theta)} \quad (2)$$

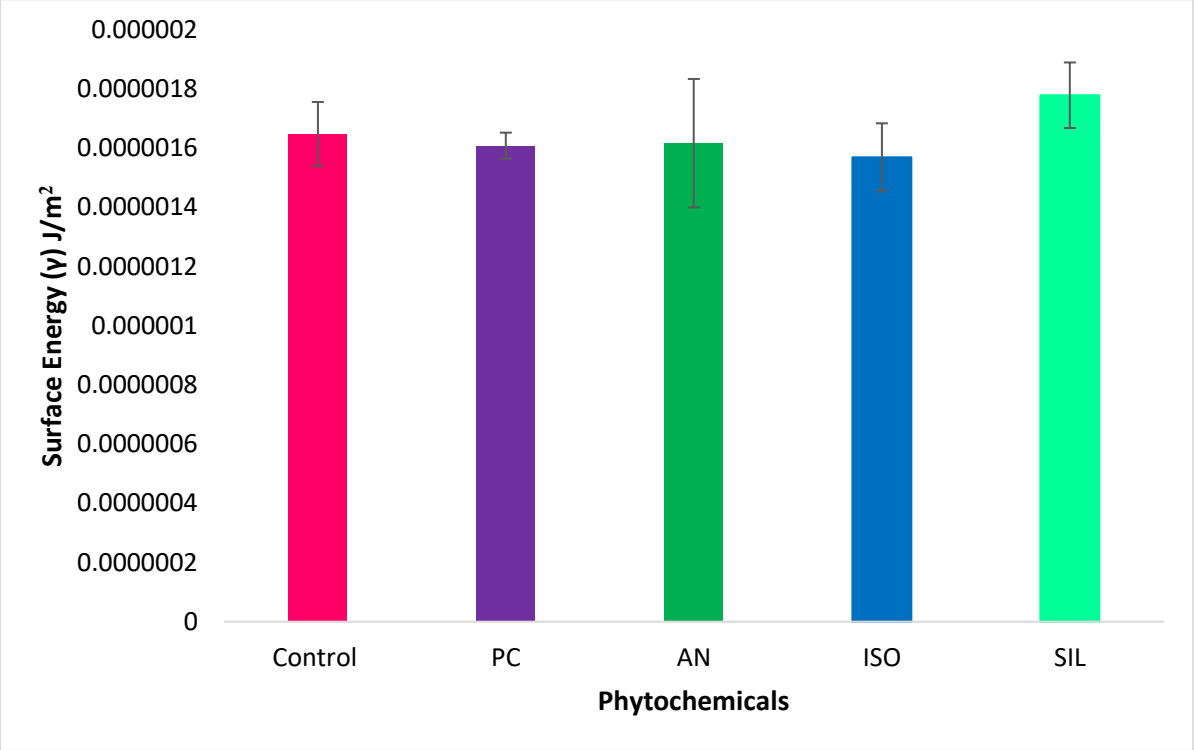

Figure 6.42: Surface energy of calcium oxalate with and without phytochemicals. The data are presented as mean ± SEM (n=3) of measurements from three independent experiments.

The surface energy values of calcium oxalate crystals formed under different conditions are summarized in Figure 6.42. The results suggest that the presence of phytochemicals generally reduced the surface energy compared to the control, except in the case of silibinin, where it was higher. As we can see, all the compounds' surface energy is around the control values except silibinin, which is higher than the control. The more the surface energy, the lesser the nucleation rate, as can also be seen in Figure 6.42. Here, increasing supersaturation increases the nucleation rate. Except for silibinin, all other compounds show similar nucleation rates to that of the control across all the supersaturation ratios. This indicates that silibinin can greatly slow down the nucleation process. X-ray diffraction (XRD) analysis confirmed that the formed

crystals, regardless of the presence of phytochemicals, were primarily calcium oxalate monohydrate. As a result, the constants for COM crystals were used to calculate the surface energy of nuclei under both conditions. The calculated surface energy for PC, AN, and ISO was lower than that of the control, whereas for SIL, it was higher due to variations in crystal structure.

6.14.3 Nucleation rate (Js)

The rate of nuclei formed per unit time is referred as nucleation rate and calculated from equation 3 (Lancia et al., 1999; Myerson, 2002) derived from classical homogeneous nucleation theory Here Js is nucleation rate, and F is Frequency constant (10^{30} nuclei/cm3) (Izmailov et al., 1999).

$$Js = F\frac{exp[-\beta\gamma 3V2NAf(\theta)]}{(RT)3ln2S} \qquad (3)$$

Knowing the Surface energy (γ) of calcium oxalate aids in calculating the nucleation rate (Js). Also, it is challenging to apply at lower supersaturation ratios (Myerson, 2002) due to its error in log calculations, hence, the lower three supersaturation ratios were eliminated for calculations of surface energy and nucleation rate.

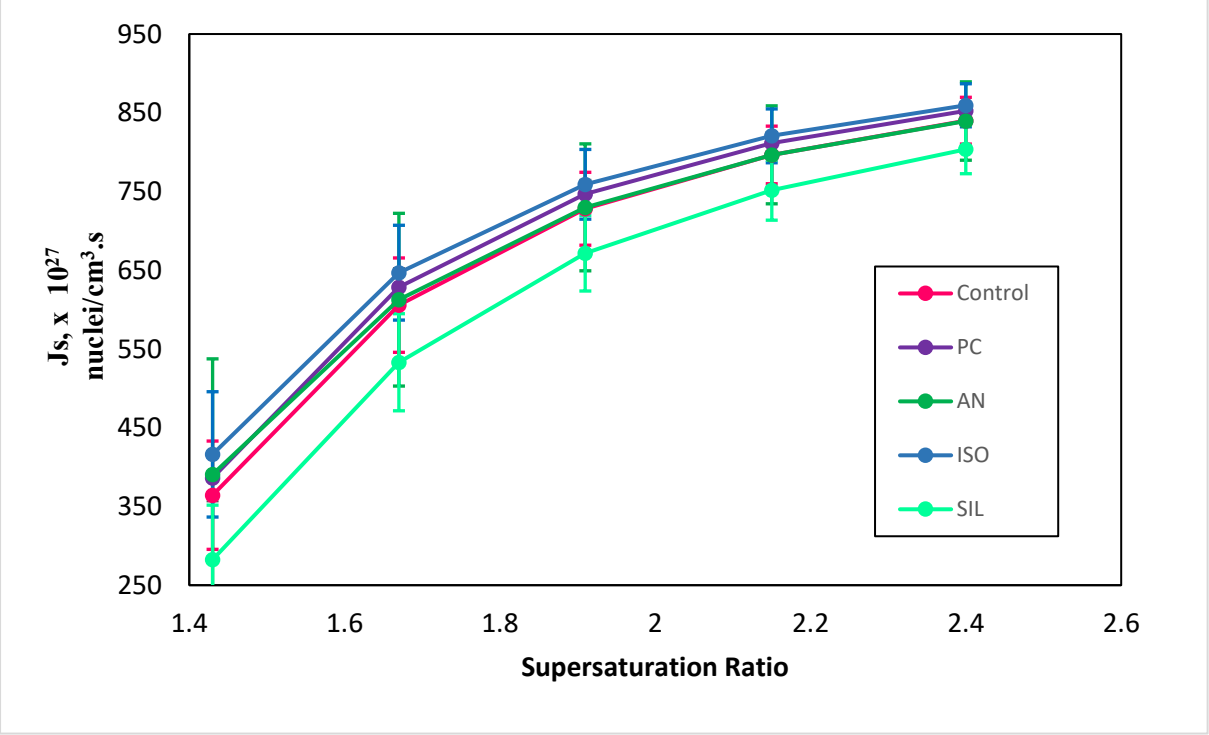

Figure 6.43: Nucleation rate (Js) of calcium oxalate with and without phytochemicals. The data are presented as mean ± SEM (n=3) of measurements from three independent experiments.

The calculated nucleation rates for calcium oxalate crystals, both with and without phytochemical additives at high supersaturation ratios (SRs), are presented in Figure 6.43. The results indicate that nucleation rates increase as SR rises, regardless of the presence of phytochemicals. However, the addition of silibinin consistently reduces the nucleation rate across all studied SRs compared to the control, while the other phytochemicals showed no significant impact.

A lower SR results in fewer nuclei formation and a slower growth rate of existing crystals. As a result, these nuclei have a reduced probability of developing into larger crystals compared to those formed under higher SR conditions. At an SR of 2.4, the recorded nucleation rates were 839.96×10^{27} nuclei/cm³·s for the control (CON), 852.46×10^{27} nuclei/cm³·s for PC, 839.52×10^{27} nuclei/cm³·s for AN, 859.51×10^{27} nuclei/cm³·s for ISO, and 803.58×10^{27} nuclei/cm³·s for SIL.

6.14.4 Calculation of free energy change (ΔGcr) and critical nucleus radius (r)

Classical Nucleation Theory explains the energy barrier to nucleation in terms of Gibbs free energy, which consists of surface and volume free energy. In a supersaturated solution, the total energy reaches its highest point at a specific particle size known as the critical size. When a cluster grows to this critical size, it is identified as a nucleus (Abdel-Aal EA et al., 2017).

Interfacial free energy is the difference of free energy between single molecule of bulk and that of the surface. In a supersaturated solution, ions or molecules join together to form a cluster or nucleus, which leads to the exchange of excess free energy between the nucleus and solutes of the supersaturated solutions, referred to as Gibbs free energy changes (ΔGcr).

Gibbs free energy changes (ΔGcr) for critical nucleus size formation are calculated by the following equation, where K is Boltzmann constant (1.380649×10^{-23} joule per kelvin) and T is absolute temperature.

$$Js = F \exp[-\frac{\Delta Gcr}{KT}]$$

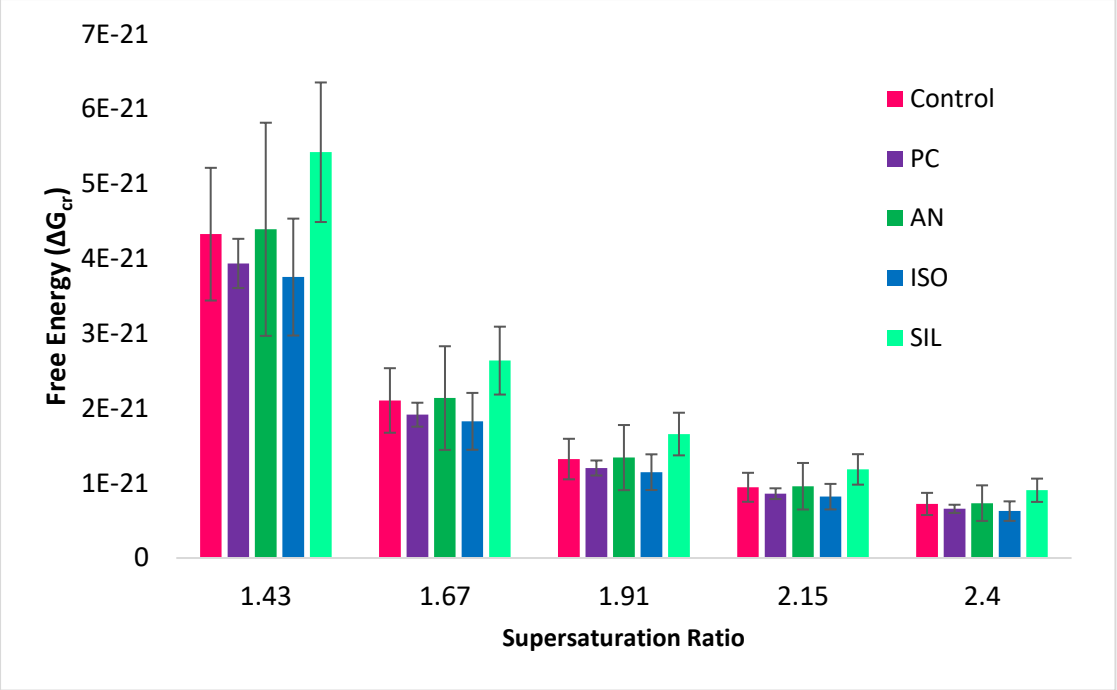

Figure 6.44: Free energy change of calcium oxalate with and without phytochemicals. The data are presented as mean ± SEM (n=3) of measurements from three independent experiments. Here, CON- control, PC- positive control, AN- anethole, ISO- isoeugenol, SIL- silibinin

The calculated free energy changes (ΔGcr) for the formation of critical nucleus sizes are presented in Figure 6.44. The findings indicate that as the supersaturation ratio (SR) increases, the Gibbs free energy required for the formation of a critical nucleus decreases. However, the addition of silibinin and anethole led to an increase in ΔGcr compared to the control. Notably, at high SRs, a lower energy barrier allows nuclei to stabilise and grow more rapidly.

The critical radius (r) is then calculated by the following equation.

$$\Delta Gcr = (4/3)\pi r^2 \gamma$$

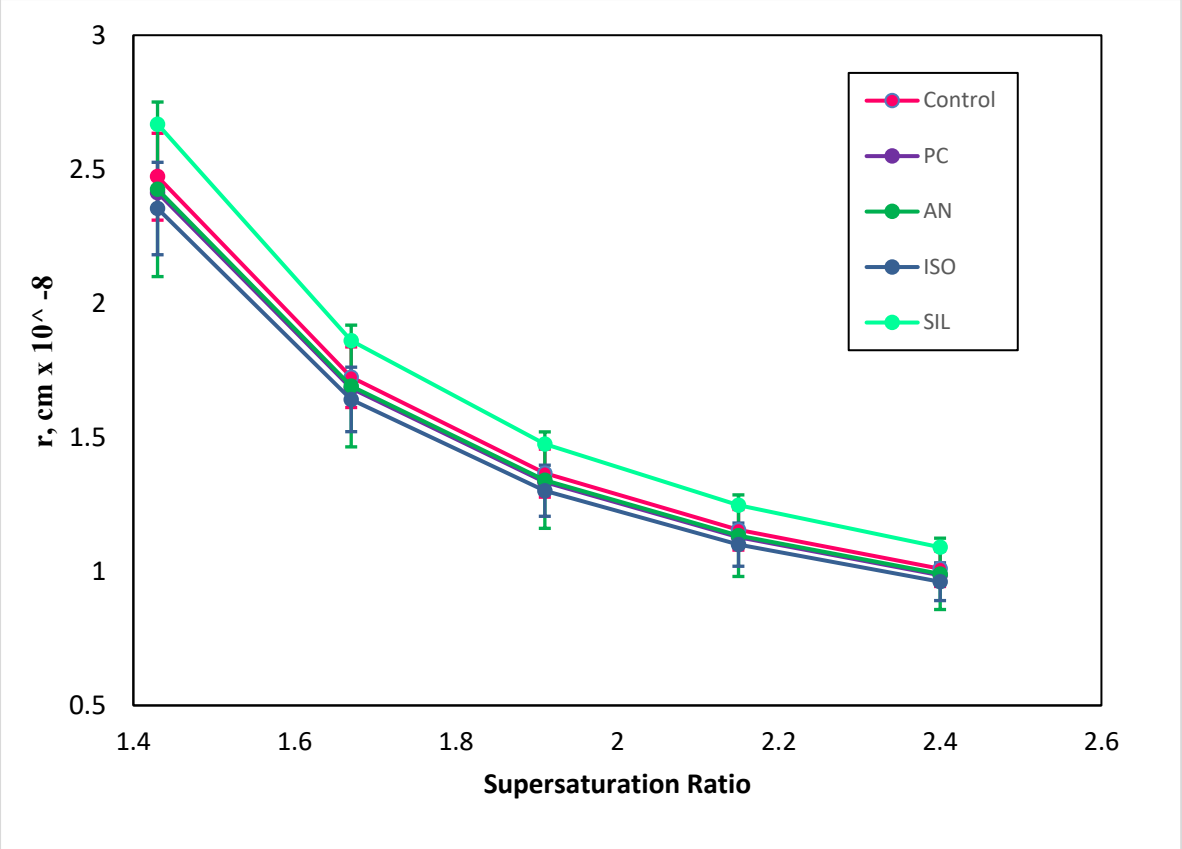

Figure 6.45: Critical radius of nucleus changes of calcium oxalate with and without phytochemicals. The data are presented as mean ± SEM (n=3) of measurements from three independent experiments. Here, CON- control, PC- positive control, AN- anethole, ISO- isoeugenol, SIL- silibinin

Figure 6.45 presents the calculated critical nucleus radius (r) at different SRs, both with and without phytochemical additives. The findings show that as SR rises, the critical nucleus radius necessary for stable nucleus formation decreases. In contrast, the addition of silibinin leads to an increase in the critical nucleus radius compared to both the control and other phytochemicals at all studied SRs.

6.14.5 Fourier Transform Infrared Spectroscopy (FTIR)

Fourier Transform Infrared Spectroscopy (FTIR) is a valuable technique used to identify chemical structures by analysing how molecules vibrate when exposed to infrared light. In this case (Figure 6.46), FTIR helps confirm the presence of calcium oxalate monohydrate (COM), a common component of kidney stones, and reveals how different substances may interact with it.

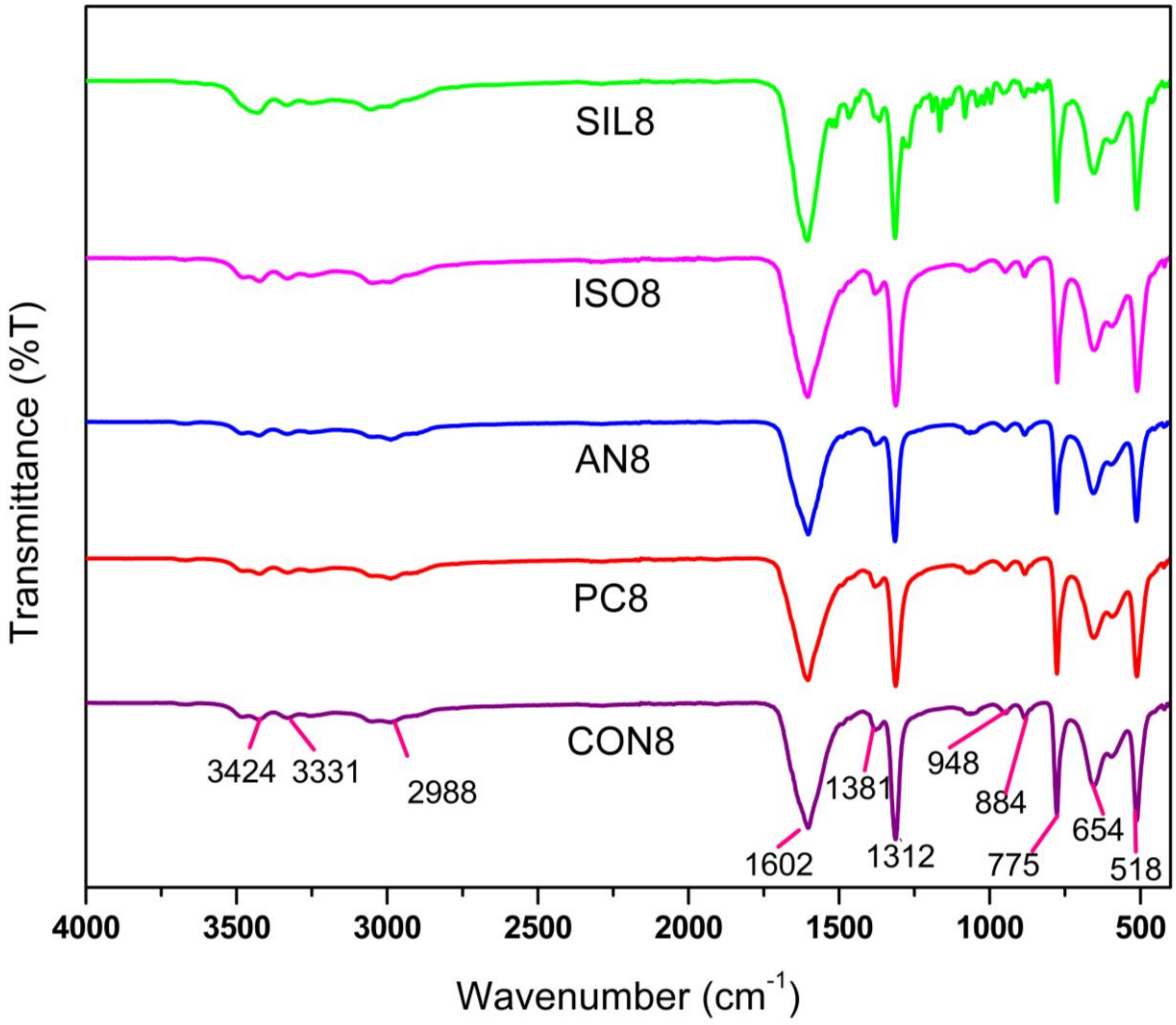

Figure 6.46: FTIR spectrum of all the groups. Here, CON- control, PC- positive control, AN- anethole, ISO- isoeugenol, SIL- silibinin. 8-8th supersaturation ratio (2.6).

FTIR spectra provide insights into the chemical structure and interactions within the various samples at 8th supersaturation ratio, including control (CON8), potassium citrate (PC8), anethole (AN8), isoeugenol (ISO8), and silibinin (SIL8).

Breaking Down the Key FTIR Peaks

1. **948 cm^{-1} (C–O Stretching Vibration)**
    - This peak is associated with C–O stretching, a key feature of the oxalate molecule in COM.
    - It provides insight into the stability of the oxalate structure, and any changes in this peak might indicate interactions that alter crystal formation.

2. **775 cm^{-1} (C–C Stretching Vibration)**
    - This peak corresponds to the stretching of carbon-carbon (C–C) bonds within the oxalate group.
    - It helps confirm the connectivity within the molecule, and shifts in its position could suggest structural changes in the crystal.
3. **654 cm^{-1} (Hydroxyl Group Bending Vibration)**
    - This peak is linked to the bending movement of hydroxyl (-OH) groups, which are important for hydration in COM.
    - Since COM retains water molecules, this peak helps determine how hydration levels affect crystal stability.
4. **1602 cm^{-1}, 1381 cm^{-1}, and 1312 cm^{-1} (Carbonyl Group Vibrations)**
    - These peaks represent the stretching movements of carbonyl (C=O) groups found in oxalate.
    - The 1602 cm^{-1} peak corresponds to asymmetrical stretching, while 1381 cm^{-1} and 1312 cm^{-1} are linked to symmetrical stretching.
    - If these peaks shift or change in intensity, it could mean that a substance is interacting with the crystal, potentially disrupting its growth.
5. **3000–3400 cm^{-1} (Hydroxyl Group Stretching Vibrations)**
    - This broad peak represents hydroxyl (-OH) stretching, commonly linked to water molecules in hydrated compounds.
    - Since COM contains water, this peak confirms its hydrated nature and could change if a substance affects hydrogen bonding.
    - A decrease in this peak might indicate reduced hydration, which could impact how stable or soluble the crystal is.

6.14.6 Particle Size and Zeta Potential Measurements

Zeta potential measures system stability and the surface charge of molecules by analysing the intensity with which mutual attraction and repulsion occur between particles (Xie et al., 2021). High surface charge density indicates lower particle aggregation due to electrostatic repulsion and stability, and vice-versa (Miyake et al., 1998; Polat et al., 2021). Particles with higher negative or positive zeta potential repel each other, whereas particle with lower negative or positive zeta potential (near to zero) tends to aggregate (Cho et al., 2014).

Table: 6.13 Size and potential of calcium oxalate with and without phytochemicals. Here, CON- control, PC- positive control, AN- anethole, ISO- isoeugenol, SIL- silibinin. 1- 1st supersaturation ratio (1.4) 8-8th supersaturation ratio (2.6).

Sample	Size (nm)	Zeta potential (mV)
CON1	11530 ± 1160	-19.1 ± 1.45
PC1	801.9 ± 31	-20 ± 1.22
AN1	1626.5 ± 145.5	-19.73 ± 1.15
ISO1	1196 ± 42	-17.1± 1.35
SIL1	1705 ± 27	-16.33 ± 0.37
CON8	19310 ± 1560	-22.26 ± 0.06
PC8	807.15 ± 61.55	-28.5 ± 0.75
AN8	3980.5 ± 65.5	-38.8 ± 0.75
ISO8	1379 ± 171	-23.2 ± 0.75
SIL8	1737 ± 18	-25.66 ± 1.43

Factors that directly affect zeta potential include surface structure, composition and ionic strength of solution (Sun et al., 2018). Human kidneys are generally isotonic with slightly acidic pH (Odya et al., 1978). The Zeta potential of all the groups is mentioned in Table 6.13. We can see that for the lower supersaturation ratio, no specific pattern was observed for the control but at higher control group had the lowest zeta potential, indicating system stability by all the compounds. Also, a significant size difference was observed when compared to control at both supersaturation ratios.

6.14.7 X-Ray Diffraction

Peaks found in the XRD graph (Figure 6.47) are specific to the monohydrate form of calcium oxalate when compared with PDF card 00-020-0231 and also mentioned in reference papers (Montealegre et al., 2017; Akyol, 2014; Stanković et al., 2024).

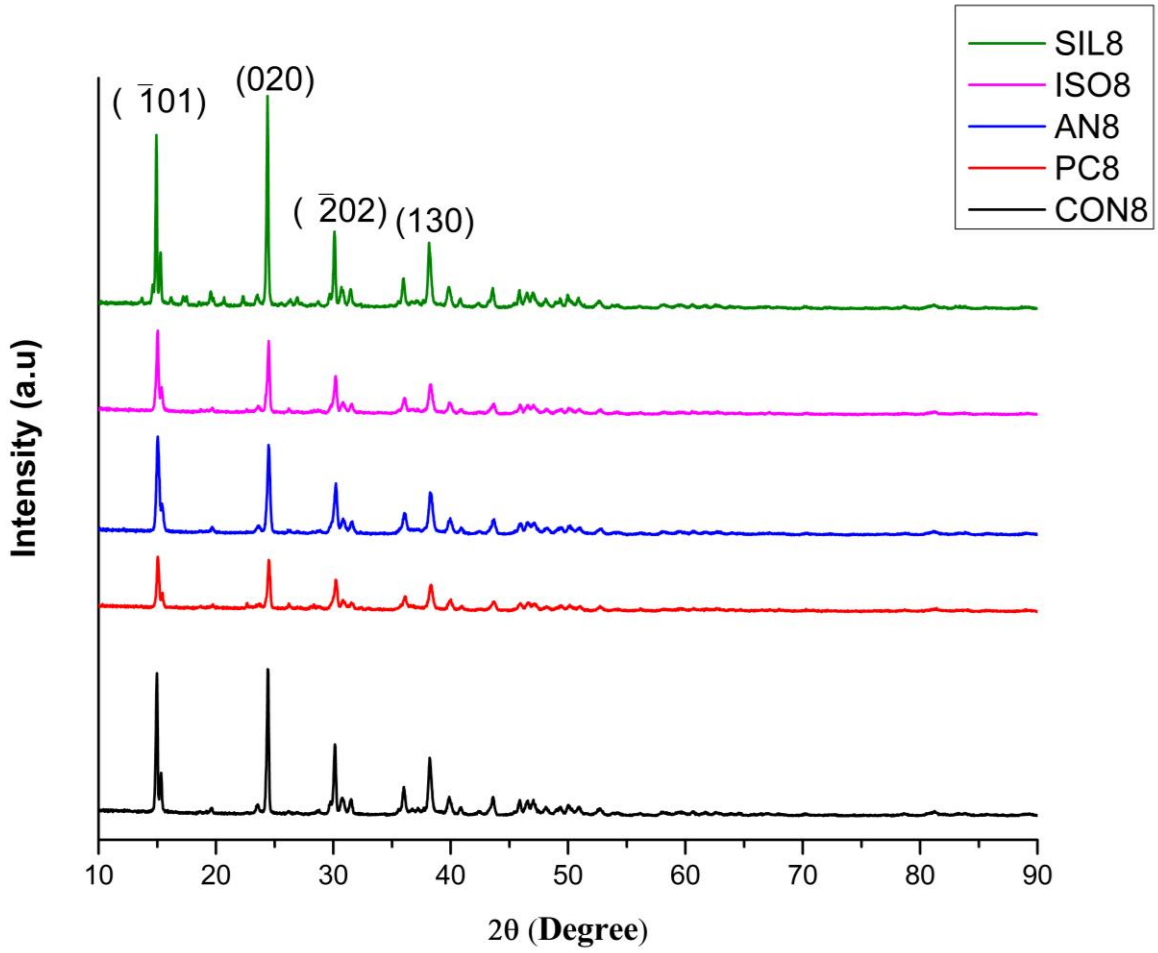

Figure 6.47: XRD spectrum of calcium oxalate with and without phytochemicals. Here, CON- control, PC- positive control, AN- anethole, ISO- isoeugenol, SIL- silibinin. 8-8th supersaturation ratio (2.6).

Similar peaks are observed across all the treatment groups. Still, the intensity of the peaks was higher in the case of silibinin and lower in the case of anethole, isoeugenol and potassium citrate when compared with the control group. Mainly exposed COM faces are ¯101 at 2θ values of 14.929, 020 at 2θ values of 24.396, ¯202 at 2θ values of 30.098, 130 at 2θ values of 38.167. Sample preparations were pure, as no other impurity peak was observed in any group. The potassium citrate XRD graph was also compared against PDF card number - 00-001-0008, where calcium citrate hydrate was found in minor quantities.

6.14.8 Field Emission Scanning Electron Microscopy (FESEM)

Calcium oxalate's morphology was studied using FESEM and is represented in Figure 6.38. The crystal morphology of calcium oxalate without additives (Figure 6.48A) is more

aggregated compared to the same supersaturation value with different additives (6.48B-E). The obtained crystal shape is rectangular with different length-to-width ratios based on the type of additive. Silibinin (Figure 6.48E) additive showed the highest length-to-width ratio, while the Anethole (Figure 6.48C) additive showed the lowest length-to-width ratio. The presence of citrate ions slows crystal growth, while silibinin accelerates the crystal growth at lower supersaturation. Likewise, complexes with calcium ions are formed by citrate ions (Marangella, et al., 2004; Farmanesh et al., 2014) and chondroitin sulfate ions (Ryall, 1997; Rodgers and Jackson, 2017), thereby reducing the interaction of calcium ions with oxalate ions. Even trace amounts of phytate ions (e.g., 1 ppm) have been shown to significantly inhibit the nucleation and growth of calcium oxalate crystals (Grases et al., 2015). At higher SR, the crystal morphology of calcium oxalate changed to rhombic shape due to the low nucleation barrier, high crystal growth rate, and transient stability, with the negative effect of added inhibitors, as shown in Figure 6.49.

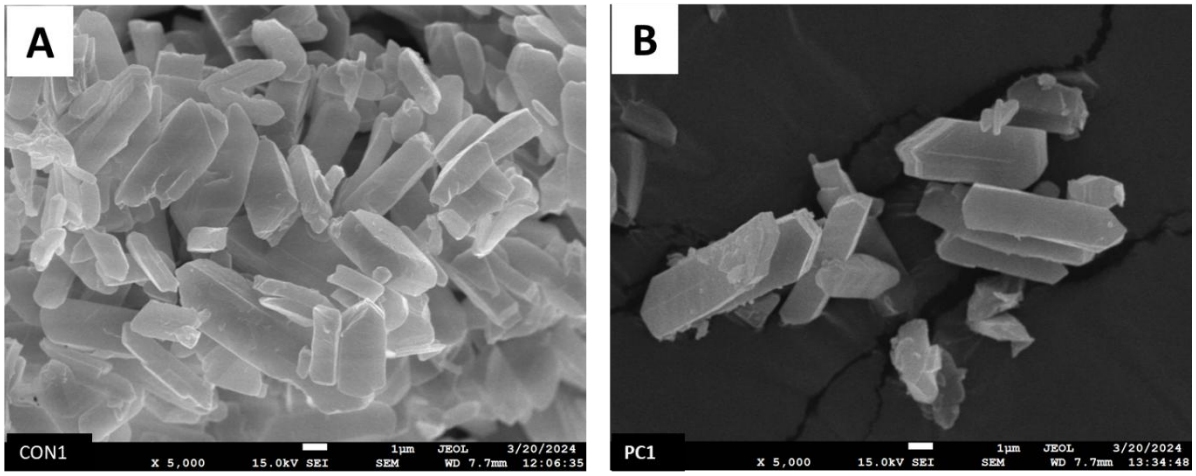

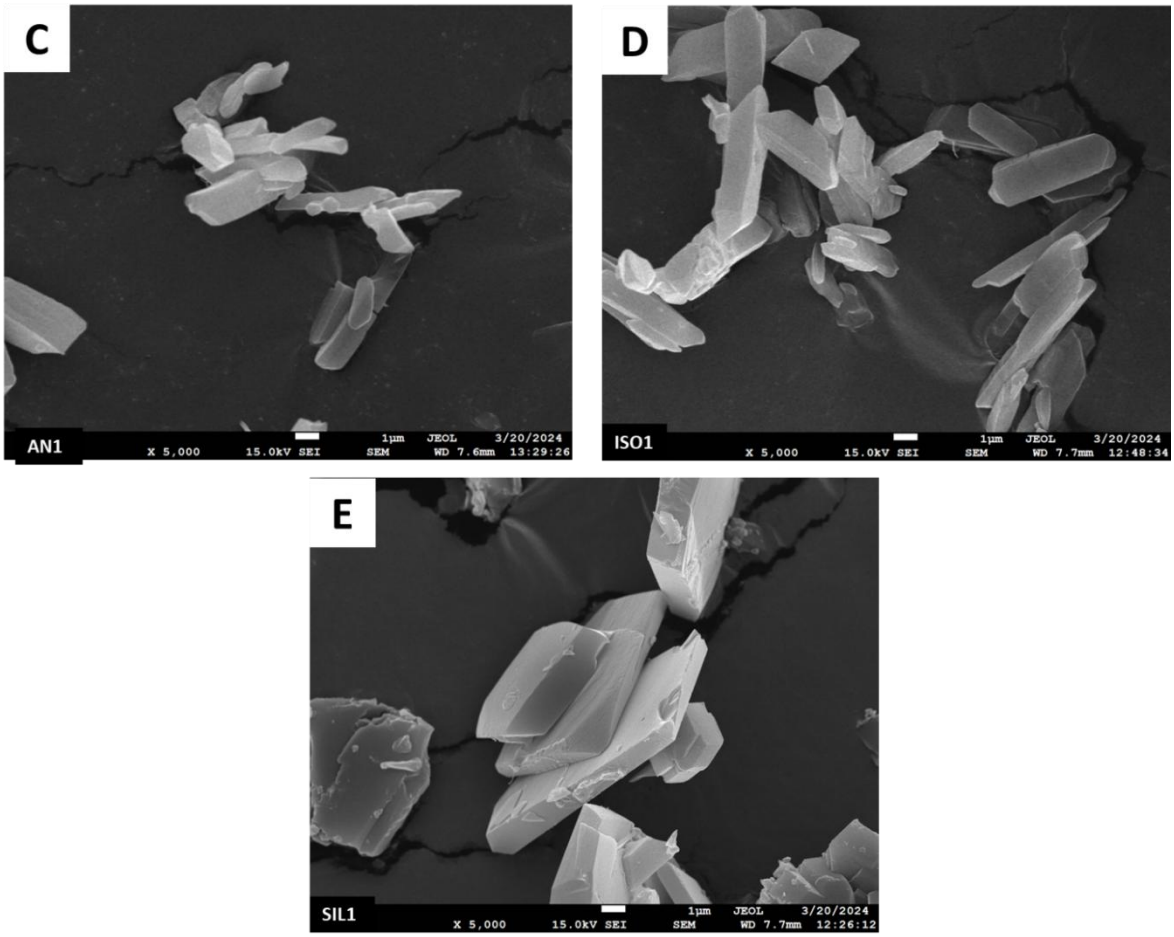

Figure 6.48: SEM images at lower supersaturation (0.72) of A) Control, B) potassium citrate, C) Anethole, D) Isoeugenol, E) Silibinin

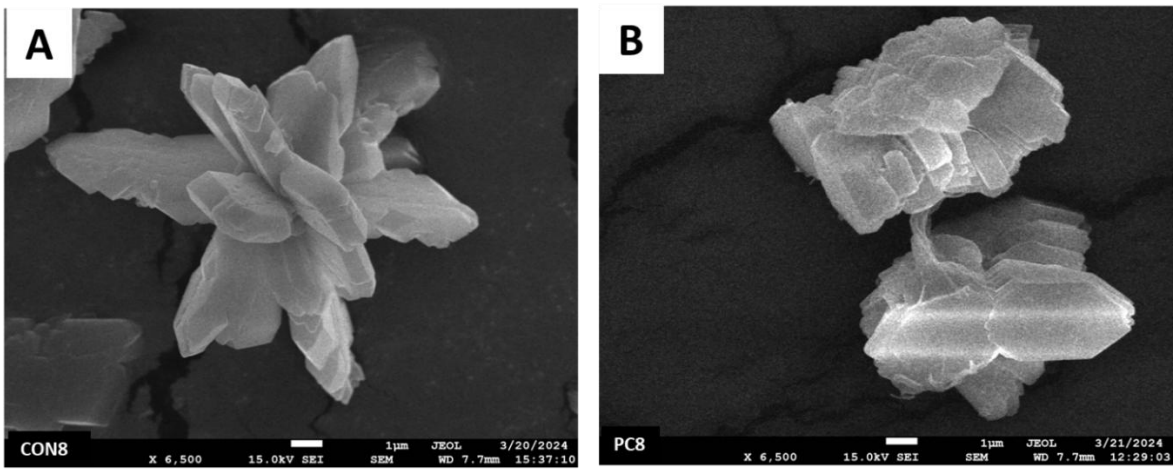

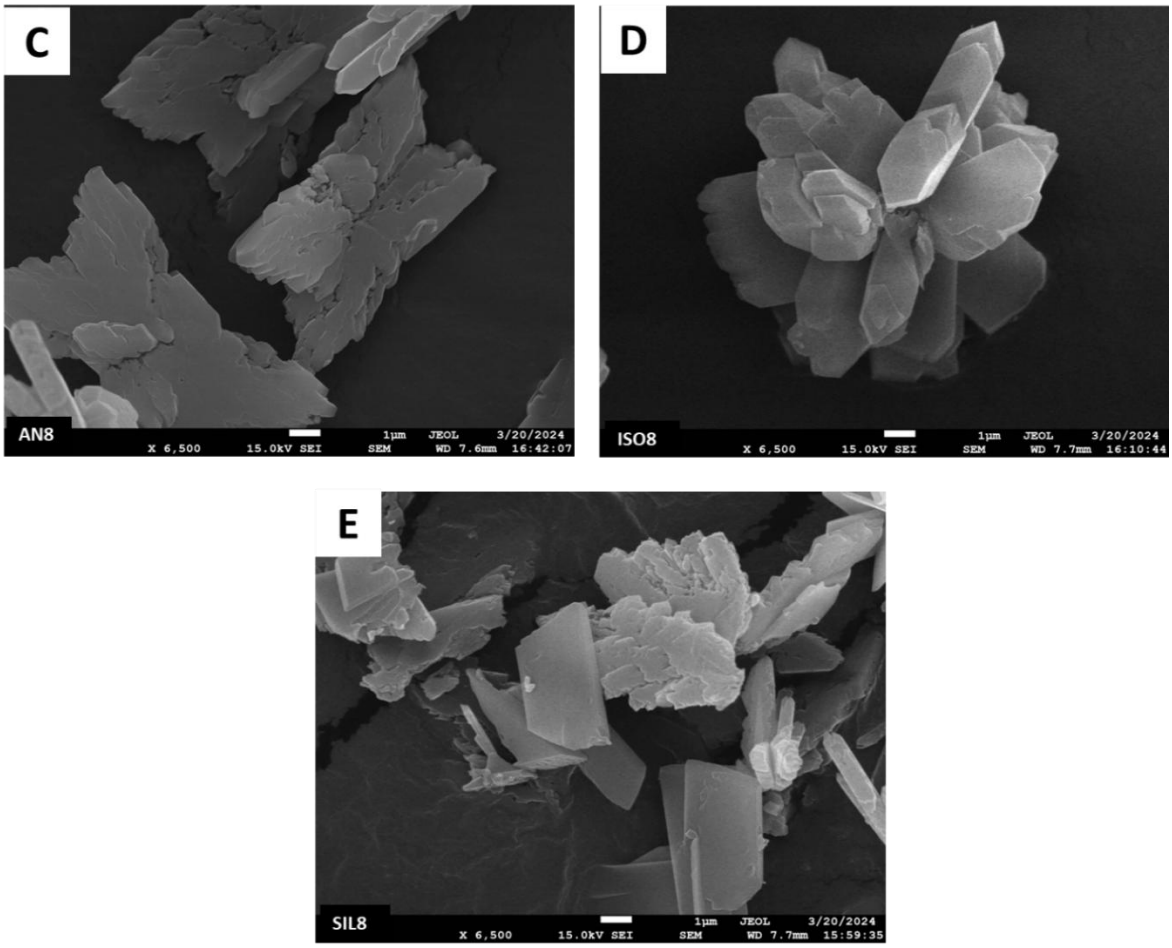

Figure 6.49**:** SEM images at higher supersaturation (2.4) of A) Control, B) potassium citrate, C) Anethole, D) Isoeugenol, and E) Silibinin

6.15 Non-Enzymatic Anti-Oxidant Assays

6.15.1 DPPH Assay

DPPH is a stable free radical reagent used to assess compounds' reducing potential and free radical scavenging activity (Asaduzzaman et al., 2020). Figure 6.50 demonstrates the DPPH inhibition for all tested compounds. Isoeugenol exhibited the strongest DPPH scavenging ability, ranging from 25-45%, followed by silibinin (10-20%) and anethole (7-15%). Ascorbic acid was used as a reference compound. Notably, isoeugenol showed significantly better activity at most concentrations compared to ascorbic acid. In contrast, silibinin and anethole exhibited DPPH scavenging activity, but at much lower levels than ascorbic acid.

Silibinin-rich *Silybum marianum* was shown to scavenge 50% of DPPH at a concentration of 19.2 ± 2.3 µg/mL (Lekmine et al., 2025). Isoeugenol has been reported to achieve 50%

inhibition at 40 µM (Fındık et al., 2011), which is consistent with the present study, where its DPPH inhibition was observed around 120 µM. The DPPH scavenging activity of Anethole is also consistent with previous literature (Freire et al., 2005; Ryu et al., 2014). Anethole may not show DPPH activity due to its reaction with peroxyl radicals (Huang et al., 2005).

6.15.2 ABTS Assay

ABTS inhibition, commonly used for free radical trapping (Re R, Pellegrini et al., 1999), is depicted in Figure 6.50 for all the tested compounds, highlighting their effective inhibition activity. Silibinin exhibited inhibition in the range of 25-70%, Isoeugenol ranged from 30-90%, and Anethole demonstrated a range of 8-18% inhibition. Previously, *Silybum marianum* scavenged 50% of ABTS at a concentration of 7.2 ± 1.7 µg/mL (Lekmine et al., 2025).

Isoeugenol showed superior inhibition activity at concentrations of 80 µM ($p < 0.05$) and 100 µM ($p < 0.0001$), whereas silibinin and anethole displayed significantly lower inhibition ($p < 0.0001$) compared to ascorbic acid at all concentrations. Isoeugenol exhibited 50% inhibition at around 40 µM, consistent with a previously reported study (Fındık et al., 2011).

6.15.3 FRAP Assay

The FRAP % inhibition results, as shown in the figure, indicate that all compounds exhibit strong inhibition activity. Except for 20 µM, where isoeugenol showed less activity than ascorbic acid, isoeugenol demonstrated superior FRAP scavenging activity compared to ascorbic acid, silibinin, and anethole at other concentrations (Figure 6.50).

Previously, *Silybum marianum* scavenged 50% of FRAP at a concentration of 24.1 ± 1.2 µg/mL (Lekmine et al., 2025). Isoeugenol achieved 50% inhibition of FRAP at 122 µM, which is in contrast to a previously reported value of 18.4 mM (Zhang et al., 2017), showing a significant difference in activity levels.

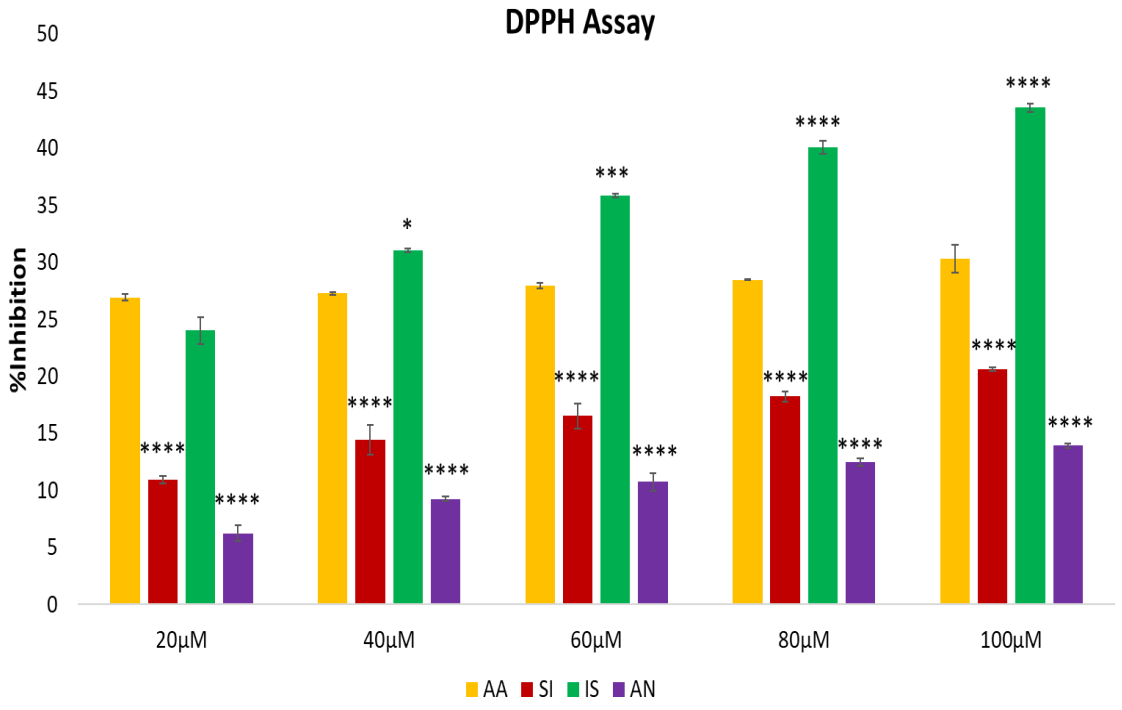
DPPH Assay
%Inhibition
50
45
40
35
30
25
20
15
10
5
0
20µM
40µM
60µM
80µM
100µM
AA
SI
IS
AN

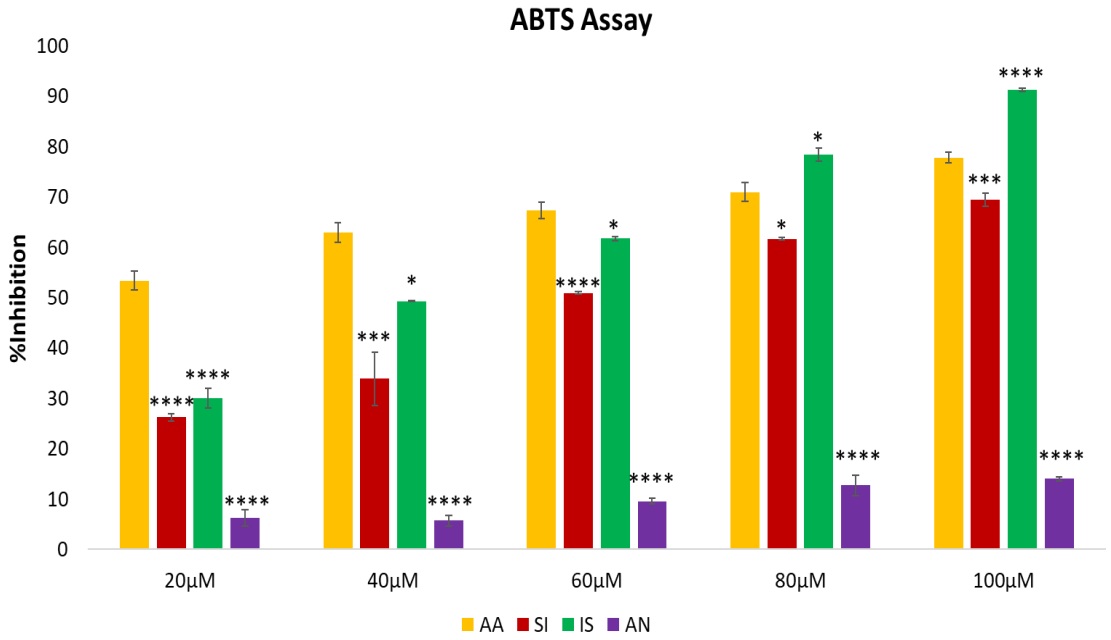
ABTS Assay
%Inhibition
100
90
80
70
60
50
40
30
20
10
0
20µM
40µM
60µM
80µM
100µM
AA
SI
IS
AN

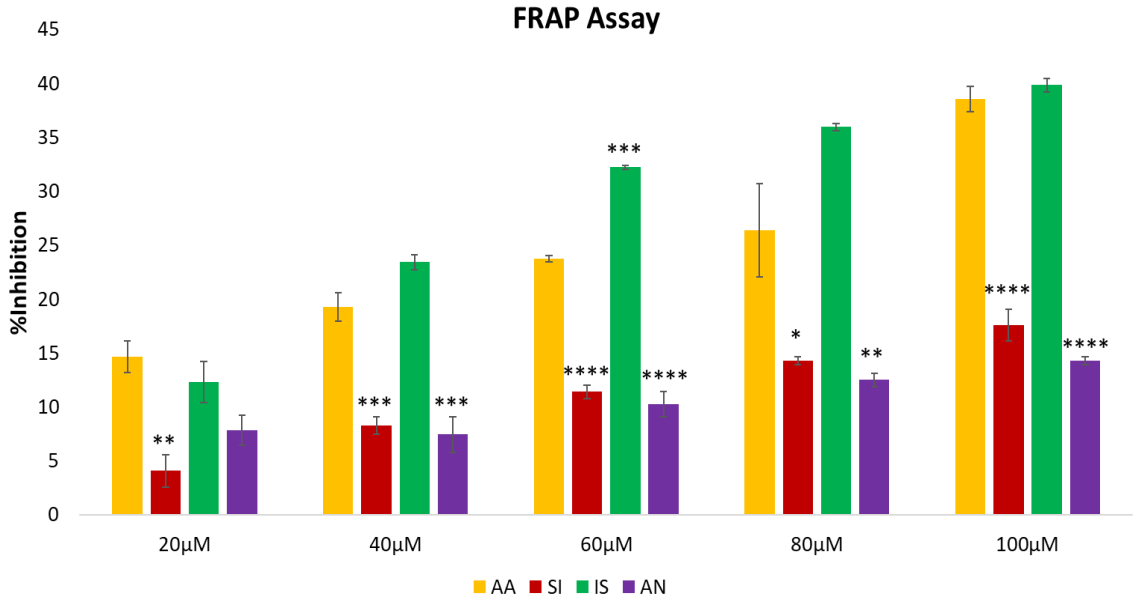

Figure 6.50: Antioxidant activities of phytochemicals at various concentrations, where AA= Ascorbic acid, SI= Silibinin, IS= Isoeugenol and AN= Anethole. All the data are represented as mean ± SEM (n = 3). Data was analysed with one-way ANOVA and Tukey's multiple comparisons test. *P < 0.05, **P < 0.01, ***P < 0.001; ****P < 0.0001 vs AA.

6.16 Enzymatic Anti-Oxidant Assays

6.16.1 MTT Assay

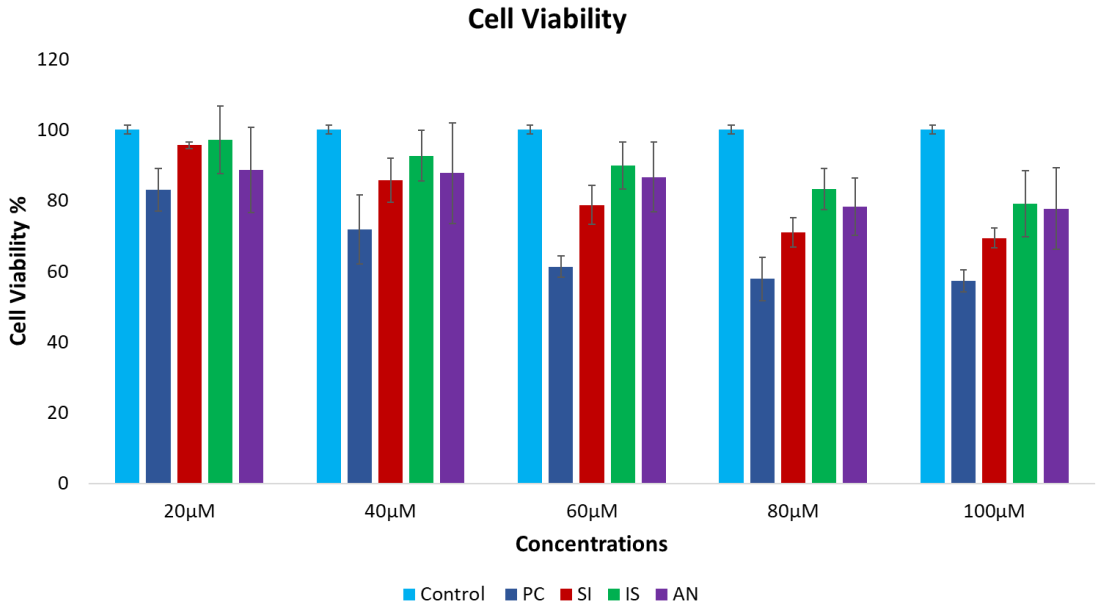

Figure 6.51: Cell line toxicity assay using NRK-52E cell line.

The cell viability of all phytochemicals is shown in Figure 6.51. As we can see, all of them showed good cell viability, with potassium citrate having a viability range of 57-83%, Silibinin having a viability range of 69- 95%, Isoeugenol having a viability range of 79-97% and Anethole having viability range of 77 -88%.

Table 6.14: Groups used in Enzymatic Anti-Oxidant Assays

Groups	**Description**
Control	Without any crystals
SI 100µM	100µM Silibinin treatment
IS 100µM	100µM Isoeugenol treatment
AN 100µM	100µM Anethole treatment
Disease	Cells containing crystals
PCD 100µM	Crystals + 100µM Potassium citrate treatment
SD 50µM	Crystals + 50µM Silibinin treatment
SD 100µM	Crystals + 100µM Silibinin treatment
ISD 50µM	Crystals + 50µM Isoeugenol treatment
ISD 100µM	Crystals + 100µM Isoeugenol treatment
AND 50µM	Crystals + 50µM Anethole treatment
AND 100µM	Crystals + 100µM Anethole treatment

6.16.2 Lipid Peroxidation

The disease group was significantly higher than the control group ($p>0.001$) as shown in Figure 6.52A. PD 100µM was able to reduce the damage ($p>0.001$) significantly. Silibinin and Isoeugenol in the treatment group at both the doses (50 and 100 µM) were able to reduce the formation of malondialdehyde (MDA) ($p>0.001$) significantly, whereas Anethole didn't have significant improvement.

6.16.3 Superoxide dismutase (SOD)

Nitroblue tetrazolium (NBT) was reduced in the disease group the most ($p>0.001$) as depicted in Figure 6.52B. On the contrary, treatment groups such as SD (50µM), SD (100µM), ISD (50µM), ISD (100µM), and AND (100µM) were able to reduce this inhibition ($p>0.001$), along

with positive control PD (100µM) (p>0.05) quite significantly. Additionally, Silibinin and Anethole at (100µM) without disease also showed a difference from the control.

6.16.4 Glutathione-S-Transferase (GST)

GST activity was significantly lower in the disease group (p>0.05) than in the control group as depicted in Figure 6.52C. Isoeugenol in the treatment group (P>0.05) ISD (50µM), ISD (100µM), and Anethole in the treatment group (P>0.001) AND (50µM), AND (100µM), were able to increase this activity. However, Silibinin didn't have any significant change in GST activity.

6.16.5 Catalase

Decomposition of hydrogen peroxide was lowest in the disease group (p>0.001), and treatment groups were able to elevate it quite significantly, as depicted in Figure 6.52D. SD (50µM) (P>0.01) and SD (100µM) (p>0.001), ISD (50µM) (p>0.05), ISD (100µM) (p>0.01), and AND (100µM) (p>0.01) did increase this decomposition of peroxide.

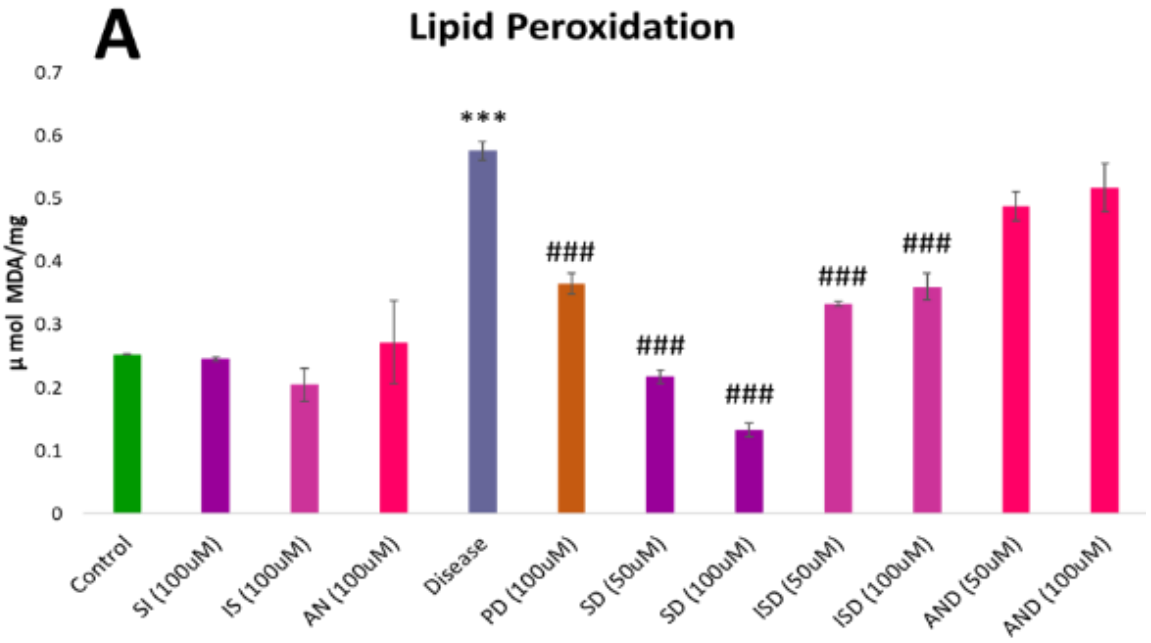

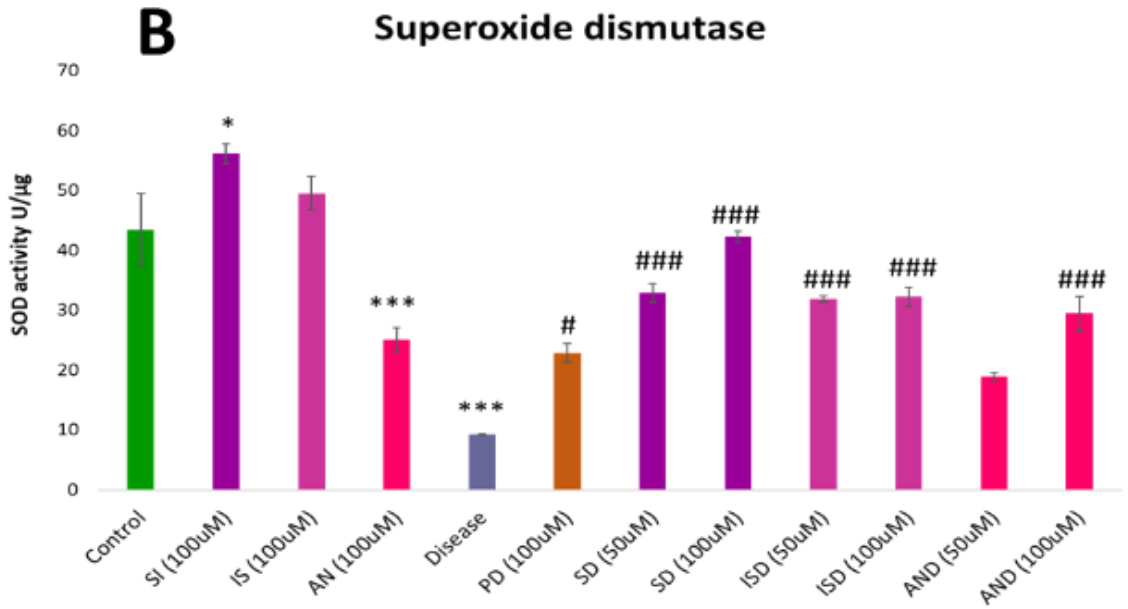
B
Superoxide dismutase
SOD activity U/µg
70
60
50
40
30
20
10
0
*
***
***
#
###
###
###
###
###
Control
SI (100uM)
IS (100uM)
AN (100uM)
Disease
PD (100uM)
SD (50uM)
SD (100uM)
ISD (50uM)
ISD (100uM)
AND (50uM)
AND (100uM)

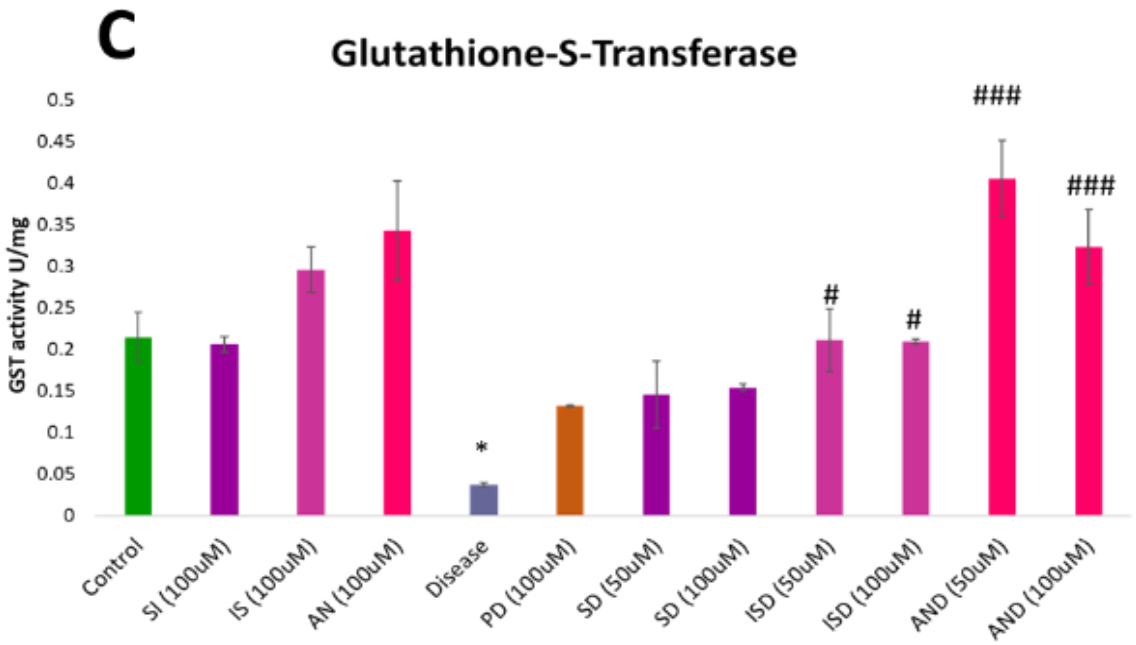
C
Glutathione-S-Transferase
GST activity U/mg
0.5
0.45
0.4
0.35
0.3
0.25
0.2
0.15
0.1
0.05
0
*
#
#
###
###
Control
SI (100uM)
IS (100uM)
AN (100uM)
Disease
PD (100uM)
SD (50uM)
SD (100uM)
ISD (50uM)
ISD (100uM)
AND (50uM)
AND (100uM)

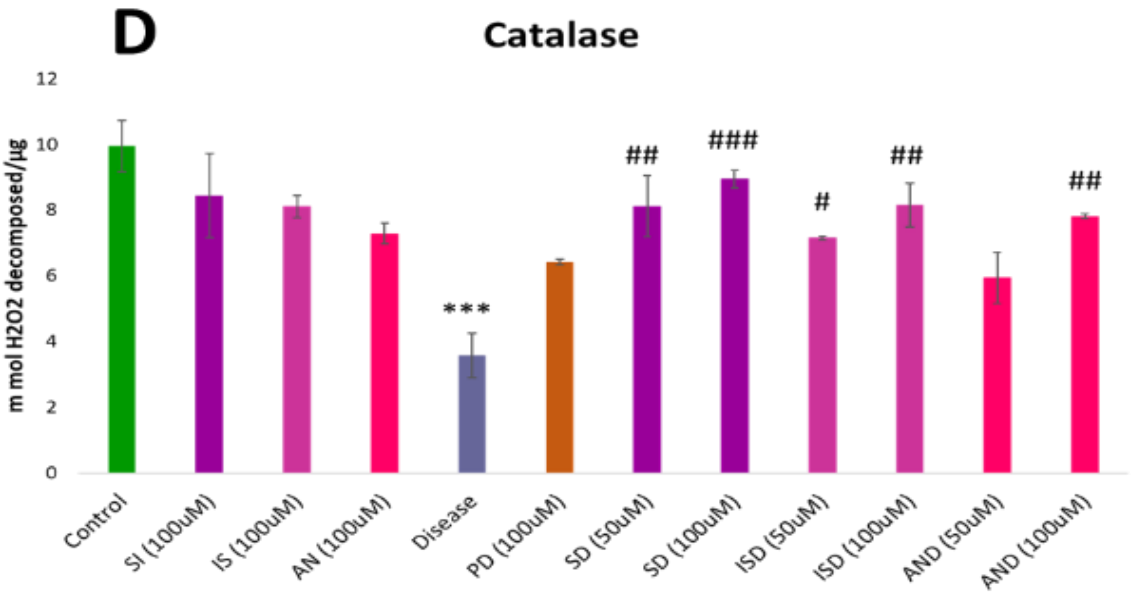

Figure 6.52: Effect of phytochemicals on enzymatic anti-oxidant assays A) Lipid Peroxidation, B) Superoxide dismutase (SOD), C) Glutathione-S-Transferase (GST), and D) Catalase

6.16.6 Cell-crystal adhesion assay

Microscopic images of cell lines affected by crystals are depicted in Figure 6.53 give insights into various shapes such as rectangular and rhomboid structures formed across the cell surface. The number of crystals that are attached to the cells is represented in Figure 6.54. We can see that potassium citrate didn't have any significant change in the number of crystals adhered when compared to the disease group. However, all the treatment groups had a significant reduction in crystal numbers ($P<0.0001$) when compared with the control. When compared with potassium citrate, isoeugenol at both concentrations showed the highest reduction and significance ($P<0.0001$), followed by silibinin at both concentrations and anethole at 100µM concentration ($P= 0.001$) and lastly with anethole at 50µM concentration ($P<0.001$).

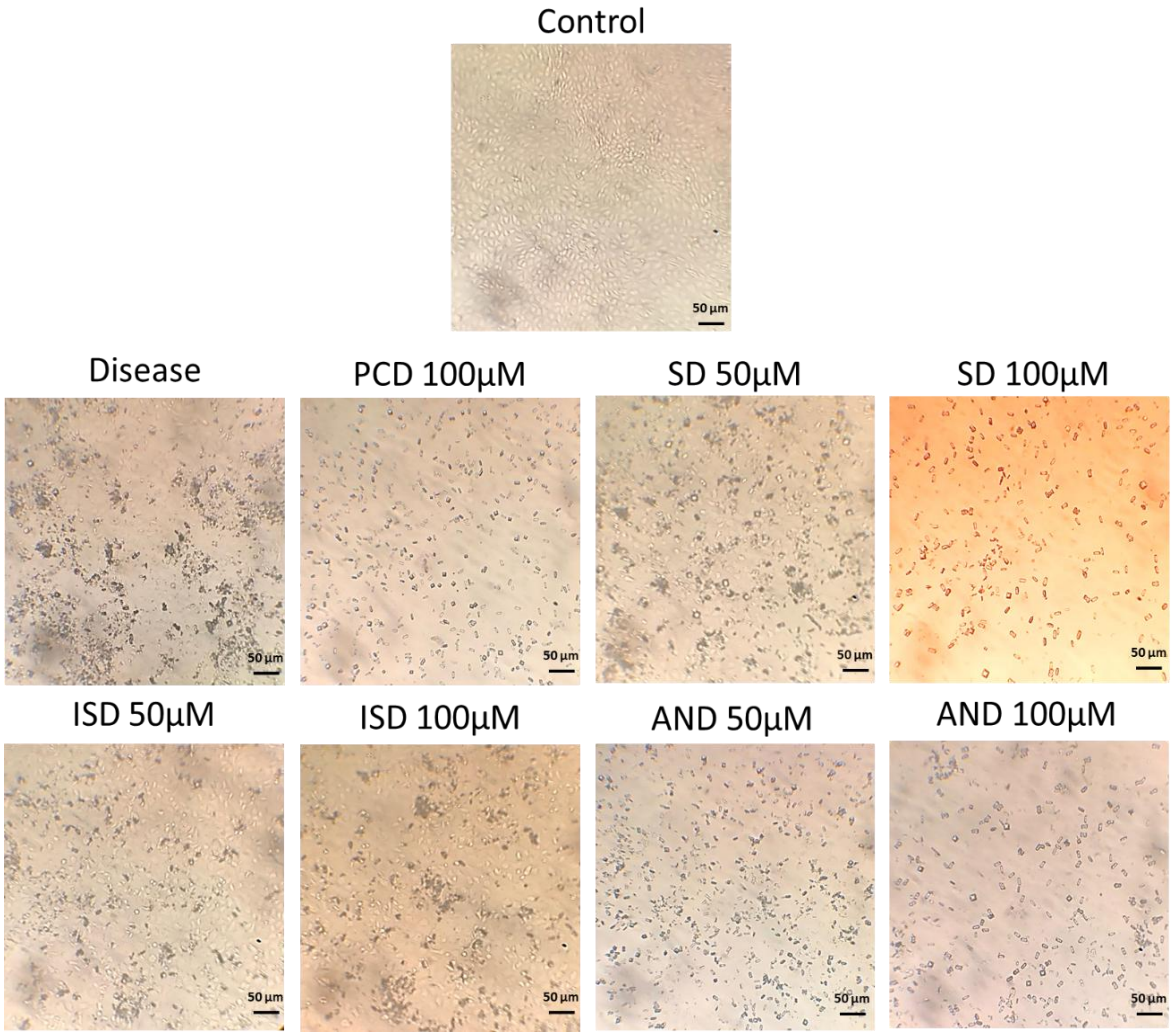

Figure 6.53: Microscopic images of NRK-52E cell lines infected with crystals developed from sodium oxalate (2mM) at 100X magnification.

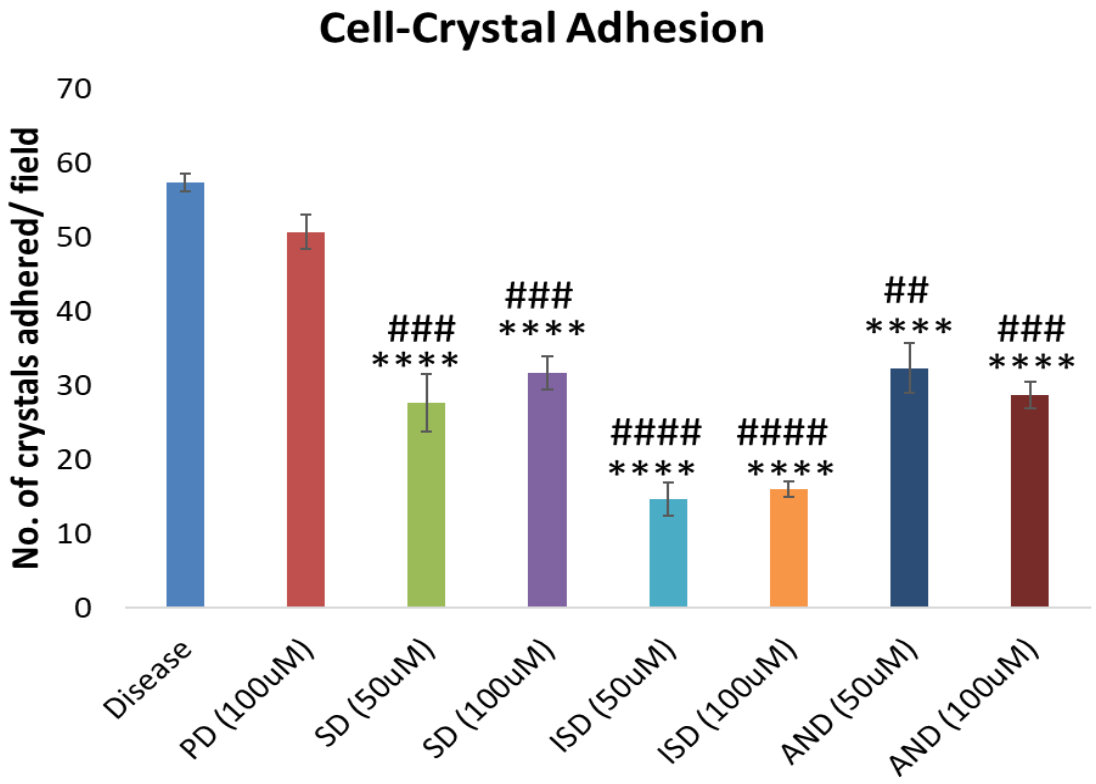

Figure 6.54: Effect of phytochemicals on crystal adhered kidney cells. Data was analyzed with one-way ANOVA and Tukey's multiple comparisons test. *P < 0.05, **P < 0.01, ***P < 0.001; ****P < 0.0001 vs AA.

6.17 Western Blotting

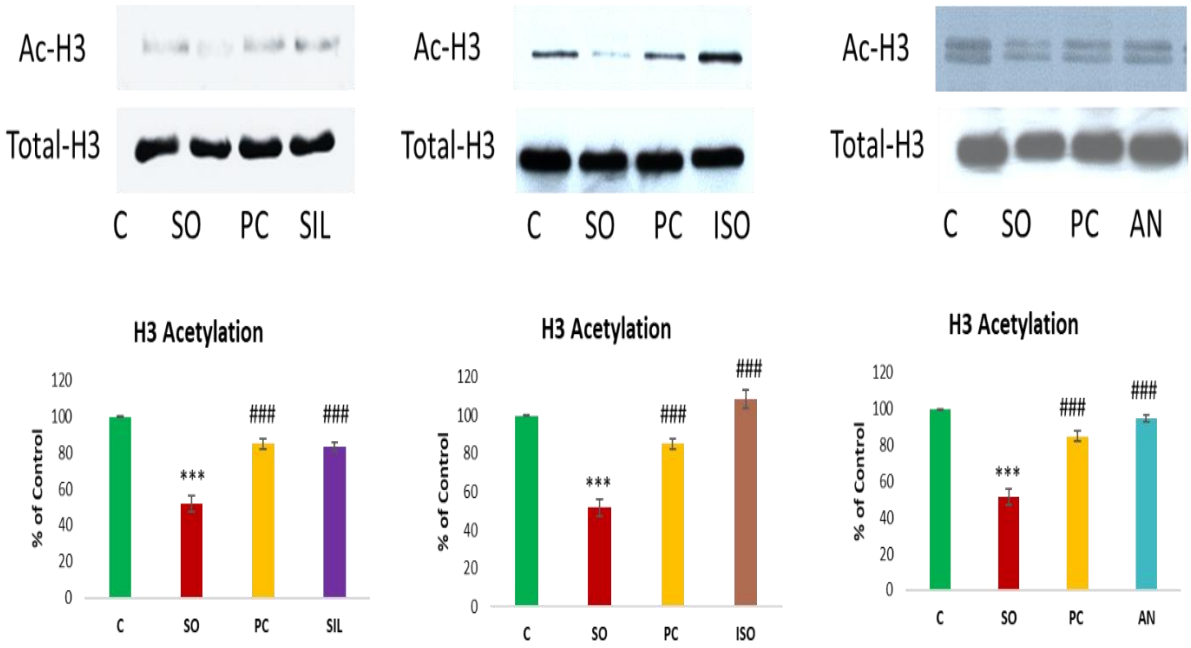

Figure 6.55: Histone 3 acetylation levels as determined by western blot in NRK-52E cell line upon no treatment (C), treatment with sodium oxalate (SO), Potassium Citrate (PC), silibinin (SIL), isoeugenol (ISO), anethole (AN). Data was analyzed with one-way ANOVA and Tukey's multiple comparisons test. $^{***}p < 0.001$ vs C, $^{###}p < 0.001$ vs SO, n=3 ± SEM.

Our result shows that expression of H3 acetylation was significantly lower in the sodium oxalate treated group when compared against the control (Figure 6.55). Treatment with phytochemicals elevated this expression significantly ($p<0.001$)

6.18 Animal Studies

6.18.1 Effect of silibinin on body weight, organ coefficient, and kidney morphology

Body weight was measured weekly, showing no significant differences between weeks or groups (Figure 6.56). Kidney and liver coefficients were higher in disease control rats receiving only ethylene glycol and ammonium chloride compared to the control group receiving CMC (65.01% and 42%, respectively; $p<0.001$ and $p<0.05$). No significant differences ($p>0.05$) were found in the length and width of kidneys across treatment groups (Table 6.15). A significant decrease in crystal size was noted in the disease group compared to the control group ($p<0.001$), as the control had no crystal formation. Treatment also significantly reduced crystal size ($p<0.001$), as shown in Table 6.15.

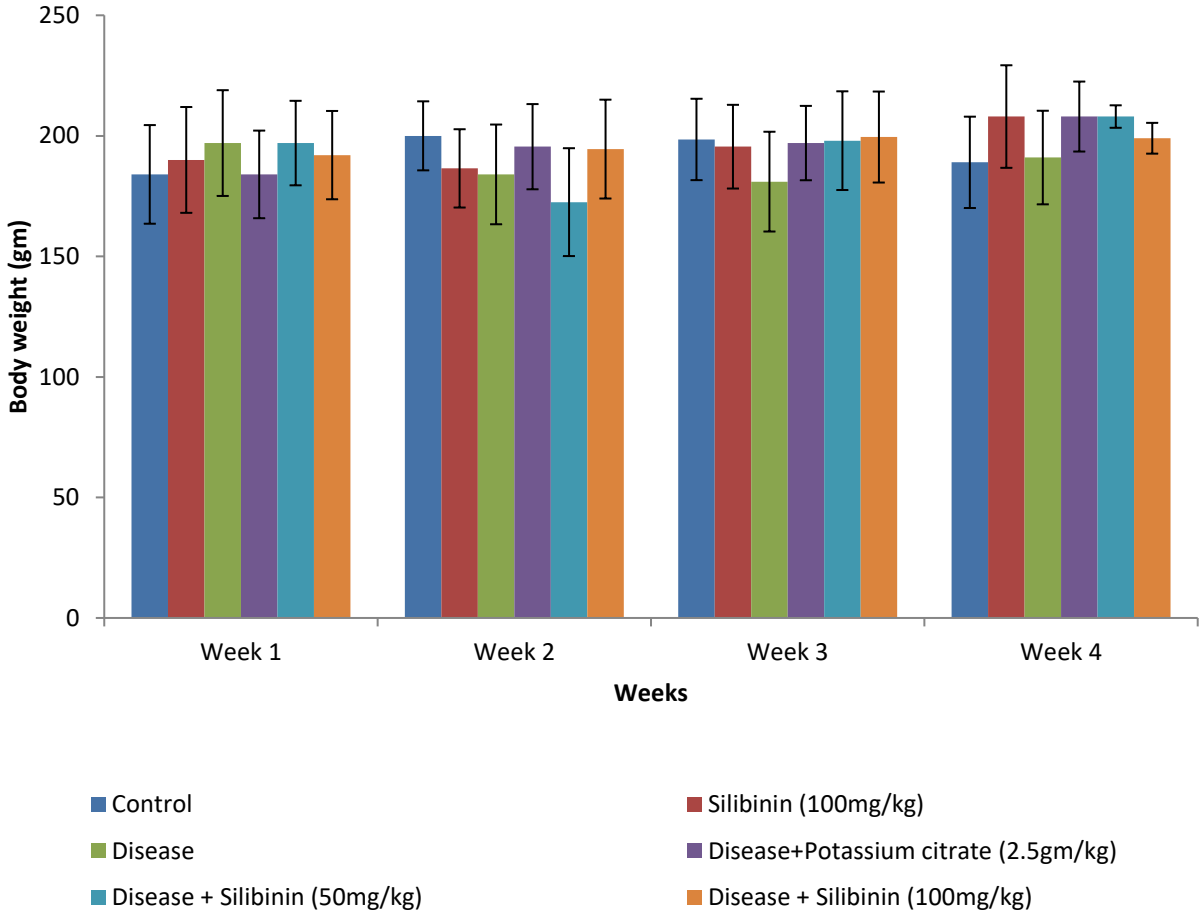

Figure 6.56: Change in body weight of the experimental groups during four weeks.

Table 6.15: Morphological characteristics of kidney and organ coefficient

Parameters	**Control**	**Silibinin (100mg/kg)**	**Disease**	**Disease+ Potassium citrate (2.5gm/kg)**	**Disease + Silibinin (50mg/kg)**	**Disease + Silibinin (100mg/kg)**
Length (mm)	14.1 ± 2.40	15.36 ± 0.20	16 ± 1.46	20.1 ± 0.05	18.66 ± 0.23	20.5 ± 2.73
Width (mm)	8.3 ± 0.11	9.34 ± 0.54	8.7 ± 1.32	10.4 ± 0.12	11.9 ± 0.63	10.5 ± 0.73
Thickness (mm)	5 ± 0.88	5.4 ± 0.36	8 ± 1.83	5.5 ± 0.49	9 ± 1.43	8.4 ± 0.36

kidney coefficient	0.0036 ± 0.001	0.0038 ± 0.001	0.0103 ± 0.001***	0.0047 ± 0.001$^{\#\#}$	0.0092 ± 0.001$^{\#}$	0.0076 ± 0.001$^{\#}$
Liver coefficient	0.0364 ± 0.001	0.0390 ± 0.002	0.0638 ± 0.007*	0.0497 ± 0.004	0.0380 ± 0.001$^{\#}$	0.0412 ± 0.003$^{\#}$
Crystal size (µm^2)	0	0	223.94 ± 22.77***	74.15 ± 6.62$^{\#\#\#}$	108.18 ± 15.03$^{\#\#\#}$	91.42 ± 8.92$^{\#\#\#}$

Values are presented as mean ± S.E.M. (n=6). Statistical significance is indicated as follows: ***p<0.001, **p<0.01, and *p<0.05 for disease vs. control; ###p<0.001, ##p<0.01, and #p<0.05 for potassium citrate, silibinin 50 mg/kg, and silibinin 100 mg/kg vs. disease.

6.18.2 Effect of silibinin on serum, urine analysis and stone markers

Urea, creatinine, and uric acid levels were elevated in the diseased group (62.5%, 49.35%, and 44.44% higher than control, respectively; p<0.001, p<0.01, p<0.001). Potassium citrate (2.5 gm/kg) significantly reduced urea (68.3%, p<0.001) and uric acid (24.44%, p<0.05) compared to the disease group. Silibinin (50 mg/kg) also lowered urea (20.49%, p<0.001), creatinine (41.55%, p<0.05), and uric acid (28.88%, p<0.05) in the diseased group. Silibinin (100 mg/kg) significantly reduced urea (23.46%, p<0.001) compared to the disease group (Table 6.16).

In the diseased group, water consumption (65%, p<0.01) and urine output (24.44%, p<0.01) were significantly higher than in the treatment and control groups. Potassium citrate reduced urine output (32.8%, p<0.001) compared to the disease group. Silibinin (50 mg/kg) significantly decreased water consumption (51.79%, p<0.05) and urine output (34.44%, p<0.001) in the diseased group. Silibinin (100 mg/kg) also significantly reduced water consumption (42.35%, p<0.05) and urine output (26.66%, p<0.01).

Calcium levels were high, and magnesium levels were low in the diseased group (p<0.001) compared to the control. Treatment with silibinin and potassium citrate significantly reversed these effects (Table 6.16).

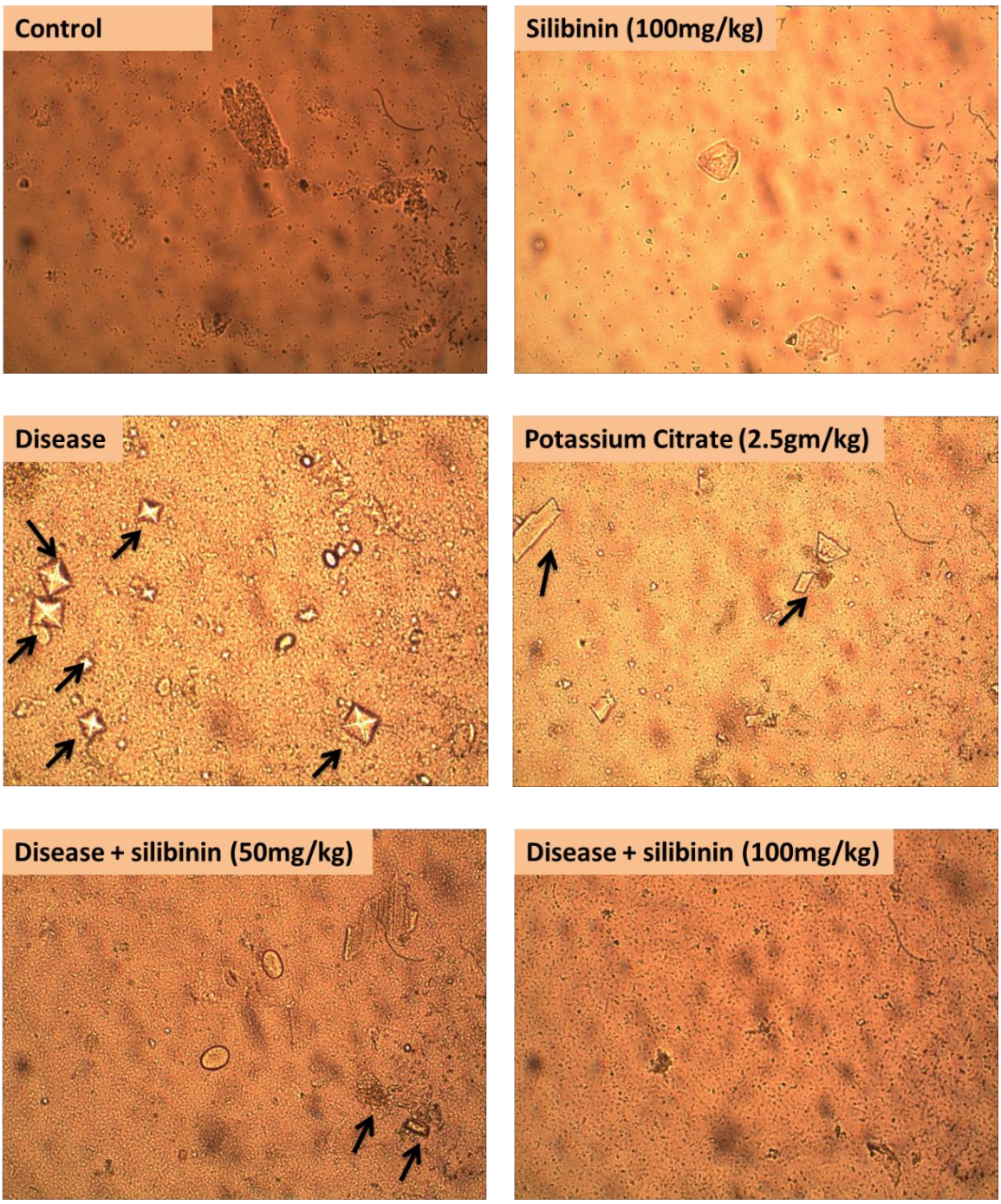

Figure 6.57: Urine microscopy of experimental groups at 100X. The black arrow highlights crystals

Urine microscopy showed no crystals in the control or silibinin (100 mg/kg) groups, while the diseased control group had many crystals. Both potassium citrate and silibinin (50 and 100 mg) reduced crystal size and density (Figure 6.57). No significant changes were observed in urine pH across experimental groups (Table 6.16). Urine samples were tested for albumin, sugar, pus cells, RBCs, epithelial cells, and ketones, with none found.

Table 6.16: Stone parameters in various animal groups

Parameters	Control	Silibinin (100mg/kg)	Disease	Disease + Potassium citrate (2.5gm/kg)	Disease + Silibinin (50mg/kg)	Disease + Silibinin (100mg/kg)
pH	7 ± 0.2	6 ± 0.3	8 ± 0.1	7 ± 0.2	8 ± 0.3	8 ± 0.2
Urea (mg/dl)	42.8 ± 0.72	29.2 ± 0.48*	114.2 ± 1.69***	36.2 ± 0.72###	90.8 ± 4.34###	87.4 ± 2.40###
Creatinine (mg/dl)	0.39 ± 0.01	0.33 ± 0.01	0.77 ± 0.08**	0.50 ± 0.05	0.45 ± 0.08#	0.5 ± 0.05
Uric acid (mg/dl)	1.25 ± 0.02	1.3 ± 0.05	2.25 ± 0.08***	1.7 ± 0.23#	1.6 ± 0.05#	1.75 ± 0.02
Water consumption (ml)	20 ± 7.31	33.6 ± 3.33	57.25 ± 5.13**	35 ± 0.33	27.6 ± 0.81#	33 ± 5.13#
Urine output (ml)	17 ± 0.30	13 ± 0.24*	22.5 ± 1.12**	15.1 ± 0.04###	14.75 ± 0.48###	16.5 ± 1.40##
Calcium (mg/ g tissue)	0.63 ± 0.07	1.24 ± 0.05***	1.70 ± 0.06***	1.18 ± 0.04 ###	0.76 ±0.03 ### ^^^	1.01 ± 0.05 ###
Magnesium (mg/ g tissue)	2.08 ± 0.04	1.77 ± 0.05**	1.23 ± 0.07 ***	1.98 ± 0.03 ###	1.54 ± 0.03 ##^^^	1.66 ± 0.06 ###^^

Values are presented as mean ± S.E.M. (n=6). Statistical significance is indicated as follows: ***p<0.001, **p<0.01, and *p<0.05 vs. control; ###p<0.001, ##p<0.01, and #p<0.05 vs. disease; ^^^p<0.001, ^^p<0.01, and ^p<0.05 vs potassium citrate (2.5 gm/kg).

6.18.3 Effect of silibinin on renal oxidative damage

Oxidative stress is a key contributor to renal injury in nephrolithiasis, driven by an imbalance between reactive oxygen species (ROS) generation and antioxidant defence mechanisms. We assessed oxidative damage through five biomarkers: lipid peroxidation (LPO), superoxide dismutase (SOD), catalase (CAT), glutathione S-transferase (GST), and reduced glutathione

(GSH). Silibinin's protective effects were compared across doses (50 mg/kg and 100 mg/kg), with potassium citrate (2.5 g/kg) serving as a reference standard.

6.18.3.1 Lipid Peroxidation (LPO)

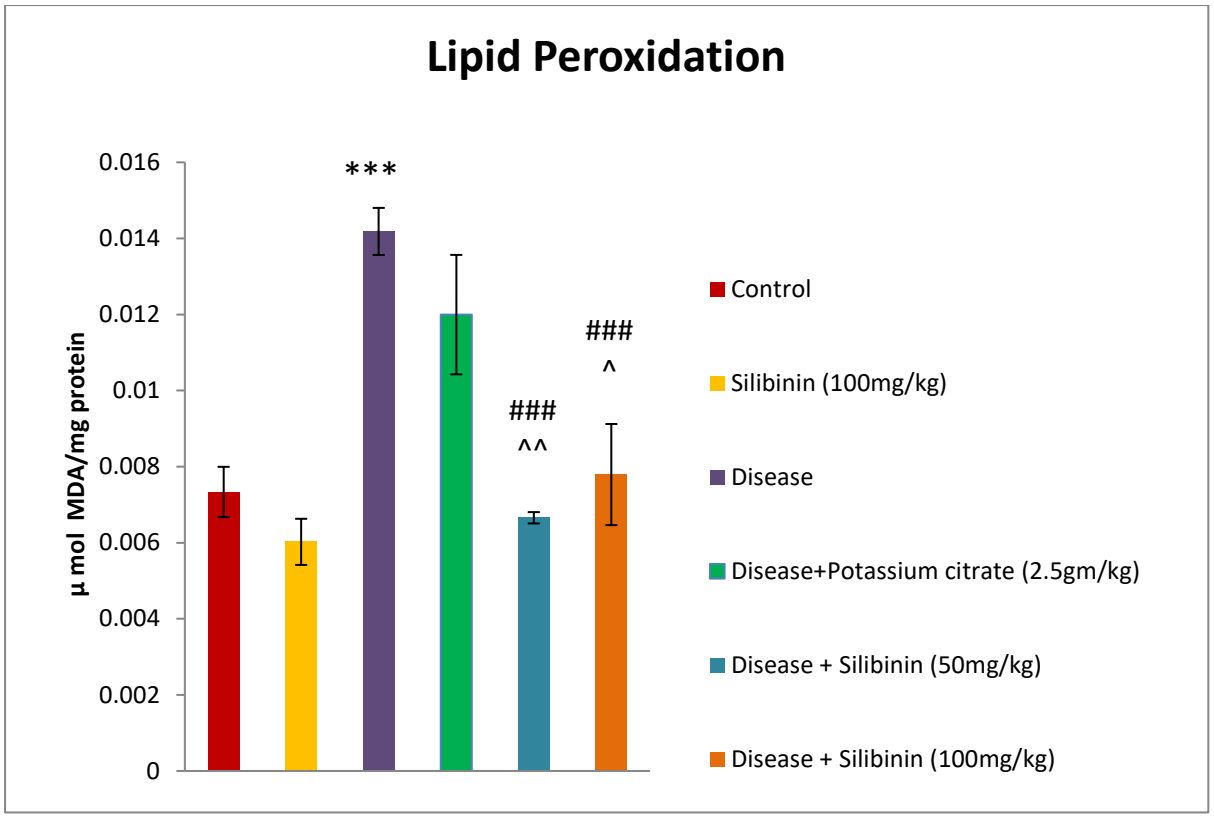

Figure 6.58: Effect of silibinin on renal lipid peroxidation (LPO). Values are shown as mean ± S.E.M. (n=6). Statistical significance is indicated as follows: ***p<0.001 vs. control; ###p<0.001 vs. disease; ^^p<0.01, and ^p<0.05 vs. potassium citrate (2.5 gm/kg).

Malondialdehyde (MDA), a byproduct of lipid peroxidation, was significantly elevated in the disease group, indicating enhanced oxidative stress and cellular membrane damage. LPO was significantly elevated (48.29%) in the disease group (0.0147 ± 0.0007 µmol MDA/mg protein) compared to the control (0.0075 ± 0.0006, ***p<0.001). Silibinin treatment at 50 mg/kg and 100 mg/kg brought MDA levels down to 0.0069 ± 0.0005 (44.51%) and 0.0079 ± 0.0008 (53.07%) respectively (###p<0.001 vs. disease), nearly normalising oxidative damage. Potassium citrate also showed efficacy (0.012 ± 0.00157, ###p<0.001), although 50 mg/kg silibinin showed slightly superior lipid peroxidation suppression (44.51%, p<0.01) compared to potassium citrate, as shown in Figure 6.58.

6.18.3.2 Superoxide Dismutase (SOD)

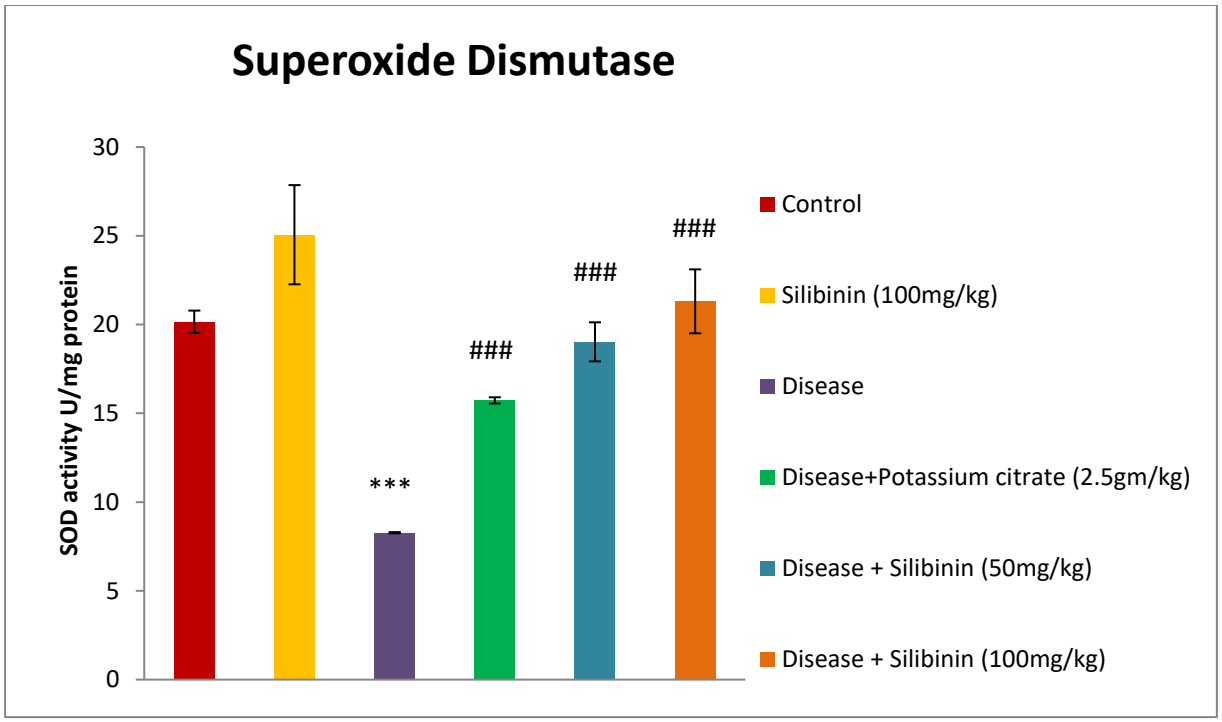

Figure 6.59: Effect of silibinin on renal superoxide dismutase (SOD). Values are shown as mean ± S.E.M. (n=6). Statistical significance is indicated as follows: ***p<0.001, vs. control; ###p<0.001 vs. disease.

The activity of superoxide dismutase (SOD), a primary antioxidant enzyme responsible for neutralising superoxide radicals, was markedly reduced in the disease group (8.27 ± 0.03 U/mg protein), showing a 41.04% decrease compared to the control group (20.15 ± 0.63, ***p<0.001). Treatment with silibinin significantly restored SOD activity in a dose-dependent manner. At 50 mg/kg and 100 mg/kg, SOD levels increased to 19.02 ± 1.1 and 21.30 ± 1.8 U/mg protein, corresponding to improvements of 56.50% and 61.16%, respectively (###p<0.001 vs. disease). Potassium citrate also elevated SOD activity to 15.72 ± 0.17 U/mg protein (47.38% improvement), although silibinin, particularly at the higher dose, demonstrated superior antioxidant restoration (Figure 6.59).

6.18.3.3 Catalase (CAT)

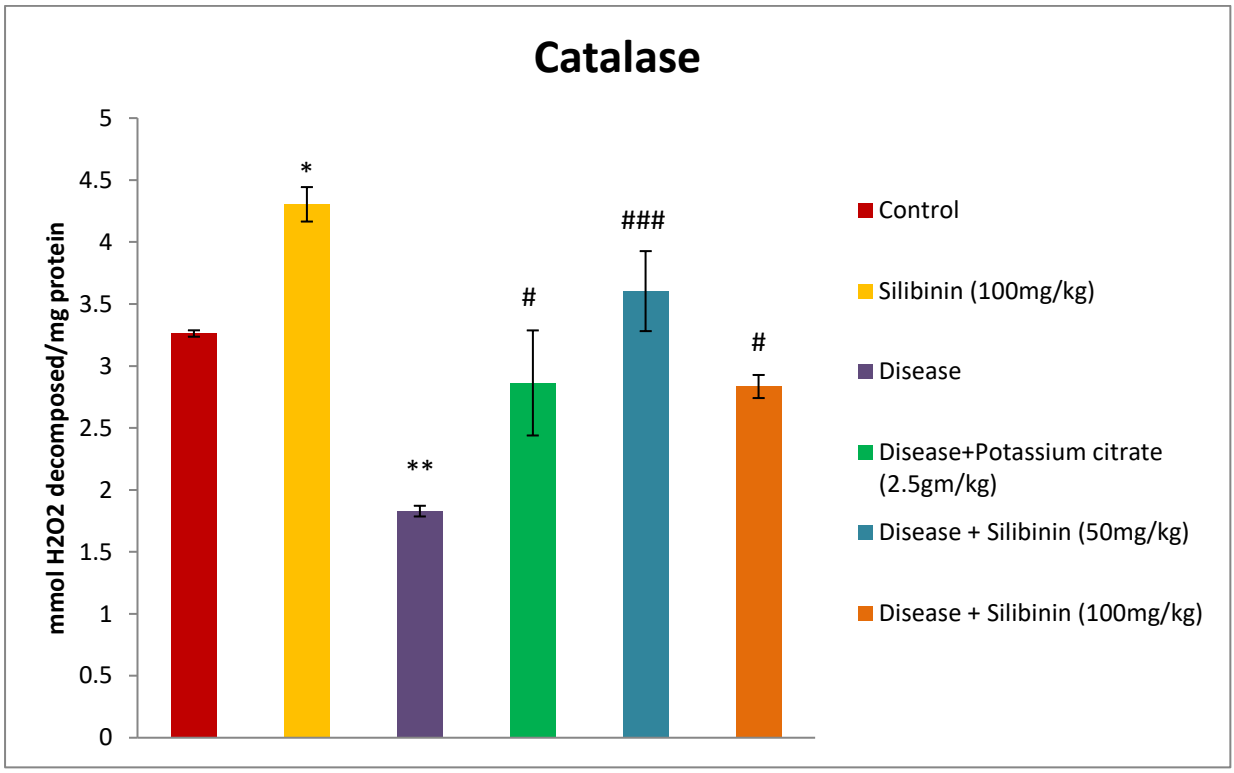

Figure 6.60: Effect of silibinin on renal catalase (CAT). Values are shown as mean ± S.E.M. (n=6). Statistical significance is indicated as follows: **p<0.01, and *p<0.05 vs. control; ###p<0.001, ##p<0.01, and #p<0.05 vs. disease.

Silibinin (100 mg/kg) significantly increased CAT (35.48%, p<0.05), compared to the disease group. Silibinin (100 mg/kg) significantly increased CAT (57.51%, p<0.05) compared to the control. Silibinin (50 mg/kg) in the diseased group significantly increased CAT (49.26%, p<0.001) compared to the disease group. Potassium citrate also significantly raised CAT (36.12%, p<0.05), compared to the disease group (Figure 6.60).

6.18.3.4 Glutathione-S-Transferase (GST)

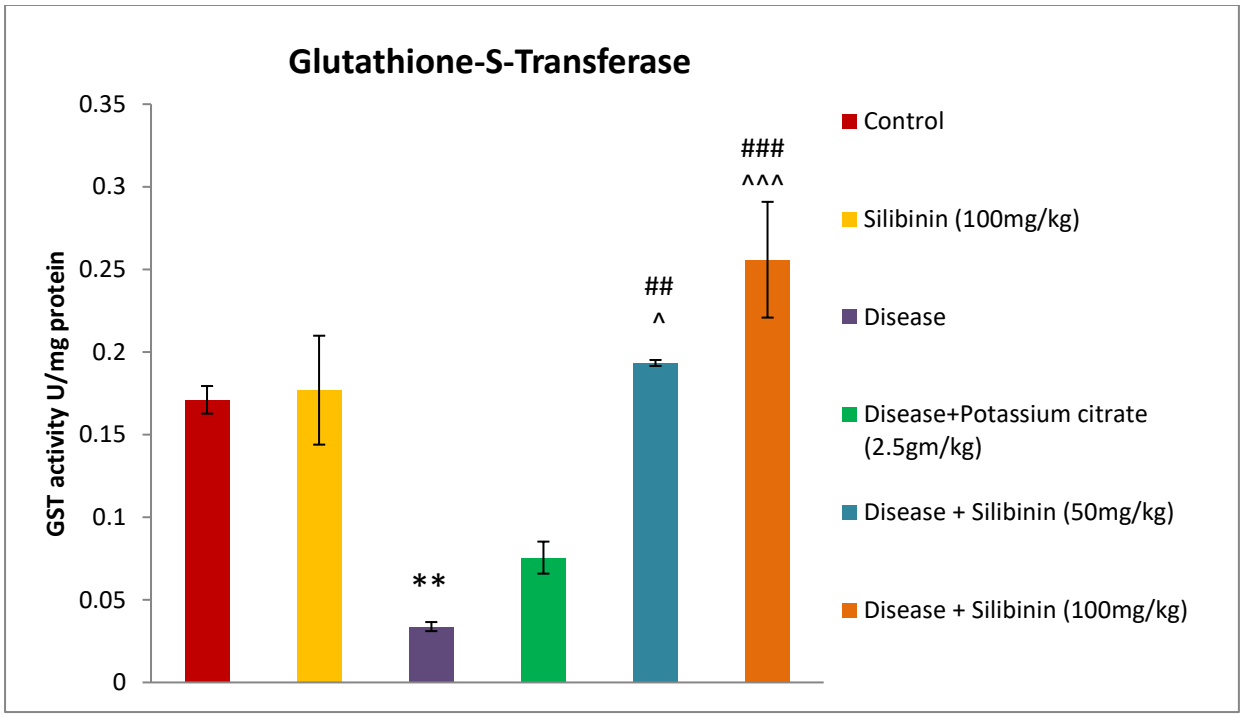

Figure 6.61: Effects of silibinin on renal Glutathione S-transferase (GST) activity. Values are shown as mean ± S.E.M. (n=6). Statistical significance is indicated as follows: **p<0.01, vs. control; ###p<0.001, and ##p<0.01 vs. disease; ^^^p<0.001, ^^p<0.01, and ^p<0.05 vs. potassium citrate (2.5 gm/kg).

Silibinin (100 mg/kg) significantly increased GST (86.79%, p<0.001) compared to the disease group and significantly reduced GST (70.47%, p<0.001) compared to potassium citrate.Silibinin (50 mg/kg) in the diseased group significantly increased GST (82.52%, p<0.01), compared to the disease group (Figure 6.61).

6.18.3.5 Reduced Glutathione (GSH)

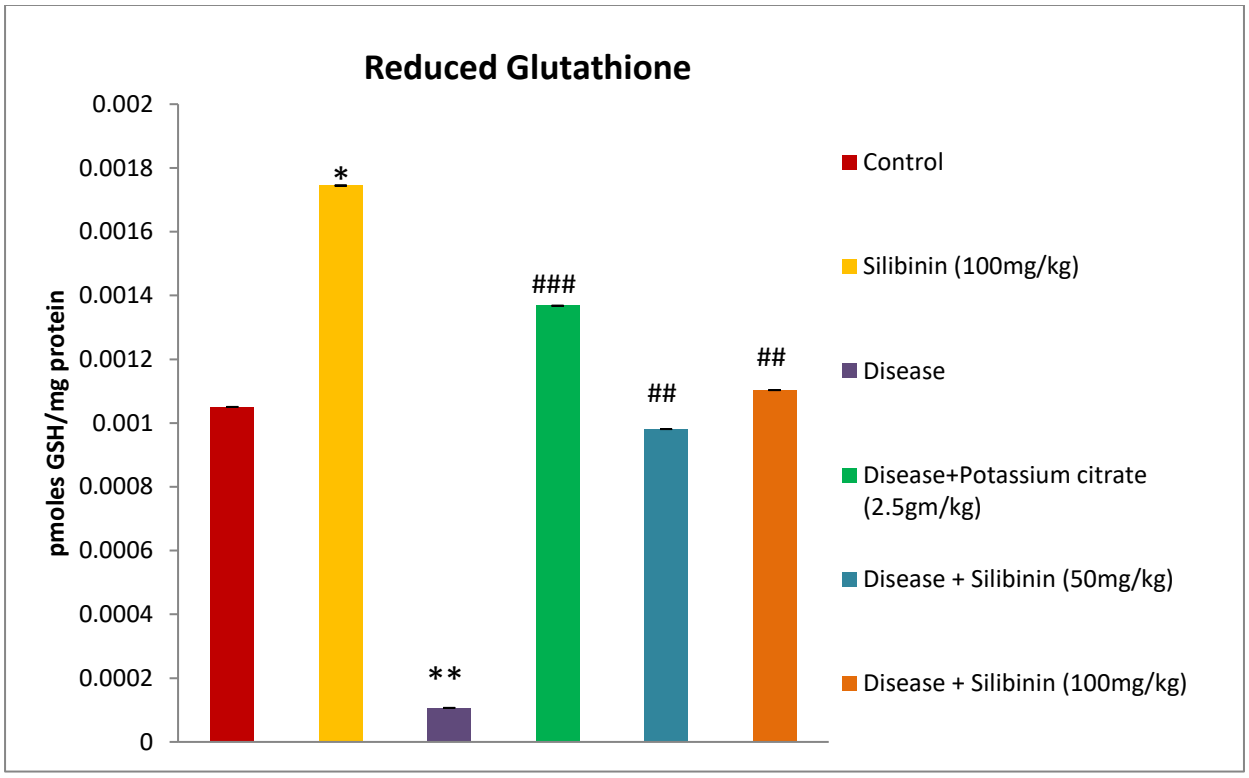

Figure 6.62: Effects of silibinin on renal reduced glutathione (GSH) activity. Values are shown as mean ± S.E.M. (n=6). Statistical significance is indicated as follows: ***p<0.001, **p<0.01, and *p<0.05 vs. control; ###p<0.001, ##p<0.01, and #p<0.05 vs. disease; ^^^p<0.001, ^^p<0.01, and ^p<0.05 vs. potassium citrate (2.5 gm/kg).

Silibinin (100 mg/kg) significantly increased GSH (39.78%, p<0.05) compared to the control, GSH (90.33%, p<0.01) compared to the disease group, silibinin (50 mg/kg) in the diseased group significantly increased GSH (89.13%, p<0.01) compared to the disease group (Figure 6.62).

Antioxidant enzyme activities were decreased in diseased rats: SOD (58.94%, p<0.001), CAT (43.93%, p<0.01), GST (67.46%, p<0.01), and GSH (89.85%, p<0.01) compared to controls. Silibinin demonstrated robust antioxidant effects in nephrolithiasis-induced oxidative stress. Both doses improved antioxidant defence and reduced oxidative biomarkers, with 100 mg/kg generally providing optimal benefits. Silibinin's efficacy was comparable to or exceeded that of potassium citrate in parameters like LPO, GST, and SOD, supporting its role as a promising therapeutic candidate in the management of kidney stone-associated oxidative injury.

6.18.4 Effect of silibinin on kidney histopathology

Multiple crystals were seen in the histopathological slides of disease and treatment groups (Figure 6.63), while no crystals were present in the control and silibinin (100 mg/kg) groups. The diseased group showed significant inflammation, renal tubule swelling, glomerulus shrinkage, necrosis, and tubular casts ($p<0.001$) compared to the control.

Potassium citrate treatment significantly reduced inflammation ($p<0.01$), tubular casts ($p<0.001$), tubular necrosis ($p<0.01$), and glomerular shrinkage ($p<0.01$) compared to the diseased group. Silibinin (50 mg/kg) also significantly reduced inflammation ($p<0.001$), tubular necrosis ($p<0.01$), tubule swelling ($p<0.01$), and glomerular shrinkage ($p<0.001$) in the diseased group. Silibinin (100 mg/kg) further reduced inflammation ($p<0.001$), tubular casts ($p<0.01$), tubular necrosis ($p<0.001$), tubule swelling ($p<0.001$), and glomerular shrinkage ($p<0.001$) significantly compared to the diseased group (Table 6.17 & Figure 6.64). Scoring and interpretation of structures were based on published literature (Yousefi et al., 2018; Yılmaz et al., 2023; Azimi et al., 2021; Singh et al., 2020; Kocaturk et al., 2020).

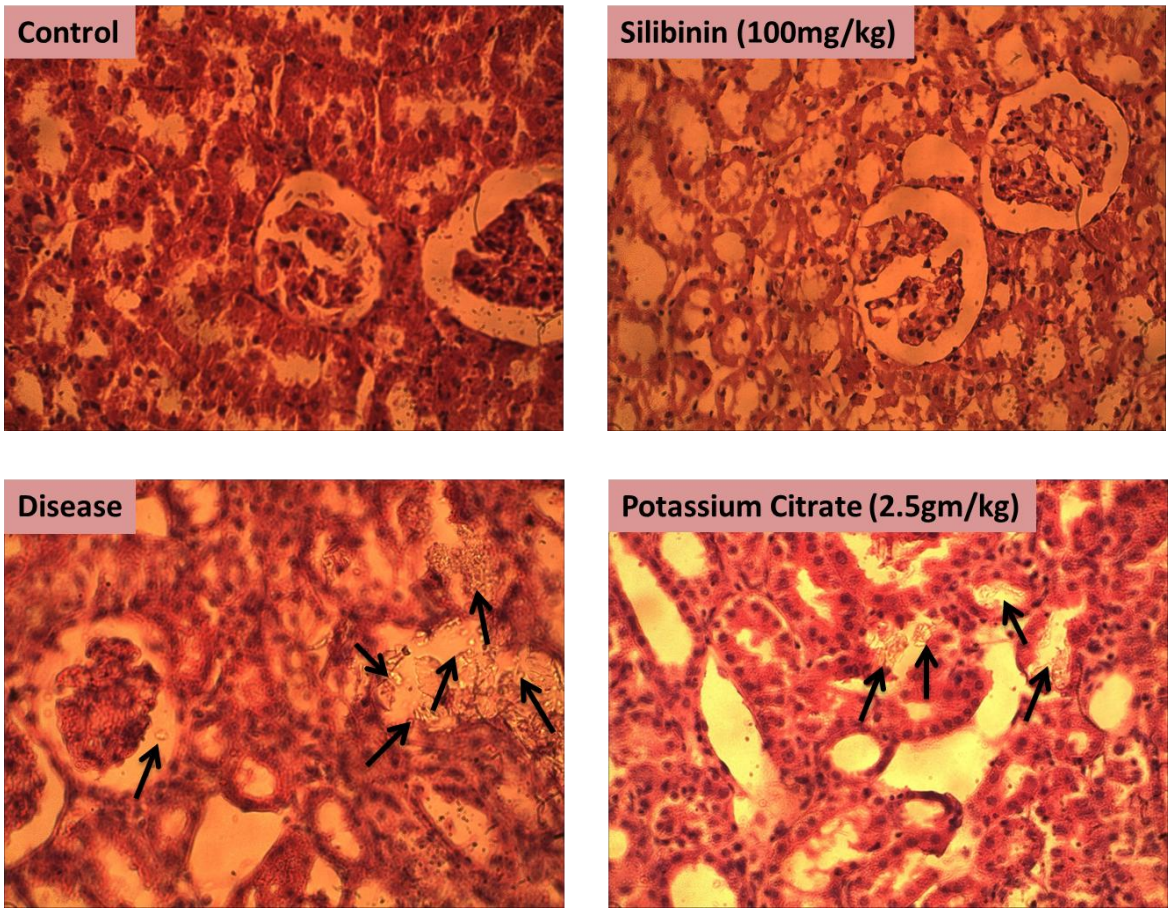

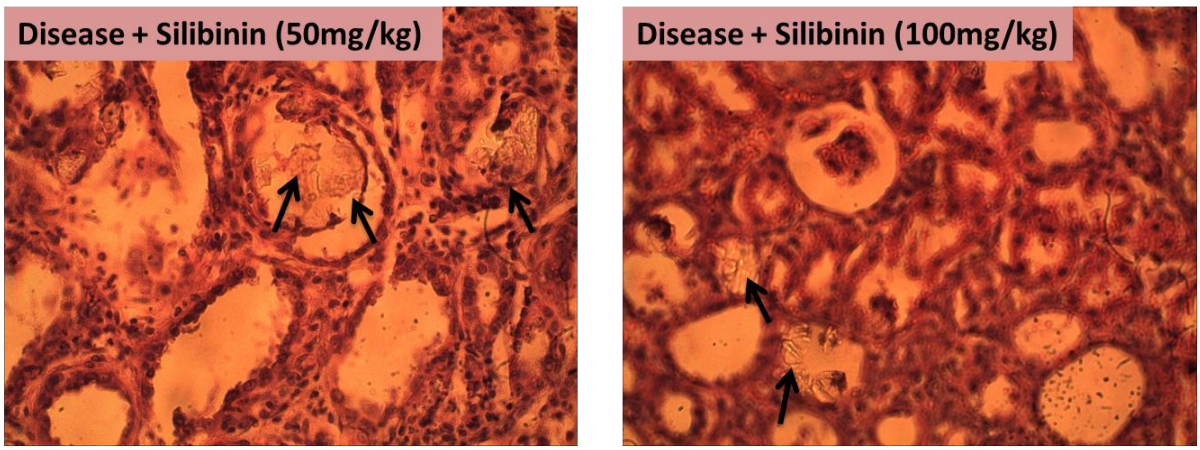

Figure 6.63: Renal histopathology of experimental groups. The black arrow shows crystals. All Figures are at 400X magnification.

Table 6.17: Histopathological changes in the experimental groups.

Parameters	**Control**	**Silibinin (100mg/kg)**	**Disease**	**Disease+Potassium citrate (2.5gm/kg)**	**Disease + Silibinin (50mg/kg)**	**Disease + Silibinin (100mg/kg)**
Inflammation	0.0 ± 0.00	0.0 ± 0.00	2.57 ± 0.20***	1.57 ± 0.29##	1.42 ± 0.20###	1.14 ± 0.14###
Tubular cast	0.0 ± 0.00	0.0 ± 0.00	2.28 ± 0.18***	0.71 ± 0.35###	1.42 ± 0.20	1.00 ± 0.21##
Tubular necrosis	0.0 ± 0.00	0.0 ± 0.00	2.28 ± 0.18***	1.14 ± 0.26##	1.28 ± 0.28##	0.71 ± 0.18###
Tubule Swelling	0.0 ± 0.00	0.0 ± 0.00	1.57 ± 0.29***	0.71 ± 0.28	0.42 ± 0.20##	0.28 ± 0.18###
Glomerular shrink	0.0 ± 0.00	0.0 ± 0.00	2.57 ± 0.29***	1.14 ± 0.40##	0.14 ± 0.14###	0.85 ± 0.40###

All values are expressed as mean ± S.E.M. (n=6). Statistical significance is indicated as follows: ***p<0.001, **p<0.01, and *p<0.05 for disease vs. control; ###p<0.001, #p<0.01, and #p<0.05 for potassium citrate, silibinin 50 mg/kg, and silibinin 100 mg/kg vs. disease. Inflammation: 0 = no inflammation, 1 = less than 25% of the tissue, 2 = 25–50% of the tissue,

3 = 50- 100% of the tissue. Tubular casts (tubules in 5 light microscopic fields): 0 = No cast, 1 ≤25% tubules 2 = 25–50% tubules 3 = 50-100% tubules. Tubular necrosis (each of 100 tubules): 0 = No necrosis, 1 ≤25% necrosis, 2 = 25–50% necrosis, 3 = 50–100% necrosis. Tubule Swelling or filled with proteinaceous fluid (each of 100 tubules): 0 = No swelling, 1 ≤25% tubules, 2 = 25–50% tubules, 3 = 50–100% tubules. Glomerular shrink 0 = No shrinkage, 1 ≤25% glomerulus, 2 = 25–50% glomerulus, 3 = 50–100% glomerulus.

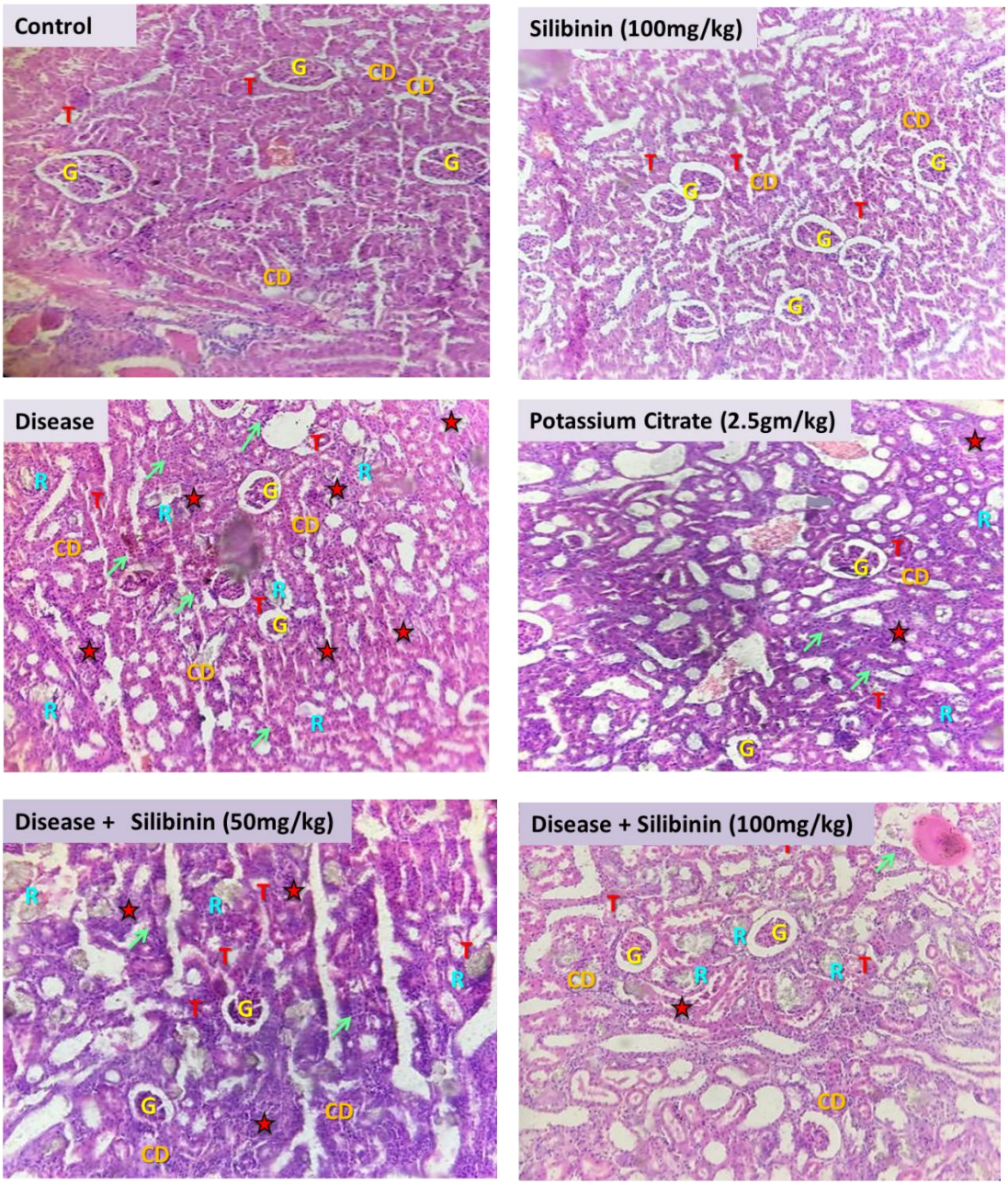

Figure 6.64: Histopathological findings of the kidneys in experimental groups**.** Key: CD =Collecting duct, G = Glomerulus, T = Tubules, R = Crystals. Green arrow indicates necrosis, and red star indicates inflammation. All images are at 100X magnification.

CHAPTER 7
DISCUSSION

Nephrolithiasis is the most common urinary system disease, with incidence rates rising each year (Li et al., 2020). The recurrence rate is 70-80% in men and 47-60% in women, with calcium oxalate stones being the most prevalent (80%) type (Queiroz et al., 2019; Tsujihata, 2008; Ivanovski and Drüeke, 2013). Approximately 12% of the global population is affected by kidney stones, with calcium oxalate comprising 75% of these cases. Despite this prevalence, the exact mechanisms of stone formation remain poorly understood (Alelign and Petros, 2018; Daudon and Jungers, 2004; Gambaro et al., 2004; Lee et al., 2011). Phytochemicals, particularly polyphenols and essential oils, possess antioxidant properties that provide protection against various diseases, including cancer, cardiovascular disorders, and neurodegenerative conditions (Valko et al., 2007; Mukherjee et al., 2007; Amorati et al.). Among these, Anethole, a major component of anise and fennel essential oils, has shown strong reactivity with peroxyl radicals, suggesting potential therapeutic benefits in kidney stone prevention. Similarly, Silibinin, a flavonoid derived from milk thistle (*Silybum marianum*), and Isoeugenol have demonstrated significant anti-inflammatory and antioxidant activities (Jahanafrooz et al., 2018; Singh et al., 2023; Chainy et al., 2000; Ritter et al., 2013). However, their role in preventing nephrolithiasis has not been explored. To the best of the authors' knowledge, this is the first study investigating their anti-lithiatic potential in in-vitro conditions.

Kidney stones (KS) can be inhibited by increased consumption of fibre, potassium and magnesium. Increased dairy intake also reduces the chances of KS, especially milk is recommended for uric acid stones (Legay et al., 2023; Taylor and Curhan, 2013; Brardi et al., 2016). KS is the multifaceted combination of genetic, dietary, environmental and lifestyle in addition to metabolic disorders which could affect the urine's pH and composition (Ferraro et al., 2020; Liu et al., 2023; Soligo et al., 2022; Siener, 2021).

Although extensive knowledge of crystallization and stone formation, effective treatments for nephrolithiasis remain scarce due to an incomplete understanding and slow progress in its pathophysiology (Liu et al., 2023). The current study applied a structured approach for the screening and identification of potential phytochemicals for the treatment of nephrolithiasis, using various computational methods. This multi-level screening included Lipinski's Rule of

Five (RO5), ADME properties, toxicity evaluation, ultimately highlighting five promising phytochemicals: 4-Vinylguaiacol, Anethole, Isoeugenol, Nadolol, and Silibinin. These compounds were subjected to various analyses, including protein-protein interaction (PPI) networks and molecular docking, to identify potential mechanisms for targeting nephrolithiasis.

The screening process began with Lipinski's Rule of Five (RO5), where 51 out of 67 compounds met the criteria, confirming the importance of structure in predicting drug-likeness. However, variability in drug-likeness across similar structures emphasized the complexity of drug development. CYP inhibition is of the parameters of druglikeliness and ADME studies. Protein pump inhibition (PPI) in suppressed form induces renal damage and risk of kidney stones increases, CYP2C19 which is related PPI metabolism could also affect the rate of kidney stones, hence was included in ADME studies (Zhang et al., 2024). And similar CYP family as parameters was taken in another survey for anti-nephrolithiatic agents (Mohan et al., 2022) and toxicity screening, whose parameters were taken from the literature (Medoro et al., 2023) narrowed the list to five promising candidates (4-Vinylguaiacol, Anethole, Isoeugenol, Nadolol, and Silibinin), which showed favourable pharmacokinetic properties. PPARγ activation helps restore mitochondrial balance, reducing oxidative stress, apoptosis, fibrosis, and inflammation caused by calcium oxalate crystals, thereby protecting against CaOx-induced renal injury (Liu et al., 2024), hence it was also included in toxicity studies. Toxicity screening of the shortlisted phytochemicals revealed favourable profiles; however, it is important to consider potential off-target effects or organ-specific toxicity when considering their therapeutic application. Further preclinical and clinical studies are necessary to confirm the safety of these compounds in long-term treatment regimens for nephrolithiasis patients.

Several predisposing factors of kidney stone formation, including hypertension, dyslipidemia, obesity, diabetes, and other components of metabolic syndrome, also increase the likelihood of renal cancer (McCredie et al., 1992; Li et al., 2020; Carbone et al., 2018; Khan et al., 2016; Johri et al., 2010). The study by Hou et al. and Guimerà et al. reported that Hepatitis B infection raises urinary pH above 6, increasing the risk of calcium phosphate stone formation in men due to suspected renal tubular acidosis, a pathogenic factor involved in calculus formation (Guimerà et al., 2020; Hou et al., 2022).

Gene Ontology (GO) and KEGG pathway enrichment analyses of the targets associated with these compounds revealed their involvement in relevant biological processes such as "response to organic substance" and "cellular response to chemical stimulus," both of which play central

roles in kidney stone formation. KEGG pathways such as Hepatitis B, Kaposi sarcoma-associated herpesvirus infection, and pathways in cancer were among the top hits. While Kaposi sarcoma-associated herpesvirus infection has no established link to nephrolithiasis in current literature, its frequent appearance across enrichment results suggests a possible unexplored pathway which might be worth investigating. The connection between Hepatitis B and nephrolithiasis is more evident, with studies reporting elevated urinary pH and an increased risk of staghorn calculi in infected individuals (Hou et al., 2022; Guimerà et al., 2020). Similar results were also reported by other studies (Liu et al., 2023; Zhang et al., 2023). Inflammatory responses to calculi may also induce hyperplasia in renal epithelia, contributing to carcinogenic progression (van de Pol et al., 2019).

Network pharmacology and protein-protein interaction (PPI) analysis identified BCL2, EGFR, MMP9, STAT3, and EP300 as key hub genes. These genes are implicated in various aspects of renal stone pathophysiology. For example, BCL2 downregulation enhances renal cell apoptosis and promotes calcium oxalate crystal adhesion (Ahmed et al., 2020). EGFR signaling has an indirect connection to nephrolithiasis via magnesium homeostasis, with its inhibition potentially impairing the protective effect of magnesium on stone formation (Vincenzi et al., 2008; Chen et al., 2003). MMP9 plays a vital role in uric acid metabolism and extracellular matrix remodeling, with SNPs linked to increased stone risk (Hess, 2006; Gruszka et al., 2021; Bu et al., 2020). Notably, recent evidence highlights STAT3 as a key regulator in nephrolithiasis, promoting RTEC ossification and enhancing claudin-14 expression via the CaSR-PKA-STAT3 pathway, thereby facilitating calcium oxalate crystal formation (Song et al., 2022; Luo et al., 2024). Progesterone receptor (PGR) influences calcium balance through modulation of parathyroid hormone, potentially affecting stone formation (Epstein et al., 1996; Seifert-Klauss et al., 2009; Wen et al., 2021). EP300, a known regulator of renal fibrosis via HIF2α modulation, is also overexpressed in diabetic nephropathy and represents another novel target in nephrolithiasis (Gong et al., 2022). Similar targets were also reported by another study (Liu et al., 2023)

Molecular docking is a critical tool for studying the binding interactions between two entities (Istrefi et al., 2020; Türkeş et al., 2021; Demir et al., 2020). When the binding energy is low (highly negative), it indicates a strong binding affinity (Hsin et al., 2013). SIRT1, a protein involved in multiple diseases such as tumorogenesis, cardiovascular, and neurodegenerative

diseases, also plays a critical role in kidney stone formation (Chen et al., 2020). The activation or inhibition of SIRT1 can influence kidney stone formation, and many natural compounds have been shown to interact with SIRT1 (Vyas et al., 2015), which is also important in the case of kidney stones. SIRT1 gets activated if any compound binds to its allosteric site, whereas it gets deacetylated if any compound binds to its catalytic site. In our study, docking simulations revealed that all three phytochemicals bind to the SIRT1 protein with favourable binding energies ranging from -5.9 to -7.9 kcal/mol, exhibiting significant interactions with residues such as GLU230, ASN226, and PHE273. Phytochemicals such as crocin, bichalcones, quercetin and metformin have previously been reported as SIRT1 interactors (Medoro et al., 2023; Karaman et al., 2018; Cuyàs et al., 2018; Iside et al., 2020). Molecular dynamics simulations (100ns) further revealed that the phytochemicals exhibited good structural stability in complex with SIRT1, with RMSD values in the range of 0.2 to 1.1 nm, which is consistent with previously reported results (Sinha et al., 2019). PCA is used to identify dominant collective motions of the protein during molecular dynamics, helping to understand how ligand binding influences the overall flexibility and conformational behaviour of the system. Although PCA does not directly identify specific residues, further projection of eigenvectors or fluctuation analysis along principal components can highlight residues that contribute most to the collective motions. In terms of MD simulation trajectory, it interprets covariance matrix of atomic fluctuations, extract components playing the major role in motion. By projecting trajectory in 2D space PCA helps in elucidating dominant structural variation and dynamic behaviour of the protein (Khan et al., 2025; Sharma et al., 2022).

Taken together, these findings suggest that the three phytochemicals, particularly silibinin form stable, compact, and well-integrated complexes with SIRT1, consistent with their docking results and previous literature on SIRT1-targeting phytochemicals such as crocin, bichalcones, quercetin, and metformin (Medoro et al., 2023; Karaman et al., 2018; Cuyàs et al., 2018; Iside et al., 2020).

Trans-anethole, which is aromatic, a phenylpropanoid commonly found in essential oil, particularly star anise and more than 20 other species such as anise, fennel, etc., is considered safe by the FDA (Sheikh et al. 2015; Aprotosoaie et al. 2016). It has many biological activities such as antimicrobial (Wieczyńska and Cavoski, 2018); antioxidant (Sá et al. 2020) anti-inflammatory (Zhang et al. 2018), anti-proliferative (Harakeh et al., 2023) but has not been explored against nephrolithiasis. Isoeugenol is a phenylpropanoid is a pale-yellow liquid found in many plant species that exhibits numerous biological activities other than being used

as a flavoring or fragrance agent (Zhang et al., 2022) such as antibacterial, antioxidant, and DNA damage protective effect (Zhang et al., 2017), anticholinergic and antidiabetic (Topal, 2019). Silibinin, a bioactive compound of milk thistle possesses anticancer (Zhu et al., 2016; Binienda et al., 2020; Tuli et al., 2021) anti-apoptotic and anti-inflammatory (Shen et al., 2019), anti-diabetic properties (Zare et al., 2024), cytochrome P-450 inhibitor (Beckmann-Knopp, 2000), improves cognitive impairment (Wei et al., 2022), neuroprotectant (Thayumanavan et al., 2022). Above mentioned phytochemicals have not been studied in nephrolithiasis but most of their biological properties are crucial when dealing with calculi.

In healthy urine, natural inhibitors like magnesium-containing complexes play a vital role in the prevention of calcium oxalate supersaturation, which is a major contributor to kidney stones (Dinnimath et al., 2017; Carvalho et al., 2004). The formation of calcium oxalate involves multiple processes such as nucleation, aggregation and growth (or oxalate depletion) (Khare et al., 2014). The present study aimed to study these processes by evaluating the inhibitory effect of Silibinin, Isoeugenol and Anethole and comparing them with potassium citrate. Isoeugenol which is found in many vegetables such as monkey orange contains methoxyphenol in its structure, which imparts anti-oxidant properties (Sitrit et al., 2003; Fujisawa et al., 2002).

The most critical step in stone formation is nucleation, in which multiple salts of stones combine to form loose clusters in a solution, when added with new components can also increase in size. The effect of phytochemicals in the range of 20µM -100µM on nucleation assay was studied in the present study, which yielded better results than potassium citrate. This nucleation assay provides valuable insights into the potential of phytochemicals as inhibitors of calcium oxalate crystallization. Silibinin and Anethole emerge as the most promising candidates due to their significant dose-dependent and time-dependent inhibitory effects. While Isoeugenol demonstrates inhibition, its inconsistency at certain concentrations warrants further investigation. The findings emphasize the importance of dose optimization and long-term efficacy evaluation in the development of anti-nucleation therapies. Future studies should explore the molecular mechanisms underlying these inhibitory effects to enhance our understanding of crystal growth prevention strategies.

Another process is aggregation assay, which is used to make kidney stones. Small crystals tend to stick together to form large particles, a process known as aggregation or agglomeration (Aggarwal et al., 2013). Aggregation of calcium oxalate was measured in the presence and absence of phytochemicals in the range of 20µM -100µM and was compared to PC in the same

range. Although not much of the significant data was obtained, it can be said that all the compounds had similar anti-aggregation capacity as that of PC. Crystal growth or oxalate depletion which is the final nail in the coffin in the formation of calculi is the process in which any crystal when achieves critical size, starts forming small solid masses known as stones (N. Kulkarni, et al., 2017). In this study, three concentrations (20µM, 60µM and 100µM) have been taken to study this process. At all three concentrations, the phytochemicals showed better activity than the standard potassium citrate.

Another aspect of nephrolithiasis is the adhesion of crystal-forming substances, their numbers and their shape on the surface of renal cells (Thongboonkerd, 2019). The more the crystal adhesion, the more the damage. Our data revealed all three phytochemicals (Silibinin, Isoeugenol and Anethole) at both concentrations (50µM and 100µM) had very low adhesion. Many polyphenols, flavonoids, and plant extracts such as Diosmin, EGCG, and trigonelline were able to reduce this cell adhesion (Bawari et al., 2023; Peerapen and Thongboonkerd, 2025; Fong-ngern et al., 2017; Khamchun et al., 2021). When crystals adhere to the cell surface, they damage the cell integrity, leading to the formation of reactive oxygen species (ROS) (Sun et al., 2015; Motskin et al., 2009; Kong et al., 2015). Hence complementary therapies should also focus on anti-oxidative properties along with anti-lithiatic properties when dealing with nephrolithiasis. In reducing power assay, reactions between antioxidants and potassium ferricyanide form potassium ferrocynanide, which further reacts with ferric chloride to form an intense blue colour, which has absorption maxima at 700nm. Now this reaction is dependent on the hydrogen atom donation capacity of any anti-oxidant (Dontha, 2016; Loganayaki et al., 2013). In our study, the reducing capacity is in the order of Isoeugenol > Silibinin > Anethole.

When talking about stone-forming elements, urinary supersaturation takes the upper hand because it is the most vital thermodynamic factor in urolith production. Once this supersaturation crosses the metastability limit, kinetic factors get overpowered by thermodynamic factors. Due to this, stone inhibitors are deemed unfit at abnormally high supersaturation states in inhibition or reduction of stone progression (Carvalho and Vieira, 2004; Khan and Canales, 2009, Konigsberger and Konigsberger, 2001). Hence, the phytochemicals must also be evaluated against the supersaturation ratio which will be the scope of our future studies.

Classical Nucleation Theory explains the energy barrier to nucleation in terms of Gibbs free energy, which consists of surface and volume free energy. In a supersaturated solution, the total

energy reaches its highest point at a specific particle size known as the critical size. When a cluster grows to this critical size, it is identified as a nucleus (Abdel-Aal EA et al., 2017).

Interfacial free energy is the difference of free energy between single molecule of bulk and that of surface. In a supersaturated solution, ions or molecules joins together to form a cluster or nucleus, which leads to the exchange of excess of free energy change between nucleus and solutes of the supersaturated solutions, referred as Gibbs free energy changes (ΔGcr).

Zeta potential measures system stability and surface charge of molecules by analysing the intensity with which mutual attraction and repulsion occur between particles (Xie et al., 2021). High surface charge density indicates lower particle aggregation due to electrostatic repulsion and stability and vice-versa (Miyake et al., 1998; Polat et al., 2021). Particles with higher negative or positive zeta potential repel each other whereas particle with lower negative or positive zeta potential (near to zero) tends to aggregate (Cho et al., 2014).

In this study, a rat model of calcium oxalate (CaOx) nephrolithiasis was developed using ethylene glycol to investigate the effects of silibinin on kidney stone formation.

Ethylene glycol acts as an oxalate precursor; it is absorbed in the intestine and metabolized to oxalate in the liver, resulting in hyperoxaluria. This condition promotes the formation of calcium oxalate crystals in the kidneys, primarily due to the poor solubility of calcium oxalate in urine (Fan et al., 1999; Karadi et al., 2006; Nizami et al., 2012; Scheid et al., 2004). Additionally, when ethylene glycol is administered alongside ammonium chloride, it accelerates the formation of kidney stones, making this combination ideal for short-term animal studies (Bobbitt et al., 1986).

Microscopic examination of urine samples revealed the presence of crystals in both diseased and treatment groups, corroborating findings from previous studies (Azimi et al., 2021; Marhoume et al., 2021). Importantly, no significant differences in kidney morphology were noted between the various experimental groups, which aligns with earlier reports (Yılmaz et al., 2023). Silibinin and potassium citrate were found to reduce organ coefficients in comparison to disease control rats, likely due to their effects in decreasing inflammation and calcium oxalate deposits (Yousefi et al., 2018).

The glomerular filtration rate (GFR), an indicator of kidney function, was found to be reduced in nephrolithiasis due to obstructed urine flow caused by the presence of stones. This obstruction leads to increased levels of non-protein nitrogenous substances, such as urea, creatinine, and uric acid, in the blood (Grover and Resnick, 1995). In the current study, silibinin

was shown to lower these levels and improve the GFR, highlighting its potential therapeutic effects. Furthermore, calcium ions are known to promote stone formation, while magnesium ions inhibit this process (Penniston and Nakada, 2018). The results indicated a reduction in calcium and an elevation in magnesium levels in silibinin-treated groups compared to the diseased group.

Numerous studies suggest that antioxidants may play a critical role in managing kidney stones by mitigating oxidative stress (Khan, 2013). Oxalate can accumulate in renal tubular epithelial cells when antioxidant mechanisms are poorly regulated, which decreases the activity of crucial enzymes such as superoxide dismutase (SOD), catalase (CAT), and glutathione (GSH), while simultaneously increasing lipid peroxidation (Khand et al., 2002; Cao et al., 2004). This oxidative stress can diminish mitochondrial membrane potential and cause damage to cellular components (Joshi et al., 2013; Joshi et al., 2012; Zuo et al., 2011). Increased SOD levels can mitigate calcium oxalate formation by decomposing reactive oxygen species and inhibiting stress responses (Kang et al., 2020). In this study, lipid peroxidation was found to be elevated, while the activities of antioxidant enzymes were decreased in the diseased group compared to controls. Notably, silibinin treatment increased the activity of these antioxidant enzymes, thereby helping to prevent renal damage.

The study also highlighted significant histopathological damage caused by ethylene glycol, including inflammation, glomerular shrinkage, necrosis, and tubular swelling. Silibinin treatment was effective in reversing these conditions. Similar protective effects were reported with other treatments, such as apigenin, fucoxanthin, lipoic acid, and 6-shogaol in ethylene glycol-induced kidney stones in male Wistar rats (Azimi et al., 2021; Wang et al., 2020; Wang et al., 2020; Afzal et al., 2021). Additionally, various plant extracts, such as *Myrtus communis* and *Aerva lanata*, have been evaluated for their effects on kidney stones, although many studies do not clarify the bioactive components involved (Yılmaz et al., 2023; Bano et al., 2018; Singh et al., 2022). Therefore, further research is necessary to assess the safety and efficacy of these treatments.

CHAPTER 8
CONCLUSION

Nephrolithiasis, a multifactorial disorder driven by oxidative stress, inflammation, and metabolic imbalances, remains a pressing global health concern. Despite advancements in surgical and pharmacological interventions, the high recurrence rate of kidney stones necessitates the exploration of alternative therapeutic strategies. This study aimed to identify natural phytochemicals with potential anti-nephrolithiatic properties using an integrated in-silico, in-vitro, and in-vivo approach. The findings highlight the therapeutic promise of Anethole, Isoeugenol, and Silibinin as effective modulators of calcium oxalate crystallization and oxidative stress, positioning them as potential candidates for nephrolithiasis management.

The multi-level screening process, involving molecular docking, ADME analysis, and pharmacokinetic profiling, demonstrated the suitability of these phytochemicals as therapeutic agents. The in-silico studies provided insights into their molecular interactions with key targets involved in nephrolithiasis, particularly SIRT1, EP300, and MMP9. The strong binding affinities observed suggest that these compounds exert their effects by modulating epigenetic regulators and pathways associated with kidney stone formation, oxidative stress, and inflammation.

In-vitro studies further validated the computational findings by demonstrating the ability of Anethole, Isoeugenol, and Silibinin to inhibit calcium oxalate crystallization. These compounds effectively reduced crystal size and numbers at lower supersaturation ratios, thereby decreasing the likelihood of crystal aggregation and retention within renal tubules. Although challenges persist at higher supersaturation ratios, these preliminary findings underscore the potential of phytochemicals in modulating crystallization dynamics and preventing kidney stone formation.

The in-vivo studies, conducted using an ethylene glycol-induced nephrolithiasis rat model, further reinforced the protective effects of these phytochemicals. Silibinin, in particular, demonstrated significant antioxidant properties, effectively reducing oxidative damage and renal injury. The observed improvements in renal function parameters, including decreased serum creatinine, urea, and uric acid levels, highlight the ability of these compounds to preserve kidney function under lithogenic conditions. Additionally, histopathological analyses confirmed reduced renal inflammation, crystal deposition, and tubular damage in treated groups compared to the disease control group.

Beyond their direct impact on calcium oxalate crystallization, these phytochemicals exhibited strong antioxidant and anti-inflammatory properties. Oxidative stress plays a critical role in kidney stone pathogenesis by triggering lipid peroxidation, mitochondrial dysfunction, and renal epithelial injury. The ability of Anethole, Isoeugenol, and Silibinin to enhance endogenous antioxidant enzyme activity (SOD, CAT, GSH) and suppress pro-inflammatory cytokines (TNF-α, IL-6, NF-κB) suggests a multifaceted approach to nephrolithiasis prevention. By targeting multiple pathological pathways, these compounds offer a promising alternative to conventional treatments that primarily focus on stone dissolution and urinary pH modulation.

While this study provides compelling evidence supporting the therapeutic potential of Anethole, Isoeugenol, and Silibinin, further research is warranted to bridge the gap between experimental findings and clinical application. Future studies should explore their pharmacokinetic behavior in human models, including bioavailability, metabolism, and long-term safety. Additionally, detailed mechanistic studies investigating their interactions with epigenetic regulators, renal epithelial cells, and immune responses will provide deeper insights into their mode of action.

Moreover, a personalized approach to nephrolithiasis treatment remains crucial. Factors such as stone composition, genetic predisposition, metabolic conditions, and lifestyle habits should be considered when developing therapeutic strategies. The integration of artificial intelligence (AI) in drug discovery and patient management may offer novel insights into optimizing treatment plans based on individual risk factors. AI-assisted diagnostics and robotic innovations in urology are already revolutionizing kidney stone management, offering precision-guided interventions and minimally invasive surgical techniques.

The future of nephrolithiasis treatment lies in a multi-pronged strategy that combines natural therapeutics with advanced technological innovations. Research into bioengineered stone dissolution therapies and targeted drug delivery systems holds promise for reducing the need for invasive interventions. Additionally, the role of gut microbiota in kidney stone formation is an emerging area of interest, with potential implications for developing probiotic-based therapies.

In conclusion, this study highlights the potential of Anethole, Isoeugenol, and Silibinin as promising natural modulators of nephrolithiasis through their anti-lithiatic, antioxidant, and epigenetic regulatory properties. By integrating computational modeling, biochemical

validation, and in-vivo assessments, this research provides a strong foundation for further investigations into plant-derived therapies for kidney stone prevention. While challenges remain in translating these findings into clinical practice, continued research efforts focusing on safety, efficacy, and personalized treatment approaches will pave the way for novel, non-invasive interventions. The insights gained from this study contribute to the broader field of nephrology, offering a step forward in the quest for safer and more effective therapies for kidney stone disease.

BIBLIOGRAPHY

- Abdel-Aal EA, Abdel-Ghafar HM, El-Sayed D, El-Shazly AN, Hoinkis J. Crystallization study of reverse osmosis desalination scales at low salinity with and without inhibitor. Particulate Science and Technology. 2017 Nov 2;35(6):749-54.
- Abdel-Aal EA, Daosukho S, El-Shall H. Effect of supersaturation ratio and Khella extract on nucleation and morphology of kidney stones. Journal of crystal growth. 2009 Apr 15;311(9):2673-81.
- Abed A, El-Nahas AR, Al-Kandari AM, Shokeir AA. Percutaneous Nephrolithotomy (PCNL) in the Treatment of Stones Within Horseshoe Kidneys and in Patients with Autosomal Dominant Polycystic Kidney Disease. InDifficult Cases in Endourology 2012 Sep 17 (pp. 115-121). London: Springer London.
- Abraham MJ, Murtola T, Schulz R, Páll S, Smith JC, Hess B, Lindahl E. GROMACS: High performance molecular simulations through multi-level parallelism from laptops to supercomputers. SoftwareX. 2015 Sep 1;1:19-25.
- Abu Zarin M, Tan JS, Murugan P, Ahmad R. Investigation of potential anti-urolithiatic activity from different types of Musa pseudo-stem extracts in inhibition of calcium oxalate crystallization. BMC complementary medicine and therapies. 2020 Dec;20:1-2.
- Afgar A, Keyhani A, Afgar A, Mirzaei-Parsa MJ, Kermani MR, Rezaei M, Ebrahimipour M, Langroudi L, Bardsiri MS, Vahidi R. Catechin-Induced changes in PODXL, DNMTs, and miRNA expression in Nalm6 cells: an integrated in silico and in vitro approach. BMC Complementary Medicine and Therapies. 2024 Jun 15;24(1):234.
- Afzal M, Kazmi I, Quazi AM, Ahmad A, Al-Abaasi FA, Imam F, Alharbi KS, Alzarea SI, Zafar A. 6-Shogaol attenuated ethylene glycol and aluminium chloride induced urolithiasis and renal injuries in rodents. Saudi Journal of Biological Sciences. 2021 Jun 1;28(6):3418-23.
- Agarwal A, Kansal V, Farooqi H, Prasad R, Singh VK. Epigallocatechin Gallate (EGCG), an active phenolic compound of Green Tea, inhibits Tumor Growth of Head and Neck Cancer cells by targeting DNA hypermethylation. Biomedicines. 2023 Mar 5;11(3):789.
- Aggarwal KP, Narula S, Kakkar M, Tandon C. Nephrolithiasis: molecular mechanism of renal stone formation and the critical role played by modulators. BioMed research international. 2013;2013(1):292953.

- AHMED L, Rebaz O. The relationship between kidney stones and Dietary habits using XRF technique. J Phys Chem Funct Mater. 2023;6(1):18–33
- Akyol E, Öner M. Controlling of morphology and polymorph of calcium oxalate crystals by using polyelectrolytes. Journal of crystal growth. 2014 Sep 1;401:260-5.
- Alelign T, Petros B. Kidney stone disease: an update on current concepts. Advances in urology. 2018;2018(1):3068365.
- Alexander B, Fishman AI, Grasso M. Ureteroscopy and laser lithotripsy: technologic advancements. World journal of urology. 2015 Feb;33:247-56.
- Alexander RT, Hemmelgarn BR, Wiebe N, Bello A, Morgan C, Samuel S, Klarenbach SW, Curhan GC, Tonelli M. Kidney stones and kidney function loss: a cohort study. Bmj. 2012 Aug 30;345.
- Amadei A, Linssen AB, Berendsen HJ. Essential dynamics of proteins. Proteins: Structure, Function, and Bioinformatics. 1993 Dec;17(4):412-25.
- Amjad Z. Applications of antiscalants to control calcium sulfate scaling in reverse osmosis systems. Desalination. 1985 Jan 1;54:263-76.
- Amorati R, Foti MC, Valgimigli L. Antioxidant activity of essential oils. Journal of agricultural and food chemistry. 2013 Nov 20;61(46):10835-47.
- Antonelli JA, Maalouf NM, Pearle MS, Lotan Y. Use of the National Health and Nutrition Examination Survey to calculate the impact of obesity and diabetes on cost and prevalence of urolithiasis in 2030. European urology. 2014 Oct 1;66(4):724-9.
- Aprotosoaie AC, Costache II, Miron A. Anethole and its role in chronic diseases. Drug discovery from mother nature. 2016:247-67.
- Aruoma OI. Free radicals, oxidative stress, and antioxidants in human health and disease. Journal of the American oil chemists' society. 1998 Feb;75(2):199-212.
- Asplin JR. Hyperoxaluric calcium nephrolithiasis. Endocrinology and Metabolism Clinics. 2002 Dec 1;31(4):927-49.
- Assadi F, Moghtaderi M. Preventive kidney stones: continue medical education. International journal of preventive medicine. 2017 Jan 1;8(1):67.
- Assimos D, Krambeck A, Miller NL, Monga M, Murad MH, Nelson CP, Pace KT, Pais VM, Pearle MS, Preminger GM, Razvi H. Surgical management of stones: American urological association/endourological society guideline, PART I. The Journal of urology. 2016 Oct;196(4):1153-60.

- Atanasov AG, Zotchev SB, Dirsch VM, Supuran CT. Natural products in drug discovery: advances and opportunities. Nature reviews Drug discovery. 2021 Mar;20(3):200-16.
- Baidya AT, Kumar A, Kumar R, Darreh-Shori T. Allosteric binding sites of Aβ peptides on the acetylcholine synthesizing enzyme ChAT as deduced by in silico molecular modeling. International Journal of Molecular Sciences. 2022 May 28;23(11):6073.
- Bakulski KM, Fallin MD. Epigenetic epidemiology: promises for public health research. Environmental and molecular mutagenesis. 2014 Apr;55(3):171-83.
- Bammens B, Evenepoel P, Verbeke K, Vanrenterghem Y. Removal of middle molecules and protein-bound solutes by peritoneal dialysis and relation with uremic symptoms. Kidney international. 2003 Dec 1;64(6):2238-43.
- Banerjee P, Eckert AO, Schrey AK, Preissner R. ProTox-II: a webserver for the prediction of toxicity of chemicals. Nucleic acids research. 2018 Jul 2;46(W1):W257-63.
- Bano H, Jahan N, Makbul SA, Kumar BN, Husain S, Sayed A. Effect of Piper cubeba L. fruit on ethylene glycol and ammonium chloride induced urolithiasis in male Sprague Dawley rats. Integrative Medicine Research. 2018 Dec 1;7(4):358-65.
- Barghouthy Y, Corrales M, Somani B. The relationship between modern fad diets and kidney stone disease: a systematic review of literature. Nutrients. 2021 Nov 26;13(12):4270.
- Barja G (2004) Free radicals and aging. Trends Neurosci 27:595–600
- Bashyal J, Raut BK, Upadhyaya SR, Sharma K, Parajuli N. Exploration of Potent Human α-Glucosidase Inhibitors Using In Silico Approaches: Molecular Docking, DFT, Molecular Dynamics Simulations, and MMPBSA. Journal of Chemistry. 2024;2024(1):2086167
- Bawari S, Sah AN, Gupta P, Zengin G, Tewari D. Himalayan Citrus jambhiri juice reduced renal crystallization in nephrolithiasis by possible inhibition of glycolate oxidase and matrix metalloproteinases. Journal of Ethnopharmacology. 2023 Apr 24; 306:116157.
- Beckmann-Knopp S, Rietbrock S, Weyhenmeyer R, Böcker RH, Beckurts KT, Lang W, Hunz M, Fuhr U. Inhibitory effects of silibinin on cytochrome P-450 enzymes in human liver microsomes. Pharmacology & toxicology. 2000 Jun;86(6):250-6.

- Berg EL. Systems biology in drug discovery and development. Drug discovery today. 2014 Feb 1;19(2):113-25.
- Bergmeyer HU, editor. Methods of enzymatic analysis. Elsevier; 2012 Dec 2.
- Bevernage J, Brouwers J, Brewster ME, Augustijns P. Evaluation of gastrointestinal drug supersaturation and precipitation: strategies and issues. International journal of pharmaceutics. 2013 Aug 30;453(1):25-35.
- Bevernage J, Brouwers J, Clarysse S, Vertzoni M, Tack JA, Annaert P, Augustijns P. Drug supersaturation in simulated human intestinal fluids representing different nutritional states. Journal of pharmaceutical sciences. 2010 Nov 1;99(11):4525-34.
- Bhattacharya S, Joshi NK, Jain YK, Bajpai N, Bhardwaj P, Chaturvedi M et al. Dietary determinants of renal calculi: a case-control study from a Tertiary Care Hospital of Western Rajasthan. Cureus. 2022;14(11).
- Bigoniya P, Sohgaura AK, Shrivastava B. Antilithiatic effect of C. dactylon, E. officinalis, K. pinnata, and B. nutans ethyl acetate fraction on glyoxylate-induced nephrolithiasis. Future Journal of Pharmaceutical Sciences. 2021 Dec;7:1-9.
- Binbay M, Istanbulluoglu O, Sofikerim M, Beytur A, Skolarikos A, Akman T, Huri E, Ozturk B, Kural AR, Muslumanoglu AY. Effect of simple malrotation on percutaneous nephrolithotomy: a matched pair multicenter analysis. The Journal of urology. 2011 May 1;185(5):1737-41.
- Binienda A, Ziolkowska S, Pluciennik E. The anticancer properties of silibinin: its molecular mechanism and therapeutic effect in breast cancer. Anti-Cancer Agents in Medicinal Chemistry (Formerly Current Medicinal Chemistry-Anti-Cancer Agents). 2020 Oct 1;20(15):1787-96.
- Bobbitt WH, Williams RM, Freed CR. Severe ethylene glycol intoxication with multisystem failure. Western journal of medicine. 1986 Feb;144(2):225.
- Bondi AV. van der Waals Volumes and Radii. The Journal of physical chemistry. 1964 Mar;68(3):441-51.
- Bonini NM, Berger SL. The sustained impact of model organisms—in genetics and epigenetics. Genetics. 2017 Jan;205(1):1.
- Brardi S, Verdacchi T, Paoletti G, Giovannelli V, Duranti E. Does milk intake play a specific role in the pathogenesis of kidney stones? Archives Ren Dis Manage. 2016;2(1):026–30
- Bu Q, Zhu Y, Chen QY, Li H, Pan Y. A polymorphism in the 3′-untranslated region of the matrix metallopeptidase 9 gene is associated with susceptibility to idiopathic

calcium nephrolithiasis in the Chinese population. Journal of International Medical Research. 2020 Dec;48(12):0300060520980211.

- Buege JA, Aust SD. [30] Microsomal lipid peroxidation. InMethods in enzymology 1978 Jan 1 (Vol. 52, pp. 302-310). Academic press.
- Bussi G, Donadio D, Parrinello M. Canonical sampling through velocity rescaling. The Journal of chemical physics. 2007 Jan 7;126(1).
- Butterweck V, Khan SR. Herbal medicines in the management of urolithiasis: alternative or complementary?. Planta medica. 2009 Aug;75(10):1095-103.
- Cao LC, Honeyman TW, Cooney R, Kennington L, Scheid CR, Jonassen JA. Mitochondrial dysfunction is a primary event in renal cell oxalate toxicity. Kidney international. 2004 Nov 1;66(5):1890-900.
- Carbone A, Al Salhi Y, Tasca A, Palleschi G, Fuschi A, De Nunzio C, Bozzini G, Mazzaferro S, Pastore AL. Obesity and kidney stone disease. A systematic review. Minerva urologica e nefrologica. 2018:393-400.
- Carvalho M, Vieira MA. Changes in calcium oxalate crystal morphology as a function of supersaturation. International braz j urol. 2004;30:205-9.
- Chainy GBN, Manna SK, Chaturvedi MM, Aggarwal BB (2000) Anethole blocks both early and late cellular responses transduced by tomor necrosis factor: effect on NF-κB, AP-1, JNK, MAPKK and apoptosis. Oncogene 19:2943–2950
- Chaiyarit S, Pikham S, Thongboonkerd V. Quercetin inhibits calcium oxalate crystallization and growth but promotes crystal aggregation and invasion. Current Research in Food Science. 2024 Jan 1;8:1006
- Chang HC, Guarente L. SIRT1 and other sirtuins in metabolism. Trends in Endocrinology & Metabolism. 2014 Mar 1;25(3):138-45.
- Chavan RB, Thipparaboina R, Kumar D, Shastri NR. Evaluation of the inhibitory potential of HPMC, PVP and HPC polymers on nucleation and crystal growth. RSC advances. 2016;6(81):77569-76.
- Chen C, Zhou M, Ge Y, Wang X. SIRT1 and aging related signaling pathways. Mechanisms of ageing and development. 2020 Apr 1;187:111215.
- Chen WC, Chen HY, Wu HC, Wu MC, Hsu CD, Tsai FJ. Vascular endothelial growth factor gene polymorphism is associated with calcium oxalate stone disease. Urological research. 2003 Jul;31:218-22.

- Chmiel JA, Stuivenberg GA, Al KF, Akouris PP, Razvi H, Burton JP, Bjazevic J. Vitamins as regulators of calcium-containing kidney stones—new perspectives on the role of the gut microbiome. Nature Reviews Urology. 2023 Oct;20(10):615-37.
- Cho WS, Thielbeer F, Duffin R, Johansson EM, Megson IL, MacNee W, Bradley M, Donaldson K. Surface functionalization affects the zeta potential, coronal stability and membranolytic activity of polymeric nanoparticles. Nanotoxicology. 2014 Mar 1;8(2):202-11.
- Coe FL, Evan A, Worcester E. Kidney stone disease. The Journal of clinical investigation. 2005 Oct 3;115(10):2598-608.
- Conti C, Casati M, Colombo C, Realini M, Brambilla L, Zerbi G. Phase transformation of calcium oxalate dihydrate–monohydrate: Effects of relative humidity and new spectroscopic data. Spectrochimica Acta Part A: Molecular and Biomolecular Spectroscopy. 2014 Jul 15;128:413-9.
- Contreras SM, Ganuza A, Corvi MM, Angel SO. Resveratrol induces H3 and H4K16 deacetylation and H2A. X phosphorylation in Toxoplasma gondii. BMC Research Notes. 2021 Dec;14:1-8.
- Cupisti A, Giannese D, D'Alessandro C, Benedetti A, Panichi V, Alfieri C, Castellano G, Messa P. Kidney stone prevention: is there a role for complementary and alternative medicine?. Nutrients. 2023 Feb 9;15(4):877.
- Curhan GC. Epidemiology of stone disease. Urologic Clinics of North America. 2007 Aug 1;34(3):287-93.
- Cuyàs E, Verdura S, Llorach-Parés L, Fernández-Arroyo S, Joven J, Martin-Castillo B, Bosch-Barrera J, Brunet J, Nonell-Canals A, Sanchez-Martinez M, Menendez JA. Metformin is a direct SIRT1-activating compound: computational modeling and experimental validation. Frontiers in endocrinology. 2018 Nov 6;9:657.
- Dahl NK, Goldfarb DS. Nutritional prevention and treatment of urinary tract stones. Nutritional Management of Renal Disease: Elsevier; 2022. p. 685–97
- Dai H, Case AW, Riera TV, Considine T, Lee JE, Hamuro Y, Zhao H, Jiang Y, Sweitzer SM, Pietrak B, Schwartz B. Crystallographic structure of a small molecule SIRT1 activator-enzyme complex. Nature communications. 2015 Jul 2;6(1):7645.
- Daina A, Michielin O, Zoete V. SwissTargetPrediction: updated data and new features for efficient prediction of protein targets of small molecules. Nucleic acids research. 2019 Jul 2;47(W1):W357-64.

- D'Angelo S, Scafuro M, Meccariello R. BPA and nutraceuticals, simultaneous effects on endocrine functions. Endocrine, Metabolic & Immune Disorders-Drug Targets (Formerly Current Drug Targets-Immune, Endocrine & Metabolic Disorders). 2019 Aug 1;19(5):594-604.
- Daosukho S. Effect of Khella (Ammi visnaga) plant extract on in vitro crystallization of calcium oxalate monohydrate. 2007.
- Daudon M, Jungers P. Clinical value of crystalluria and quantitative morphoconstitutional analysis of urinary calculi. Nephron Physiology. 2004 Oct 19;98(2):p31-6.
- Demir Y, Taslimi P, Koçyiğit ÜM, Akkuş M, Özaslan MS, Duran HE, Budak Y, Tüzün B, Gürdere MB, Ceylan M, Taysi S. Determination of the inhibition profiles of pyrazolyl–thiazole derivatives against aldose reductase and α-glycosidase and molecular docking studies. Archiv der pharmazie. 2020 Dec;353(12):2000118.
- Devi A, Chaitanya NS. Designing of peptide aptamer targeting the receptor-binding domain of spike protein of SARS-CoV-2: an in silico study. Molecular Diversity. 2021 Jan 2:1-3.
- Dinnimath BM, Jalalpure SS, Patil UK. Antiurolithiatic activity of natural constituents isolated from Aerva lanata. Journal of Ayurveda and integrative medicine. 2017 Oct 1;8(4):226-32.
- Dong R, Zhang X, Liu Y, Zhao T, Sun Z, Liu P, Xiang Q, Xiong J, Du X, Yang X, Gui D. Rutin alleviates EndMT by restoring autophagy through inhibiting HDAC1 via PI3K/AKT/mTOR pathway in diabetic kidney disease. Phytomedicine. 2023 Apr 1;112:154700.
- Dontha S. A review on antioxidant methods. Asian J. Pharm. Clin. Res. 2016 Oct;9(2):14-32.
- Eberhardt J, Santos-Martins D, Tillack AF, Forli S. AutoDock Vina 1.2. 0: New docking methods, expanded force field, and python bindings. Journal of chemical information and modeling. 2021 Jul 19;61(8):3891-8.
- Edvardsson VO, Goldfarb DS, Lieske JC, Beara-Lasic L, Anglani F, Milliner DS, Palsson R. Hereditary causes of kidney stones and chronic kidney disease. Pediatric nephrology. 2013 Oct;28:1923-42.
- Epstein EY, Silver JU, Almogi GI, Livni NE, Naveh-Many TA. Parathyroid hormone mRNA levels are increased by progestins and vary during rat estrous cycle. American Journal of Physiology-Endocrinology and Metabolism. 1996 Jan 1;270(1):E158-63.

- Evan AP. Physiopathology and etiology of stone formation in the kidney and the urinary tract. Pediatric nephrology. 2010 May;25:831-41.
- Fan J, Glass MA, Chandhoke PS. Impact of ammonium chloride administration on a rat ethylene glycol urolithiasis model. Scanning Microsc. 1999;13(2-3):299-306.
- Farmanesh S, Ramamoorthy S, Chung J, Asplin JR, Karande P, Rimer JD. Specificity of growth inhibitors and their cooperative effects in calcium oxalate monohydrate crystallization. Journal of the American Chemical Society. 2014 Jan 8;136(1):367-76.
- Ferraro PM, Bargagli M, Trinchieri A, Gambaro G. Risk of kidney stones: influence of dietary factors, dietary patterns, and vegetarian-vegan diets. Nutrients. 2020;12:779.
- Ferraro PM, Taylor EN, Eisner BH, Gambaro G, Rimm EB, Mukamal KJ, Curhan GC. History of kidney stones and the risk of coronary heart disease. Jama. 2013 Jul 24;310(4).
- Fong-ngern K, Vinaiphat A, Thongboonkerd V. Microvillar injury in renal tubular epithelial cells induced by calcium oxalate crystal and the protective role of epigallocatechin-3-gallate. The FASEB Journal. 2017 Jan;31(1):120-31.
- Fujisawa S, Atsumi T, Kadoma Y, Sakagami H. Antioxidant and prooxidant action of eugenol-related compounds and their cytotoxicity. Toxicology. 2002 Aug 1;177(1):39-54.
- Gaikwad AB, Gupta J, Tikoo K. Epigenetic changes and alteration of Fbn1 and Col3A1 gene expression under hyperglycaemic and hyperinsulinaemic conditions. Biochemical Journal. 2010 Dec 1;432(2):333-41.
- Galicka A, Krętowski R, Nazaruk J, Cechowska-Pasko M. Anethole prevents hydrogen peroxide-induced apoptosis and collagen metabolism alterations in human skin fibroblasts. Molecular and cellular biochemistry. 2014 Sep;394:217-24.
- Gamage KN, Jamnadass E, Sulaiman SK, Pietropaolo A, Aboumarzouk O, Somani BK. The role of fluid intake in the prevention of kidney stone disease: A systematic review over the last two decades. Turkish journal of urology. 2020 Jun 5;46(Suppl 1):S92.
- Gambaro G, Vezzoli G, Casari G, Rampoldi L, D'Angelo A, Borghi L. Genetics of hypercalciuria and calcium nephrolithiasis: from the rare monogenic to the common polygenic forms. American journal of kidney diseases. 2004 Dec 1;44(6):963-86.
- Gao B, Yasui T, Itoh Y, Li Z, Okada A, Tozawa K, Hayashi Y, Kohri K. Association of osteopontin gene haplotypes with nephrolithiasis. Kidney international. 2007 Sep 1;72(5):592-8.

- Gao B, Yasui T, Lu X, Zhou H, Liu J, Liu P, Okada A, Xiao C, Kohri K. Matrix Gla protein expression in NRK-52E cells exposed to oxalate and calcium oxalate monohydrate crystals. Urologia Internationalis. 2010 Aug 4;85(2):237-41.
- Gauhar V, Chew BH, Traxer O, Tailly T, Emiliani E, Inoue T, Tiong HC, Chai CA, Lakmichi MA, Tanidir Y, Bin Hamri S. Indications, preferences, global practice patterns and outcomes in retrograde intrarenal surgery (RIRS) for renal stones in adults: results from a multicenter database of 6669 patients of the global FLEXible ureteroscopy Outcomes Registry (FLEXOR). World journal of urology. 2023 Feb;41(2):567-74.
- Ge SX, Jung D, Yao R. ShinyGO: a graphical gene-set enrichment tool for animals and plants. Bioinformatics. 2020 Apr 15;36(8):2628-9.
- Genheden, S., & Ryde, U. (2015). The MM/PBSA and MM/GBSA methods to estimate ligand-binding affinities. Expert opinion on drug discovery, 10(5), 449-461.
- Geraghty RM, Davis NF, Tzelves L, Lombardo R, Yuan C, Thomas K, Petrik A, Neisius A, Türk C, Gambaro G, Skolarikos A. Best practice in interventional management of urolithiasis: an update from the European Association of Urology Guidelines Panel for Urolithiasis 2022. European urology focus. 2023 Jan 1;9(1):199-208.
- Giannakou, M. E., & Partridge, L. (2004). The interaction between FOXO and SIRT1: tipping the balance towards survival. Trends in cell biology, 14(8), 408-412.
- Gilani AH. Trends in ethnopharmacology. Journal of ethnopharmacology. 2005 Aug 22;100(1-2):43-9.
- Gillen DL, Coe FL, Worcester EM. Nephrolithiasis and increased blood pressure among females with high body mass index. American journal of kidney diseases. 2005 Aug 1;46(2):263-9.
- Goel R, Yadav R, Gupta NP, Aron M. Laparoscopic assisted percutaneous nephrolithotomy (PCNL) in ectopic kidneys: two different techniques. International urology and nephrology. 2006 Feb;38:75-8.
- Goldfarb DS, Fischer ME, Keich Y, Goldberg J. A twin study of genetic and dietary influences on nephrolithiasis: a report from the Vietnam Era Twin (VET) Registry. Kidney international. 2005 Mar 1;67(3):1053-61..
- Gong Y, Dou Y, Wang L, Wang X, Zhao Z. EP300 promotes renal tubular epithelial cell fibrosis by increasing HIF2α expression in diabetic nephropathy. Cellular Signalling. 2022 Oct 1;98:110407.

- Grases F, Rodriguez A, Costa-Bauza A. Efficacy of mixtures of magnesium, citrate and phytate as calcium oxalate crystallization inhibitors in urine. The Journal of Urology. 2015 Sep;194(3):812-9.
- Gruszka K, Rajzer M, Drożdż T, Wojciechowska W, Pizoń T, Migacz-Gruszka K, Czarnecka D. Selected matrix metalloproteinases activity and hypertension-mediated organ damage in relation to uric acid serum level. Cardiology Journal. 2021;28(6):905-13.
- Guimerà J, Martínez A, Tubau V, Sabate A, Bauza JL, Rios A, Lopez M, Piza P, Grases F, Pieras E. Prevalence of distal renal tubular acidosis in patients with calcium phosphate stones. World Journal of Urology. 2020 Mar;38:789-94.
- Guzel A, Yunusoglu S, Calapoglu M, Candan IA, Onaran I, Oncu M, Ergun O, Oksay T. Protective effects of quercetin on oxidative stress-induced tubular epithelial damage in the experimental rat hyperoxaluria model. Medicina. 2021 Jun 3;57(6):566.
- Habig, W.H., M.J. Pabst, and W.B. Jakoby, Glutathione S-transferases: the first enzymatic step in mercapturic acid formation. Journal of biological Chemistry, 1974. 249(22): p. 7130-7139.
- Haley WE, Enders FT, Vaughan LE, Mehta RA, Thoman ME, Vrtiska TJ, Krambeck AE, Lieske JC, Rule AD. Kidney function after the first kidney stone event. InMayo Clinic Proceedings 2016 Dec 1 (Vol. 91, No. 12, pp. 1744-1752). Elsevier.
- Han H, Segal AM, Seifter JL, Dwyer JT. Nutritional management of kidney stones (nephrolithiasis). Clinical nutrition research. 2015 Jul 1;4(3):137-52.
- Han X, Shen T, Lou H. Dietary polyphenols and their biological significance. International Journal of Molecular Sciences. 2007 Sep;8(9):950-88.
- Harakeh S, Al-Raddadi R, Alamri T, Al-Jaouni S, Qari M, Qari Y, Kumar A, Tashkandi HM, Moulay M, Aldahlawi AM, Slama P. Apoptosis induction in human hepatoma cell line HepG2 cells by trans-Anethole via activation of mitochondria-mediated apoptotic pathways. Biomedicine & Pharmacotherapy. 2023 Sep 1;165:115236.
- He M, Dong Y, Cai W, Cai J, Xie Y, Yu M, Li C, Wen L. Recent advances in the treatment of renal stones using flexible ureteroscopys. International Journal of Surgery. 2024 Jul 1;110(7):4320-8.
- Hess B. Acid–base metabolism: implications for kidney stosne formation. Urological research. 2006 Apr;34(2):134-8.
- Hill AJ, Basourakos SP, Lewicki P, Wu X, Arenas-Gallo C, Chuang D, Bodner D, Jaeger I, Nevo A, Zell M, Markt SC. Incidence of kidney stones in the United States: the

continuous national health and nutrition examination survey. The Journal of urology. 2022 Apr;207(4):851-6.

- Hou B, Lin C, Hao Z. Chronic hepatitis B virus infection increases the risk of upper urinary calculi. BMC urology. 2022 Jun 6;22(1):82.
- Hsin KY, Ghosh S, Kitano H. Combining machine learning systems and multiple docking simulation packages to improve docking prediction reliability for network pharmacology. PloS one. 2013 Dec 31;8(12):e83922.
- Huang J, Rauscher S, Nawrocki G, Ran T, Feig M, De Groot BL, Grubmüller H, MacKerell Jr AD. CHARMM36m: an improved force field for folded and intrinsically disordered proteins. Nature methods. 2017 Jan;14(1):71-3.
- Icer MA, Gezmen-Karadag M. The multiple functions and mechanisms of osteopontin. Clinical biochemistry. 2018 Sep 1;59:17-24.
- Ilevbare GA, Liu H, Edgar KJ, Taylor LS. Maintaining supersaturation in aqueous drug solutions: impact of different polymers on induction times. Crystal Growth & Design. 2013 Feb 6;13(2):740-51.
- Irwin JJ, Shoichet BK. ZINC− a free database of commercially available compounds for virtual screening. Journal of chemical information and modeling. 2005 Jan 24;45(1):177-82.
- Istrefi Q, Türkeş C, Arslan M, Demir Y, Nixha AR, Beydemir Ş, Küfrevioğlu Öİ. Sulfonamides incorporating ketene N, S-acetal bioisosteres as potent carbonic anhydrase and acetylcholinesterase inhibitors. Archiv der Pharmazie. 2020 Jun;353(6):1900383.
- Ivanovski O, Drüeke TB. A new era in the treatment of calcium oxalate stones?. Kidney international. 2013 Jun 1;83(6):998-1000.
- Izmailov AF, Myerson AS, Arnold S. A statistical understanding of nucleation. Journal of Crystal Growth. 1999 Jan 15;196(2-4):234-42.
- Jahanafrooz Z, Motamed N, Rinner B, Mokhtarzadeh A, Baradaran B. Silibinin to improve cancer therapeutic, as an apoptotic inducer, autophagy modulator, cell cycle inhibitor, and microRNAs regulator. Life sciences. 2018 Nov 15;213:236-47.
- Jain M, Manohar CS, Nagabhushan M, Keshavamurthy R. A comparative study of minimally invasive percutaneous nephrolithotomy and retrograde intrarenal surgery for solitary renal stone of 1–2 cm. Urology Annals. 2021 Jul 1;13(3):226-31.
- Jakubek P, Rajić J, Kuczyńska M, Suliborska K, Heldt M, Dziedziul K, Vidaković M, Namieśnik J, Bartoszek A. Beyond antioxidant activity: redox properties of catechins

may affect changes in the DNA methylation profile—the example of SRXN1 gene. Antioxidants. 2023 Mar 20;12(3):754.

- Jeong BC, Kim BS, Kim JI, Kim HH. Effects of green tea on urinary stone formation: an in vivo and in vitro study. Journal of endourology. 2006 May 1;20(5):356-61.
- Jo, S., Kim, T., Iyer, V. G., & Im, W. (2008). CHARMM-GUI: a web-based graphical user interface for CHARMM. Journal of computational chemistry, 29(11), 1859-1865.
- Johri N, Cooper B, Robertson W, Choong S, Rickards D, Unwin R. An update and practical guide to renal stone management. Nephron Clinical Practice. 2010 Jul 2;116(3):c159-71.
- Joshi S, Peck AB, Khan SR. NADPH oxidase as a therapeutic target for oxalate induced injury in kidneys. Oxidative medicine and cellular longevity. 2013;2013(1):462361.
- Joshi S, Saylor BT, Wang W, Peck AB, Khan SR. Apocynin-treatment reverses hyperoxaluria induced changes in NADPH oxidase system expression in rat kidneys: a transcriptional study. 2012
- Jungers P, Joly D, Barbey F, Choukroun G, Daudon M. ESRD caused by nephrolithiasis: prevalence, mechanisms, and prevention. American journal of kidney diseases. 2004 Nov 1;44(5):799-805.
- Kakkar M, Kakkar R. A 13 year hospital based study on the trend of urinary stone disease in Uttarakhand, India. Nepal Journal of Epidemiology. 2021 Mar 31;11(1):949.
- Kang J, Sun Y, Deng Y, Liu Q, Li D, Liu Y, Guan X, Tao Z, Wang X. Autophagy-endoplasmic reticulum stress inhibition mechanism of superoxide dismutase in the formation of calcium oxalate kidney stones. Biomedicine & Pharmacotherapy. 2020 Jan 1;121:109649.
- Kanlaya R, Kuljiratansiri R, Peerapen P, Thongboonkerd V. The inhibitory effects of epigallocatechin-3-gallate on calcium oxalate monohydrate crystal growth, aggregation and crystal-cell adhesion. Biomedicine & Pharmacotherapy. 2024 Jan 1;170:115988.
- Karadi RV, Gadge NB, Alagawadi KR, Savadi RV. Effect of Moringa oleifera Lam. root-wood on ethylene glycol induced urolithiasis in rats. Journal of ethnopharmacology. 2006 Apr 21;105(1-2):306-11.
- Karagözler AA, Erdağ B, Emek YÇ, Uygun DA. Antioxidant activity and proline content of leaf extracts from Dorystoechas hastata. Food Chemistry. 2008 Nov 15;111(2):400-7.

- Karaman B, Alhalabi Z, Swyter S, Mihigo SO, Andrae-Marobela K, Jung M, Sippl W, Ntie-Kang F. Identification of bichalcones as sirtuin inhibitors by virtual screening and in vitro testing. Molecules. 2018 Feb 14;23(2):416.
- Kasote DM, Jagtap SD, Thapa D, Khyade MS, Russell WR. Herbal remedies for urinary stones used in India and China: A review. Journal of ethnopharmacology. 2017 May 5;203:55-68
- Khamchun S, Yoodee S, Thongboonkerd V. Dual modulatory effects of diosmin on calcium oxalate kidney stone formation processes: Crystallization, growth, aggregation, crystal-cell adhesion, internalization into renal tubular cells, and invasion through extracellular matrix. Biomedicine & Pharmacotherapy. 2021 Sep 1;141:111903.
- Khan A, Bashir S, Khan SR. Antiurolithic effects of medicinal plants: results of in vivo studies in rat models of calcium oxalate nephrolithiasis—a systematic review. Urolithiasis. 2021 Apr;49(2):95-122.
- Khan MN, Farooq U, Khushal A, Wani TA, Zargar S, Khan S. Unraveling potential EGFR kinase inhibitors: Computational screening, molecular dynamics insights, and MMPBSA analysis for targeted cancer therapy development. PLoS One. 2025 May 9;20(5):e0321500.
- Khan SR, Canales BK. Genetic basis of renal cellular dysfunction and the formation of kidney stones. Urological Research. 2009 Aug;37:169-80.
- Khan SR, Pearle MS, Robertson WG, Gambaro G, Canales BK, Doizi S, Traxer O, Tiselius HG. Kidney stones. Nature reviews Disease primers. 2016 Feb 25;2(1):1-23.
- Khan SR. Reactive oxygen species as the molecular modulators of calcium oxalate kidney stone formation: evidence from clinical and experimental investigations. The Journal of urology. 2013 Mar;189(3):803-11.
- Khand FD, Gordge MP, Robertson WG, Noronha-Dutra AA, Hothersall JS. Mitochondrial superoxide production during oxalate-mediated oxidative stress in renal epithelial cells. Free Radical Biology and Medicine. 2002 Jun 15;32(12):1339-50.
- Khare P, Mishra VK, Arun K, Bais N, Singh R. Study on in vitro anti-lithiatic activity of Phyllanthus niruri linn. leaves by homogenous precipitation and turbiditory method. Int J Pharm Pharm Sci. 2014;6(4):124-7.
- Kittanamongkolchai W, Vaughan LE, Enders FT, Dhondup T, Mehta RA, Krambeck AE, McCollough CH, Vrtiska TJ, Lieske JC, Rule AD. The changing incidence and

presentation of urinary stones over 3 decades. InMayo Clinic Proceedings 2018 Mar 1 (Vol. 93, No. 3, pp. 291-299). Elsevier.

- Kizivat T, Smolić M, Marić I, Tolušić Levak M, Smolić R, Bilić Čurčić I, Kuna L, Mihaljević I, Včev A, Tucak-Zorić S. Antioxidant pre-treatment reduces the toxic effects of oxalate on renal epithelial cells in a cell culture model of urolithiasis. International journal of environmental research and public health. 2017 Jan;14(1):109.
- Kohjimoto Y, Sasaki Y, Iguchi M, Matsumura N, Inagaki T, Hara I. Association of metabolic syndrome traits and severity of kidney stones: results from a nationwide survey on urolithiasis in Japan. American Journal of Kidney Diseases. 2013 Jun 1;61(6):923-9.
- Kong W, Li H, Liu J, Han Y, Huang H, Liu Y, Kang Z. Size-dependent and real-time effect of SiO 2 nanoparticles on a single living HeLa Cell's membrane permeability. Journal of Materials Chemistry B. 2015;3(7):1198-203.
- Königsberger E, Königsberger LC. Thermodynamic modeling of crystal deposition in humans. Pure and Applied Chemistry. 2001 May 1;73(5):785-97.
- Kono, Y., Generation of superoxide radical during autoxidation of hydroxylamine and an assay for superoxide dismutase. Archives of biochemistry and biophysics, 1978. 186(1): p. 189-195.
- Kulkarni N, Kapse N, Pachori R, Sadar P. Studies on inhibition of calcium oxalate crystallisation by using plant extract and soil microflora. Eur J Pharm Med Res. 2017;4(8):329-34.
- Kumar A, Zhang KY. Advances in the development of shape similarity methods and their application in drug discovery. Frontiers in chemistry. 2018 Jul 25;6:315.
- Kume A, Kawai S, Kato R, Iwata S, Shimizu K, Honda H. Exploring high-affinity binding properties of octamer peptides by principal component analysis of tetramer peptides. Journal of bioscience and bioengineering. 2017 Feb 1;123(2):230-8.
- Kushwaha K, Garg SS, Mandal D, Khurana N, Gupta J. Screening of natural epigenetic modifiers for managing glycemic memory and diabetic nephropathy. Journal of Drug Targeting. 2024 Aug 8;32(7):807-19.
- Lai Y, Zheng H, Sun X, Lin J, Li Q, Huang H, Hou Y, Zhong H, Zhang D, Fucai T, He Z. The advances of calcium oxalate calculi associated drugs and targets. European Journal of Pharmacology. 2022 Nov 15;935:175324.

- Lambert EH, Miller NL, Herrell SD. Urologic instrumentation: endoscopes and lasers. InPractical Urology: Essential Principles and Practice: Essential Principles and Practice 2011 Feb 9 (pp. 283-291). London: Springer London.
- Lancia A, Musmarra D, Prisciandaro M. Measuring induction period for calcium sulfate dihydrate precipitation. AIChE Journal. 1999 Feb;45(2):390-7.
- Lee HJ, Jeong SJ, Lee HJ, Lee EO, Bae H, Lieske JC, Kim SH. 1, 2, 3, 4, 6-Penta-O-galloyl-beta-D-glucose reduces renal crystallization and oxidative stress in a hyperoxaluric rat model. Kidney international. 2011 Mar 1;79(5):538-45.
- Lee J, Cheng X, Jo S, MacKerell AD, Klauda JB, Im W. CHARMM-GUI input generator for NAMD, GROMACS, AMBER, OpenMM, and CHARMM/OpenMM simulations using the CHARMM36 additive force field. Biophysical journal. 2016 Feb 16;110(3):641a.
- Legay C, Haeusermann T, Pasquier J, Chatelan A, Fuster DG, Dhayat N, Seeger H, Ritter A, Mohebbi N, Ernandez T, Chopard CS. Differences in the food consumption between kidney stone formers and nonformers in the Swiss Kidney Stone Cohort. Journal of renal nutrition. 2023 Jul 1;33(4):555-65.
- Li DF, Gao YL, Liu HC, Huang XC, Zhu RF, Zhu CT. Use of thiazide diuretics for the prevention of recurrent kidney calculi: a systematic review and meta-analysis. Journal of Translational Medicine. 2020 Dec;18:1-2.
- Li X, Li N, Wen Y, Lyu ZY, Feng XS, Wei LP, Chen YH, Chen HD, Wang G, Chen SH, Ren JS. Metabolic syndrome components and renal cell cancer risk in Chinese males: a population-based prospective study. Zhonghua yu Fang yi xue za zhi [Chinese Journal of Preventive Medicine]. 2020 Jun 1;54(6):638-43.
- Li X, Wu G, Shang P, Bao J, Lu J, Yue Z. Anti-nephrolithic potential of catechin in melamine-related urolithiasis via the inhibition of ROS, apoptosis, phospho-p38, and osteopontin in male Sprague-Dawley rats. Free radical research. 2015 Oct 3;49(10):1249-58.
- Li Y, Li X, Hussain SA, Daddam JR, Chen Z. Therapeutic Effect of Epigallocatechin-3-Gallate and Quercetin on Renal Stone Formation in Rats. Pakistan Journal of Zoology. 2024 Jun 1;56(3):1015.
- Liu H, Cao M, Jin Y, Jia B, Wang L, Dong M, Han L, Abankwah J, Liu J, Zhou T, Chen B. Network pharmacology and experimental validation to elucidate the pharmacological mechanisms of Bushen Huashi decoction against kidney stones. Frontiers in Endocrinology. 2023 Feb 14;14:1031895.

- Liu M, Wu J, Gao M, Li Y, Xia W, Zhang Y, Chen J, Chen Z, Zhu Z, Chen H. Lifestyle factors, serum parameters, metabolic comorbidities, and the risk of kidney stones: a Mendelian randomization study. Frontiers in endocrinology. 2023 Sep 22;14:1240171.
- Liu T, Ma X, Ouyang T, Chen H, Lin J, Liu J, Xiao Y, Yu J, Huang Y. SIRT1 reverses senescence via enhancing autophagy and attenuates oxidative stress-induced apoptosis through promoting p53 degradation. International journal of biological macromolecules. 2018 Oct 1;117:225-34.
- Liu Y, Chen Y, Liao B, Luo D, Wang K, Li H, Zeng G. Epidemiology of urolithiasis in Asia. Asian journal of urology. 2018 Oct 1;5(4):205-14.
- Liu Y, Ye J, Cao Y, Zhang R, Wang Y, Zhang S, Dai W, Ye S. Silibinin ameliorates diabetic nephropathy via improving diabetic condition in the mice. European Journal of Pharmacology. 2019 Feb 15;845:24-31.
- Loganayaki N, Siddhuraju P, Manian S. Antioxidant activity and free radical scavenging capacity of phenolic extracts from Helicteres isora L. and Ceiba pentandra L. Journal of food science and technology. 2013 Aug;50:687-95.
- Lohiya A, Kant S, Kapil A, Gupta SK, Misra P, Rai SK. Population-based estimate of urinary stones from Ballabgarh, northern India. The National medical journal of India. 2017 Jul 1;30(4):198-200.
- López M, Hoppe B. History, epidemiology and regional diversities of urolithiasis. Pediatric nephrology. 2010 Jan;25(1):49-59.
- López-Vallejo F, Caulfield T, Martínez-Mayorga K, A Giulianotti M, Nefzi A, A Houghten R, L Medina-Franco J. Integrating virtual screening and combinatorial chemistry for accelerated drug discovery. Combinatorial Chemistry & High Throughput Screening. 2011 Jul 1;14(6):475-87.
- Lothuvachai T, Likittanasombat K, Milindankura S, Sakulsaengprapha A, Kitiyakara C. Chryseobacterium meningosepticum infection and cardiac tamponade in a long-term hemodialysis patient. American Journal of Kidney Diseases. 2006 Oct 1;48(4):e49-53.
- Lowry OH, Rosebrough NJ, Farr AL, Randall RJ. Protein measurement with the Folin phenol reagent.
- Lu X, Sun D, Xu B, Pan J, Wei Y, Mao X, Yu D, Liu H, Gao B. In silico screening and molecular dynamic study of nonsynonymous single nucleotide polymorphisms associated with kidney stones in the SLC26A6 gene. The Journal of urology. 2016 Jul 1;196(1):118-23.

- Luo P, Chen T, Zheng L, Zou J, Zou J, Li W, Chen Q, Cheng L, Qian B. Calcium sensing receptor regulate claudin-14 via PKA-STAT3 pathway in rat model of nephrolithiasis. Frontiers in Pharmacology. 2024 Dec 4;15:1477122.
- Luo W, Brouwer C. Pathview: an R/Bioconductor package for pathway-based data integration and visualization. Bioinformatics. 2013 Jul 15;29(14):1830-1.
- Maisuradze GG, Liwo A, Scheraga HA. Relation between free energy landscapes of proteins and dynamics. Journal of chemical theory and computation. 2010 Feb 9;6(2):583-95
- Malinaric R, Mantica G, Martini M, Balzarini F, Mariano F, Marchi G, Tognoni P, Panarello D, Bottino P, Terrone C. The lifetime history of the first Italian public extra-corporeal shock wave lithotripsy (ESWL) lithotripter as a Mirror of the evolution of Endourology over the last decade. International Journal of Environmental Research and Public Health. 2023 Feb 25;20(5):4127.
- Maline GE, Goldfarb DS. Climate change and kidney stones. Current opinion in nephrology and hypertension. 2024 Jan 1;33(1):89-96.
- Marangella M, Bagnis C, Bruno M, Vitale C, Petrarulo M, Ramello A. Crystallization inhibitors in the pathophysiology and treatment of nephrolithiasis. Urologia internationalis. 2004;72(Suppl. 1):6-10.
- Marhoume FZ, Aboufatima R, Zaid Y, Limami Y, Duval RE, Laadraoui J, Belbachir A, Chait A, Bagri A. Antioxidant and polyphenol-rich ethanolic extract of Rubia tinctorum L. prevents urolithiasis in an ethylene glycol experimental model in rats. Molecules. 2021 Feb 14;26(4):1005.
- Mark, P., & Nilsson, L. (2001). Structure and dynamics of the TIP3P, SPC, and SPC/E water models at 298 K. The Journal of Physical Chemistry A, 105(43), 9954-9960.
- Mayans L. Nephrolithiasis. Primary care. 2019 Jun 1;46(2):203-12.
- McClinton S, Starr K, Thomas R, MacLennan G, Lam T, Hernandez R, Pickard R, Anson K, Clark T, MacLennan S, Thomas D. The clinical and cost effectiveness of surgical interventions for stones in the lower pole of the kidney: the percutaneous nephrolithotomy, flexible ureterorenoscopy and extracorporeal shockwave lithotripsy for lower pole kidney stones randomised controlled trial (PUrE RCT) protocol. Trials. 2020 Dec;21:1-5.
- McCredie M, Stewart JH. Risk factors for kidney cancer in New South Wales, Australia. II. Urologic disease, hypertension, obesity, and hormonal factors. Cancer Causes & Control. 1992 Jul;3:323-31.

- Medoro A, Jafar TH, Ali S, Trung TT, Sorrenti V, Intrieri M, Scapagnini G, Davinelli S. In silico evaluation of geroprotective phytochemicals as potential sirtuin 1 interactors. Biomedicine & Pharmacotherapy. 2023 May 1;161:114425.
- Meng XY, Zhang HX, Mezei M, Cui M. Molecular docking: a powerful approach for structure-based drug discovery. Current computer-aided drug design. 2011 Jun 1;7(2):146-57.
- Miyake O, Yoshimura K, Yoshioka T, Koide T, Okuyama A. High urinary excretion level of citrate and magnesium in children: potential etiology for the reduced incidence of pediatric urolithiasis. Urological research. 1998 Jun;26:209-13.
- Moe OW. Kidney stones: pathophysiology and medical management. The lancet. 2006 Jan 28;367(9507):333-44.
- Moftakhar L, Jafari F, Ghoddusi Johari M, Rezaeianzadeh R, Hosseini SV, Rezaianzadeh A. Prevalence and risk factors of kidney stone disease in population aged 40–70 years old in Kharameh cohort study: a cross-sectional population-based study in southern Iran. BMC urology. 2022 Dec 19;22(1):205.
- Mohamed DA, Mabrok HB, Ramadan AA, Elbakry HF. The potential role of alkaline diets in prevention of calcium oxalate kidney stone formation. Food & Function. 2024;15(24):12033-46.
- Mohan PK, Krishna TA, Thirumurugan A, Kumar TS, Kumari BR. Chemical profiling and in vitro antiurolithiatic activity of Pleurolobus gangeticus (L.) J. St.-Hil. ex H. Ohashi & K. Ohashi along with its antioxidant and antibacterial properties. Applied Biochemistry and Biotechnology. 2022 Nov;194(11):5037-59.
- Montealegre CM, De Leon RL. Effect of Blumea balsamifera extract on the phase and morphology of calcium oxalate crystals. Asian Journal of Urology. 2017 Oct 1;4(4):201-7.
- Moore DS. Behavioral epigenetics. Wiley Interdisciplinary Reviews: Systems Biology and Medicine. 2017 Jan;9(1):e1333.
- Morgan MS, Pearle MS. Medical management of renal stones. Bmj. 2016 Mar 14;352:i52.
- Morris GM, Goodsell DS, Halliday RS, Huey R, Hart WE, Belew RK, Olson AJ. Automated docking using a Lamarckian genetic algorithm and an empirical binding free energy function. Journal of computational chemistry. 1998 Nov 15;19(14):1639-62.

- Motskin M, Wright DM, Muller K, Kyle N, Gard TG, Porter AE, Skepper JN. Hydroxyapatite nano and microparticles: correlation of particle properties with cytotoxicity and biostability. Biomaterials. 2009 Jul 1;30(19):3307-17.
- Mukherjee PK, Maity N, Nema NK, Sarkar BK (2011) Bioactive compounds from natural resources against skin aging. Phytomedicine 19:64–73
- Muñoz E, Nováček V, Vandenbussche PY. Using drug similarities for discovery of possible adverse reactions. InAMIA Annual Symposium Proceedings 2017 Feb 10 (Vol. 2016, p. 924).
- Myerson A. Handbook of industrial crystallization. Butterworth-Heinemann; 2002 Jan 8.
- Nagula S, Subhashini NJ, Bhikshapathi DV, Mamatha P. Anti-urolithiatic and nephroprotective activity of quercetin and betulin in conjunction with a bio enhancer–an in vivo study. Biomedical and Pharmacology Journal. 2023 Jun 30;16(2):847-62.
- NEPHROLITHIASIS O. Managing acute and chronic renal stone disease. Practitioner. 2016;260(1790):17-20.
- Nicoglou A, Merlin F. Epigenetics: A way to bridge the gap between biological fields. Studies in History and Philosophy of Science Part C: Studies in History and Philosophy of Biological and Biomedical Sciences. 2017 Dec 1;66:73-82.
- Nirumand MC, Hajialyani M, Rahimi R, Farzaei MH, Zingue S, Nabavi SM, Bishayee A. Dietary plants for the prevention and management of kidney stones: preclinical and clinical evidence and molecular mechanisms. International journal of molecular sciences. 2018 Mar 7;19(3):765.
- Nischitha R, Shivanna MB. Diversity and in silico docking of antibacterial potent compounds in endophytic fungus Chaetomium subaffine Sergeeva and host Heteropogon contortus (L.) P. Beauv. Process Biochemistry. 2022 Jan 1;112:124-38.
- Nizami AN, Rahman MA, Ahmed NU, Islam MS. Whole Leea macrophylla ethanolic extract normalizes kidney deposits and recovers renal impairments in an ethylene glycol–induced urolithiasis model of rats. Asian Pacific Journal of Tropical Medicine. 2012 Jul 1;5(7):533-8.
- Noor F, Rehman A, Ashfaq UA, Saleem MH, Okla MK, Al-Hashimi A, AbdElgawad H, Aslam S. Integrating network pharmacology and molecular docking approaches to decipher the multi-target pharmacological mechanism of Abrus precatorius L. acting on diabetes. Pharmaceuticals. 2022 Mar 29;15(4):414.

- Noorafshan A, Karbalay-Doust S, Karimi F. Diosmin reduces calcium oxalate deposition and tissue degeneration in nephrolithiasis in rats: a stereological study. Korean journal of urology. 2013 Apr 1;54(4):252-7.
- O'Boyle NM, Banck M, James CA, Morley C, Vandermeersch T, Hutchison GR. Open Babel: An open chemical toolbox. Journal of cheminformatics. 2011 Dec;3:1-4.
- Odya CE, Marinkovic DV, Hammon KJ, Stewart TA, Erdös EG. Purification and properties of prolylcarboxypeptidase (angiotensinase C) from human kidney. Journal of Biological Chemistry. 1978 Sep 10;253(17):5927-31.
- Oksay T, Yunusoğlu S, Calapoğlu M, Aydın Candan I, Onaran I, Ergün O, Özorak A. Protective impact of resveratrol in experimental rat model of hyperoxaluria. International urology and nephrology. 2017 May;49:769-75.
- Oliveros JC, Venny C. An interactive tool for comparing lists with Venn's diagrams. BioinfoGP, CNB-CSIC. 2007 Mar 13.
- Opo FA, Rahman MM, Ahammad F, Ahmed I, Bhuiyan MA, Asiri AM. Structure based pharmacophore modeling, virtual screening, molecular docking and ADMET approaches for identification of natural anti-cancer agents targeting XIAP protein. Scientific reports. 2021 Feb 18;11(1):4049.
- Ouahhoud S, Khoulati A, Kadda S, Bencheikh N, Mamri S, Ziani A, Baddaoui S, Eddabbeh FE, Lahmass I, Benabbes R, Addi M. Antioxidant activity, metal chelating ability and dna protective effect of the hydroethanolic extracts of crocus sativus stigmas, tepals and leaves. Antioxidants. 2022 May 9;11(5):932.
- Oucherif KA, Raina S, Taylor LS, Litster JD. Quantitative analysis of the inhibitory effect of HPMC on felodipine crystallization kinetics using population balance modeling. CrystEngComm. 2013;15(12):2197-205.
- Oxtoby DW. Homogeneous nucleation: theory and experiment. Journal of Physics: Condensed Matter. 1992 Sep 21;4(38):7627.
- Parmar MS. Kidney stones. Bmj. 2004 Jun 10;328(7453):1420-4.
- Parrinello M, Rahman A. Crystal structure and pair potentials: A molecular-dynamics study. Physical review letters. 1980 Oct 6;45(14):1196.
- Peerapen P, Putpeerawit P, Boonmark W, Thongboonkerd V. Resveratrol inhibits calcium oxalate crystal growth, reduces adhesion to renal cells and induces crystal internalization into the cells, but promotes crystal aggregation. Current Research in Food Science. 2024 Jan 1;8:100740.
- Peerapen P, Thongboonkerd V. Kidney stone prevention. Adv Nutr. 2023;14:555–69.

- Peerapen P, Thongboonkerd V. Role of trigonelline, a bioactive alkaloid in coffee, for kidney stone prevention. InCoffee in Health and Disease Prevention 2025 Jan 1 (pp. 641-649). Academic Press.
- Penniston KL, Nakada SY. Updates in the metabolic management of calcium stones. Current urology reports. 2018 Jun;19:1-1.
- Petit I, Belletti GD, Debroise T, Llansola-Portoles MJ, Lucas IT, Leroy C, Bonhomme C, Bonhomme-Coury L, Bazin D, Daudon M, Letavernier E. Vibrational signatures of calcium oxalate polyhydrates. ChemistrySelect. 2018 Aug 23;3(31):8801-12.
- Petrović A, Kizivat T, Bilić Ćurčić I, Smolić R, Smolić M. In vitro cell culture models of hyperoxaluric states: Calcium oxalate and renal epithelial cell interactions. Crystals. 2021 Jun 25;11(7):735.
- Pettersen, E. F., Goddard, T. D., Huang, C. C., Couch, G. S., Greenblatt, D. M., Meng, E. C., & Ferrin, T. E. (2004). UCSF Chimera—a visualization system for exploratory research and analysis. Journal of computational chemistry, 25(13), 1605-1612.
- Polat S, Eral HB. Elucidating the role of hyaluronic acid in the structure and morphology of calcium oxalate crystals. Advanced Powder Technology. 2021 Oct 1;32(10):3650-9.
- Poloni LN, Ford AP, Ward MD. Site discrimination and anisotropic growth inhibition by molecular imposters on highly dissymmetric crystal surfaces. Crystal Growth & Design. 2016 Sep 7;16(9):5525-41.
- Prada-Gracia D, Gómez-Gardeñes J, Echenique P, Falo F. Exploring the free energy landscape: from dynamics to networks and back. PLoS computational biology. 2009 Jun 26;5(6):e1000415.
- Queiroz MF, Melo KR, Sabry DA, Sassaki GL, Rocha HA, Costa LS. Gallic acid-chitosan conjugate inhibits the formation of calcium oxalate crystals. Molecules. 2019 May 31;24(11):2074.
- Raja A, Wood F, Joshi HB. The impact of urinary stone disease and their treatment on patients' quality of life: a qualitative study. Urolithiasis. 2020 Jun;48(3):227-34.
- Rampogu S, Baek A, Gajula RG, Zeb A, Bavi RS, Kumar R, Kim Y, Kwon YJ, Lee KW. Ginger (Zingiber officinale) phytochemicals—gingerenone-A and shogaol inhibit SaHPPK: molecular docking, molecular dynamics simulations and in vitro approaches. Annals of clinical microbiology and antimicrobials. 2018 Dec;17:1-5.
- Rathi S, Chavan RB, Shastri NR. Classification of the crystallization tendency of active pharmaceutical ingredients (APIs) and nutraceuticals based on their nucleation and

crystal growth behaviour in solution state. Drug Delivery and Translational Research. 2020 Feb;1

- Ren, Y., Du, C., Shi, Y., Wei, J., Wu, H., & Cui, H. (2017). The Sirt1 activator, SRT1720, attenuates renal fibrosis by inhibiting CTGF and oxidative stress. International journal of molecular medicine, 39(5), 1317-1324.
- Ritter AMV, Domiciano TP, Verri WA Jr, Zarpelon AC, da Silva LG, Barbosa CP, Natali MR, Cuman RK, Bersani-Amado CA (2013) Antihypernociceptive activity of Anethole in experimental inflammatory pain. Inflammopharmacology 21:187–197
- Rodgers AL, Jackson GE. Determination of thermodynamic parameters for complexation of calcium and magnesium with chondroitin sulfate isomers using isothermal titration calorimetry: Implications for calcium kidney-stone research. Journal of Crystal Growth. 2017 Apr 1;463:14-8.
- Romero V, Akpinar H, Assimos DG. Kidney stones: a global picture of prevalence, incidence, and associated risk factors. Reviews in urology. 2010;12(2-3):e86.
- Rule AD, Bergstralh EJ, Melton III LJ, Li X, Weaver AL, Lieske JC. Kidney stones and the risk for chronic kidney disease. Clinical Journal of the American Society of Nephrology. 2009 Apr 1;4(4):804-11.
- Rule AD, Roger VL, Melton III LJ, Bergstralh EJ, Li X, Peyser PA, Krambeck AE, Lieske JC. Kidney stones associate with increased risk for myocardial infarction. Journal of the American Society of Nephrology. 2010 Oct 1;21(10):1641-4.
- Ryall RL. Urinary inhibitors of calcium oxalate crystallization and their potential role in stone formation. World journal of urology. 1997 Jun;15:155-64.
- Sá NA, Vieira LA, Ferreira AC, Cadenas J, Bruno JB, Maside C, Sousa FG, Cibin FW, Alves BG, Rodrigues AP, Leal-Cardoso JH. Anethole supplementation during oocyte maturation improves in vitro production of bovine embryos. Reproductive Sciences. 2020 Aug;27:1602-8.
- Saha S, Mishra A. Rutin-loaded polymeric nanorods alleviate nephrolithiasis by inhibiting inflammation and oxidative stress in vivo and in vitro. Food & Function. 2022;13(6):3632-48.
- Sakamoto T, Tanimoto K, Eguchi H, Sasaki S, Tsuboi K, Hayashi SI, Ichihara S. Resveratrol exhibits diverse anti-cancer activities through epigenetic regulation of E-cadherin and p21 in triple-negative breast cancer cells. Breast Cancer. 2023 Sep;30(5):727-38.

- Sakhaee K, Maalouf NM, Sinnott B. Kidney stones 2012: pathogenesis, diagnosis, and management. The Journal of Clinical Endocrinology & Metabolism. 2012 Jun 1;97(6):1847-60.
- Sani A, Beheshti R, Khalichi R, Taraghikhah M, Nourollahi E, Shafigh A, Pashazadeh F, Ghojazadeh M, Mostafaei H, Salehi-Pourmehr H, Hajebrahimi S. Urolithiasis management: An umbrella review on the efficacy and safety of extracorporeal shock wave lithotripsy (ESWL) versus the ureteroscopic approach. Urologia Journal. 2025 Jan 22:03915603241313162.
- Sayer JA. Progress in understanding the genetics of calcium-containing nephrolithiasis. Journal of the American Society of Nephrology. 2017 Mar 1;28(3):748-59.
- Scales Jr CD, Smith AC, Hanley JM, Saigal CS, Urologic Diseases in America Project. Prevalence of kidney stones in the United States. European urology. 2012 Jul 1;62(1):160-5.
- Scheid CR, Cao LC, Honeyman T, Jonassen JA. How elevated oxalate can promote kidney stone disease: changes at the surface and in the cytosol of renal cells that promote crystal adherence and growth. Front Biosci. 2004 Jan 1;9(797):e808.
- Schwarz RD, Dwyer NT. Pediatric kidney stones: long-term outcomes. Urology. 2006 Apr 1;67(4):812-6.
- Seifert-Klauss V, Prior JC. Progesterone and bone: actions promoting bone health in women. Journal of osteoporosis. 2010;2010(1):845180.
- Seke F, Manhivi VE, Shoko T, Slabbert RM, Sultanbawa Y, Sivakumar D. Effect of freeze drying and simulated gastrointestinal digestion on phenolic metabolites and antioxidant property of the Natal plum (Carissa macrocarpa). Foods. 2021 Jun 18;10(6):1420.
- Sequira L, Hebbar S, Ravishanker N. Prevalence and associated risk factors of urinary stone in India, a systematic review. Biomedicine 2023;43:572-6
- Shadman A, Bastani B. Kidney calculi: Pathophysiology and as a systemic disorder. Iranian journal of kidney diseases. 2017 May 1;11(3):180.
- Shafi S, Khurana N, Gupta J. PPAR gamma agonistic activity of dillapiole: protective effects against diabetic nephropathy. Natural Product Research. 2024 Mar 22:1-6.
- Shannon P, Markiel A, Ozier O, Baliga NS, Wang JT, Ramage D, Amin N, Schwikowski B, Ideker T. Cytoscape: a software environment for integrated models of biomolecular interaction networks. Genome research. 2003 Nov 1;13(11):2498-504.

- Sharma A, Vora J, Patel D, Sinha S, Jha PC, Shrivastava N. Identification of natural inhibitors against prime targets of SARS-CoV-2 using molecular docking, molecular dynamics simulation and MM-PBSA approaches. Journal of Biomolecular Structure and Dynamics. 2022 May 3;40(7):3296-311.
- Sheikh BA, Pari L, Rathinam A, Chandramohan R. 2015. Trans-anethole, a terpenoid ameliorates hyperglycemia by regulating key enzymes of carbohydrate metabolism in streptozotocin induced diabetic rats. Biochimie. 112:57–65.
- Shen Y, Zhao H, Wang Z, Guan W, Kang X, Tai X, Sun Y. Silibinin declines blue light-induced apoptosis and inflammation through MEK/ERK/CREB of retinal ganglion cells. Artificial cells, nanomedicine, and biotechnology. 2019 Dec 4;47(1):4059-65.
- Shoag J, Tasian GE, Goldfarb DS, Eisner BH. The new epidemiology of nephrolithiasis. Advances in chronic kidney disease. 2015 Jul 1;22(4):273-8.
- Siener R. Nutrition and kidney stone disease. Nutrients. 2021;13(6):1917.
- Sigurjonsdottir VK, Runolfsdottir HL, Indridason OS, Palsson R, Edvardsson VO. Impact of nephrolithiasis on kidney function. BMC nephrology. 2015 Dec;16:1-7.
- Simon LL, Nagy ZK, Hungerbuhler K. Comparison of external bulk video imaging with focused beam reflectance measurement and ultra-violet visible spectroscopy for metastable zone identification in food and pharmaceutical crystallization processes. Chemical Engineering Science. 2009 Jul 15;64(14):3344-51.
- Singh A, Vellapandian C, Krishna G. Preventive and therapeutic effects of Aerva lanata (L.) extract on ethylene glycol-induced nephrolithiasis in male Wistar albino rats. Digital Chinese Medicine. 2022 Jun 1;5(2):199-209.
- Singh M, Kadhim MM, Turki Jalil A, Oudah SK, Aminov Z, Alsaikhan F, Jawhar ZH, Ramírez-Coronel AA, Farhood B. A systematic review of the protective effects of silymarin/silibinin against doxorubicin-induced cardiotoxicity. Cancer Cell International. 2023 May 10;23(1):88.
- Singh S, Gupta S, Mishra T, Banerjee BD, Sharma T, Mishra TS. Risk factors of incident kidney stones in Indian adults: a hospital-based cross-sectional study. Cureus. 2023 Feb 27;15(2).
- Sinha, S., Patel, S., Athar, M., Vora, J., Chhabria, M. T., Jha, P. C., & Shrivastava, N. (2019). Structure based identification of novel sirtuin inhibitors against triple negative breast cancer: An in silico and in vitro study. International journal of biological macromolecules, 140, 454-468.

- Sitrit Y, Loison S, Ninio R, Dishon E, Bar E, Lewinsohn E, Mizrahi Y. Characterization of monkey orange (Strychnos spinosa Lam.), a potential new crop for arid regions. Journal of agricultural and food chemistry. 2003 Oct 8;51(21):6256-60.
- Soligo M, Morlacco A, Zattoni F, Valotto C, Beltrami P. Metabolic syndrome and stone disease. Panminerva Medica. 2021 Oct 5;64(3):344-58.
- Song Q, Liao W, He Z, Li D, Dong C, Song C, Yang S. Oxalate induces the ossification of RTECs by activating the JAK2/STAT3 signaling pathway and participates in the formation of kidney stones. Archives of biochemistry and biophysics. 2022 Sep 30;727:109325.
- Song Q, Song C, Chen X, Xiong Y, Li L, Liao W, Xue L, Yang S. FKBP5 deficiency attenuates calcium oxalate kidney stone formation by suppressing cell–crystal adhesion, apoptosis and macrophage M1 polarization via inhibition of NF-κB signaling. Cellular and Molecular Life Sciences. 2023 Oct;80(10):301.
- Sorokin I, Mamoulakis C, Miyazawa K, Rodgers A, Talati J, Lotan Y. Epidemiology of stone disease across the world. World journal of urology. 2017 Sep;35:1301-20.
- Souid I, Korchef A, Souid S. In silico evaluation of Vitis amurensis Rupr. polyphenol compounds for their inhibition potency against CoVID-19 main enzymes Mpro and RdRp. Saudi Pharmaceutical Journal. 2022 May 1;30(5):570-84.
- Sowers MR, Jannausch M, Wood C, Pope SK, Lachance LL, Peterson B. Prevalence of renal stones in a population-based study with dietary calcium, oxalate, and medication exposures. American journal of epidemiology. 1998 May 15;147(10):914-20.
- Spivacow FR, Del Valle EE, Lores E, Rey PG. Kidney stones: Composition, frequency and relation to metabolic diagnosis. Medicina (Buenos Aires). 2016 Dec;76(6):343-8.
- Stamatelou K, Goldfarb DS. Epidemiology of kidney stones. InHealthcare 2023 Feb 2 (Vol. 11, No. 3, p. 424). MDPI.
- Stanković A, Matijaković Mlinarić N, Kontrec J, Njegić Džakula B, Lyons DM, Marković B, Kralj D. Influence of Amino Acids on Calcium Oxalate Precipitation in Systems of Different Chemical Complexity. Crystals. 2024 Jun 28;14(7):599.
- Stelzer G, Rosen N, Plaschkes I, Zimmerman S, Twik M, Fishilevich S, Stein TI, Nudel R, Lieder I, Mazor Y, Kaplan S. The GeneCards suite: from gene data mining to disease genome sequence analyses. Current protocols in bioinformatics. 2016 Jun;54(1):1-30.
- Stroup SP, Auge BK. Urinary infection and struvite stones. InUrinary tract stone disease 2010 Dec 2 (pp. 217-224). London: Springer London.

- Sun XY, Ouyang JM, Li YB, Wen XL. Mechanism of cytotoxicity of micron/nano calcium oxalate monohydrate and dihydrate crystals on renal epithelial cells. Rsc Advances. 2015;5(56):45393-406.
- Sun XY, Ouyang JM, Xu M. Synthesis, characterization, and cytotoxicity assay of calcium oxalate dihydrate crystals in various shapes. CrystEngComm. 2016;18(29):5463-73.
- Sun XY, Zhang CY, Bhadja P, Ouyang JM. Preparation, properties, formation mechanisms, and cytotoxicity of calcium oxalate monohydrate with various morphologies. CrystEngComm. 2018;20(1):75-87.
- Sun Y, Liu Y, Guan X, Kang J, Wang X, Liu Q, Li D, Xu H, Tao Z, Deng Y. Atorvastatin inhibits renal inflammatory response induced by calcium oxalate crystals via inhibiting the activation of TLR4/NF-κB and NLRP3 inflammasome. IUBMB life. 2020 May;72(5):1065-74.
- Taguchi K, Okada A, Hamamoto S, Iwatsuki S, Naiki T, Ando R, Mizuno K, Tozawa K, Kohri K, Yasui T. Proinflammatory and metabolic changes facilitate renal crystal deposition in an obese mouse model of metabolic syndrome. The Journal of urology. 2015 Dec;194(6):1787-96.
- Tamborino F, Cicchetti R, Mascitti M, Litterio G, Orsini A, Ferretti S, Basconi M, De Palma A, Ferro M, Marchioni M, Schips L. Pathophysiology and main molecular mechanisms of urinary stone formation and recurrence. International journal of molecular sciences. 2024 Mar 6;25(5):3075.
- Tattevin P, Revest M, Chapplain JM, Ratajczak-Enselme M, Arvieux C, Michelet C. Increased risk of renal stones in patients treated with atazanavir. Clinical infectious diseases. 2013 Apr 15;56(8):1186-.
- Taylor EN, Curhan GC. Dietary calcium from dairy and nondairy sources, and risk of symptomatic kidney stones. The Journal of urology. 2013 Oct 1;190(4):1255-9.
- Taylor EN, Feskanich D, Paik JM, Curhan GC. Nephrolithiasis and risk of incident bone fracture. The Journal of urology. 2016 May 1;195(5):1482-6.
- Taylor EN, Stampfer MJ, Curhan GC. Obesity, weight gain, and the risk of kidney stones. Jama. 2005 Jan 26;293(4):455-62.
- Thabet NM, Moustafa EM. Protective effect of rutin against brain injury induced by acrylamide or gamma radiation: role of PI3K/AKT/GSK-3β/NRF-2 signalling pathway. Archives of physiology and biochemistry. 2018 Mar 15;124(2):185-93.

- Thayumanavan G, Jeyabalan S, Fuloria S, Sekar M, Ravi M, Selvaraj LK, Bala L, Chidambaram K, Gan SH, Rani NN, Begum MY. Silibinin and Naringenin against Bisphenol A-Induced neurotoxicity in zebrafish model—Potential flavonoid molecules for new drug design, development, and therapy for neurological disorders. Molecules. 2022 Apr 15;27(8):2572.
- Thongboonkerd V. Proteomics of crystal–cell interactions: a model for kidney stone research. Cells. 2019 Sep 12;8(9):1076.
- Topal F. Anticholinergic and antidiabetic effects of isoeugenol from clove (Eugenia caryophylata) oil. International Journal of Food Properties. 2019 Jan 1;22(1):583-92.
- Trott O, Olson AJ. AutoDock Vina: improving the speed and accuracy of docking with a new scoring function, efficient optimization, and multithreading. Journal of computational chemistry. 2010 Jan 30;31(2):455-61.
- Tsujihata M. Mechanism of calcium oxalate renal stone formation and renal tubular cell injury. International Journal of Urology. 2008 Feb;15(2):115-20.
- Tuli HS, Mittal S, Aggarwal D, Parashar G, Parashar NC, Upadhyay SK, Barwal TS, Jain A, Kaur G, Savla R, Sak K. Path of Silibinin from diet to medicine: A dietary polyphenolic flavonoid having potential anti-cancer therapeutic significance. InSeminars in Cancer Biology 2021 Aug 1 (Vol. 73, pp. 196-218). Academic Press.
- Türk C, Knoll T, Petrik A, Sarica K, Straub M, Seitz C. Guidelines on urolithiasis. European association of urology. 2011 Mar 30.
- Türkeş C, Demir Y, Beydemir Ş. Calcium channel blockers: molecular docking and inhibition studies on carbonic anhydrase I and II isoenzymes. Journal of Biomolecular Structure and Dynamics. 2021 Mar 8;39(5):1672-80.
- Uk S, Tk D. Mutational landscape of K-Ras substitutions at 12th position-a systematic molecular dynamics approach. Journal of Biomolecular Structure & Dynamics. 2020 Oct 9;40(4):1571-85.
- Ushimoto C, Sugiki S, Kunii K, Inoue S, Kuroda E, Akai R, Iwawaki T, Miyazawa K. Dynamic change and preventive role of stress response via Keap1-Nrf2 during renal crystal formation. Free Radical Biology and Medicine. 2023 Oct 1;207:120-32.
- Valko M, Leibfritz D, Moncol J, Cronin MT, Mazur M, Telser J. Free radicals and antioxidants in normal physiological functions and human disease. The international journal of biochemistry & cell biology. 2007 Jan 1;39(1):44-84.

- van de Pol JA, van den Brandt PA, Schouten LJ. Kidney stones and the risk of renal cell carcinoma and upper tract urothelial carcinoma: the Netherlands Cohort Study. British journal of cancer. 2019 Feb 5;120(3):368-74.
- Vanitha S, Vyshnavi PS. Determination of chemical composition in cooked and raw banana stem (Musa accuminata) and its efficacy on kidney stones-in vitro study. Journal of Scientific Research. 2020;64(03):66-74.
- Vijayakumar M, Ganpule A, Singh A, Sabnis R, Desai M. Review of techniques for ultrasonic determination of kidney stone size. Research and reports in urology. 2018 Aug 10:57-61.
- Vincenzi B, Santini D, Tonini G. Biological interaction between anti-epidermal growth factor receptor agent cetuximab and magnesium. Expert Opinion on Pharmacotherapy. 2008 Jun 1;9(8):1267-9.
- Vyas, V. K., Goel, A., Ghate, M., & Patel, P. (2015). Ligand and structure-based approaches for the identification of SIRT1 activators. Chemico-Biological Interactions, 228, 9-17.
- Wallace, A. C., Laskowski, R. A., & Thornton, J. M. (1995). LIGPLOT: a program to generate schematic diagrams of protein-ligand interactions. Protein engineering, design and selection, 8(2), 127-134.
- Wang H, Liu Z, Liu S, Yang R, Wang Y, Gu Y, Wu M, Dong R, Chen B. The Therapeutic Effect of Catechin on Nephrolithiasis Induced by Co-Exposure to Melamine and Cyanuric Acid in Sprague–Dawley Rats. Toxics. 2023 Sep 21;11(9):799.
- Wang R, Younis EM, Veeraraghavan VP, Tian C. Antiurolithiatic effect of Fucoxanthin on ethylene glycol-induced renal calculus in experimental rats. Journal of King Saud University-Science. 2020 Apr 1;32(3):1896-901.
- Wang Z, Bai Y, Wang J, Wang J. The preventive and therapeutic effects of α-lipoic acid on ethylene glycol-induced calcium oxalate deposition in rats. International urology and Nephrology. 2020 Jul;52:1227-34.
- Wei P, Li X, Wang S, Dong Y, Yin H, Gu Z, Na X, Wei X, Yuan J, Cao J, Gao H. Silibinin ameliorates formaldehyde-induced cognitive impairment by inhibiting oxidative stress. Oxidative Medicine and Cellular Longevity. 2022;2022(1):5981353.
- Wen J, Cao Y, Li Y, Zhu F, Yuan M, Xu J, Li J. Metabolomics analysis of the serum from children with urolithiasis using UPLC-MS. Clinical and Translational Science. 2021 Jul;14(4):1327-37.

- Werner H, Bapat S, Schobesberger M, Segets D, Schwaminger SP. Calcium oxalate crystallization: Influence of pH, energy input, and supersaturation ratio on the synthesis of artificial kidney stones. ACS omega. 2021 Oct 1;6(40):26566-74.
- Wieczyńska J, Cavoski I. Antimicrobial, antioxidant and sensory features of eugenol, carvacrol and trans-anethole in active packaging for organic ready-to-eat iceberg lettuce. Food chemistry. 2018 Sep 1;259:251-60.
- Wiederkehr MR, Moe OW. Uric acid nephrolithiasis: a systemic metabolic disorder. Clinical reviews in bone and mineral metabolism. 2011 Dec;9:207-17.
- Wishart DS, Feunang YD, Guo AC, Lo EJ, Marcu A, Grant JR, Sajed T, Johnson D, Li C, Sayeeda Z, Assempour N. DrugBank 5.0: a major update to the DrugBank database for 2018. Nucleic acids research. 2018 Jan 4;46(D1):D1074-82.
- Wong Y, Cook P, Roderick P, Somani BK. Metabolic syndrome and kidney stone disease: a systematic review of literature. Journal of endourology. 2016 Mar 1;30(3):246-53.
- Wu F, Hua Y, Kaochar S, Nie S, Lin YL, Yao Y, Wu J, Wu X, Fu X, Schiff R, Davis CM. Discovery, structure–activity relationship, and biological activity of histone-competitive inhibitors of histone acetyltransferases P300/CBP. Journal of medicinal chemistry. 2020 Apr 21;63(9):4716-31.
- Wu X, Shi X, Chen X, Yin Z. Epigallocatechin gallate (EGCG) can epigenetically regulate the receptor of advanced glycation end products (RAGE) to ameliorate Osteoarthritis. Journal of Functional Foods. 2023 Aug 1;107:105682.
- Wu Y, Xun Y, Zhang J, Hu H, Qin B, Wang T, Wang S, Li C, Lu Y. Resveratrol attenuates oxalate-induced renal oxidative injury and calcium oxalate crystal deposition by regulating TFEB-induced autophagy pathway. Frontiers in Cell and Developmental Biology. 2021 Feb 25;9:638759.
- Xie H, Zhang S, Liu J, Hu J, Tang A. A novel calcium oxalate/sepiolite composite for highly selective adsorption of Pb (II) from aqueous solutions. Minerals. 2021 May 23;11(6):552.
- Yadav A, Das R, Mehta DK, Yatin. Benefaction of Herbals in the Management of Urolithiasis. Current Traditional Medicine. 2021 Aug 1;7(4):541-51.
- Yadav A, Mohite S. Anticancer activity and In-Silico ADMET analysis of malvastrum coromandelianum. International Journal of Pharma Sciences and Research. 2020;11(5):71-3.

- Yasir F, Wahab AT, Choudhary MI. Protective effect of dietary polyphenol caffeic acid on ethylene glycol-induced kidney stones in rats. Urolithiasis. 2018 Apr;46(2):157-66.
- Ye QL, Wang DM, Wang X, Zhang ZQ, Tian QX, Feng SY, Zhang ZH, Yu DX, Ding DM, Xie DD. Sirt1 inhibits kidney stones formation by attenuating calcium oxalate-induced cell injury. Chemico-Biological Interactions. 2021 Sep 25;347:109605.
- Yen GC, Chen HY. Antioxidant activity of various tea extracts in relation to their antimutagenicity. Journal of agricultural and food chemistry. 1995 Jan;43(1):27-32.
- Yousefi Ghale-Salimi M, Eidi M, Ghaemi N, Khavari-Nejad RA. Antiurolithiatic effect of the taraxasterol on ethylene glycol induced kidney calculi in male rats. Urolithiasis. 2018 Oct;46(5):419-28.
- Yu L, Gan X, Bai Y, An R. CREB1 protects against the renal injury in a rat model of kidney stone disease and calcium oxalate monohydrate crystals-induced injury in NRK-52E cells. Toxicology and applied pharmacology. 2021 Feb 15;413:115394.
- Zaki S, Jahan N, Kalim M, Islam G. In vitro antilithiatic activity of the hydro-alcoholic extract of Cinnamomum zeylanicum Blume bark on calcium oxalate crystallization. Journal of integrative medicine. 2019 Jul 1;17(4):273-81.
- Zare Mehrjerdi P, Asadi S, Ehsani E, Askari VR, Baradaran Rahimi V. Silibinin as a major component of milk thistle seed provides promising influences against diabetes and its complications: a systematic review. Naunyn-Schmiedeberg's Archives of Pharmacology. 2024 May 27:1-9.
- Zeferino AS, Mira AR, Delgadinho M, Brito M, Ponte T, Ribeiro E. Drug resistance and epigenetic modulatory potential of epigallocatechin-3-gallate against staphylococcus aureus. Current Microbiology. 2022 May;79(5):149.
- Zeng X, Xi Y, Jiang W. Protective roles of flavonoids and flavonoid-rich plant extracts against urolithiasis: A review. Critical reviews in food science and nutrition. 2019 Jul 20;59(13):2125-35.
- Zhai W, Zheng J, Yao X, Peng B, Liu M, Huang J, Wang G, Xu Y. Catechin prevents the calcium oxalate monohydrate induced renal calcium crystallization in NRK-52E cells and the ethylene glycol induced renal stone formation in rat. BMC complementary and alternative medicine. 2013 Dec;13:1-1.
- Zhang LL, Zhang LF, Xu JG, Hu QP. Comparison study on antioxidant, DNA damage protective and antibacterial activities of eugenol and isoeugenol against several foodborne pathogens. Food & nutrition research. 2017 Jul 18.

- Zhang S, Chen X, Devshilt I, Yun Q, Huang C, An LJ, Dorjbat S, He X. 2018. Fennel main constituent, trans-anethole treatment against LPS-induced acute lung injury by regulation of Th17/Treg function. Mol Med Rep. 18(2):1369–1376.
- Zhang S, Zhu J, Ju Y, Lv M, Yang R, Li Y, Miao Y, Wang Y. Drosophila model and network pharmacology to explore novel targets and novel active components of Chinese traditional medications for treating kidney stones. Pharmacological Research-Modern Chinese Medicine. 2023 Mar 1;6:100220.
- Zhang X, Felter SP, Api AM, Joshi K, Selechnik D. A Cautionary tale for using read-across for cancer hazard classification: Case study of isoeugenol and methyl eugenol. Regulatory Toxicology and Pharmacology. 2022 Dec 1;136:105280.
- Zhang Y, Liu M, Zhu Z, Chen H. Proton pump inhibitors use is associated with a higher prevalence of kidney stones: NHANES 2007–2018. BMC Public Health. 2024 May 2;24(1):1215.
- Zhu XX, Ding YH, Wu Y, Qian LY, Zou H, He Q. Silibinin: a potential old drug for cancer therapy. Expert review of clinical pharmacology. 2016 Oct 2;9(10):1323-30.
- Zuo J, Khan A, Glenton PA, Khan SR. Effect of NADPH oxidase inhibition on the expression of kidney injury molecule and calcium oxalate crystal deposition in hydroxy-L-proline-induced hyperoxaluria in the male Sprague–Dawley rats. Nephrology Dialysis Transplantation. 2011 Jun 1;26(6):1785-96.

CONFERENCES AND WORKSHOPS

CHAITANYA BHARATHI INSTITUTE OF TECHNOLOGY (A)
Kokapet (Village), Gandipet, Hyderabad, Telangana-500075. www.cbit.ac.in
ISO Certified 9001:2015
COMMITTED TO RESEARCH, INNOVATION AND EDUCATION 42 years

3rd Research Day
Saturday, 28th August 2021

Certificate

This is to certify that Mr./Ms./Dr. **Nancy Bhura** of **Lovely Professional University** has participated in **"3rd Research Day"** and presented a paper entitled **Anti-oxidant and nephroprotective effects of Basil Polysaccharides in pharmacological diabetic model** on 28th August 2021 at **Chaitanya Bharathi Institute of Technology (A),** Hyderabad – 500 075, Telangana, INDIA.

Dr. A. D. Sarma
Director, R & D

Dr. P. Ravinder Reddy
Principal

DIVISION OF RESEARCH AND DEVELOPMENT

[Under the Aegis of Lovely Professional University, Jalandhar-Delhi G.T. Road, Phagwara (Punjab)]

Certificate No.240167

Certificate of Participation

This is to certify that **Ms. Nancy Bhura** of **Lovely Professional University, Phagwara, Punjab, India** has presented paper on **Cancer therapy by histone deacetyase inhibitors based nanomedicines** in the **International Conference on Materials for Emerging Technologies (ICMET-21)** held on February 18-19, 2022, organized by Department of Research Impact and Outcome, Division of Research and Development, Lovely Professional University, Punjab.

Date of Issue: 16-03-2022
Place: Phagwara (Punjab), India

Prepared by
(Administrative Officer-Records)

Dr. Vipul Srivastava
Convener
(ICMET-21)

Dr. Manish Vyas
Organizing Secretary
(ICMET-21)

Dr. Chander Prakash
Co-Chairperson
(ICMET-21)

CERTIFICATE

PROUDLY PRESENTED TO

Nancy Bhura

Molecular modeling for the medicinal chemistry toolkit

May 27, 2021	*Chemistry World Webinars*	CHEMISTRY WORLD SCHRÖDINGER.
Date of Completion	Organizer	

NATIONAL INSTITUTE OF PHARMACEUTICAL EDUCATION & RESEARCH (NIPER) KOLKATA

Chunilal Bhawan, 168, Maniktala Main Road, Kolkata 700054

कोलकाता KOLKATA

औषध विभाग Department of Pharmaceuticals

Participation Certificate

This is to certify that Dr./Mr./Miss./Mrs.

Nancy Bhura

has participated in one day workshop entitled as "One Day - Workshop on Publications, Systematic Review & Meta-Analysis" held on December 6th, 2021 at NIPER, Kolkata.

Prof. V. Ravichandiran
Director, NIPER-Kolkata

Ganpat University | Shree S.K. Patel College of Pharmaceutical Education and Research

25 years of Cultivating Next-Gen Pharma Profession through Research & Innovations

CERTIFICATE
OF PARTICIPATION

It is our pleasure to certify that Prof./Dr./Mr./Ms.

Nancy Bhura

from **Lovely Professional University**

has participated as a delegate in Online-webinar on

"Current Trends in Clinical Research"

on 24th July, 2021,
at Ganpat University,
Shree S. K. Patel College of Pharmaceutical Education
and Research, Gujarat, India.

Dr. Pawan Kumar Gupta
Coordinator
Assistant Professor

Prof. Bhaswat S. Chakraborty
Moderator
Professor Emeritus

Dr. S. S. Pancholi
Convener
Executive Dean
SoP and Principal

HUMAN RESOURCE DEVELOPMENT CENTER

[Under the Aegis of Lovely Professional University, Jalandhar-Delhi G.T. Road, Phagwara (Punjab)]

Certificate No. 241680

Certificate of Participation

This is to certify that **Ms. Nancy Bhura** D/o Sh. Suresh Kumar Bhura participated in **Training on The Care and Use of Laboratory Animals in Accordance with Ethical Guidelines** organized by Lovely Professional University w.e.f. **March 11, 2022** to **March 12, 2022** and obtained **"O"** Grade.

Deputy Dean
Human Resource Development Center

Professor and Dean
Human Resource Development Center

CSIR-IIIM

International Conference on Emerging Trends in Biosciences and Chemical Technology-2022

December 3-5, 2022

Organised by

School of Biotechnology, Shri Mata Vaishno Devi University, Katra

Certificate of Participation

This is to certify that Prof./Dr./Mr./Ms. Nancy Bhura

has presented Poster / Oral Presentation entitled Evaluation of Trans-Anethole as Anti-Oxidant & Anti-Lithiatic Agent at

International Conference on Emerging Trends in Biosciences and Chemical Technology (ETBCT-2022) held at Shri Mata Vaishno Devi University, Katra, J&K in collaboration with CSIR-IIM Jammu and BRSI, India.

Dr. Indu Bhushan, Convener, ETBCT-2022

Dr. Asha Chaubey, Convener, ETBCT-2022

Prof. Ashok Pandey, Conference Chair, ETBCT-2022

Dr. Ratna Chandra, Organizing Secretary, ETBCT-2022

DST@ 1971-2021 — DEPARTMENT OF SCIENCE & TECHNOLOGY

THAPAR INSTITUTE OF ENGINEERING & TECHNOLOGY (Deemed to be University)

CERTIFICATE OF PARTICIPATION

This acknowledges that

NANCY BHURA

from LOVELY PROFESSIONAL UNIVERSITY, PHAGWARA, JALANDHAR

has attended DST-PURSE sponsored three-day workshop & hands-on training on *"Spectroscopy, Separation, and Surface Characterization Techniques"*, organized by Department of Chemistry and Biochemistry (DCBC), during March 04-06, 2024 at Thapar Institute of Engineering and Technology (TIET), Patiala, Punjab

Prof. Amjad Ali, Organizer of Workshop, TIET, Patiala, Punjab

Prof. Soumen Basu, Organizer of Workshop, TIET, Patiala, Punjab

Prof. Manmohan Chhiber, Head DCBC, TIET, Patiala, Punjab

International Conference on Drug Discovery

Nov. 10th & 11th 2022, BITS Pilani, K K Birla Goa Campus

ICDD 2022

Certificate

This is to certify that

Nancy Bhura

has successfully participated in International Conference on Drug Discovery held at BITS-Pilani K K Birla Goa Campus on 10th & 11th Nov. 2022 and presented a poster.

R. Raghu
Vice President

Prof. Suman Kundu
Director, BITS Pilani,
K.K. Birla Goa Campus

Schrödinger | BITS Pilani
K K Birla Goa Campus


विज्ञान एवं प्रौद्योगिकी विभाग
DEPARTMENT OF
SCIENCE & TECHNOLOGY
Azadi Ka Amrit Mahotsav
THAPAR INSTITUTE
Certificate of Participation
This certificate is awarded to
Nancy Bhura
For successful participation in 7 Days,
Hands-on training program on Insights into the
Applications of High-End Instruments in Chemical Sciences,
held under the scheme of Synergistic Training Program
Utilizing the Scientific and Technological Infrastructure (STUTI),
an initiative by Department of Science and Technology, India.
Held from 21st February to 27th February 2023
At Thapar Institute of Engineering and Technology, Patiala, Punjab
Dr. Ratnesh Jain
DST-STUTI ICT
Coordinator
Dr. Satnam Singh
Prof. & Head,
School of Chemistry & Biochemistry
Dr. Anoop Verma
Associate Professor & Head,
School of Energy & Environment

JOURNAL OF RECEPTORS AND SIGNAL TRANSDUCTION
2022, VOL. 42, NO. 5, 521–530
https://doi.org/10.1080/10799893.2022.2058016

Taylor & Francis
Taylor & Francis Group

ORIGINAL ARTICLE

Target-based in-silico screening of basil polysaccharides against different epigenetic targets responsible for breast cancer

Nancy Bhura[a#], Pawan Gupta[b,c#] and Jeena Gupta[d]

[a]Department of Biotechnology, School of Bioengineering and Biosciences, Lovely Professional University, Phagwara, Punjab, India; [b]Department of Research and Development, Lovely Professional University, Phagwara, Punjab, India; [c]Department of Pharmacology, Shree SK Patel College of Pharmaceutical Education and Research, Ganpat University, Mehsana, Gujarat, India; [d]Department of Biochemistry, School of Bioengineering and Biosciences, Lovely Professional University, Phagwara, Punjab, India

ABSTRACT

Purpose: Breast cancer (BC) is one of the leading types of cancer found in women. One of the causes reported for BC is improper regulation of epigenetic modifications. Various epigenetic targets such as histone deacetylases (HDAC) and histone acetyltransferases (HAT) regulate many types of cancer, including BC. Basil is known to possess anti-cancer properties; however, the role of its polysaccharides against different epigenetic targets is still not very clear. Therefore, the molecular docking method is used to find out the binding potential of the BPSs against different epigenetic targets responsible for BC.

Methods: All the basil polysaccharides (BPSs) were screened against the diverse epigenetic targets reported for BC (HDAC1-2, 4-8, and HAT) using molecular docking studies alongwith swissADME studies to check the drug likeliness of the BPSs.

Results: It was found that glucosamine ring, glucosamine linear, glucuronic acid linear, rhamnose linear, glucuronic acid ring, galactose ring, mannose, glucose, and xylose were exhibited consistent binding potential against the epigenetic targets (HDAC1, HDAC2, HDAC4, HDAC5, HDAC6, HDAC7, HDAC8, and HAT,) responsible for BC.

Conclusion: This is the first report where BPSs were reported against these epigenetic targets. These studies can help to understand the underlying mechanism of BPSs used against epigenetic targets for BC. These results can be further validated experimentally to confirm their potential as a promising inhibitor against the epigenetic targets (HDAC1-2, 4-8, and HAT) having a role in BC.

ARTICLE HISTORY
Received 22 September 2021
Revised 19 January 2022
Accepted 21 January 2022

KEYWORDS
Basil polysaccharides; breast cancer; epigenetics; target based in-silico screening; molecular docking

1. Introduction

Breast cancer (BC) remains the most frequent form of the disease and the second leading cause of death in women [1]. The development of therapies targeting anti-HER2 has made substantial progress in the prognosis of metastatic BC. Also, emerging immunotherapy provides scope for efficient management of these BC patients [2]. However, most demises caused by BC come from the deterioration and growth of secondary malignant tumors to other distant organs. This is when conventional treatments like surgery or curative chemotherapy aren't available any longer an option. That is the reason why only 26% of stage 4 patients reach five years of survival [3]. Thus, exploring the basis of genetic and epigenetic changes in BC can ease the development process of diagnosis and therapeutic strategies aiding in the treatment of deadly disease.

Epigenetic studies have evolved as crucial players in BC development and progression [4]. The attention to epigenetics as a therapeutic target comes from the fact that in contrast to gene alterations, aberrant hypermethylation and histone PTMs are possibly reversible. In addition, combined treatments with epigenetic drugs can exploit the dynamic nature of epigenetic changes to potentially modulate responses to immunotherapy [5]. At present, there are two types of epigenetic drugs approved in the clinical studies: the first one is DNMT inhibitors (DNMTi) for treating cancers of colon, ovarian, and lung cancer (with serious side effects) [6]. And another is histone deacetylase small-molecule inhibitors (HDACi) for treating cancer of the lymphatic system and plasma cells [7]. To date, 18 HDAC family members have been identified and classified into four groups based on their homology to yeast HDAC: Classes, which are taken in this study, have been discussed briefly in Table 1.

No HDAC inhibitor has been available in the market approved by the US-FDA for BC treatment to date but registered under clinical trials for BC treatment [22]. Pracinostat (SB939) is a novel HDAC inhibitor that has been reported to have better pharmaceutical properties than other inhibitors like vorinostat [23] and is effective against brain metastasis

CONTACT Pawan Gupta pawanpharma79@gmail.com Department of Pharmacology, Shree SK College of Pharmaceutical Education and Research, Ganpat University, Ganpat Vidyanagar, Mehsana-384012, Gujarat, India
#Both the authors are contributed equally

Supplemental data for this article can be accessed online at https://doi.org/10.1080/10799893.2022.2058016.

ScienceDirect

Journal of Manufacturing Processes
Volume 119, 15 June 2024, Pages 666-681

On 3D printed thermoresponsive PCL-PLA nanofibers based architected smart nanoporous scaffolds for tissue reconstruction

Ranvijay Kumar [a b], Rupinder Singh [b], Vinay Kumar [a], Nishant Ranjan [a], Jeena Gupta [c], Nancy Bhura [c]

[a] University Centre for Research and Development, Chandigarh University, Punjab, India
[b] Department of Mechanical Engineering, National Institute of Technical Teachers Training and Research, Chandigarh, India
[c] School of Bioengineering and Biosciences, Lovely Professional University, Punjab, India

Received 14 May 2023, Revised 31 December 2023, Accepted 2 April 2024, Available online 8 April 2024, Version of Record 8 April 2024.

What do these dates mean?

Check for updates

Show less

Share Cite

https://doi.org/10.1016/j.jmapro.2024.04.008

Get rights and content

Abstract

Previous studies have reported that polycaprolactone (PCL)-polylactic acid (PLA) based scaffolds are one of the most acceptable composite materials in tissue engineering/reconstruction applications. However, little has been reported on the

Volume 2800, Issue 1
8 September 2023

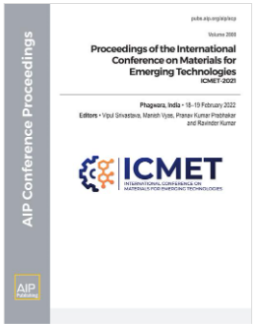

PROCEEDINGS OF THE INTERNATIONAL CONFERENCE ON MATERIALS FOR EMERGING TECHNOLOGIES: ICMET-2021
18–19 February 2022
Phagwara, India

RESEARCH ARTICLE | SEPTEMBER 08 2023

Cancer therapy by histone deacetylase inhibitors based nanomedicines

Nancy Bhura; Jeena Gupta
+ Author & Article Information

AIP Conf. Proc. 2800, 020037 (2023)
https://doi.org/10.1063/5.0164153

The inhibitors of histone deacetylases are approved for the treatment of different malignancies and have also achieved therapeutic success. However, still due to their low efficiency of treatment, their application in the treatment of chronic tumors is challenging. There are wide applications of nanotechnology in cancer treatment as nanomedicine are presumed to improve the stability of the drug, increasing drug accumulation in tumors and prolonging the half-life of circulation. Nanomedicine, therefore, emerges as a promising strategy for enhancing the therapeutic efficacy of histone deacetylase inhibitors. However, the associated nanotoxicity of nanomaterials used in drug delivery systems eased the success of nanomedicine. We summarized the advances of histone deacetylase inhibitor-based nanomedicines and their therapeutic efficacy with a focus on designing targeted drug delivery systems for histone deacetylase inhibitors.